DOCTORAL DISSERTATION

GDAŃSK UNIVERSITY OF TECHNOLOGY

FACULTY OF CHEMISTRY

Preparation, characterization, and manufacturing of new polymeric materials for 3D printing for medical applications

by

AGNIESZKA HARYŃSKA, MSc Eng.

DEPARTMENT OF POLYMER TECHNOLOGY

The author of the Ph.D. dissertation: Agnieszka Haryńska, MSc Eng.

Scientific discipline: Chemical sciences

DOCTORAL DISSERTATION

Title of Ph.D. dissertation: Preparation, characterization, and manufacturing of new polymeric materials for 3D printing for medical applications.

Title of Ph.D. dissertation (in Polish): Otrzymywanie, charakterystyka i wytwarzanie nowych materiałów polimerowych do druku 3D dla zastosowań medycznych.

`

Supervisor *signature*
PhD DSc. Eng., Justyna Kucińska-Lipka, Assoc. Prof. of GUT

Gdańsk, 2022

STATEMENT

The author of the Ph.D. dissertation: Agnieszka Haryńska, MSc Eng.

I, the undersigned, agree that my Ph.D. dissertation entitled:

"Preparation, characterization, and manufacturing of new polymeric materials for 3D printing for medical applications".

may be used for scientific or didactic purposes.[1]

Gdańsk,…… ……

signature of the Ph.D. student

Aware of criminal liability for violations of the Act of 4th February 1994 on Copyright and Related Rights (Journal of Laws 2006, No. 90, item 631) and disciplinary actions set out in the Law on Higher Education (Journal of Laws 2012, item 572 with later amendments),[2] as well as civil liability, I declare, that the submitted Ph.D. dissertation is my own work.

I declare, that the submitted Ph.D. dissertation is my own work performed under and in cooperation with the supervision of PhD DSc. Eng., Justyna Kucińska-Lipka, Assoc. Prof. of GUT.

This submitted Ph.D. dissertation has never before been the basis of an official procedure associated with the awarding of a Ph.D. degree.

All the information contained in the above thesis which is derived from written and electronic sources is documented in a list of relevant literature in accordance with art. 34 of the Copyright and Related Rights Act.

I confirm that this Ph.D. dissertation is identical to the attached electronic version.

Gdańsk,…… ……

signature of the Ph.D. student

I, the undersigned, agree to include an electronic version of the above Ph.D. dissertation in the open, institutional, digital repository of Gdańsk University of Technology, Pomeranian Digital Library, and for it to be submitted to the processes of verification and protection against misappropriation of authorship.

Gdańsk,…… ……

signature of the Ph.D. student

[1] Decree of Rector of Gdansk University of Technology No. 34/2009 of 9th November 2009, TUG archive instruction addendum No. 8.

[2] Act of 27th July 2005, Law on Higher Education: Chapter 7, Criminal responsibility of PhD students, Article 226.

DESCRIPTION OF DOCTORAL DISSERTATION

The Author of the Ph.D. dissertation: Agnieszka Haryńska, MSc Eng.

Title of Ph.D. dissertation: Preparation, characterization, and manufacturing of new polymeric materials for 3D printing for medical applications.

Title of Ph.D. dissertation in Polish: Otrzymywanie, charakterystyka i wytwarzanie nowych materiałów polimerowych do druku 3D dla zastosowań medycznych.

Language of Ph.D. dissertation: English

Supervision: PhD DSc. Eng., Justyna Kucińska-Lipka, Assoc. Prof. of GUT

Date of doctoral defense:

Keywords of Ph.D. dissertation in Polish: biopolimery; polimery klasy medycznej; synteza polimerów; osadzanie topionego materiału; druk 3D; produkcja filamentów; charakterystyka materiałowa.

Keywords of Ph.D. dissertation in English: bio-based polymers; medical-grade polymers; polymer synthesis; fused filament fabrication; 3D printing; filament manufacturing; material characterization.

Summary of Ph.D. dissertation in Polish:

Niniejsza rozprawa dotyczy syntezy, formowania oraz charakterystyki nowych filamentów do druku 3D w technologii FDM™/FFF dla celów medycznych. Opracowano dwa rodzaje nowych filamentów, tj. degradowalne filamenty poliuretanowe, oraz biodegradowalne filamenty polilaktydowo-skrobiowe. Zbadano wpływ procesu druku 3D na wybrane właściwości tych filamentów. Przeprowadzono szczegółową analizę procesu formowania filamentów przy użyciu metody wytłaczania, co w znaczący sposób uzupełnia dotychczasowe piśmiennictwo. Zaprojektowano oraz wydrukowano w 3D porowate struktury oraz modele anatomiczne wykorzystując m.in. opracowane filamenty. Tak otrzymane detale poddano serii wstępnych badań biologicznych mających na celu określenie ich przydatności dla konkretnych zastosowań medycznych. Wyniki badań wykazały, że opracowane filamenty poliuretanowe są biokompatybilne i podatne na degradację krótkoterminową, a proces formowania nie wpływa na ich właściwości strukturalne, termiczne i biologiczne. Natomiast, modyfikacja polilaktydu dodatkiem skrobii termoplastycznej spowodowała wzrost hydrofilowości oraz podatności na degradację hydrolityczną opracowanego bio-

filamentu. Wykazano, że wydrukowane poliuretanowe porowate struktury 3D spełniają wstępne wymagania dla rusztowań tkanki kostnej gąbczastej. Z kolei, personalizowane modele anatomiczne wydrukowane z użyciem opracowanego bio-filamentu charakteryzują się zwiększoną podatnością na kompostowanie oraz nie odbiegają jakością od wydruków otrzymanych z komercyjnego filamentu polilaktydowego (PLA). Podstawą niniejszej rozprawy doktorskiej jest cykl sześciu artykułów naukowych opublikowanych w czasopismach z listy JCR.

Summary of Ph.D. dissertation in English:

This work concerns the synthesis, formation, and characteristics of new filaments for 3D printing in FDM™/FFF technology for medical purposes. Two types of filaments were developed, i.e. degradable polyurethane and biodegradable polylactide-starch. The influence of the 3D printing process on selected filament properties was investigated. A detailed analysis of the filament formation process by the extrusion method was carried out, thus complementing the current state of knowledge. Porous structures and anatomical models were designed and 3D printed using, among others, developed filaments. The obtained details were subjected to a series of preliminary biological *(in vitro*) tests to determine their suitability for medical applications. The research results showed that the developed polyurethane filaments are biocompatible and susceptible to degradation, and the forming process does not affect their structural, thermal, and biological properties. Whereas, modification of polylactide with the addition of thermoplastic starch increased the hydrophilicity and susceptibility to hydrolytic degradation of the developed bio-filament. It has been shown that 3D printed polyurethane porous structures meet the prerequisites of cancellous bone tissue scaffolds. In turn, personalized anatomical models printed with the use of the developed bio-filament are characterized by increased compostability while maintaining the quality of printouts from commercial polylactide (PLA) filament. The basis of the presented doctoral dissertation is a series of six scientific articles published in journals indexed in the JCR list.

To my husband, the only love and best friend.

"Time well spent is time spent together".

CONTENTS

ABBREVIATIONS AND ACRONYMS

^{1}H NMR	-	proton nuclear magnetic resonance
3DP	-	3D printing
ATR	-	attenuated total reflection technique used in FTIR spectroscopy
BDO	-	1,4-butanediol
C-HAp	-	carbonated-hydroxyapatite
CT	-	computer tomography
DICOM	-	digital imaging and communications in medicine
DMA	-	dynamic mechanical analysis
DSC	-	differential scanning calorimetry
EDS	-	energy-dispersive X-ray spectroscopy
ESO	-	epoxidized soybean oil
FDM	-	fused deposition modelling
FFF	-	fused filament fabrication
FTIR	-	Fourier transform infrared spectroscopy
HAp	-	hydroxyapatite
HDI	-	1,6-hexamethylene di-isocyanate
HS	-	hard segment
IPDI	-	isophorone di-isocyanate
MDI	-	4,4'-methylenediphenyl di-isocyanate
MFR	-	melt flow rate
OM	-	optical microscope
PBS	-	phosphate-buffered saline
PCL	-	polycaprolactone diol
PDO	-	polydioxanone
PEBA	-	α,ω-dihydroxy(ethylene-butylene adipate) diol
pG	-	plant glycerin
PLA	-	polylactide
PLGA	-	poly(lactic-co-glycolic) acid
PLA/TPS	-	term adopted for developed bio-composition consisting of PLA, TPS and ESO
polyol	-	term adopted for oligomeric chemical compounds containing hydroxyl groups
PUR	-	polyurethane (in general)
SBF	-	simulated body fluid
SEM	-	scanning electron microscope
SFE	-	surface free energy
SS	-	soft segment
TDI	-	toluene di-isocyanate
TDS	-	technical data sheet
TGA	-	thermogravimetry
TPE	-	thermoplastic elastomer

TPS	-	thermoplastic potato starch
TPU	-	thermoplastic polyurethane
TPU(E)	-	term adopted for developed poly(ester urethane) filament (Epaline®)
TPU(PCL)	-	term adopted for synthesized poly(ester urethanes) with PCL as a polyol
TPU(PEBA)	-	term adopted for synthesized poly(ester urethanes) with PEBA as a polyol
XRD	-	X-ray powder diffraction
wCA	-	water contact angle

CHAPTER I

THEORETICAL BACKGROUND

1.1. Outline

Additive manufacturing (AM), colloquially known as 3D printing (3DP), is a set of modern techniques that, along with computer modeling tools, allows for obtaining complex structures and personalized products. The objects are precisely formed layer by layer, unlike the removal of material in traditional means (carving, milling, machining, etc.). The use of AM in medicine is of great interest to academia and industry. Advanced AM technologies are no longer limited to the formation of prototypes but also functional/finished products such as implants, prostheses, drug delivery systems, tissue scaffolds, or even human tissues. 3D printing appears to be one of the most in-demand moulding methods for custom medical products. This is due to design freedom and the ability to work directly with DICOM (Digital Imaging and Communications in Medicine) files, which greatly facilitates the preparation of complex and patient-matched structures. Due to the huge increase in the availability of 3D printers, the demand for materials suitable for 3D printing that meet stringent medical requirements has increased. Therefore, the factor limiting the widespread use of 3D printing in medicine is the insufficient amount and variety of materials that are compatible with AM technologies and meet medical-grade criteria. Many 3DP techniques are used for medical purposes, including SLS (Selective Laser Sintering), bio-printing, PJ (PolyJet), and SLA (Stereolithography). However, FFF (Fused Filament Fabrication) appears to be the easiest way to utilize AM due to its attractive cost of purchase, ease of service and feedstock preparation. It utilizes a raw material in the form of a filament, i.e. thermoplastic-based wire with a constant diameter (mostly 1.75/2.85 cm). Most often, filament is obtained by extruding polymer granules (or composites), which are then wound on a spool of specific dimensions. This process requires appropriate processing line and strict parameters, thanks to which the resulted material will retain its properties and a constant diameter. The filament is formed continuously and it is possible to form the product on a mass scale. However, this is not the only method of forming filaments. The literature is dominated by discontinuous forming methods in which only short sections of filament are obtained in the form of extrudate collected manually from the extrusion die (information on the process flow and parameters is rather omitted). The market supplies many solutions based on petrochemical polymers, acrylonitrile butadiene styrene (ABS), polyamide (PA), thermoplastic elastomer (TPE) or polylactide (PLA) and their modifications with fillers, thus providing a wide range of various properties. 3D-printable solutions for

medicine are most often based on biocompatible, bioresorbable and/or biodegradable polymers. The example of such commercial products are Lactoprene® 100M (PLA), Caproprene® 100M (PCL), Bioflex® (TPE), or Dioxactisse® 100 (PDO). The number of medical grade filaments available has visibly increased, however the choice is still limited. An interesting alternative to the mentioned product might be properly designed thermoplastic polyurethanes (TPU). For many years, polyurethanes have been successfully used in medicine as breast implants, stents, surgical dressings, dialysis membranes, and artificial blood vessels, due to the unique properties of flexibility, toughness, biocompatibility, and hemocompatibility. Their unique features are also utilized in tissue engineering for scaffolding, in which proper design of the porous structure is one of the crucial factors. Therefore, the use of 3D printing tools seems to be very advisable in this regard. Nevertheless, TPU's common use as filaments for FFF 3DP is still missing. Another interesting solution increasing the variety of medical filaments can be plant-based biodegradable polymers. Healthcare is increasingly using 3D printing, among others, for pre-operative planning, thus producing a significant number of disposable details. As the amount of such waste is increasing, research into sustainable systems seems to be the right direction. It would seem, however, that the commonly available PLA filament is a ready-made solution, but it is a difficult and long-term degradable polymer, effective biodegradation of which requires special conditions. Despite its common label as "bio and environmental friendly", PLA waste began to be perceived as difficult to effectively and sustainably manage. In addition, such PLA filaments are enriched with printability-improving agents (plasticizers, oils, pigments), which additionally may hinder biodegradation and contribute to greater environmental plastic pollution. One way to overcome these issues is blending PLA with fast-degradable and compostable polymers such as thermoplastic starch (TPS). TPS benefits include high renewability and biodegradability rate along with comparatively low cost. Nevertheless, unsatisfactory mechanical properties, fragile and susceptibility to retrogradation discourage the polymer industry to widespread use of TPS. Thus, proper modification and plasticization of TPS in a way that will not affect biodegradability is highly desirable. Such PLA/TPS bio-composites adapted to 3D printing with FFF technology might challenge traditional petroleum-based or long-term degradable filaments as a sustainable alternative. However, the literature on the subject is limited and, to the best of our knowledge, the market does not yet provide solutions in this regard.

In the following chapters, the theoretical foundations of the above considerations are presented and supplemented with the literature and market review.

1.2. Introduction to the studied biopolymers

1.2.1. Polyurethanes (PUR) as biomaterials

Polyurethanes (PUR) have been used as biomedical polymers since the 1960s [1]. For decades, PURs have been modified and adapted to medical requirements. This has resulted in the modern biopolymers that exhibit a wide range of properties, such as excellent biostability and bio-, and hemo-compatibility, antiseptic, or satisfactory biomimetic properties [2–4]. PURs are widely used in drug delivery systems (DDS), vascular surgery, cardiology, and tissue engineering, hence the methods of their processing are constantly being improved. The unique feature of polyurethanes is their versatility, which allows customizing the properties to the desired needs and applications. PURs show a strong structure-properties relationship. By changing the components and/or the method of synthesis and forming, various classes of plastics can be obtained, i.e. thermoplastic elastomers (TPE), rigid and flexible foams, elastomers (thermosetting), or waterborne dispersions (coatings, adhesives, binders) [5]. Generally, the chemistry of polyurethanes is based on a urethane group (–NCOOH–), usually formed by the nucleophilic substitution reaction of isocyanate (–NCO) group with electrophilic agent (–OH). A less common solution involves the reaction of amine-based molecules with polycarbonate derivatives (including carbamates), resulting in so-called non-isocyanate polyurethanes (NIPUs) [6]. A common method for the synthesis of polyurethanes is the polyaddition reaction of polyisocyanates (aromatic or aliphatic) with long-chain polyols (hydroxyl- or amino-terminated) and low molecular weight chain extenders (glycols or diamines) in the presence of a catalyst (organometallic or amine). The process can be carried out in a one-step or two-step method. In the first one, all the reagents are mixed to react simultaneously. It does not require the use of additional apparatus and is time-effective. One-step polymerization is most often used in the synthesis of PUR foams. However, the control of the process is limited and the resulting polymers might have a large molar mass distribution which affects the properties. Thus, the synthesis of cast PURs usually takes place in a two-step manner. The first stage comprises a so-called pre-polymerization step in which a molar excess of polyisocyanate reacts with

a polyol with active hydrogen atoms. The isocyanate-terminated prepolymer is then reacted with a low molecular weight chain extender (terminated with isocyanate-reactive groups –OH/–NH2), leading to the formation of macromolecular PUR. Although the reaction time is longer, the product shows a lower molar mass dispersion and has a more orderly structure compared to the compounds obtained with the one-step method. This in turn favours the phenomenon of phase separation which is responsible for the unique properties of PURs. While the structure of elastomeric PURs is crosslinked with phases composed of chemically linked chain networks, thermoplastic polyurethanes (TPU) have a segmented structure consisting of linear chains with hard (HS) and soft (SS) segments. The soft segments contain long-chain polyols which, due to their relatively low glass transition temperature (T_g), provide high elasticity. The urethane groups bound to isocyanate residues and low molecular weight chain extenders form HS that provide increased mechanical strength of the material. The segmented structure described is responsible for the thermoplastic nature of TPU (ability to plasticize at a certain elevated temperature) and elastomeric nature (resilience). Since the polyurethane segments are thermodynamically incompatible, the phase separation phenomenon occurs, which leads to the formation of ordered supermolecural structures (nanometric domains, but also, in certain instances, microstructures of globules and spherulites) [7]. Interactions between hard segments forming the domain structure (mainly hydrogen bonds and London dispersion forces LDF) act like physical crosslinking of polymer chains [8]. Such complex TPU morphology ensures resilience comparable to chemically crosslinked elastomers while being a thermoplastic, as intermolecular forces weaken at elevated temperatures and are renewed. Moreover, by selecting a type and ratio of reagents in the TPU synthesis, the nature of the obtained segments can be controlled. This has a direct impact on the material properties (strength, hardness, susceptibility to degradation or biocompatibility), but also, along with the synthesis conditions, affects morphological factors (type and size of supermolecural structures, degree of phase separation or crystallinity), which further adjusts the properties of the material [9,10].

In the synthesis of medical-grade TPU, usually two types of di-isocyanates are used, i.e. aromatic and aliphatic. Aromatic di-isocyanates, such as 4,4'-methylenediphenyl diisocyanate (MDI) and toluene diisocyanate (TDI) are most commonly used in the synthesis of commercial biostable TPUs (Texin Rx®, ChronoFlex C®, Elasthane®, Pellethane®) due to high availability, relatively low cost, and higher reactivity than

aliphatic di-isocyanates. These products are distinguished by high mechanical strength, resistance to abrasion, oils and greases, and resistance to hydrolysis. Therefore, they are perfect for external contact with the human body (short- and long-term) as medical and surgical equipment or as biostable intra-tissue structures. However, UV sterilization of aromatic TPUs can lead to photodegradation and deterioration of properties [11]. Since TPUs are required to be highly resistant to degradation and biostable in permanent and long-term implant applications, biodegradable and resorbable systems are most in-demand in tissue engineering and drug delivery. In the process of aromatic TPU degradation, toxic residues containing carcinogenic aromatic amines, such as methylenedianiline (MDA) and toluene diamine (TDA), can be released [12–15]. Nevertheless, the detected concentrations of potentially carcinogenic amines were negligible, and the preliminary tests of toxic and mutagenic properties did not qualify the tested materials as carcinogenic. However, this topic is still being discussed, leaving some doubts behind. Therefore, the use of aliphatic and cycloaliphatic di-isocyanates in the synthesis of degradable and medical TPU seems reasonable, as the resulting amine residues are non-toxic and removed from the body in the natural life cycle [16]. The literature predominates in aliphatic TPUs based on 1,4-diisocyanatobutane (BDI), l-lysine di-isocyanate (LDI), isophorone diisocyanate (IPDI), hexamethylene di-isocyanate (HDI), or 4,4'-methylenebis(cyclohexyl isocyanate (HMDI) [16–20]. The results of these studies show the high potential of formed aliphatic TPUs as biostable and biocompatible implantable biomaterials, but non- or slow-degradable. According to Cauich-Rodríguez's review [21] on the degradation of medical polyurethanes, it can be concluded that, among other factors, the use of aliphatic di-isocyanates increases susceptibility to polyurethane degradation in relation to aromatic systems. The commercial solutions of aliphatic TPUs cover Carbothane®, MillaMed®, or Tecoflex MG®. The features of these products include excellent oxidative stability, resistance to yellowing by aging and sterilization, and moderate mechanical properties. Those systems are biostable, biocompatible, and not adapted to biodegradation. The values of strength parameters and the characteristics of the commercial medical TPUs are attached in **Appendix 1** (**Table A1**). Another important substrate influencing the chemistry and properties of polyurethanes is polyol, i.e. oligomeric organic compound containing several hydroxyl groups.

Biodegradable TPUs are synthesized with prone to hydrolysis polyester-diols, or a mixture with polyether-diols, usually with polycaprolactone-diol (PCL), polylactide-diol (PLA), poly(glycolic acid) (PGA), poly(ethylene glycol) (PEG), and poly(tetramethylene glycol) (PTMG) [22–25]. These polyols are widely used in medicine and provide different properties. However, the semi-crystalline nature of these soft segments may hinder the TPU degradation. Thus, the use of amorphous polyols in the synthesis of degradable TPUs may facilitate hydrolytic or enzyme breakdown. The literature on amorphous polyols in the synthesis of TPU is limited. This is most likely due to the deterioration of the mechanical and thermal properties of polyurethanes containing amorphous flexible segments in the structure with respect to the semi-crystalline ones [26]. However, tissue engineering products such as tissue scaffolds, dressings, and artificial blood vessels require slightly different material properties (appropriate strength, elasticity, biocompatibility, rapid degradation, etc.), and then amorphous polyols appear to be preferable to those that are crystallizable.

One way to increase the degradability rate of slow-degradable segmented polyurethanes is to use biodegradable block polyols enriched with amorphous segments. Henry et al. [27] synthesized poly(ester-urethane) with block polyol consisting of crystalline PHB and amorphous poly(caprolactone-co-glycolide) segments. The material had satisfactory mechanical properties (tensile strength of ~20 MPa, tensile modulus ~8 MPa), and the formed tissue scaffolds showed good *in vitro* biocompatibility. However, degradation study in PBS demonstrated that the porous scaffolds were resistant to hydrolytic degradation and remain stable till 168 days of incubation after which degradation starts with the amorphous region of the TPU soft segment. More promising results in fast-degradable polyurethane systems were presented by Wang et. al [28]. They synthesized novel amorphous and biodegradable polyol BPD, consisting of 1,3 propanediol (PDO), 1,4 butanediol (BDO), succinic acid (SU), sebacic acid (SA) and furamic acid (FA). Then biodegradable polyurethane (BTPU) was synthesized with MDI and BDO (hard segment) and BPD (soft amorphous segment). The results of enzymatic degradation of the BTPU showed an increase in mass lost with rising amorphous soft segment content in the BPTU structure (mass lost over 38% after 14 days of incubation).

Another issue worth discussing is the use of catalysts in the synthesis of degradable, medical polyurethanes. As mentioned before, most common used catalysts for TPU synthesis are amine based (1,4-diazabicyclo[2.2.2]octane DABCO) and metal-organic (dibutyltin dilaurate DBTDL, stannous octoate ($Sn(Oct)_2$). The catalysts accelerate the reaction between hydroxyl and isocyanate groups leading to the formation of urethane bonds. In addition to improving the kinetics of the process, the catalyst leads to higher molecular weights improving the mechanical properties and processing of the TPU [29]. Both amines and tin compounds, however, belong to the group of highly toxic substances. The study of Tanzi et. al [30] showed that all the catalysts are cytotoxic relative to the cell line of the 3T3 mouse fibroblasts. However, the cytotoxicity test was conducted by directly adding a given catalyst into culture medium. The results of the experiment conducted in such drastic conditions cannot be referred to materials containing such catalysts, as the concentration of a catalyst released from polyurethane matrix in degradation processes is incomparably smaller. Nevertheless, more and more scientists are developing polyurethane systems without using a synthesis catalyst to avoid a presumed/reputed decrease in biocompatibility [31–33].

In summary, the use of biodegradable, amorphous polyols and aliphatic di-isocyanates in the synthesis of TPUs may contribute to the improvement of their susceptibility to degradation, while maintaining biocompatibility, as the toxicity of the degradation products is not expected. Moreover, the synthesis of TPUs without the use of catalysts potentially harmful to the human body may increase the material biocompatibility.

1.2.2. Thermoplastic starch (TPS)

The main raw material for the production of thermoplastic starch (TPS) is native starch obtained from plants such as corn, potatoes, wheat, cassava, and rice. They are mass-grown plants available in many parts of the world. Therefore starch is considered a versatile, cheap, and abundant raw material that meets the criteria of plastic sustainability [34]. The botanical origin of starch defines its chemical and structural characteristic, including content of lipids, proteins and minerals, crystalline structure, granules size, and proportion of amylopectin and amylose [35]. The main constituents of native starch are the D-glucose polymers, amylopectin, and amylose. Amylopectin is a highly branched polysaccharide that builds the shell of the starch grains and is

responsible for the ability to swell and form soles. Amylose has a linear structure that forms helical structures which are mainly packed inside starch grains forming core [36]. Both components of starch (amylose and amylopectin) can crystallize and the degree of crystallinity depends on the origin of the starch, the external conditions and the processing method. The content of amylose in starch depends on its origin and usually ranges from 20% to 30%. Along with native starch, TPS is a completely biodegradable and compostable polymer material that is sensitive to environmental humidity due to its hydrophilic nature. Positive features of TPS are shown in **Figure 1**.

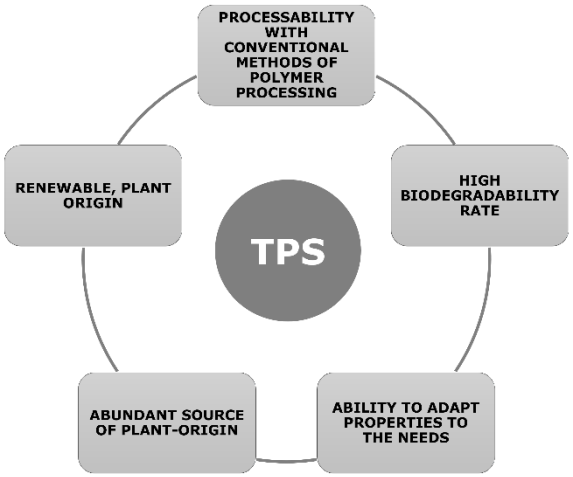

Figure 1 Advantageous material features of thermoplastic starch.

However, the final properties of TPS depend on several factors, including the origin of native starch that determines the structural properties of the granules, but also the processing parameters and type and ratio of the plasticizer used. Numerous studies have shown that the chemical structure, molecular weight, and the type of functional groups of the plasticizers are crucial factors defining the performance of TPS products [37–40]. Accordingly, further considerations focus on the topic of TPS plasticization.

Thermoplastic starch (TPS) is a product of the thermal treatment of starch flour (native starch), most often by a combination of thermal and mechanical processing methods. These treatments are aimed at destroying the semicrystalline nature of the starch grains and transforming them into a homogeneous, amorphous thermoplastic. This process requires the presence of a plasticizer that lowers the processing temperature of the starch below its decomposition temperature. Plasticizer molecules

penetrate the starch granules, destroying the internal hydrogen bonds. Therefore, the molecular interactions between the starch chains weaken, leading to a decrease in glass transition temperature (T_g), thereby improving processability, plasticity, and flexibility. There are many substances used as native starch plasticizers including water, sugars, polyols, amides, and carboxylic acids [41] [42]. They are rich in polar groups (OH, COOH, and NH_2), which make them able to form strong hydrogen bonds between monomeric starch chains. Water seems to be the top choice, however, high volatility of H_2O molecules precludes its effective operation since starch transformation requires high temperature and shear forces. Glycerol is currently the most common, especially on a commercial scale, due to its high availability and relatively low price, as well as a well-described plasticization mechanism [43]. Zuo et. al [38] showed that the performance of TPS can be tailored to the desired application by selecting the appropriate plasticizer. They used a range of different polyalcohol's and amine plasticizers (i.e.: ethylene glycol, glycerol, sorbitol, formamide, urea) to obtain thermoplastic corn-based starch and to study the effect of the plasticizer type on its properties. The degree of TPS plasticization was assessed on the basic of the endothermic peak analysis and the calculated gelatinization enthalpy obtained from the DSC thermograms. They noticed that as the number of carbon atoms in the plasticizer structure increases, the plasticization effect gradually decreases. This is attributed to the easier penetration of smaller molecules between the starch chains and thus simpler disruption intermolecular hydrogen bonds. This trend was noticed for both types of plasticizers i.e. polyols and amine. As the sorbitol has the highest number of carbon atoms among the alcohol plasticizers, the plasticization effect was marked as the lowest. For the same reason, urea plasticizer showed a lower degree of plasticization than formamide. However, the analysis of XRD patterns revealed that the polyol-based TPS had a significantly higher crystallization degree than amine-based, which suggests a better plasticization effect of amine over polyol-based plasticizers. These results were reflected in the study of mechanical properties and water sorption test. It has been noticed that as the molecular weight of the TPS plasticizer increases, the toughness increases while the ductility decreases. Moreover, the tensile strength (T_{Sb}) values were significantly higher for polyol plasticizers (sorbitol-based TPS T_{Sb} ~ 6.6 MPa, glycol-based TPS T_{Sb} ~ 5.2 MPa) than for urea- (T_{Sb} ~ 4.4 MPa) and formamide-plasticized TPS (T_{Sb} ~ 3.4 MPa). The opposite tendency was noted for the value of elongation at break, which proves that with an

increase in the degree of TPS plasticization, the degree of crystallization decreases, internal hydrogen bonds weaken, and chains mobility increases which is reflected in a decrease in strength and an increase in TPS ductility. In turn, incubation in the water of TPS samples revealed that with the increase of the plasticization degree, the water absorption of the TPS noticeably increases; as the starch chains mobility increases and crystallization degree decreases, the absorption of the water molecules increases. The results indicate that the degree of plasticization has a direct influence on TPS features. Consequently, by selecting the type of plasticizer, the properties of the TPS can be adjusted to a certain extent.

Retrogradation, also called re-crystallization, is one of the biggest disadvantages of TPS. It is an aging process that progresses during storage. The starch plasticization process is aimed at transforming crystal- into amorphous-structure, while the amount of the amorphous phase can reach 90% [44]. However, the formed amorphous regions are highly metastable, which in turn causes self-reorganization of the starch chains and the formation of amylose, and amylopectin crystal clusters [45]. The hydrogen bonds are the main, and sometimes the only, interactions between plasticizer molecules and starch chains. Therefore, as a result of mechanical stress or the hygroscopicity of the plasticizer weak hydrogen bonds are destroyed, and thus plasticizer migration takes place which accelerates the retrogradation process. The retrogradation and migration of the plasticizer on the TPS surface strongly affect its functional properties (increase in brittleness or deterioration of product aesthetic). The most common ways to overcome these drawbacks are to select an appropriate plasticizer, their mixtures [46], and/or an addition of an extra modifier that will strengthen the interaction between starch chains [37].

Amine derivative plasticizers (urea, formamide, acetamide) have recently been very popular in starch plasticization due to their high availability, low price, and chemical properties. The highly polarized oxygen present in the amide group is responsible for the greater ability to form strong hydrogen bonds with starch than popular polyols (glycerol, sorbitol). This has a direct impact on limiting the process of TPS retrogradation and migration of the plasticizer molecules from TPS matrix [47]. The use of a mixture of plasticizers (urea and ethanolamine) additionally increased the effect by significantly reducing the aging process (rigidity, plasticizer migration) of TPS [48]. While the use of urea-formamide plasticizer enhanced water resistance and

improved thermal resistance compared to glycerol-plasticized TPS [49]. However, amine compounds are known to be toxic as they can degrade into cancerogenic compounds (nitramines, nitrosamines) [50]. Thus, their application is limited to non-food and non-medical products. But the limitation should also cover other applications since the toxic wastes can accumulate in surface water [51] or soil [52] increasing environmental pollution.

Polyol-plasticizers appear to be the most used in TPS molding. Glycerol, sorbitol, isosorbide, and their mixtures plasticize starch effectively, but relatively high hygroscopicity enhances retrogradation of the TPS products. And while glycerol is a substance that has no negative effects on the environment, is highly available, quite cheap, and is the most efficient in mobilizing the starch chains [53], it does not provide satisfactory results on its own. To overcome the moisture absorption of TPS, Ahmed et al. undertook research into the use of amphiphilic plasticizers such as isoleucine and butyric acid [54]. They found that although these plasticizers resulted in resistance toward moisture, the mechanical properties were unsatisfactory. Isoleucine-plasticized samples showed high crystallinity which made them to fragile. Butyric acid-TPS were amorphous, but the plasticization degree was too low, causing the mechanical properties to be well below expectations. In order to support the plasticizers, co-plastification with malic acid, a well-known starch crosslinking agent [55,56], was applied. This resulted in the improvement of ductile properties in both amphiphilic-plasticized TPS films as the carboxylic acids promote hydrogen bonding and mobilization of starch chains. The combination of hydrophilic and amphiphilic starch plasticizers can provide a favorable balance between ductility, strength, and susceptibility to the retrogradation of TPS, which seems to be a promising research trend.

Generally, the use of carboxylic acids with starch in the presence of a strong base leads to the esterification of glucose units and thus a grafting or crosslinking [57,58]. The acid-treated starch is enriched with so-called resistant starch (RS), which has recently gained interest in the functional food industry [59]. The application of RS mainly covers flavouring ingredients, stabilizers or thickeners, nevertheless it is not suitable as a processable/functional polymer.

Another novel and noteworthy idea for the effective plasticization of TPS is the use of Deep Eutectic Solvents (DES) [60]. DES are mixtures or alloys whose melting point is lower than the melting point of their individual components. DES structure includes the HBA (hydrogen bond acceptor) and HBD (hydrogen bond donor) units. Most often HBA are based on quaternary amines (polyatomic ions of the structure $-NR_4^+$) e.g. choline chloride (CC), while HBA are represented by substances rich in strong polar groups (amides, polyols, carboxylic acids, amines). The properties of DES are similar to ionic liquids, i.e. (low vapor pressure, high dissolution ability, and low melting point). They are marked as cheap and easy to prepare, non-toxic mixtures that can be obtained from compounds of natural origin [61]. Research undertaken by Zdanowicz et al. showed that along with a remarkable plasticizing effect, DES can act as a cross-linker of starch units, thus significantly improving the mechanical properties, reducing hygroscopicity and retrogradation of TPS [62,63]. However, the papers focus on material characterization, while the mechanism of TPS plasticization and interactions between starch molecules and DES is still unknown. Thus, the research in this content are highly desirable.

The discussed studies on starch plasticization process allowed to determine the desired properties of plasticizers. **Figure 2** presents the plasticizers' features that promote effective starch plasticization and lead to the formation of high-quality TPS.

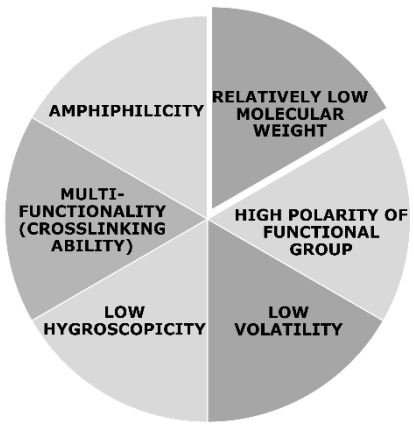

Figure 2 Properties of plasticizers favoring effective starch gelatinization.

Although the use of novel plasticizers or their mixtures generating strong molecular interactions with starch has resulted in an improvement in TPS performance, the

"plasticization itself" still seems insufficient to meet the requirements of polymers used in the plastics industry (high processing and thermal stability, moisture resistance, mechanical strength etc.). Therefore, along with the use of modern starch plasticizers, the disadvantages of TPS are overcome by mixing (blending) with other biopolymers, such as poly(hydroxybutyrate) (PHB) or polylactide (PLA) [64,65]. In this way, TPS gains sufficient processability, thermal stability, and resistance to aging without losing its biodegradability. This approach can also result in lower costs of biodegradable products such as PLA and PHB, which are relatively expensive biopolymers.

1.2.3. Polylactide (PLA)

Polylactide (PLA) is referred to as the material of the 21st century. It combines the properties of conventional synthetic thermoplastics with biodegradability, and natural origin (synthesized with monomers of plant origin, most often fermented starch from cassava, corn, and sugar cane). It is one of the most popular bioplastic with the second global production capacities (the 1st place is taken by polybutylene adipate terephthalate (PBAT), and the 3st place is for starch-based compositions) [66]. The packaging industry is the main market for PLA, but 3D printing has also become relevant because polylactide filaments are the most commonly used. Nowadays, PLA is obtained on an industrial scale *via* polycondensation of lactic acid monomers or the ring-opening polymerization (ROP) of cyclic lactides in an organometallic catalyst environment [67]. PLA belongs to the group of linear polyesters with mechanical strength, processability, and gas permeability of commercial synthetic polymers. PLA is a crystalline polymer with a relatively high melting point (from 130 to 210°C) depending on the chemistry and microstructure. It shows good resistance to oils and fats, and moreover PLA is biocompatible and bio-absorbable. It is a biodegradable material whose breakdown is most often induced by the hydrolysis of ester bonds (at a temperature of ~60°C) to lactic acid that is metabolized intracellularly or excreted in the urine/breath in the form of carbon dioxide and water [68].

The biodegradation process of polymers usually consists of two stages - disintegration and bio-assimilation, known as mineralization. The disintegration process proceeds in aerobic conditions under abiotic factors and consists of the initial fragmentation of the polymer chains. While the process of bio-assimilation is carried out by microorganisms, it involves the initial digestion and enzymatic breakdown of

hydrocarbon chains, followed by assimilation and metabolization into inorganic matter (mainly water, carbon dioxide, and biomass) [69]. Biodegradability refers to the decomposition of material into the inorganic matter under the influence of microorganisms, while the decomposition conditions and duration of the process are not strictly defined. The course and efficiency of the biodegradation process depends on three main factors: environmental conditions, type and amount of microorganisms, and material properties. Abiotic factors influence the intensity of the fragmentation process which may occur through thermal, oxidative and photo-degradation, or mechanical disintegration. Enzymes, as macromolecular substances, do not penetrate the interior of the material, but they cause the efficient breakdown of the fragmented polymer chains on its surface. For example, esterases are responsible for the hydrolysis of ester bonds, lipases catalyze their breakdown, the proteinase K, in turn, can hydrolyze the amorphous phase by cutting off lactic acid units from the ends of the chain, thus ensuring enzymatic decomposition of polymers such as polylactide (PLA). The properties of the material are also an important aspect determining the biodegradation process. Chemical structure (functional groups, type of bonds, branching, molecular weight, stereochemistry), surface (degree of roughness, hydrophilicity), and mechanical properties (flexibility, hardness), degree of crystallinity, are some of the many factors determining the susceptibility to fragmentation of the material and thus further mineralization processes. The properties of polymers favouring biodegradation include; low degree of crystallinity, low molecular weight, non-cross-linked structure, highly developed surface (roughness and porosity), the presence of functional groups susceptible to hydrolysis and/or oxidation, as well as the dimensions of the material itself (high surface to volume ratio) [70]. Considering the above factors, measurements of changes in mechanical properties, surface morphology, or the degree of disintegration can be an important indicator of material degradation, but not biodegradation. The basic test for assessing the mineralization of the material in all standards for biodegradation is the measurement of the released CO_2 (CH_4 in anaerobic conditions). The fact that CO_2 was released proves that the material took part in the natural carbon cycle, not only decomposing into biologically stable microscopic particles.

For many years, PLA has been successfully used in medicine in drug delivery, tissue engineering, wound healing, dermatological treatments, and dental procedures. It was also often used to manufacture personal protective equipment (PPE) much

needed by the medical sector during the ongoing Covid-19 pandemic [71]. The degradation of PLA *in vivo* is very slow, and complete resorption occurs after more than 5 years, and strongly depends on material crystallinity, morphology, and molecular weight [72]. However, along with the high price, PLA exhibits high brittleness, low flexibility, and low degradation rate in the natural environment [73]. Studies have shown that despite biodegradability, PLA waste contributes to increasing environmental pollution, as biodegradation under ambient conditions is unsatisfactory [74]. Effective PLA biodegradation primarily requires elevated temperature (above 55°C) along with proper moisture (>60%) and oxygen content, and microorganisms-rich (thermophilic bacteria conditions) [75]. Therefore, the process of PLA biodegradation in landfill sites, soil, or aquatic environments is highly impaired/disturbed. That is why PLA biodegradation is often carried out *via* composting. Composting, or organic recycling, is a natural method of utilization and waste management, which also involves the decomposition of organic matter by microorganisms (biodegradation), however, under strictly controlled conditions (appropriate temperature, oxygenation, humidity, etc.). It is predominantly aerobic process. The products of the process are heat, carbon dioxide, and ammonium absorbable for plants. Therefore, compostable materials must undergo the process of biodegradation within strictly defined time and conditions, and their decomposition products must not be harmful to the compost. Compostable plastics are a subgroup of biodegradable plastics [76]. The degradation products of PLA acidify the decomposition environment, which adversely affects microbial growth and inhibits further decomposition processes (mineralization). Some research indicate that effective PLA composting can be achieved when added in small amounts into compost (less than 30% of the total waste mixture) [77]. Despite plant origin and "bio" and "eco" label, PLA wastes in solid waste managements still need a care [78]. In many places, industrial composting is only adapted to green waste (without increased temperature), and the collection and separation of biodegradable/degradable plastics from plastic waste streams is difficult and often unprofitable. Also, recycling infrastructure is often not adapted to managing "eco-friendly" plastic waste, which ends up in the residual waste stream [79]. Therefore, in order to sustainably manage the waste of biodegradable polymers, one should look for materials with a compostability certificate (EN 13432, ASTM D6400), otherwise, the waste should be directed to material recycling. The latest research raises the alarm about the dangers

to human health resulting from exposure to plastic waste, which are present in all spheres of the globe [80–82]. More and more researchers raise the issue of the high risk that may be posed by the growing share of biodegradable or bio-based polymers, the inappropriate waste management of which leads to fast and uncontrolled contamination with harmful microplastic [80,83–85]. That is why it seems that the production of bio-plastics with an indefinite disposal route is an incorrect solution that can bring undesirable effects on the environment.

1.2.4. Epoxidized soybean oil (ESO) as TPS and PLA modifier

Epoxidized vegetable oils also seem to be a noteworthy group of plant-derived polymer modifiers. One of the most commonly epoxidized vegetable oils is soybean oil [86]. Oxidation of soybean oil, in the presence of peroxide or peracid and carboxylic acid (mainly acetic or formic acid), leads to the conversion of carbon-carbon double bonds into highly reactive epoxide groups [87]. Such triglyceride compound with oxirane moiety, carbonyl groups, and relatively long and elastic carbon chains seems effective in polymer plasticizing (**Figure 3**). Epoxidized soybean oil (ESO) is highly popular due to its low cost, non-toxicity, biodegradability, and abundance of the raw material from which it is made. It has proved effective in the chemical industry as a lubricant, reinforcing agent, polymer plasticizer and stabilizer. Its modifying properties have become the subject of research by many scientists, including as a biopolymers plasticizer and modifier.

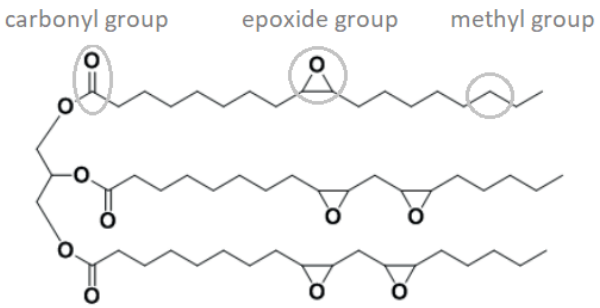

Figure 3 Scheme of chemical structure of epoxidized soybean oil (ESO).

Belhassen et. al [88] modified TPS (plasticized with glycerine) with the ESO in order to improve mechanical properties and enhance hydrophobicity. Based on FTIR spectra, it was found that there was a ring-opening condensation reaction between the reactive oxiranes of ESO and the hydroxyl groups (starch and glycerine origin).

Since ESO is a multifunctional compound with six oxirane rings, its integration into TPS chains resulted in a partly crosslinking, which led to the shift of the T_g to higher values and a huge increase in melt viscosity (over a 9-times drop in the value of MFR). This reflected in a significant increase in tensile strength (~1 to 3.5 MPa) and Young's modulus (~15 to 230 MPa), for unmodified TPS and TPS with 3%wt of ESO, respectively. However, as the ESO content increased, the elongation at break dropped, reaching 40% for the sample with 4%wt ESO. The water contact angle of the unmodified sample was 65° and reached 88° for the sample containing 4 wt% ESO. An increase in the hydrophobicity of the TPS-ESO was also demonstrated by extending the water absorption time relative to the unmodified TPS sample. Although the obtained samples had improved mechanical and hydrophobic properties, such high melt viscosity adversely affects the processing, and the resulted stiffness limits the use of the modified TPS. Accordingly, lower contents of ESO or changes of ESO to plasticizer ratio might help reduce the negative impact of the TPS crosslinking effect. A more common issue in the literature is the addition of ESO as a green plasticizer of PLA [89–91]. Since PLA is not a hydroxyl group-rich compound, the result of ESO incorporation is the opposite, as ESO does not efficiently covalently bind to the PLA chains. Only weak interaction between ESO and PLA are expected, i.e. hydrogen bonds between the epoxy group of ESO and the terminal -OH groups of PLA, eventually H-bonding between epoxy-ESO and ester-PLA groups. ESO can penetrate into PLA increasing chains mobility and thus T_g and flexibility. Consequently, a typical plasticizing effect is observed, which is mainly manifested by an increase in elongation at break and a decrease in the tensile strength of the relatively brittle PLA. Fathilah et. al [90] showed a significant reduction in T_g, complex viscosity and dynamic storage modulus already at 5% ESO content in PLA matrix. In turn, Xu et. al [91] noticed that for the ESO content of 3%, the PLA melt flow rate increases around 50% and the elongation at break more than 2 times. While the incorporation of 6% ESO resulted in a sharp increase in the melt and tensile strength. The further addition of ESO (up to 15%) led to a decrease in melt strength and a sharp increase in MFR. The authors [91] chose the optimal content of ESO 6%, which ensures sufficient performance balance of the PLA. The plasticizing effect of ESO was also found in study of Vijayarajan et. al [89], where during the impact test, a transition of PLA behaviour from brittle to ductile was noted along with increasing ESO content. In addition, they observed an increase in impact strength (over 5 times) of PLA with ESO content of

5-10%wt. Their further research revealed that the migration of ESO to the surface of PLA occurred within 30 days of storage at room temperature [92]. This unfavourable effect deteriorated the material properties to some extent. However, according to the results, the sufficient plasticizing effect of PLA was still maintained even after 90 days of storage, since all the material properties have not changed further. Even though the plasticizer migrated, unmodified PLA was still more brittle than PLA-ESO stored for over 90 days.

The enormous potential of ESO is probably due to the structure of its molecule, i.e. relatively high molecular weight, the content of reactive epoxy rings in the chain, and the presence of long carbon chains. It is also an amphiphilic compound of low volatility, hydrophobicity, and multi-functionality. Therefore, it meets most of the above-mentioned factors (**Figure 2**) favouring effective polymer plasticization. In addition, biodegradability and non-toxicity encourage further research on this renewable biopolymer plasticizer.

Proper plasticization of TPS and blending with PLA can result in a fully plant-based, easily biodegradable, and cost-effective composition of very promising properties. It is worth pointing out that at the time of starting doctoral studies, literature lacked reports on PLA/TPS blends modified with ESO.

1.3. Fundamentals of additive manufacturing (AM) technology

Additive manufacturing (AM) (commonly called 3D printing) represents a set of enabling technologies that are among the greatest achievements of the 4th Industrial Revolution [93]. Through the use of computer modeling tools, AM enables the combination of industrial-scale production and molding with manual precision. This feature stands out AM technologies from other manufacturing methods. American Society for Testing and Materials (ASTM) defines the principle of AM operation as the opposite of the subtractive production methods [94]. In this way, a 3D object is fabricated based on the provided digital model by controlled fusion of material. Although Charles Hull is considered "the father" of 3D printing, the beginnings of additive technologies date back to the '70s. In 1973, the first reports appeared, laying the foundations for the technology known today as Selective Laser Sintering (SLS). In his patent, Pierre A. L. Ciraud described the method of manufacturing products of

any geometry by fusing material in the form of a powder using an energy source [95]. Since then, successive generations of visionaries and inventors have presented new AM solutions, revolutionizing subsequent branches of industry. In **Figure 4**, I highlighted the events and inventors that, in my opinion, shaped the development of AM technology.

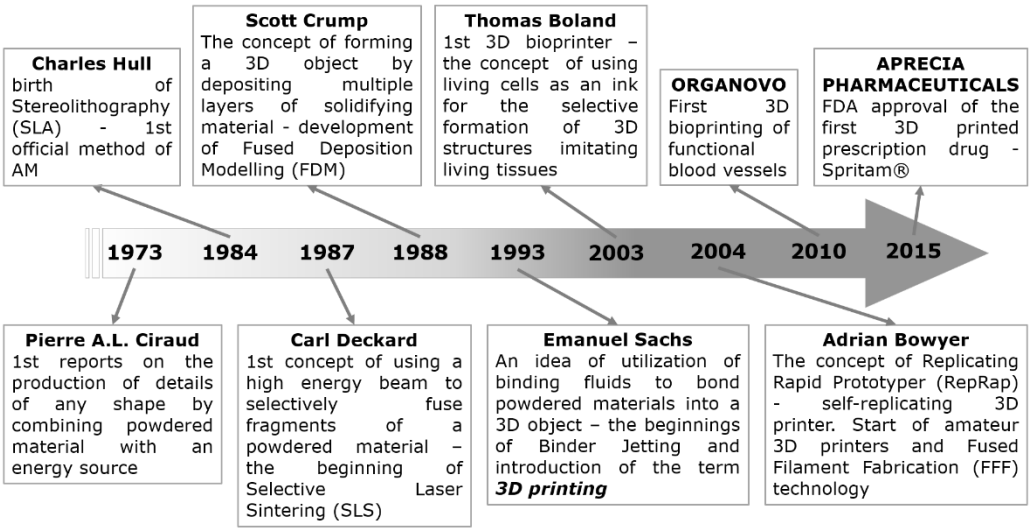

Figure 4 Milestones driving Additive Manufacturing technology.

In the beginning, 3D printing was considered a platform for prototyping – the formation of early-stage samples/models to test a concept or process. However, along with the improvement of AM machines and raw materials, 3D printers began produce functional products even on a large-scale [96]. Thus, AM has found application in many industries, including automotive, aerospace, architectural, educational, healthcare, artistic, military, or even nowadays medicine. The enormous interest in AM technologies is reflected in the global market size valued at 13.7 billion USD in 2020. Grand View Research market analysis report showed that 2.1 million units of 3D printers were purchased worldwide in 2020. Moreover, long-term forecasts predict continued revenue growth of AM expected to reach over 62 billion USD by 2028 [97]. These data show how important aspect of the global economy and technology is 3D printing. The biggest feature that stands out 3D printing beyond other forming techniques is accelerated time from the design to the final customized product. Moreover, some literature reports consider AM as a more sustainable and ecological technology compared to the conventional manufacturing methods [98–100]. The

most frequently mentioned ecological aspects of 3D printing include easy design optimization resulting in weight reduction and less material usage [101], the possibility of effective waste recycling [102–104], and a lower carbon footprint due to the lower energy consumption of the 3D printers [105,106]. Nevertheless, Liu et. al [107] notice that among positive features, there are also negative environmental aspects of 3D printing in particular about mass-scale production. It turns out that, with the increase in the scale of production, the average energy consumption per 3D printed part increases, while this value decreases in the case of molding with traditional methods [108–110]. In addition to the energy aspect, the negative impact of AM also includes relatively long production time (which increases energy consumption), possible non-recyclable photosensitive resin wastes [111], or hazardous agents emissions during the 3D printing process [112,113]. It is undeniable that additive technologies are a powerful tool for prototyping and the formation of personalized details. However, the overall environmental impact of AM depends on many factors, including the type of 3D printing technology and raw material used, production scale, or even printing parameters settings [114,115]. Although there are many positive aspects to 3D printing, according to the research conducted so far, it cannot be clearly stated that AM is a sustainable or more environmentally friendly technology than standard molding techniques [107,115–117]. It should also be noted that the term additive technologies covers a multitude of techniques differing in the type of material used, the method of the material fusion, and operational principles. This directly affects energy consumption, the possibility of effective material recycling, production time, or the machine and operation costs. Therefore it seems reasonable to not consider susceptibility and/or ecological aspects of AM in a general sense but in relation to a specific 3D printing technique and a scale of production.

Additive manufacturing contains several techniques differing in the way the material is fused, apparatus, and used material. A few of the most widespread AM technologies are Stereolithography (SLA), Selective Laser Sintering (SLS), Direct Metal Laser Sintering (DMLS), Fused Deposition Modeling (FDM)™/Fused Filament Fabrication (FFF), Binder jetting, PolyJet™/MultiJet™ and Electron Beam Melting (EBM). The first commercialized 3D printing apparatus was Stereolithography (SLA-1). Introduced in the late 80s by 3D Systems (the first 3D printing company) quickly gained great popularity as a novel machine that allows for the rapid production of 3D objects. The

basic principle of the process is layered curing of the liquid photosensitive resin with a precisely directed beam of UV light until a 3D object is formed. The resin solidifies as a result of the photopolymerization process, i.e. the polymerization of monomers in the presence of a photoinitiator, which decomposes under the influence of UV radiation, with the formation of active centers (free radicals, ions) initiating the polymerization reaction. Laser power needed to initiate the process typically does not exceed 1 W capacity [118]. In general, materials for SLA are based on epoxy and/or acrylate resins containing numerous functional groups that ensure the formation of a polymer network. These photo-curable systems contain liquid mixtures of monomer, polymer base, oligomers, and photo-initiators, and optionally, optical absorbers, stabilizers, and fillers to improve the printability of the resin. Thus, the SLA process results in a highly cross-linked product with an infusible and insoluble polymer network (thermoset). The standard SLA machines consist of a resin tank, a movable build platform, and a UV laser whose beam is controlled by an optical system with galvanometers. The current solutions proposed by the SLA technology giants (3D Systems, FormLabs) allow printing details with dimensions of the order of 20 μm, which makes SLA the technology of the highest resolution among all 3D printing techniques [119,120]. It would seem that SLA is a kind of hassle-free forming technology, but it has some limitations. The post-printed parts require additional treatment that covers support removal, cleaning (by rinsing in solvent to remove any uncured resign), post-curing in UV light to stabilize and enhance the mechanical and thermal properties of the printout, and finally surface finishing. Only after these treatments details obtained with SLA are characterized by a very smooth surface and one of the highest resolutions. Despite the many advantages of resin printouts, such as smooth (injection mold-like) surface, dimensional stability, and chemical resistance, hindered path of effective and sustainable recycling of the SLA wastes is a major limitation of this 3D printing technology.

SLS, DMLS, and EBM belong to, so-called powder bed fusion (PBF) 3D printing technology. These methods use a high-energy source, mainly laser or electron beam, to fuse powder particles layer-by-layer, thus forming a solid part. In the beginning, the build chamber of the 3D printer is filled with an inert gas, e.g. argon or nitrogen, to minimize the powder oxidation process. Then the build material is placed inside the build chamber while a recoater (coating system) disperses a thin layer of the powder on the top of the platform. The powder is then preheated to facilitate the subsequent

fusing of the material with the energy beam. Once the laser/electron beam finishes scanning and sintering the first layer, the platform lowers and the process repeats until the 3D object is completed. As the object fusion takes place inside the powder bed the unfused powder acts as a support structure hence process does not require the use of dedicated supports structures. After completing the process, the printout slowly cools down in the printer chamber, thus avoiding possible warping and thermal stresses. Finally, the printed object undergoes post-processing of cleaning the rest of the powder and eventually media tumbling or polishing. It should be noticed that PBF technologies do not generate a large amount of production waste. The powder used is recyclable (to some extent) and can be reused. After completion of the process, the unused powder is sequentially collected and then suitably screened and replenished with fresh material. The layer resolution of PBF technology is typically between 50 to 200 μm and is strictly dependent on the type and quality of the powder used (i.e. flowability, shape, and particle size distribution). SLS and DMLS technologies use lasers, typically single fiber lasers of 200 W to 1 KW capacity, to selectively fuse powder particles [121]. Unlike SLS, the DMLS technique uses only metallic and alloy materials such as aluminum, titanium, stainless steel, cobalt-chromium alloy, or nickel-chrome-iron superalloy. The SLS focuses on thermoplastic polymers, mainly polyamides (PA6, PA11, PA12), thermoplastic elastomers (TPE), polystyrene (PS), polypropylene (PP), and composites. Electron Beam Melting (EBM) is a distinctive type of PBF in which an electron beam produced by an electron gun (usually capacity of 3-6 kW) is used to melt and fuse powder particles. This process was developed at the Chalmers University of Technology in Sweden in 1993 and commercialized 4 years later by Arcam AB [122]. Since the EBM uses electrical charges, the material type is limited to electrically conductive ones. Otherwise, there would be no interaction between powder particles and electron beams. Consequently, titanium and chromium-cobalt alloys are the most common feedstocks in EBM technology. To avoid the scattering of the electron beam by air molecules, the EBM 3D printing process takes place under a vacuum ($\sim 10^{-2}$-10^{-3} Pa) [123]. A vacuumed build chamber also prevents the possible oxidation of reactive materials such as titanium alloys [124]. Mention should also be made of the powder preheating step. Namely, just before starting the EBM printing process, the first layer of the material is heated to above 500°C to initially bind the powder particles, minimizing its spreading during manufacturing. This approach also avoids the accumulation of residual stress and

provides better support for printed models. What distinguishes EBM from laser-based 3D printing (SLS, DMLS) is primarily the manufacturing speed. Controlling the energy beam using a magnetic field, unlike the mirror system used in laser-based 3D printers, allows significantly speeds up production. However, as the spot of the electron beam is wider than that of the laser, the precision and accuracy of the printing are noticeably lower.

The feature that distinguishes the described PBF technologies from other 3D printing techniques is the availability of industrial-scale printers ensuring large build volumes and production capacity. Solutions provided by PBF world leaders (EOS, 3D Systems, Farsoon – laser PBF and Arcam AB, Wayland Additive – electron beam PBF) allow for automated production of the end-products with dimensions exceeding 400 mm. Therefore, PBF technologies are the most widely used on an industrial scale, especially for automotive, aviation, medical, dental, and jewelry industries [125].

AM technologies that stand up one of the highest resolutions, accuracy, and precisions are material jetting (MJ) types (PJ/MJP). MJ is based on injecting printing process which uses photo-curable plastic resins and/or casting wax materials. A series of tiny nozzles on the print-head jet droplets of photoactive material in ultra-thin layers onto a build platform. Then each layer is immediately cured with UV light into a constantly growing solid part. The presence of several print-heads allows objects of different materials (or various colors) to be formed at once. This is especially important when printing structures that require supports. Stratasys and 3D Systems (3D printing tycoons) are mainly responsible for the development of MJ technologies. PolyJet™ and MultiJet™ use the same principle of material fusing. However, the main difference between the solutions is the type of support material used and the method of its removal from the finished product. MultiJet™, from 3D Systems, uses paraffin wax as a support material, which is removed by melting in an oven. Whereas, PolyJet™ utilizes soluble support consisting of polyethylene, propylene, and glycerin which is removed by dissolving in an organic solvent. The distinguishing feature of MJ technology is the possibility of multi-material printing at once, high layer resolution, and exceptionally smooth surface of the printouts. The unique features of MJ turned out to be extremely useful in the medical sector. The combination of precision, and multicolor printing allows replicating the complexity of the human body and the formation of patient-matched models useful in surgical planning or tools in medical

education and training [126–128]. 3D printing with ultra-high resolution and smooth surface is also in great demand in prototyping and tooling.

Binder jetting represents one of the fastest AM processes. Developed at the Massachusetts Institute of Technology in 1993 by Emanuel Sachs who introduces the term 3D printing (3DP). In this process liquid binder is selectively applied to a thin layer of powder (metallic, ceramic, or composite), layer by layer, thus forming a solid part. The selective dosing system that uses a cartridge allows for very fast printing. As with PBF systems, Binder Jetting does not require the use of support structures - the surrounding powder prevents destabilization of the printed structure. However, the usage of binding agents does not provide sufficient adhesion between powder particles. Accordingly, as-printed parts show relatively high porosity, surface roughness, and brittleness therefore post-processing steps are required [129]. These stages include curing, sintering and/or infiltration, and surface finishing. Once the binding agent is cured (heating in an oven ~200°C) the printout remains porous due to the superficial adhesion between the powder particles. Therefore further heat treatment is necessary to achieve the required density and thus mechanical strength. Typically, the printout is sinter in a furnace with a controlled atmosphere, where the binder burns out and fusion of the particles takes place. However, as the binder is removed, some voids remain and the print density may still be insufficient, thereby an infiltration process is proposed. It involves a densification process in which an infiltrating liquid such as epoxy resin, cyanoacrylate, magnesium sulfate, or molten alloys penetrates the porous structure by capillary action [130]. Each type of infiltrate has different processing procedures, including application method, temperature, and solidification time. Usually, the infiltrate is applied manually by dribbling, brushing, or immersing, whereas the hardening takes place at room temperature or during the sintering process in the furnace. The combination of both treatments (sintering and infiltration) allows to increase the printout density up to 95 % and thus significantly improves the mechanical properties [130]. However, the surface of binder jetted parts is still extremely rough (average roughness ~6 μm [131]), therefore an additional post-treatment step is also needed. The most common surface finishing processes are tumble and hand polishing, bead blasting, and plating [129]. Despite the many advantages of Binder Jetting, such as print speed, large build size, diversity of materials, or lack of supports, the as-printed parts cannot be considered as finished and must undergo a series of post-treatment stages. This generates additional time,

materials, and operating costs. Nevertheless, Binder Jetting has found application in many industries including, medicine, automotive, electronics with a particular interest in the rapid casting field (indirect 3D printing) [132]. Several works have been published showing a great potential of BJ molds and cores [133–135] where the seemingly disadvantages of this method (porosity and insufficient strength) ensure adequate gas evacuation or simple removal from the final part.

The first 3D printing device adapted to desktop platforms was Fused Deposition Modeling (FDM™). It is a technology that belongs to the group of material extrusion 3D printing. The technology invented in the late 80s by Scott Crump and commercialized by Stratasys revolutionized the 3D printing industry. This method consists in applying a plasticized polymer material in layers to the build platform. For this purpose, the FDM uses a numerically controlled miniature head equipped with a heated nozzle. The head is attached to the guides that enable the movement in a given direction. FDM printers most often use the material in the form of a filament – a thin fiber of a strictly defined diameter (1.75 or 2.85 cm) wound on a spool. The feed roller system transfers filament to the heat block where plasticization takes place. The material is then pushed/moved to the nozzle and layered on the build plate along the given path, creating a 3D object. In this process, the material does not fully melt (only plasticizes). As a result of the cooling of the plasticized material, successive layers are fused. Thus, the detail is only hardened/solidified by the adhesive forces and further molecular diffusion and entanglement of the polymer chains. As the basic feedstock for FDM are thermoplastic polymers, the variety of materials available is enormous and constantly growing. The most popular are conventional thermoplastics i.e. PLA, ABS, PA, PC, and TPU, but also composites and nanocomposites [136]. Such a variety of available filaments allows adjusting the properties of the printed detail to a given application, starting from everyday products to high-performance engineering details and medical devices. The advantages of this technology have been used since the early 90s, mainly for industry, but the real revolution in 3D printing came with the expiry of the FDM 3D printing patent in 2009. Since then people started manufacturing their own FDM-inspired 3D printers. Consequently, a new, low-cost, and open-source process called Fused Filament Fabrication (FFF) was born. However, anisotropic properties resulting from poor interlayer adhesion and insufficient surface finish of the printouts are the main drawbacks of material extrusion 3D printing [137]. This hinders the widespread use of FFF 3DP as a production tool, leaving it mainly for

prototype applications. Due to the method of layered deposition, the FFF-printouts obtained from either conventional polymers or engineering composites exhibit inferior properties to their counterparts molded with traditional processing such as injection, casting, or extrusion [138]. The weakest link of FFF printouts is the mechanical strength along the build direction (along the z-axis) which may decrease by up to 60% in relation to other directions [139]. The mechanical anisotropy, but also the relatively low accuracy and resolution, make the FFF printouts the most anisotropic among all 3D printing techniques. However, methods of improving inter-layer adhesion have been developed, which significantly improve the functional properties of printouts and make the FFF 3D printing technology still attractive and desirable. The enhancement of the interfacial bond can be improved by optimizing the printing parameters, post-processing, and/or chemical and physical modification of the polymer feedstock [140–142]. It was found that by changing the nozzle temperature towards higher values the polymer viscosity lowers, increasing chains mobility and thus facilitating the so-called neck growth through which the molecular diffusion and entanglement of the polymer chains occurs between successive layers [143]. However, this optimization requires additional control by examining the thermal stability of the given material, so that the resulting reduction in melt viscosity is not due to thermal degradation. Shish et. al [144] used cold plasma treatment (CLT) to improves interlayer bonding strength of the PLA printouts. They set up a low-energy laser system that processed the sample during the printing which resulted with significant increase in bonding strength (up to 100%), depending on the treatment time. Chemical modification of the FFF raw materials covers the chemical cross-linking that enhances interlayer bonding. One way is to blend the polymer raw material with specific radiation sensitizers and use ionizing radiation to generate the radicals that cross-link the polymer structure and significant strengthen the printout [145]. The simpler and less expensive way is the physical modification by preparation of polymer composite with organic/inorganic fillers and nanofillers such as talk, silica, calcium carbonate, montmorillonite, or carbon nanotubes. The additives decrease the melt viscosity and enhance the formation of interlayer bonding [146,147].

The accessibility, simplicity of operation, variety of materials, and affordability are the main pros of extrusion-based 3D printing that made this technology widely recognized and used by consumers, industry, and academia. However, further research on 3D printing in FFF technology is needed both in the context of reducing the anisotropy of

printouts and increasing the resolution, but also in developing new raw materials (filaments) with advanced and specialized properties.

A summarized description of the discussed AM technologies is presented in **Table 1**.

Table 1 Review of selected additive manufacturing technologies.

AM technology	Material fusion principle	Material type	Machine, material, and operational costs	Resolution (approx.)
Stereolithography (SLA)	selective curing of photosensitive resin with UV-laser	UV-curable resin	medium	< 25 µm
Selective Laser Sintering (SLS)	a high-power laser melt and fuse the material in the form of a micro powder	thermoplastic polymer powder	high	< 30 µm
Direct Metal Laser Sintering (DMLS)		metallic powder	high	< 30 µm
Fused Deposition Modeling (FDM)™ / Fused Filament Fabrication (FFF)	plasticization of thermoplastic polymer and layered deposition on the build platform via a heated nozzle	thermoplastic polymer filament	low	< 0.4 mm
Binder Jetting	selective deposition of a liquid binding agent onto a thin layer of powder material	powder particles (metal, ceramic, sand, polymer, and composite)	high	< 0.3 mm
PolyJet (PJ)™/MultiJet (MJP)™	jetting of photosensitive resin droplets onto a movable platform and solidifying with a UV light	UV-curable resin	medium	< 20 µm
Electron Beam Melting (EBM)	selective fusion of a powder metal using an electron beam	metallic powder	very high	< 0.2 mm

The 3D printing process is a complex operation that begins with the preparation of the digital model and ends at the stage of finishing the obtained 3D object. It includes five main stages, the correct execution of which guarantees a positive result of the process (**Figure 5**).

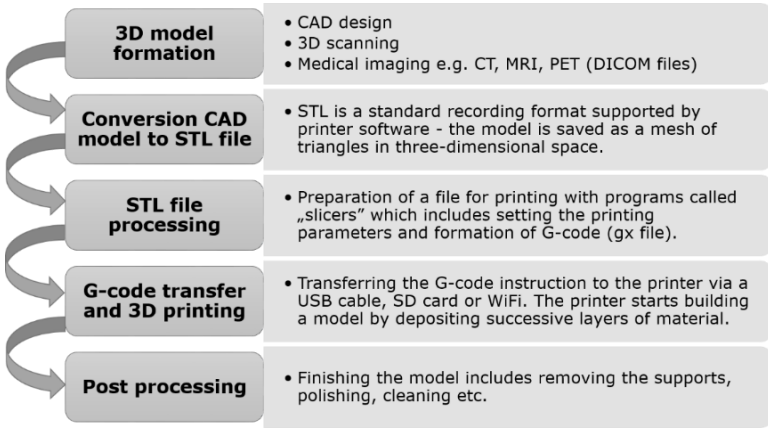

Figure 5 General stages of the 3D printing process.

The desired 3D model is most often created using computer-aided design (CAD) tools, however, 3D scanning or medical imaging is increasingly being used. The created model should be saved in the STL format, which is then prepared for 3D printing in programs called *slicers*. A slicer converts the STL file into specific instructions (such as G-code) that the 3D printer traces to create a 3D object. The code contains a set of settings and printing parameters including the layout of the printout on the working table, shape, and type of support structures. The processed file is sent to the printer and the 3D printing process begins. The last stage is post-processing, which varies depending on the 3D printing technique and material, and most often includes the removal of supports, polishing, cleaning, and annealing. **Figure 6** shows the process of preparing a file for 3D printing, using the example of forming a personalized spine structure directly from the computer tomography (CT) image. The 3D Slicer platform enables the processing and conversion of medical imaging files to 3D models, which are then optimized and cut in programs such as Meshixer or SLic3r. In this way, it is possible to obtain customized anatomical structures directly from the patient's imaging. It is worth noting that the programs presented here are open-source and additionally supported by databases with a huge community that significantly facilitates the process of preparing such complex medical structures.

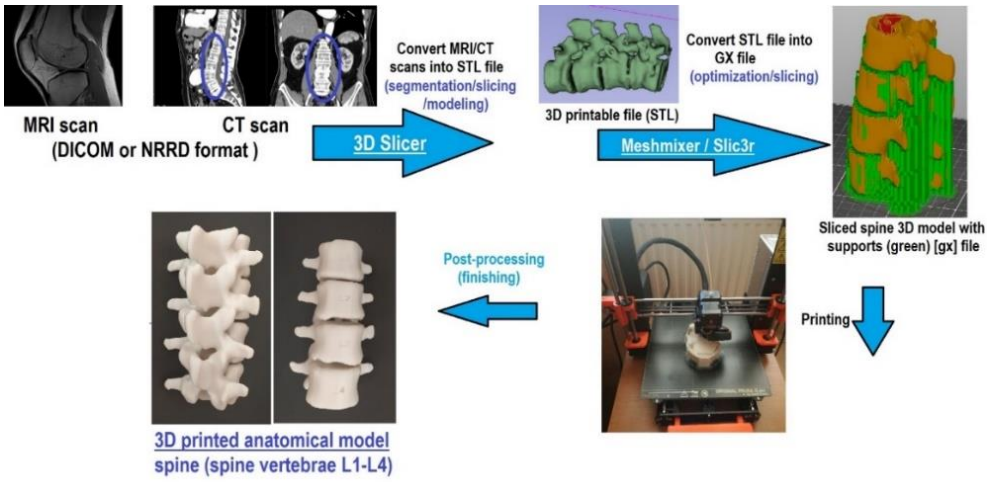

Figure 6 Converting a radiographic image (CT) to 3D printing of the spine anatomical model.

1.3.1. Additive manufacturing (AM) in modern medicine

The use of additive manufacturing in medicine is no longer a future prospect. Innovative solutions combining 3D printing technologies, modern materials, medical imaging, or 3D scanning change the current approach to forming medical devices, ensuring greater personalization, precision, and affordability. One of the greatest advantages of 3DP in medicine is the direct link between medical imaging and product development. This significantly shortens the distance from design to product, and thus greater availability and facilitates the work of medics. Medical applications for 3DP can be classified into several broad categories, including medical products and equipment; implants and prosthetics; anatomical models for surgical planning and education; tissue engineering and organs; personalized drug delivery systems [148,149]. Depending on the application, these products are formed using various 3D printing methods and materials. A technology of particular importance in medicine is bioprinting, however, this work does not deal with this issue because it differs too much from the scope of the dissertation.

Bertol et. al [150] used a direct metal laser sintering (DMLS) 3DP with titanium alloy powder (Ti-6Al-4V) to prepare a customized preoperative implant (mandible prosthesis) based on the patient's CT scan. In turn, Hao et. al [151] demonstrated the potential of selective laser sintering (SLS) in 3D printing of bioactive implants. They used composite powder of high-density polyethylene enriched with

hydroxyapatite (HA-HDPE) to 3D print of block specimens. The study showed that the processing parameters (laser power and scanning speed) have a significant effect on the degree of particle fusion and porosity of the sample. Moreover, it was found that the SLS process allows the exposure of HA particles to the sample surface, thereby enhancing bioactive properties. Similar observations were noticed in study of the Kasper et. al [152]. They used Stereolithography (SLA) to produce patient-matched bone grafting implant of composite containing poly(trimethylene carbonate) (PTMC) enriched with high amounts of osteoconductive β-tricalcium phosphate (β-TCP). SEM showed that the surface of formed porous scaffolds was rich in bioactive agents (PTMC) and had microscale roughness. Such morphology is desirable as it facilitates the attachment of osteogenic cells and surface bioactivity is intensified. Therefore, it can be assumed that along with SLS, SLA 3D printing promotes the accumulation of composite filler on the surface of the printouts, therefore, in this case, increasing the printout's bioactivity [153]. A technology of particular importance in the dental industry is power bed fusion PBF (direct metal laser sintering DMLS or selective laser melting SLM). Computer-aided metal or alloy powder sintering allows for the formation of structures with the desired surface morphology and controlled functionally graded architecture. Many studies have shown that implant surfaces with a suitably rough surface, as well as gradually changed porosity, support the process of osseointegration, i.e. a key and multi-stage process that permanently connects and stabilizes the dental implant with the patient's bone [154–156]. The nature of DMLS/SLM printouts is a rough and porous surface hence it is possible to obtain structures of biomaterials, such as titanium, with an inherently porous structure meeting the requirements of bioactive dental implants. Mullen et. al presented novel titanium, bone in-growth constructs with a morphology similar to that of natural human bone [157]. The use of SLM 3D printing allowed obtaining structures with gradually changing roughness and porosity and a high level of pores interconnectivity and open-pored type morphology, so desired for effective bone ingrowth and vascularization of the bone implant. Already in the years 2012-2014, the first results of clinical trials on powder-based 3D printed titanium implants were presented, and the results confirm the high potential of such structures in personalized prosthetics [158–160]. Further research was devoted to improving the design of implants to better adapt to patients' anatomy and enhance osseointegration [161,162], and modifying powder materials to increase bioactivity [163] hereby nowadays custom-

matched 3D printed dental implants are common practice [164]. Pioneering research on the use of FDM/FFF 3D printing for tissue engineering belongs to professor Hutmacher. Among others, he described the method of obtaining novel bioresorbable PCL-based porous scaffolds with diverse architecture [165] as well as starch-based structures with micro- and macro porosity [166]. Initial mechanical and biological studies showed a significant potential of the obtained structures as scaffolds in soft tissue engineering.

Along with the growing amount of research on additive technologies for medical applications, more and more commercial solutions are noticed. Biotech companies such as Organovo, Triastek, or Fasotec supply ready-made solutions for medical products obtained using 3D printing technologies. Examples of such products with a short description are presented in **Table 2.** In addition to very popular solutions of personalized implants or preoperative planning systems, 3D printed pharmaceuticals are gaining importance in the market. Since the first FDA-approved 3D-printed drug of Spritam®, the articles describing the novel solutions in 3D printing pharmaceuticals have increased rapidly [167]. Such interest in this molding method is reflected in numbers, the valued 3D-printed pharmaceuticals market is over $159 million in 2020, and forecasts show an increase to over $285 million by 2025 [168]. In 2021, Triastek, Chinese pharmaceutical giant, has granted approval to clinical trials of T19 – 3D printed drug designed for the treatment of rheumatoid arthritis. Triastek uses Melt Extrusion Deposition (MED®) system, a platform combining reactive extrusion of a medicine with layered deposition. Developed tablets are characterized by a complex internal architecture which provides high control of drug dosing. The systems being developed may revolutionize the pharmaceuticals market, leading to the personalization of drugs.

Table 2 Examples of biotech companies providing products formed with 3D printing.

Company	3DP technology	Product	Type of material
Organovo	Bioprinting	Functional human tissues/organs, e.g. vascular tubular grafts	1) filling - vascular cell types; smooth muscle cells (SMCs) and fibroblasts 2) scaffold - agarose rods
K2M	Selective laser sintering (SLS) (Lamellar 3D Titanium Technology®)	Spinal implants	Titanium powders

Company	3DP technology	Product	Type of material
Apercia Pharmaceuticals	Powder bed and inkjet 3DP (PBIH) (ZipDose® Technology)	Spritam® antiepileptic drug (highly porous pill)	1) Powdered pharmaceutical med (levetiracetam) 2) Binding fluid* * - more data is not available
Triastek	Melt Extrusion Deposition® (MED)	T19® drug for rheumatoid arthritis (porous pill with customized geometry)	The mixture of active pharmaceutical ingredient (API) with resorbable polymer matrix* * - more data is not available
Regenovo	Bioprinting / 3DP	Tissue scaffolds, anatomical models, drug discovery models, metabolic syndrome models	- Bone tissue materials: hydroxyapatite, tricalcium phosphate, polyetherketoneketone - Soft tissue scaffolds; Gelatin, Alginate, Fibrin, Collagen, Agar, Chitosan. - Controlled release drug systems: PLLA, PLGA, PCL, Sodium Starch Glycolate
Cognionics	Fused deposition modeling FDM	Dry EEG electrodes	No data available
L'Oreal – Organovo (*in progress)	Bioprinting	Human skin tissue	Embryonic stem cells, adipose-derived stem cells, bone marrow-derived mesenchymal stem cells
Fasotec (Fasolab)	MultiJet printing (MJP)	Surgical training systems Tissue and organs models	Silicone, Polyurethane
Stryker	Direct metal laser sintering (DMLS)	Permanent implants	Hydroxyapatite, cobalt chrome alloy, titanium, high impact polyethylene,

Progress in medicine through the use of modern technologies is undeniably visible and extremely necessary, however, certain aspects raise some concerns. The proposed solutions in the field of 3D printed preoperative planning systems facilitate the surgeons preparation and course of surgery. They are a great achievement that increases the accuracy and success of the operation and also makes surgery planning less complicated, as the 3D printed structures are customized and patient-matched. Nevertheless, this makes them disposable products that can, at best, be destined for

the educational purposes of medical students. Considering the enormous demand for such systems, as well as the fact that more and more medical centres are equipped with 3D printers and the necessary software, a huge amount of such waste can be expected to be generated. The 3D printing system of great importance in this regard is FDM/FFF due to its relative ease of use, and low operating and material costs. The most commonly used material in FDM/FFF 3D printing is polylactide (PLA), which is characterized by a high quality-to-price ratio, as well as being easy to print [169]. As PLA is a biodegradable polymer of plant origin, it has the label of a pro-ecological product, nevertheless, its eco-properties were questioned in an earlier chapter. Therefore, I believe that at the moment attention should be paid to developing novel solutions for FDM/FFF 3DP surgical training systems and/or artificial organs as teaching aids, which will correspond to the printability of PLA but will be a more responsible solution in terms of sustainability.

1.4. 3D printable filaments and their production

In this work and in the field of 3D printing, the term "filament" defines the raw material for 3D printing in FDM™ and FFF technology. It is a fiber with a well-defined and constant diameter, made of a thermoplastic polymer or a composite. Standard filament diameters available on the market are 1.75 and 2.85 mm, respectively. Generally, filament formation is performed *via* hot-melt extrusion (HME) of the thermoplastic-based pellets [170]. The process can be carried out discontinuously and continuously depending on the complexity of the production line. A conventional extruder equipped with an appropriate forming nozzle and external extrudate cooling is sufficient to form a filament in a discontinuous manner. In such a system, the extrudate diameter is controlled manually and the filament is collected in the form of relatively short wires. Due to the simplicity of operation, such systems work well in academia during preliminary research on new filaments. Professional filament production lines are more complex and allow receiving filament continuously. They are provided by companies (ThermoFisher Scientific, Filabot, Conair, Boco Pardubice, Zamak Mercator) or independently constructed. The main production line elements include extruder with granulate dryer, forming head, calibrators, cooling tubs, drier, diameter sensor, pulling system, compensator and winder. Working with such a system requires adjusting a series of settings including extrusion and operational parameters. The process of forming a filament for 3D printing can be divided into

three main stages, i.e. preparation of polymer granules, shaping the filament, and winding on a spool. Depending on the needs, the preparation of the granulate includes the step of cleaning and drying the polymer granulate or mixing with selected fillers and modifiers in order to contribute specific properties. The most commonly used modifiers are agents improving the extruding and printability of filaments, i.e. lubricants (microcrystalline cellulose, magnesium stearate [171]) and plasticizers (mineral and vegetable oils, PEG, glycerol, esters of citric acid [172,173]) as well as compatibilizers (anhydrides, organofunctional silanes [174]) increasing the adhesion between the filler and the matrix. Additives in the form of fillers, colorants and light stabilizers are also common. Once the polymer feedstock is properly prepared the drying step is required since the polymer granules are rather hygroscopic. Moist granulate causes interference during extrusion and can lead to degradation of the material and pressure fluctuations in the extruder barrel which in turn destabilize the extrudate. Granules are typically dried with airflow or under vacuum at 60-80°C for a few hours depending on the type of polymer (moisture level should not exceed 0.10%). The dried granules are fed into an extruder to form the filament with the desired diameter. In the extrusion process, the granulate is plasticized and combined with specific additives as a result of heat, pressure, and shear forces, and then transported in the form of a wire to the calibration zone that includes cooling tubs and diameter calibrators. The cooling process responds for the final shape and roundness of the extruded fiber. In case of insufficient heat dissipation, distortion of the filament cross-section can occur. The wire is most often cooled with water with a gradually changing temperature (hot on in, cold on out). This prevents the formation of thermal stress and possible voids defects that arise when the plastic cools too quickly. Moreover, the right temperature settings ensure the proper shape of the filament and prevent the over-shaped phenomenon. Properly selected diameters of calibrators located at the exit of the bathtubs along with adjusted pulling velocity determine the final diameter of the filament which is controlled by the laser diameter sensor. The faster pulling velocity, the smaller the filament diameter. Before entering the winding system, the filament is dried intensively, usually with a stream of air. Finally, the filament is attached to the spool and wound around.

The crucial parameters of the filament-formation process can be divided into (i) extrusion parameters and (ii) operational setting.

(i) Adjustable parameters include temperature, extrusion velocity, and dosing rate. Parameters to be controlled are the melt temperature and the head pressure. The temperature profile is selected based on the thermal and rheological characteristics of a given granulate. The parameter of the mass flow rate (MFR), which determines the flowability of a thermoplastic at a given temperature and under a given load, is very informative in this regard. Proper temperature profile ensures adequate plasticization and affects, besides melt temperature, the head pressure. Constant head pressure is one of the key determinants of a stable melt flow, so important when a profile with a constant diameter is extruded.

(ii) Essential operational settings cover optimization of pellets drying (time and temperature), calibration zones (calibrators diameter, tubs length, type and temperature of the coolant), and pulling velocity.

The literature dealing with the process of formation medical-grade filaments has increased [175–177], however, at the time of starting doctoral research, only two reports covering discontinuous manner were found. Xiao et. al [178] described the procedure of molding 3D-printable TPU filament as well as examined the 3D printing settings leading to the formation of a high-quality TPU printouts. For this purpose, they used commercial pellets of medical-grade aliphatic poly(ether)urethane (Tecoflex LM-95A - Lubrizol). The filament of 1.75 mm diameter was formed with a single-screw extruder with a screw diameter of 20 mm, an L/D ratio of 24, and a nozzle diameter of 1.3 mm in a discontinuous manner. The optimized parameters included pellet drying, temperature, and extrusion speed. Processing temperatures were selected based on the melting peak of the polymer assessed *via* DSC and were ~20°C higher than the T_g. However, the publication rather focuses on the assessment of the impact of printing parameters (print temperature and raster angle) on the mechanical properties of the printouts than on the filament-formation process. Melocchi et. al showed different approach as they prepared specialized filament with active pharmaceutical ingredients [179]. The pharmaceutical-grade filament was based on hydroxypropyl cellulose modified with various plasticizers (PEG, PEO) and enriched with drugs (triethyl citrate, acetaminophen, or furosemide). Researchers paid attention to drying the raw materials (24h, 40°C), and extrusion was carried out using a twin-screw extruder (with customized nozzle of 1.8 diameter) to ensure the proper blending of the ingredients. Both the shaping of the filament and the diameter

control were performed manually in a discontinuously manner. It was also noted that the works cited did not investigated whether the forming or 3D printing processes affect the structural, thermal or biocompatibility of the resulted filaments and printouts.

The market of filaments is still growing, and more and more different solutions are presented. The retail market focuses primarily on solutions that provide new visual and aesthetic effects, rather than specialized and functional. Due to the very favourable price-quality ratio and ease of printing, users of FDM/FFF 3D printers most often choose polylactide (PLA) and acrylonitrile butadiene styrene (ABS) filaments. Therefore, they are most widely used and known filaments [169]. Companies compete in presenting new solutions based on a polymer matrix (most common PLA) with the addition of a filler in the form of powder, nanoparticles, or fibers. These include filaments that glow in the dark (Glowfill® from colorFabb), conductive (conductive PLA from Proto-pasta), ferromagnetic (Ferro-Magnetic PLA® from Graphene 3D lab), or that have a texture resembling wood (Laywoo-D3 from Lay Filaments) or metal (Copperfill® from Prusa Research) (details in **Table 3**). And although these materials show interesting properties, their range is limited by the properties of the matrix which is at least 60% PLA. The filaments are limited to inefficient phosphorescence, low-voltage conductivity (strongly dependent on the print plane) or magnet attraction. Nevertheless, they are a great alternative to hobby projects due to relatively easy printing and affordability.

Table 3 Overview of popular filaments for 3D printing in FDM/FFF technology for hobby use.

Trade name (company)	Matrix type	Filler type	Retail price
Conductive PLA (Proto-pasta)	PLA	conductive carbon black	$50 USD (500 g spool)
Glowfill® (colorFabb)	PLA/PHA	phosphorescent pigment	$35 USD (750 g spool)
Ferro-Magnetic PLA® (Graphene 3D lab)	PLA	iron powder	$75 USD (350 g spool)
Timberfill® (Fillamentum)	PLA	wood fibers	$45 USD (750 g spool)

1.4.1. Medical-grade filaments – market and literature review

There is a deficiency of certified medical filaments on the market, and despite the increasing amount of research devoted to their production and optimization, solutions are still lacking. One of the few companies providing ready-made solutions in the field of medical FDM/FFF filaments is Poly-Med (USA), which specializes in bioresorbable polymers and provides a series of filaments such as Lactoprene® (PLA-based), Caproprene® (PCL-based), Max-Prene® (PGLA-based) and Dioxaprene® (PDO-based). Filaments are biocompatible with varying degrees of bio-resorption. Mohseni et. al performed an independent assessment of these filaments and showed that they are suitable for 3DP porous structures with diverse architectures and of different susceptibility to accelerated degradation [180]. Despite the fact that the performed studies include only mechanical- and chemical characterization, their potential in tissue engineering can be assumed. In 2018, the Taiwan biotech company Advance Biomedical Technology presented one of the first biodegradable and medical-grade filament for extrusion-based 3D printing - MedFila® (PCL-based). Currently, the company has expanded its offer with a series of PLGA-based filaments and ceramic composites. The application of those filaments covers 3D printing of bone grafting substitutes, drug delivery systems, dental fillers, and plastic surgery items. In the same year, Solvay introduced new 3D printable medical-grade filaments, KetaSpire® (polyetheretherketone PEEK) and Radel® (polyphenylsulfone PPSU), respectively. The presented filaments are characterized with superior toughness, impact strength, and chemical resistance as well as meet the ISO 10993 requirements of biomaterials for limited contact with body fluids and tissues. Another solution covers guidel!ne®, PETG (glycol-modified polyethylene terephthalate) filament provided by Tulman 3D (USA). It is a very tough material with a tensile strength of over 47 MPa and a Modulus of 1.95 GPa. The filament is made of medical raw materials, but the product itself is not certified.

It should be noted that at the time of starting doctoral studies, there were no commercially available medical-grade TPU filaments for 3D printing in FDM/FFF technology, and the number of literature reports was also limited (**Table 4**). Moreover, no commercially available medical-grade TPU filament has been found to date.

In 2016 Jung et. al presented a novel polyurethane tracheal scaffold with micro-scale architecture formed *via* self-developed 3D printing system based on syringe with TPU solution (40% solution of Tecoflex® in chloroform) [181]. The obtained implant had satisfactory mechanical properties (Young modulus of 2.8 MPa, tensile strength of 3.2 MPa, elongation at break of 725%) that were maintained stable up to 16 weeks after implantation into the anterior tracheal defect of the rabbit. In addition, bronchoscopy showed that the implanted tracheal scaffolds were permeable for a period of 16 weeks, while the histologic results revealed ingrowth of connective tissue into the scaffolds within 4 weeks after implant. The results showed very promising mechanical and biological properties of the 3D printed scaffolds due to the unique properties of thermoplastic polyurethanes. However, this process requires the preparation of the raw material in the form of a polymer solution. The need to use large amounts of organic solvents (including chloroform) does not match the trends of green chemistry therefore, in my opinion, the process should be refined.

Table 4 Literature reports on TPU systems for extrusion-based 3D printing.

Material	3DP technology	Product / application	Biological test	Image	Ref.
Tecoflex ® (TPU) medical grade - aliphatic polyether-based TPU	invented 3D printing system based on a printing syringe with a 0.2 mm nozzle that prints with TPU solution (40% in chloroform).	tracheal scaffold / patch-type prosthesis	*in vivo / implanted into the tracheal defect of rabbits*	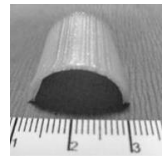	[181]
Water dispersion of TPU diols – PLA,PEBA, Diisoyanate – IPID, Chain extenders – DMPA/EDA + PEO as a viscosity enhancer	low-temperature fused deposition manufacturing (LFDM)	scaffolds for cartilage regeneration	*in vitro / rat chondrocyte cell line*	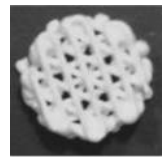	[182]
Water dispersion of TPU diols – PLA, PEBA, Diisoyanate – IPID, Chain extenders – DMPA/EDA + HAc as a viscosity enhancer	low-temperature fused deposition manufacturing (LFDM)	scaffolds for cartilage regeneration	*in vitro / human MSCs, in vivo / implanted into the chondral defects of rabbit knees*	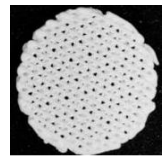	[183]

Material	3DP technology	Product / application	Biological test	Image	Ref.
TPU/PLA/GO nanocomposite – enhanced with graphene oxide (GO), TPU – Pearlthane® (PCL-based)	FFF	tissue engineering scaffolds	*in vitro / NIH3T3 cells*		[184]
TPU 90 (diol-polyether, diisocyanate - MDI, chain extender - BDO) TPU 80 (diol – PCL, diisocyanate – MDI, chain extender – BDO)	FFF	tracheal tissue / cartilaginous rings	*in vitro / HDF, BEC cells*	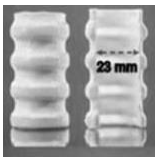	[185]

Hung et. al developed a novel method of 3D printing with low-temperature fused deposition modelling (LFDM) in which the use of toxic polymeric solvents is avoided and the printing ink is obtained in an aqueous-based process in the form of water dispersion of nanoparticles (NPs). The presented systems were based on the waterborne biodegradable aliphatic poly(ester)urethane NPs and modified with polyethylene oxide (PEO) [182] and hyaluronic acid (HAc) with mesenchymal stem cells (MSCs) growth factor (TGFβ3) and/or small molecule drug of cyclohexanecarboxamide (Y27632) [183], respectively. The printed TPU/PEO porous structures showed huge potential as cartilage tissue scaffolds due to the satisfactory seeding efficiency and proliferation of chondrocytes. In turn, TPU/HAc/Y or TG bioactive scaffolds showed induction of the chondrogenic differentiation of MSCs and the production of a matrix for cartilage repair, showing the potential as a unique tissue engineering platform. Despite the many advantages of the developed low-temperature printing system with aqueous solutions, this system requires the ongoing preparation of inks, the synthesis of which is relatively challenging, and the operation of the 3D printer itself requires specialized knowledge. Another interesting and relatively undemanding solution regarding 3D printable polyurethane systems covers the nanocomposite filament of TPU/PLA enhanced with graphene oxide (GO) presented by Chen et. al in 2017 [184]. The developed filament is suitable for printing on a conventional FDM/FFF printer. The combination of TPU and PLA resulted in a biocompatible system with sufficient elasticity and toughness, while the addition of GO increased thermal stability and mechanical properties. It has also been proven

that the 3D printed TPU/PLA/GO porous scaffolds had good biocompatibility towards NIH3T3 cells. Such a system allows fabricating elastic and biocompatible scaffolds with desired architecture in a relatively easy and cost-effective manner. Although the described filament was self-prepared, the main feedstock used was commercial (TPU pellets - Pearlthane®, PLA pellets – Nature Works). Tsai et. al presented a concept tailored to desired needs and compatible with conventional FDM/FFF 3D printers [185]. Namely, they synthesized aromatic poly(ether-ester)urethane and formed 3D printable filament to further produce with FDM a series of patient-specific with DICOM data of a CT scan cartilaginous rings for tracheal tissue engineering purposes. The resulted elastic tissue substitutes showed biomimetic properties with satisfactory mechanical strength as well as were prone to biofunctionalization thus promoting effective tissue regeneration.

The high versatility and outstanding biological and mechanical properties of TPUs encourage their use as specialized medical materials in additive technologies. The development of new TPU filaments for low-budget FDM/FFF printers may lead to the popularization of the technology in advanced medical applications, thus reducing operating costs and increasing the availability of customized and/or patient-matched products.

It should be noted that none of the above-described works analyses the process and apparatus needed to form medical-grade filament for 3D printing.

The revision of the latest literature reports on bio-based filaments for 3D printing was presented in the PAPER 6, therefore the author decided not to duplicate these issues.

1.5. Notes to the literature review and motivation of doctoral dissertation

The market and literature revision showed a deficiency of medical-grade TPU filaments for FDM/FFF 3DP. Moreover, there was a lack of research on the formation of 3D printable filaments and the stability of filaments under 3D printing conditions. In addition, the arising plastic pollution problems and thus increased society's environmental awareness has led to the huge demand for more sustainable polymeric materials with less negative environmental impact. Since the biodegradability of PLA filaments remains certain concerns, the research on the sustainable bio-filaments with

enhanced biodegradability and adequate printability for extrusion-based 3D printing are also desired.

It should also be noted that, despite years of research on materials for 3D printing in FFF/FDM technology, some issues are still unresolved. There is no clear statement on whether the 3D printing process affects pristine/original material properties (in particular regarding medical-grade materials). Also, there is a lack of literature reports that would show how to effectively form medical-grade filaments for 3D printing using extrusion in a continuous manner.

Therefore, the main focus of the doctoral dissertation was new medical filaments for 3D FDM/FFF printing. But also, attempts were made to resolve the mentioned doubts. Consequently, in the presented doctoral dissertation, I undertook research on the synthesis, formation, and detailed characterization of new medical-grade filaments for extrusion-based 3D printers (FDM™/FFF). As part of my research, I developed and characterized two types of filaments, i.e. flexible biocompatible and compostable plant-based. Furthermore, I extended my work with an analysis of the filament-forming process on a laboratory and technical scale. Subsequently, I studied the stability of the filaments (both, formed and commercial) through analysis of selected properties before and after the 3D printing process, thus complementing the current state of knowledge. Next, I designed various types of porous 3D structures and prepared personalized anatomical models directly from a CT scan. The obtained digital models were then 3D printed using, among others, developed filaments. Finally, the selected printouts were subjected to a series of preliminary biological tests (*in vitro*) to assess their potential in medical application.

1.6. References

1. Lamba, N.M.K.; Woodhouse, K.A.; Cooper, S.L.; Lelah, M.D. *Polyurethanes in Biomedical Applications*; CRC press: Washington, DC, 1998; ISBN 9780849345173.
2. Ramezani, M.; Monroe, M.B.B. Biostable Segmented Thermoplastic Polyurethane Shape Memory Polymers for Smart Biomedical Applications. *ACS Appl. Polym. Mater.* **2022**, *4*, 1956–1965, doi:10.1021/acsapm.1c01808.
3. Xu, L.C.; Siedlecki, C.A. *Antibacterial Polyurethanes*; 2016; ISBN 9780081006221.
4. Francolini, I.; Crisante, F.; Martinelli, A.; D'Ilario, L.; Piozzi, A. Synthesis of Biomimetic Segmented Polyurethanes as Antifouling Biomaterials. *Acta Biomater.* **2012**, *8*, 549–

558, doi:10.1016/j.actbio.2011.10.024.

5. Akindoyo, J.O.; Beg, M.D.H.; Ghazali, S.; Islam, M.R.; Jeyaratnam, N.; Yuvaraj, A.R. Polyurethane Types, Synthesis and Applications-a Review. *RSC Adv.* **2016**, *6*, 114453–114482, doi:10.1039/c6ra14525f.

6. Włoch, M.; Błażek, K. Isocyanate-Free Polyurethanes. In *Polyurethane Chemistry: Renewable Polyols and Isocyanates*; ACS Symposium Series; American Chemical Society, 2021; Vol. 1380, pp. 107–166 ISBN 9780841298408.

7. Janik, H. Progress in the Studies of the Supermolecular Structure of Segmented Polyurethanes. *Polimery* **2010**, *55*, 419–500.

8. Ryszkowska, J.; Waśniewski, B. Quantitative Description of the Morphology of Polyurethane Nanocomposites for Medical Applications. *WIT Trans. Eng. Sci.* **2011**, *72*, 377–386, doi:10.2495/MC110331.

9. Król, P. Synthesis Methods, Chemical Structures and Phase Structures of Linear Polyurethanes. Properties and Applications of Linear Polyurethanes in Polyurethane Elastomers, Copolymers and Ionomers. *Prog. Mater. Sci.* **2007**, *52*, 915–1015, doi:10.1016/j.pmatsci.2006.11.001.

10. Foks, J.; Janik, I.H.; Russo, R. Morphology and Thermal Properties of Polyurethanes Prepared under Different Conditions. *Eur. Polym. J.* **1989**, *25*, 31–37, doi:10.1016/0014-3057(89)90205-X.

11. Irusta, L.; Fernandez-Berridi, M.J. Aromatic Poly(Ether-Urethanes): Effect of the Polyol Molecular Weight on the Photochemical Behaviour. *Polymer (Guildf).* **1999**, *40*, 4821–4831, doi:10.1016/S0032-3861(98)00708-3.

12. Darby, T.D.; Johnson, H.J.; Northup, S.J. An Evaluation of a Polyurethane for Use as a Medical Grade Plastic. *Toxicol. Appl. Pharmacol.* **1978**, *46*, 449–453, doi:10.1016/0041-008X(78)90090-X.

13. Luu, H. Do; Hutter, J.C. Pharmacokinetic Modeling of 4,4′-Methylenedianiline Released from Reused Polyurethane Dialyzer Potting Materials. *J. Biomed. Mater. Res.* **2002**, *53*, 276–286, doi:10.1002/(SICI)1097-4636(2000)53:3<276::AID-JBM13>3.0.CO;2-E.

14. Shintani, H. Formation and Elution of Toxic Compounds from Sterilized Medical Products: Methylenedianiline Formation in Polyurethane. *J. Biomater. Appl.* **1995**, *10*, 23–58, doi:10.1177/088532829501000102.

15. Shintani, H.; Nakamura, A. Formation of 4,4′-methylenedianiline in Polyurethane Potting Materials by Either Γ-ray or Autoclave Sterilization. *J. Biomed. Mater. Res.* **1991**, *25*, 1275–1286, doi:10.1002/jbm.820251008.

16. Guelcher, S.A.; Gallagher, K.M.; Didier, J.E.; Klinedinst, D.B.; Doctor, J.S.; Goldstein, A.S.; Wilkes, G.L.; Beckman, E.J.; Hollinger, J.O. Synthesis of Biocompatible Segmented Polyurethanes from Aliphatic Diisocyanates and Diurea Diol Chain Extenders. *Acta Biomater.* **2005**, *1*, 471–484, doi:10.1016/j.actbio.2005.02.007.

17. Lim, D.I.; Park, H.S.; Park, J.H.; Knowles, J.C.; Gong, M.S. Application of High-Strength Biodegradable Polyurethanes Containing Different Ratios of Biobased Isomannide and Poly (E-Caprolactone) Diol. *J. Bioact. Compat. Polym.* **2013**, *28*, 274–288, doi:10.1177/0883911513484572.

18. Król, P.; Uram, Ł.; Król, B.; Pielichowska, K.; Sochacka-Piętal, M.; Walczak, M. Synthesis

and Property of Polyurethane Elastomer for Biomedical Applications Based on Nonaromatic Isocyanates, Polyesters, and Ethylene Glycol. *Colloid Polym. Sci.* **2020**, *298*, 1077–1093, doi:10.1007/s00396-020-04667-8.

19. He, X.; Zhai, Z.; Wang, Y.; Wu, G.; Zheng, Z.; Wang, Q.; Liu, Y. New Method for Coupling Collagen on Biodegradable Polyurethane for Biomedical Application. *J. Appl. Polym. Sci.* **2012**, *126*, 354–361, doi:10.1002/app.36742.

20. Kucinska-Lipka, J.; Gubanska, I.; Strankowski, M.; Cieśliński, H.; Filipowicz, N.; Janik, H. Synthesis and Characterization of Cycloaliphatic Hydrophilic Polyurethanes, Modified with L-Ascorbic Acid, as Materials for Soft Tissue Regeneration. *Mater. Sci. Eng. C* **2017**, *75*, 671–681, doi:10.1016/j.msec.2017.02.052.

21. Cauich-rodríguez, J. V; Chan-Chan, L.H.; Hernandez-Sánchez, F.; Cervantes-Uc, J.M. Degradation of Polyurethanes for Cardiovascular Applications. In *Advances in Biomaterials Science and Biomedical Applications*; Pignatello, R., Ed.; InTech, 2013; pp. 51–82 ISBN 978-953-51-1051-4.

22. Zhou, G.; Ma, C.; Zhang, G. Synthesis of Polyurethane-g-Poly(Ethylene Glycol) Copolymers by Macroiniferter and Their Protein Resistance. *Polym. Chem.* **2011**, *2*, 1409–1414, doi:10.1039/c1py00016k.

23. Ali, F.B.; Kang, D.J.; Kim, M.P.; Cho, C.H.; Kim, B.J. Synthesis of Biodegradable and Flexible, Polylactic Acid Based, Thermoplastic Polyurethane with High Gas Barrier Properties. *Polym. Int.* **2013**, *63*, 1620–1626, doi:10.1002/pi.4662.

24. Alishiri, M.; Shojaei, A.; Abdekhodaie, M.J.; Yeganeh, H. Synthesis and Characterization of Biodegradable Acrylated Polyurethane Based on Poly(ε-Caprolactone) and 1,6-Hexamethylene Diisocyanate. *Mater. Sci. Eng. C* **2014**, *42*, 763–773, doi:10.1016/j.msec.2014.05.056.

25. Zeng, J.B.; Li, Y.D.; Li, W. Da; Yang, K.K.; Wang, X.L.; Wang, Y.Z. Synthesis and Properties of Poly(Ester Urethane)s Consisting of Poly(L-Lactic Acid) and Poly(Ethylene Succinate) Segments. *Ind. Eng. Chem. Res.* **2009**, *48*, 1706–1711, doi:10.1021/ie801391m.

26. Tuan Ismail, T.N.M.; Ibrahim, N.A.; Sendijarevic, V.; Sendijarevic, I.; Schiffman, C.M.; Hoong, S.S.; Mohd Noor, M.A.; Poo Palam, K.D.; Yeong, S.K.; Idris, Z.; et al. Thermal and Mechanical Properties of Thermoplastic Urethanes Made from Crystalline and Amorphous Azelate Polyols. *J. Appl. Polym. Sci.* **2019**, *136*, 1–11, doi:10.1002/app.47890.

27. Henry, J.; Simonet, M.; Pandit, A.; Neuenschwander, P. Characterization of a Slowly Degrading Biodegradable Polyesterurethane for Tissue Engineering Scaffolds. *J. Biomed. Mater. Res. Part A* **2007**, *82A*, 669–679, doi:10.1002/jbm.a.31094.

28. Wang, Z.; Yan, J.; Wang, T.; Zai, Y.; Qiu, L.; Wang, Q. Fabrication and Properties of a Bio-Based Biodegradable Thermoplastic Polyurethane Elastomer. *Polymers (Basel).* **2019**, *11*, 1–13, doi:10.3390/polym11071121.

29. Marzec, M.; Kucińska-Lipka, J.; Kalaszczyńska, I.; Janik, H. Development of Polyurethanes for Bone Repair. *Mater. Sci. Eng. C* **2017**, *80*, 736–747, doi:10.1016/j.msec.2017.07.047.

30. Tanzi, M.C.; Verderio, P.; Lampugnani, M.G.; Resnati, M.; Dejana, E.; Sturani, E. Cytotoxicity of Some Catalysts Commonly Used in the Synthesis of Copolymers for

Biomedical Use. *J. Mater. Sci. Mater. Med.* **1994**, *5*, 393–396, doi:10.1007/BF00058971.

31. Kim, H.-J.; Kang, M.-S.; Knowles, J.C.; Gong, M.-S. Synthesis of Highly Elastic Biocompatible Polyurethanes Based on Bio-Based Isosorbide and Poly(Tetramethylene Glycol) and Their Properties. *J. Biomater. Appl.* **2014**, *29*, 454–464, doi:10.1177/0885328214533737.

32. Park, H.; Gong, M.-S.; Knowles, J.C. Catalyst-Free Synthesis of High Elongation Degradable Polyurethanes Containing Varying Ratios of Isosorbide and Polycaprolactone: Physical Properties and Biocompatibility. *J. Mater. Sci. Mater. Med.* **2013**, *24*, 281–294, doi:10.1007/s10856-012-4814-0.

33. Sivak, W.N.; Pollack, I.F.; Petoud, S.; Zamboni, W.C.; Zhang, J.; Beckman, E.J. Catalyst-Dependent Drug Loading of LDI-Glycerol Polyurethane Foams Leads to Differing Controlled Release Profiles. *Acta Biomater.* **2008**, *4*, 1263–1274, doi:10.1016/j.actbio.2008.01.008.

34. Singh, A.A.; Genovese, M.E. Green and Sustainable Packaging Materials Using Thermoplastic Starch. In *Sustainable Food Packaging Technology*; John Wiley & Sins, 2021; pp. 133–160.

35. Alcázar-Alay, S.C.; Meireles, M.A.A. Physicochemical Properties, Modifications and Applications of Starches from Different Botanical Sources. *Food Sci. Technol.* **2015**, *35*, 215–236, doi:10.1590/1678-457X.6749.

36. Wang, S.; Copeland, L. Effect of Acid Hydrolysis on Starch Structure and Functionality: A Review. *Crit. Rev. Food Sci. Nutr.* **2015**, *55*, 1081–1097, doi:10.1080/10408398.2012.684551.

37. Montilla-Buitrago, C.E.; Gómez-López, R.A.; Solanilla-Duque, J.F.; Serna-Cock, L.; Villada-Castillo, H.S. Effect of Plasticizers on Properties, Retrogradation, and Processing of Extrusion-Obtained Thermoplastic Starch: A Review. *Starch/Staerke* **2021**, *73*, doi:10.1002/star.202100060.

38. Zuo, Y.; Gu, J.; Tan, H.; Zhang, Y. Thermoplastic Starch Prepared with Different Plasticizers: Relation between Degree of Plasticization and Properties. *J. Wuhan Univ. Technol. Mater. Sci. Ed.* **2015**, *30*, 423–428, doi:10.1007/s11595-015-1164-z.

39. Ma, X.; Yu, J.; He, K.; Wang, N. The Effects of Different Plasticizers on the Properties of Thermoplastic Starch as Solid Polymer Electrolytes. *Macromol. Mater. Eng.* **2007**, *292*, 503–510, doi:10.1002/mame.200600445.

40. Ma, X.; Yu, J. The Effects of Plasticizers Containing Amide Groups on the Properties of Thermoplastic Starch. *Starch/Staerke* **2004**, *56*, 545–551, doi:10.1002/star.200300256.

41. Nafchi, A.M.; Moradpour, M.; Saeidi, M.; Alias, A.K. Thermoplastic Starches: Properties, Challenges, and Prospects. *Starch/Staerke* **2013**, *65*, 61–72, doi:10.1002/star.201200201.

42. Da Róz, A.L.; Carvalho, A.J.F.; Gandini, A.; Curvelo, A.A.S. The Effect of Plasticizers on Thermoplastic Starch Compositions Obtained by Melt Processing. *Carbohydr. Polym.* **2006**, *63*, 417–424, doi:10.1016/j.carbpol.2005.09.017.

43. Ivanič, F.; Kováčová, M.; Chodák, I. The Effect of Plasticizer Selection on Properties of Blends Poly(Butylene Adipate-Co-Terephthalate) with Thermoplastic Starch. *Eur. Polym.*

J. **2019**, *116*, 99–105, doi:10.1016/j.eurpolymj.2019.03.042.

44. Zhang, Y.; Han, J.H. Crystallization of High-Amylose Starch by the Addition of Plasticizers at Low and Intermediate Concentrations. *J. Food Sci.* **2010**, *75*, doi:10.1111/j.1750-3841.2009.01404.x.

45. Wang, S.; Li, C.; Copeland, L.; Niu, Q.; Wang, S. Starch Retrogradation: A Comprehensive Review. *Compr. Rev. Food Sci. Food Saf.* **2015**, *14*, 568–585, doi:10.1111/1541-4337.12143.

46. Esmaeili, M.; Pircheraghi, G.; Bagheri, R. Optimizing the Mechanical and Physical Properties of Thermoplastic Starch via Tuning the Molecular Microstructure through Co-Plasticization by Sorbitol and Glycerol. *Polym. Iternational* **2017**, *66*, 809–819, doi:10.1002/pi.5319.

47. Ma, X.; Yu, J. The Plastcizers Containing Amide Groups for Thermoplastic Starch. *Carbohydr. Polym.* **2004**, *57*, 197–203, doi:10.1016/j.carbpol.2004.04.012.

48. Schmitt, H.; Guidez, A.; Prashantha, K.; Soulestin, J.; Lacrampe, M.F.; Krawczak, P. Studies on the Effect of Storage Time and Plasticizers on the Structural Variations in Thermoplastic Starch. *Carbohydr. Polym.* **2015**, *115*, 364–372, doi:10.1016/j.carbpol.2014.09.004.

49. Xiaofei, M.; Jiugao, Y.; Jin, F. Urea and Formamide as a Mixed Plasticizer for Thermoplastic Starch. *Polym. Int.* **2004**, *53*, 1780–1785, doi:10.1002/pi.1580.

50. Ma, F.; Wan, Y.; Yuan, G.; Meng, L.; Dong, Z.; Hu, J. Occurrence and Source of Nitrosamines and Secondary Amines in Groundwater and Its Adjacent Jialu River Basin, China. *Environ. Sci. Technol.* **2012**, *46*, 3236–3243, doi:10.1021/es204520b.

51. Poste, A.E.; Grung, M.; Wright, R.F. Amines and Amine-Related Compounds in Surface Waters: A Review of Sources, Concentrations and Aquatic Toxicity. *Sci. Total Environ.* **2014**, *481*, 274–279, doi:10.1016/j.scitotenv.2014.02.066.

52. Fekete, A.; Malik, A.K.; Kumar, A.; Schmitt-Kopplin, P. Amines in the Environment. *Crit. Rev. Anal. Chem.* **2010**, *40*, 102–121, doi:10.1080/10408340903517495.

53. Šoltýs, A.; Hronský, V.; Šmídová, N.; Olčák, D.; Ivanič, F.; Chodák, I. Solid-State 1H and 13C NMR of Corn Starch Plasticized with Glycerol and Urea. *Eur. Polym. J.* **2019**, *117*, 19–27, doi:10.1016/j.eurpolymj.2019.04.042.

54. Ahmed, I.; Niazi, M.B.K.; Hussain, A.; Jahan, Z. Influence of Amphiphilic Plasticizer on Properties of Thermoplastic Starch Films. *Polym. - Plast. Technol. Eng.* **2018**, *57*, 17–27, doi:10.1080/03602559.2017.1298803.

55. Shi, M.; Jing, Y.; Yang, L.; Huang, X.; Wang, H.; Yan, Y.; Liu, Y. Structure and Physicochemical Properties of Malate Starches from Corn, Potato, and Wrinkled Pea Starches. *Polymers (Basel).* **2019**, *11*, doi:10.3390/polym11091523.

56. Shi, M.; Gao, Q.; Liu, Y. Changes in the Structure and Digestibility of Wrinkled Pea Starch with Malic Acid Treatment. *Polymers (Basel).* **2018**, *10*, 1–12, doi:10.3390/polym10121359.

57. Hung, P. Van; Vien, N.L.; Lan Phi, N.T. Resistant Starch Improvement of Rice Starches under a Combination of Acid and Heat-Moisture Treatments. *Food Chem.* **2016**, *191*, 67–73, doi:10.1016/j.foodchem.2015.02.002.

58. Xie, X.; Liu, Q. Development and Physicochemical Characterization of New Resistant Citrate Starch from Different Corn Starches. *Starch/Staerke* **2004**, *56*, 364–370, doi:10.1002/star.200300261.

59. Golachowski, A.; Drożdz, W.; Golachowska, M.; Kapelko-Zeberska, M.; Raszewski, B. Production and Properties of Starch Citrates—Current Research. *Foods* **2020**, *9*, 1–14, doi:10.3390/foods9091311.

60. Skowrońska, D.; Wilpiszewska, K. Deep Eutectic Solvents for Starch Treatment. *Polymers (Basel).* **2022**, *14*, doi:10.3390/polym14020220.

61. Zdanowicz, M.; Wilpiszewska, K.; Spychaj, T. Deep Eutectic Solvents for Polysaccharides Processing. A Review. *Carbohydr. Polym.* **2018**, *200*, 361–380, doi:10.1016/j.carbpol.2018.07.078.

62. Zdanowicz, M.; Jędrzejewski, R.; Pilawka, R. Deep Eutectic Solvents as Simultaneous Plasticizing and Crosslinking Agents for Starch. *Int. J. Biol. Macromol.* **2019**, *129*, 1040–1046, doi:10.1016/j.ijbiomac.2019.02.103.

63. Zdanowicz, M.; Sałasińska, K.; Lewandowski, K.; Skórczewska, K. Thermoplastic Starch/Ternary Deep Eutectic Solvent/Lignin Materials: Study of Physicochemical Properties and Fire Behavior. *ACS Sustain. Chem. Eng.* **2022**, *10*, 4579–4587, doi:10.1021/acssuschemeng.1c08542.

64. Lai, S.M.; Don, T.M.; Huang, Y.C. Preparation and Properties of Biodegradable Thermoplastic Starch/Poly(Hydroxy Butyrate) Blends. *J. Appl. Polym. Sci.* **2006**, *100*, 2371–2379, doi:10.1002/app.23085.

65. Park, J.W.; Im, S.S. Biodegradable Polymer Blends of Poly(L-Lactic Acid) and Gelatinized Starch. *Polym. Eng. Sci.* **2000**, *40*, 2539–2550.

66. European Bioplastics *Bioplastics Market Development Update 2021*; 2021;

67. Masutani, K.; Kimura, Y. PLA Synthesis. From the Monomer to the Polymer. In *Poly(lactic acid) Science and Technology: Processing, Properties, Additives and Applications*; The Royal Society of Chemistry, 2014; pp. 1–36 ISBN 978-1-84973-879-8.

68. da Silva, D.; Kaduri, M.; Poley, M.; Adir, O.; Krinsky, N.; Shainsky-Roitman, J.; Schroeder, A. Biocompatibility, Biodegradation and Excretion of Polylactic Acid (PLA) in Medical Implants and Theranostic Systems. *Chem. Eng. J.* **2018**, *340*, 9–14, doi:10.1016/j.cej.2018.01.010.

69. Bastioli, C. *Handbook of Biodegradable Polymers*; Bastioli, C., Ed.; 2nd Editio.; Rapa Technology Limited, 2005;

70. Lucas, N.; Bienaime, C.; Belloy, C.; Queneudec, M.; Silvestre, F.; Nava-Saucedo, J.E. Polymer Biodegradation: Mechanisms and Estimation Techniques - A Review. *Chemosphere* **2008**, *73*, 429–442, doi:10.1016/j.chemosphere.2008.06.064.

71. DeStefano, V.; Khan, S.; Tabada, A. Applications of PLA in Modern Medicine. *Eng. Regen.* **2020**, *1*, 76–87, doi:10.1016/j.engreg.2020.08.002.

72. Bergsma, J.E.; Rozema, F.R.; Bos, R.R.M.; Boering, G.; de Bruijn, W.C.; Pennings, A.J. In Vivo Degradation and Biocompatibility Study of in Vitro Pre-Degraded as-Polymerized Polylactide Particles. *Biomaterials* **1995**, *16*, 267–274, doi:10.1016/0142-9612(95)93253-A.

73. Goto, T.; Kishita, M.; Sun, Y.; Sako, T.; Okajima, I. Degradation of Polylactic Acid Using Sub-Critical Water for Compost. *Polymers (Basel).* **2020**, *12*, 1–14, doi:10.3390/polym12112434.

74. Karamanlioglu, M.; Robson, G.D. The Influence of Biotic and Abiotic Factors on the Rate of Degradation of Poly(Lactic) Acid (PLA) Coupons Buried in Compost and Soil. *Polym. Degrad. Stab.* **2013**, *98*, 2063–2071, doi:10.1016/j.polymdegradstab.2013.07.004.

75. Teixeira, S.; Eblagon, K.M.; Miranda, F.; R. Pereira, M.F.; Figueiredo, J.L. Towards Controlled Degradation of Poly(Lactic) Acid in Technical Applications. *J. Carbon Res.* **2021**, *7*, 42, doi:10.3390/c7020042.

76. Kijchavengkul, T.; Auras, R. Compostability of Polymers. *Polym. Int.* **2008**, *57*, 793–804, doi:10.1002/pi.2420.

77. Ghorpade, V.M.; Gennadios, A.; Hanna, M.A. Laboratory Composting of Extruded Poly(Lactic Acid) Sheets. *Bioresour. Technol.* **2001**, *76*, 57–61, doi:10.1016/S0960-8524(00)00077-8.

78. Ainali, N.M.; Kalaronis, D.; Evgenidou, E.; Kyzas, G.Z.; Bobori, D.C.; Kaloyianni, M.; Yang, X.; Bikiaris, D.N.; Lambropoulou, D.A. Do Poly(Lactic Acid) Microplastics Instigate a Threat? A Perception for Their Dynamic towards Environmental Pollution and Toxicity. *Sci. Total Environ.* **2022**, *832*, 155014, doi:https://doi.org/10.1016/j.scitotenv.2022.155014.

79. Napper, I.E.; Thompson, R.C. Environmental Deterioration of Biodegradable, Oxo-Biodegradable, Compostable, and Conventional Plastic Carrier Bags in the Sea, Soil, and Open-Air over a 3-Year Period. *Environ. Sci. Technol.* **2019**, *53*, 4775–4783, doi:10.1021/acs.est.8b06984.

80. Weinstein, J.E.; Dekle, J.L.; Leads, R.R.; Hunter, R.A. Degradation of Bio-Based and Biodegradable Plastics in a Salt Marsh Habitat: Another Potential Source of Microplastics in Coastal Waters. *Mar. Pollut. Bull.* **2020**, *160*, 111518, doi:10.1016/j.marpolbul.2020.111518.

81. Lim, X.Z. Microplastics Are Everywhere - but Are They Harmful? *Nature* **2021**, *593*, 22–25, doi:10.1038/d41586-021-01143-3.

82. Rahman, A.; Sarkar, A.; Yadav, O.P.; Achari, G.; Slobodnik, J. Potential Human Health Risks Due to Environmental Exposure to Nano- and Microplastics and Knowledge Gaps: A Scoping Review. *Sci. Total Environ.* **2021**, *757*, 143872, doi:10.1016/j.scitotenv.2020.143872.

83. Qin, M.; Chen, C.; Song, B.; Shen, M.; Cao, W.; Yang, H.; Zeng, G.; Gong, J. A Review of Biodegradable Plastics to Biodegradable Microplastics: Another Ecological Threat to Soil Environments? *J. Clean. Prod.* **2021**, *312*, 127816, doi:10.1016/j.jclepro.2021.127816.

84. Liao, J.; Chen, Q. Biodegradable Plastics in the Air and Soil Environment: Low Degradation Rate and High Microplastics Formation. *J. Hazard. Mater.* **2021**, *418*, 126329, doi:10.1016/j.jhazmat.2021.126329.

85. Malafaia, G.; Nascimento, Í.F.; Estrela, F.N.; Guimarães, A.T.B.; Ribeiro, F.; Luz, T.M. da; Rodrigues, A.S. de L. Green Toxicology Approach Involving Polylactic Acid Biomicroplastics and Neotropical Tadpoles: (Eco)Toxicological Safety or Environmental Hazard? *Sci. Total Environ.* **2021**, *783*, 146994, doi:10.1016/j.scitotenv.2021.146994.

86. Goud, V. V.; Patwardhan, A. V.; Pradhan, N.C. Studies on the Epoxidation of Mahua Oil (Madhumica Indica) by Hydrogen Peroxide. *Bioresour. Technol.* **2006**, *97*, 1365–1371, doi:10.1016/j.biortech.2005.07.004.

87. Tang, Q.; Chen, Y.; Gao, H.; Li, Q.; Xi, Z.; Zhao, L.; Peng, C.; Li, L. Bio-Based Epoxy Resin from Epoxidized Soybean Oil. In *Soybean - Biomass, Yield and Productivity*; IntechOpen, 2019.

88. Belhassen, R.; Vilaseca, F.; Mutjé, P.; Boufi, S. Thermoplasticized Starch Modified by Reactive Blending with Epoxidized Soybean Oil. *Ind. Crops Prod.* **2014**, *53*, 261–267, doi:10.1016/j.indcrop.2013.12.039.

89. Vijayarajan, S.; Selke, S.E.M.; Matuana, L.M. Continuous Blending Approach in the Manufacture of Epoxidized Soybean-Plasticized Poly(Lactic Acid) Sheets and Films. *Macromol. Mater. Eng.* **2014**, *299*, 622–630, doi:10.1002/mame.201300226.

90. Ali, F.; Chang, Y.-W.; Kang, S.C.; Yoon, J.Y. Thermal, Mechanical and Rheological Properties of Poly (Lactic Acid)/Epoxidized Soybean Oil Blends. *Polym. Bull.* **2009**, *62*, 91–98, doi:10.1007/s00289-008-1012-9.

91. Yu-Qiong Xu, J.-P.Q. Mechanical and Rheological Properties of Epoxidized Soybean Oil Plasticized Poly(Lactic Acid). *J. Appl. Polym. Sci.* **2009**, *112*, 3185–3191, doi:10.1002/app.

92. Xing, C.; Matuana, L.M. Epoxidized Soybean Oil-Plasticized Poly(Lactic Acid) Films Performance as Impacted by Storage. *J. Appl. Polym. Sci.* **2016**, *133*, 1–8, doi:10.1002/app.43201.

93. Skilton, M.; Hovsepian, F. The Technology of the 4th Industrial Revolution. In *The 4th Industrial Revolution*; Palgrave Macmillan, 2018; pp. 29–68 ISBN 978-3-319-62479-2.

94. ASTM. Standard Terminology for Additive Manufacturing Technologies. ASTM International, 2012.

95. Ciraud, P.A.L. A Method and Apparatus for Making Any Belongings from Any Fusible Material 1973.

96. Gosselin, C.; Duballet, R.; Roux, P.; Gaudillière, N.; Dirrenberger, J.; Morel, P. Large-Scale 3D Printing of Ultra-High Performance Concrete – a New Processing Route for Architects and Builders. *Mater. Des.* **2016**, *100*, 102–109, doi:10.1016/J.MATDES.2016.03.097.

97. 3D Printing Market Size, Share | Industry Report, 2021-2028 Available online: https://www.grandviewresearch.com/industry-analysis/3d-printing-industry-analysis (accessed on 14 August 2021).

98. Attaran, M. The Rise of 3-D Printing:The Advantages of Additive Manufacturing over Traditional Manufacturing. **2017**, doi:10.1016/j.bushor.2017.05.011.

99. Liu, Z.; Jiang, Q.; Ning, F.; Kim, H.; Cong, W.; Xu, C.; Zhang, H.C. Investigation of Energy Requirements and Environmental Performance for Additive Manufacturing Processes. *Sustain.* **2018**, *10*, doi:10.3390/SU10103606.

100. Fraţila, D.; Rotaru, H. Additive Manufacturing-a Sustainable Manufacturing Route. *MATEC Web Conf.* **2017**, *94*, doi:10.1051/MATECCONF/20179403004.

101. Yang, S.; Min, W.; Ghibaudo, J.; Zhao, Y.F. Understanding the Sustainability Potential

of Part Consolidation Design Supported by Additive Manufacturing. *J. Clean. Prod.* **2019**, *232*, 722–738, doi:10.1016/j.jclepro.2019.05.380.

102. Zhao, P.; Rao, C.; Gu, F.; Sharmin, N.; Fu, J. Close-Looped Recycling of Polylactic Acid Used in 3D Printing: An Experimental Investigation and Life Cycle Assessment. *J. Clean. Prod.* **2018**, *197*, 1046–1055, doi:10.1016/J.JCLEPRO.2018.06.275.

103. Kumar, S.; Czekanski, A. Roadmap to Sustainable Plastic Additive Manufacturing. *Mater. Today Commun.* **2018**, *15*, 109–113, doi:10.1016/j.mtcomm.2018.02.006.

104. Tang, H.P.; Qian, M.; Liu, N.; Zhang, X.Z.; Yang, G.Y.; Wang, J. Effect of Powder Reuse Times on Additive Manufacturing of Ti-6Al-4V by Selective Electron Beam Melting. *JOM 2015 673* **2015**, *67*, 555–563, doi:10.1007/S11837-015-1300-4.

105. Gebler, M.; Schoot Uiterkamp, A.J.M.; Visser, C. A Global Sustainability Perspective on 3D Printing Technologies. *Energy Policy* **2014**, *74*, 158–167, doi:10.1016/j.enpol.2014.08.033.

106. Kreiger, M.; Pearce, J.M. Environmental Life Cycle Analysis of Distributed Three-Dimensional Printing and Conventional Manufacturing of Polymer Products. *ACS Sustain. Chem. Eng.* **2013**, *1*, 1511–1519, doi:10.1021/SC400093K.

107. Liu, Z.; Jiang, Q.; Zhang, Y.; Li, T.; Zhang, H. Sustainability of 3D Printing: A Critical Review and Recommendations. In Proceedings of the International Manufacturing Science and Engineering Conference MSEC2016; Blacksburg, 2016; pp. 0–8.

108. Busachi, A.; Erkoyuncu, J.; Colegrove, P.; Martina, F.; Watts, C.; Drake, R. A Review of Additive Manufacturing Technology and Cost Estimation Techniques for the Defence Sector. *CIRP J. Manuf. Sci. Technol.* **2017**, *19*, 117–128, doi:10.1016/J.CIRPJ.2017.07.001.

109. Telenko, C.; Seepersad, C.C. A Comparison of the Energy Efficiency of Selective Laser Sintering and Injection Molding of Nylon Parts. *Rapid Prototyp. J.* **2012**, *6*, 472–481, doi:10.1108/13552541211272018.

110. Yoon, H.S.; Lee, J.Y.; Kim, H.S.; Kim, M.S.; Kim, E.S.; Shin, Y.J.; Chu, W.S.; Ahn, S.H. A Comparison of Energy Consumption in Bulk Forming, Subtractive, and Additive Processes: Review and Case Study. *Int. J. Precis. Eng. Manuf. - Green Technol.* **2014**, *1*, 261–279, doi:10.1007/s40684-014-0033-0.

111. Quan, H.; Zhang, T.; Xu, H.; Luo, S.; Nie, J.; Zhu, X. Photo-Curing 3D Printing Technique and Its Challenges. *Bioact. Mater.* **2020**, *5*, 110–115, doi:10.1016/J.BIOACTMAT.2019.12.003.

112. Wojtyła, S.; Klama, P.; Baran, T. Is 3D Printing Safe? Analysis of the Thermal Treatment of Thermoplastics: ABS, PLA, PET, and Nylon. *http://dx.doi.org/10.1080/15459624.2017.1285489* **2017**, *14*, D80–D85, doi:10.1080/15459624.2017.1285489.

113. Kim, Y.; Yoon, C.; Ham, S.; Park, J.; Kim, S.; Kwon, O.; Tsai, P.-J. Emissions of Nanoparticles and Gaseous Material from 3D Printer Operation. *Environ. Sci. Technol.* **2015**, *49*, 12044–12053, doi:10.1021/ACS.EST.5B02805.

114. Bourhis, F. Le; Kerbrat, O.; Hascoet, J.-Y.; Mognol, P. Sustainable Manufacturing: Evaluation and Modeling of Environmental Impacts in Additive Manufacturing. *Int. J. Adv. Manuf. Technol. 2013 699* **2013**, *69*, 1927–1939, doi:10.1007/S00170-013-5151-2.

115. Faludi, J.; Bayley, C.; Bhogal, S.; Iribarne, M. Comparing Environmental Impacts of Additive Manufacturing vs Traditional Machining via Life-Cycle Assessment. *Rapid Prototyp. J.* **2015**, *21*, 14–33, doi:10.1108/RPJ-07-2013-0067.

116. Khalid, M.; Peng, Q. Sustainability and Environmental Impact of Additive Manufacturing: A Literature Review. *Comput. Aided. Des. Appl.* **2021**, *18*, 1210–1232, doi:10.14733/cadaps.2021.1210-1232.

117. Ford, S.; Despeisse, M. Additive Manufacturing and Sustainability: An Exploratory Study of the Advantages and Challenges. *J. Clean. Prod.* **2016**, *137*, 1573–1587, doi:10.1016/j.jclepro.2016.04.150.

118. Esposito Corcione, C.; Greco, A.; Maffezzoli, A. Photopolymerization Kinetics of an Epoxy Based Resin for Stereolithography. *J. Therm. Anal. Calorim. 2003 722* **2003**, *72*, 687–693, doi:10.1023/A:1024558506949.

119. Gibson, I.; Rosen, D.; Stucker, B. Vat Photopolymerization Processes. *Addit. Manuf. Technol.* **2015**, 63–106, doi:10.1007/978-1-4939-2113-3_4.

120. Kazmer, D. Three-Dimensional Printing of Plastics. *Appl. Plast. Eng. Handb. Process. Mater. Appl. Second Ed.* **2017**, 617–634, doi:10.1016/B978-0-323-39040-8.00029-8.

121. Bhavar, V.; Kattire, P.; Patil, V.; Khot, S.; Gujar, K.; Singh, R. A Review on Powder Bed Fusion Technology of Metal Additive Manufacturing. *Addit. Manuf. Handb.* **2017**, 251–253, doi:10.1201/9781315119106-15.

122. History of Arcam AB Available online: https://www.ge.com/additive/who-we-are/about-arcam.

123. Zhang, L.-C.; Wang, J.; Liu, Y.; Jia, Z.; Liang, S.-X. Additive Manufacturing of Titanium Alloys. *Encycl. Mater. Met. Allloys* **2022**, 256–274, doi:10.1016/B978-0-12-819726-4.00002-8.

124. Oshida, Y. Fabrication Technologies. *Biosci. Bioeng. Titan. Mater.* **2013**, 303–340, doi:10.1016/B978-0-444-62625-7.00010-8.

125. Molitch-Hou, M. Overview of Additive Manufacturing Process. *Addit. Manuf. Mater. Process. Quantif. Appl.* **2018**, 1–38, doi:10.1016/B978-0-12-812155-9.00001-3.

126. Ionita, C.N.; Mokin, M.; Varble, N.; Bednarek, D.R.; Xiang, J.; Snyder, K. V; Siddiqui, A.H.; Levy, E.I.; Meng, H.; Rudin, S. Challenges and Limitations of Patient-Specific Vascular Phantom Fabrication Using 3D Polyjet Printing. *Proc. SPIE--the Int. Soc. Opt. Eng.* **2014**, *9038*, 90380M, doi:10.1117/12.2042266.

127. JP, C.; LJ, O.; L, S.; A, K.; F, A.; O, T.; MB, M.; SJ, Y.; PC, K.; RA, J.; et al. Incorporating Three-Dimensional Printing into a Simulation-Based Congenital Heart Disease and Critical Care Training Curriculum for Resident Physicians. *Congenit. Heart Dis.* **2015**, *10*, 185–190, doi:10.1111/CHD.12238.

128. Maddox, M.M.; Feibus, A.; Liu, J.; Wang, J.; Thomas, R.; Silberstein, J.L. 3D-Printed Soft-Tissue Physical Models of Renal Malignancies for Individualized Surgical Simulation: A Feasibility Study. *J. Robot. Surg.*, doi:10.1007/s11701-017-0680-6.

129. Mostafaei, A.; Elliott, A.M.; Barnes, J.E.; Li, F.; Tan, W.; Cramer, C.L.; Nandwana, P.; Chmielus, M. Binder Jet 3D Printing—Process Parameters, Materials, Properties, Modeling, and Challenges. *Prog. Mater. Sci.* **2021**, *119*, 100707, doi:10.1016/j.pmatsci.2020.100707.

130. Garzón, E.O.; Alves, J.L.; Neto, R.J. Post-Process Influence of Infiltration on Binder Jetting Technology. *Adv. Struct. Mater.* **2017**, *65*, 233–255, doi:10.1007/978-3-319-50784-2_19.

131. Sames, W.J.; List, F.A.; Pannala, S.; Dehoff, R.R.; Babu, S.S. The Metallurgy and Processing Science of Metal Additive Manufacturing. *http://dx.doi.org/10.1080/09506608.2015.1116649* **2016**, *61*, 315–360, doi:10.1080/09506608.2015.1116649.

132. Ziaee, M.; Crane, N.B. Binder Jetting: A Review of Process, Materials, and Methods. *Addit. Manuf.* **2019**, *28*, 781–801, doi:10.1016/J.ADDMA.2019.05.031.

133. Snelling, D.A.; Williams, C.B.; Druschitz, A.P. Mechanical and Material Properties of Castings Produced via 3D Printed Molds. *Addit. Manuf.* **2019**, *27*, 199–207, doi:10.1016/J.ADDMA.2019.03.004.

134. Le Néel, T.A.; Mognol, P.; Hascoët, J.Y. A Review on Additive Manufacturing of Sand Molds by Binder Jetting and Selective Laser Sintering. *Rapid Prototyp. J.* **2018**, *24*, 1325–1336, doi:10.1108/RPJ-10-2016-0161.

135. Upadhyay, M.; Sivarupan, T.; El Mansori, M. 3D Printing for Rapid Sand Casting—A Review. *J. Manuf. Process.* **2017**, *29*, 211–220, doi:10.1016/J.JMAPRO.2017.07.017.

136. 3D Printed Materials-Stratasys Available online: https://www.stratasys.com/en/materials/materials-catalog.

137. Gao, X.; Qi, S.; Kuang, X.; Su, Y.; Li, J.; Wang, D. Fused Filament Fabrication of Polymer Materials: A Review of Interlayer Bond. *Addit. Manuf.* **2021**, *37*, 101658, doi:10.1016/j.addma.2020.101658.

138. Ahn, S.H.; Montero, M.; Odell, D.; Roundy, S.; Wright, P.K. *Anisotropic Material Properties of Fused Deposition Modeling ABS*; 2002; Vol. 8; ISBN 1355254971019.

139. Goh, G.D.; Yap, Y.L.; Tan, H.K.J.; Sing, S.L.; Goh, G.L.; Yeong, W.Y. Process–Structure–Properties in Polymer Additive Manufacturing via Material Extrusion: A Review. *Crit. Rev. Solid State Mater. Sci.* **2020**, *45*, 113–133, doi:10.1080/10408436.2018.1549977.

140. Bhandari, S.; Lopez-Anido, R.A.; Gardner, D.J. Enhancing the Interlayer Tensile Strength of 3D Printed Short Carbon Fiber Reinforced PETG and PLA Composites via Annealing. *Addit. Manuf.* **2019**, *30*, 100922, doi:10.1016/j.addma.2019.100922.

141. Yang, K.; Grant, J.C.; Lamey, P.; Joshi-Imre, A.; Lund, B.R.; Smaldone, R.A.; Voit, W. Diels–Alder Reversible Thermoset 3D Printing: Isotropic Thermoset Polymers via Fused Filament Fabrication. *Adv. Funct. Mater.* **2017**, *27*, 1–11, doi:10.1002/adfm.201700318.

142. Nguyen, N.A.; Bowland, C.C.; Naskar, A.K. A General Method to Improve 3D-Printability and Inter-Layer Adhesion in Lignin-Based Composites. *Appl. Mater. Today* **2018**, *12*, 138–152, doi:10.1016/j.apmt.2018.03.009.

143. Gao, X.; Zhang, D.; Wen, X.; Qi, S.; Su, Y.; Dong, X. Fused Deposition Modeling with Polyamide 1012. *Rapid Prototyp. J.* **2019**, *25*, 1145–1154, doi:10.1108/RPJ-09-2018-0258.

144. Shih, C.C.; Burnette, M.; Staack, D.; Wang, J.; Tai, B.L. Effects of Cold Plasma Treatment on Interlayer Bonding Strength in FFF Process. *Addit. Manuf.* **2019**, *25*, 104–111, doi:10.1016/j.addma.2018.11.005.

145. Shaffer, S.; Yang, K.; Vargas, J.; Di Prima, M.A.; Voit, W. On Reducing Anisotropy in 3D Printed Polymers via Ionizing Radiation. *Polymer (Guildf).* **2014**, *55*, 5969–5979, doi:10.1016/j.polymer.2014.07.054.

146. Meng, S.; He, H.; Jia, Y.; Yu, P.; Huang, B.; Chen, J. Effect of Nanoparticles on the Mechanical Properties of Acrylonitrile–Butadiene–Styrene Specimens Fabricated by Fused Deposition Modeling. *J. Appl. Polym. Sci.* **2017**, *134*, 1–9, doi:10.1002/app.44470.

147. Gao, X.; Zhang, D.; Qi, S.; Wen, X.; Su, Y. Mechanical Properties of 3D Parts Fabricated by Fused Deposition Modeling: Effect of Various Fillers in Polylactide. *J. Appl. Polym. Sci.* **2019**, *136*, 1–10, doi:10.1002/app.47824.

148. Dodziuk, H. Applications of 3D Printing in Healthcare. *Kardiochirurgia i Torakochirurgia Pol.* **2016**, *13*, 283–293, doi:10.5114/kitp.2016.62625.

149. Ventola, C.L. Medical Applications for 3D Printing: Current and Projected Uses. *Pharm. Ther.* **2014**, *39*, 704–711, doi:10.1016/j.infsof.2008.09.005.

150. Bertol, L.S.; Júnior, W.K.; Silva, F.P. da; Aumund-Kopp, C. Medical Design: Direct Metal Laser Sintering of Ti-6Al-4V. *Mater. Des.* **2010**, *31*, 3982–3988, doi:10.1016/j.matdes.2010.02.050.

151. Hao, L.; Savalani, M.M.; Zhang, Y.; Tanner, K.E.; Harris, R.A. Selective Laser Sintering of Hydroxyapatite Reinforced Polyethylene Composites for Bioactive Implants and Tissue Scaffold Development. *Proc. Inst. Mech. Eng. Part H J. Eng. Med.* **2006**, *220*, 521–531, doi:10.1243/09544119JEIM67.

152. Dienel, K.E.G.; Van Bochove, B.; Seppälä, J. V. Additive Manufacturing of Bioactive Poly(Trimethylene Carbonate)/β-Tricalcium Phosphate Composites for Bone Regeneration. *Biomacromolecules* **2020**, *21*, 366–375, doi:10.1021/acs.biomac.9b01272.

153. Guillaume, O.; Geven, M.A.; Sprecher, C.M.; Stadelmann, V.A.; Grijpma, D.W.; Tang, T.T.; Qin, L.; Lai, Y.; Alini, M.; de Bruijn, J.D.; et al. Surface-Enrichment with Hydroxyapatite Nanoparticles in Stereolithography-Fabricated Composite Polymer Scaffolds Promotes Bone Repair. *Acta Biomater.* **2017**, *54*, 386–398, doi:10.1016/j.actbio.2017.03.006.

154. Larsson Wexell, C.; Thomsen, P.; Aronsson, B.O.; Tengvall, P.; Rodahl, M.; Lausmaa, J.; Kasemo, B.; Ericson, L.E. Bone Response to Surface-Modified Titanium Implants: Studies on the Early Tissue Response to Implants with Different Surface Characteristics. *Int. J. Biomater.* **2013**, doi:10.1155/2013/412482.

155. Mangano, C.; Mangano, F.; Shibli, J.A.; Ricci, M.; Sammons, R.L.; Figliuzzi, M. Morse Taper Connection Implants Supporting "Planned" Maxillary and Mandibular Bar-Retained Overdentures: A 5-Year Prospective Multicenter Study. *Clin. Oral Implants Res.* **2011**, *22*, 1117–1124, doi:10.1111/j.1600-0501.2010.02079.x.

156. Murr, L.E.; Gaytan, S.M.; Martinez, E.; Medina, F.; Wicker, R.B. Next Generation Orthopaedic Implants by Additive Manufacturing Using Electron Beam Melting. *Int. J. Biomater.* **2012**, *2012*, doi:10.1155/2012/245727.

157. Mullen, L.; Stamp, R.C.; Brooks, W.K.; Jones, E.; Sutcliffe, C.J. Selective Laser Melting: A Regular Unit Cell Approach for the Manufacture of Porous, Titanium, Bone in-Growth Constructs, Suitable for Orthopedic Applications. *J. Biomed. Mater. Res. - Part B Appl.*

Biomater. **2009**, *89*, 325–334, doi:10.1002/jbm.b.31219.

158. Mangano, F.; Pozzi-Taubert, S.; Zecca, P.A.; Luongo, G.; Sammons, R.L.; Mangano, C. Immediate Restoration of Fixed Partial Prostheses Supported by One-Piece Narrow-Diameter Selective Laser Sintering Implants: A 2-Year Prospective Study in the Posterior Jaws of 16 Patients. *Implant Dent.* **2013**, *22*, 388–393, doi:10.1097/ID.0b013e31829afa9d.

159. Mangano, F.G.; De Franco, M.; Caprioglio, A.; MacChi, A.; Piattelli, A.; Mangano, C. Immediate, Non-Submerged, Root-Analogue Direct Laser Metal Sintering (DLMS) Implants: A 1-Year Prospective Study on 15 Patients. *Lasers Med. Sci.* **2014**, *29*, 1321–1328, doi:10.1007/s10103-013-1299-0.

160. Figliuzzi, M.; Mangano, F.; Mangano, C. A Novel Root Analogue Dental Implant Using CT Scan and CAD/CAM: Selective Laser Melting Technology. *Int. J. Oral Maxillofac. Surg.* **2012**, *41*, 858–862, doi:10.1016/j.ijom.2012.01.014.

161. Wang, Z.; Zhang, M.; Liu, Z.; Wang, Y.; Dong, W.; Zhao, S.; Sun, D. Biomimetic Design Strategy of Complex Porous Structure Based on 3D Printing Ti-6Al-4V Scaffolds for Enhanced Osseointegration. *Mater. Des.* **2022**, *218*, 110721, doi:https://doi.org/10.1016/j.matdes.2022.110721.

162. Kan, J.; Roe, P.; Rungcharassaeng, K. Effects of Implant Morphology on Rotational Stability During Immediate Implant Placement in the Esthetic Zone. *Int. J. Oral Maxillofac. Implants* **2015**, *30*, 667–670, doi:10.11607/jomi.3885.

163. Barazanchi, A.; Li, K.C.; Al-Amleh, B.; Lyons, K.; Waddell, J.N. Additive Technology: Update on Current Materials and Applications in Dentistry. *J. Prosthodont.* **2017**, *26*, 156–163, doi:10.1111/jopr.12510.

164. Mangano, C.; Bianchi, A.; Mangano, F.G.; Dana, J.; Colombo, M.; Solop, I.; Admakin, O. Custom-Made 3D Printed Subperiosteal Titanium Implants for the Prosthetic Restoration of the Atrophic Posterior Mandible of Elderly Patients: A Case Series. *3D Print. Med.* **2020**, *6*, 1–14, doi:10.1186/s41205-019-0055-x.

165. Zein, I.; Hutmacher, D.W.; Tan, K.C.; Teoh, S.H. Fused Deposition Modeling of Novel Scaffold Architectures for Tissue Engineering Applications. *Biomaterials* **2002**, *23*, 1169–1185.

166. Lam, C.X..; Mo, X..; Teoh, S..; Hutmacher, D.. Scaffold Development Using 3D Printing with a Starch-Based Polymer. *Mater. Sci. Eng. C* **2002**, *20*, 49–56, doi:10.1016/S0928-4931(02)00012-7.

167. Gioumouxouzis, C.I.; Karavasili, C.; Fatouros, D.G. Recent Advances in Pharmaceutical Dosage Forms and Devices Using Additive Manufacturing Technologies. *Drug Discov. Today* **2019**, *24*, 636–643, doi:10.1016/j.drudis.2018.11.019.

168. *3D Printed Drugs Market Research Report by Technology (Direct-Write, Fused Deposition Modelling, and Inkjet Printing), End User, Region (Americas, Asia-Pacific, and Europe, Middle East & Africa) - Global Forecast to 2026 - Cumulative Impact of COVID-19*; 2022;

169. Dey, A.; Eagle, I.N.R.; Yodo, N. A Review on Filament Materials for Fused Filament Fabrication. *J. Manuf. Mater. Process.* **2021**, *5*, doi:10.3390/jmmp5030069.

170. Dumpa, N.; Butreddy, A.; Wang, H.; Komanduri, N.; Bandari, S.; Repka, M.A. 3D Printing in Personalized Drug Delivery: An Overview of Hot-Melt Extrusion-Based Fused

Deposition Modeling. *Int. J. Pharm.* **2021**, *600*, 120501, doi:10.1016/j.ijpharm.2021.120501.

171. Mora-Castaño, G.; Millán-Jiménez, M.; Linares, V.; Caraballo, I. Assessment of the Extrusion Process and Printability of Suspension-Type Drug-Loaded Affinisol™ Filaments for 3D Printing. *Pharmaceutics* **2022**, *14*, doi:10.3390/pharmaceutics14040871.

172. Kontárová, S.; Přikryl, R.; Melčová, V.; Menčík, P.; Horálek, M.; Figalla, S.; Plavec, R.; Feranc, J.; Sadílek, J.; Pospíšilová, A. Printability, Mechanical and Thermal Properties of Poly(3-Hydroxybutyrate)-Poly(Lactic Acid)-Plasticizer Blends for Three-Dimensional (3D) Printing. *Materials (Basel).* **2020**, *13*, doi:10.3390/ma13214736.

173. Bajwa, D.; Eichers, M.; Shojaeiarani, J.; Kallmeyer, A. Influence of Biobased Plasticizers on 3D Printed Polylactic Acid Composites Filled with Sustainable Biofiller. *Ind. Crops Prod.* **2021**, *173*, 114132, doi:https://doi.org/10.1016/j.indcrop.2021.114132.

174. Jayasuriya, C.K. Interfacial Bonding in Polymer–Ceramic Nanocomposites. In *Reference Module in Materials Science and Materials Engineering*; Elsevier, 2017 ISBN 978-0-12-803581-8.

175. Pascual-González, C.; de la Vega, J.; Thompson, C.; Fernández-Blázquez, J.P.; Herráez-Molinero, D.; Biurrun, N.; Lizarralde, I.; del Río, J.S.; González, C.; LLorca, J. Processing and Mechanical Properties of Novel Biodegradable Poly-Lactic Acid/Zn 3D Printed Scaffolds for Application in Tissue Regeneration. *J. Mech. Behav. Biomed. Mater.* **2022**, *132*, 105290, doi:https://doi.org/10.1016/j.jmbbm.2022.105290.

176. Pascual-González, C.; Thompson, C.; de la Vega, J.; Biurrun Churruca, N.; Fernández-Blázquez, J.P.; Lizarralde, I.; Herráez-Molinero, D.; González, C.; LLorca, J. Processing and Properties of PLA/Mg Filaments for 3D Printing of Scaffolds for Biomedical Applications. *Rapid Prototyp. J.* **2022**, *28*, 884–894, doi:10.1108/RPJ-06-2021-0152.

177. Roulon, S.; Soulairol, I.; Lavastre, V.; Payre, N.; Cazes, M.; Delbreilh, L.; Alié, J. Production of Reproducible Filament Batches for the Fabrication of 3D Printed Oral Forms. *Pharmaceutics* **2021**, *13*, doi:10.3390/pharmaceutics13040472.

178. Xiao, J.; Gao, Y. The Manufacture of 3D Printing of Medical Grade TPU. *Prog. Addit. Manuf.* **2017**, *2*, 117–123, doi:10.1007/s40964-017-0023-1.

179. Melocchi, A.; Parietti, F.; Maroni, A.; Foppoli, A.; Gazzaniga, A.; Zema, L. Hot-Melt Extruded Filaments Based on Pharmaceutical Grade Polymers for 3D Printing by Fused Deposition Modeling. *Int. J. Pharm.* **2016**, *509*, 255–263, doi:10.1016/j.ijpharm.2016.05.036.

180. Mohseni, M.; Hutmacher, D.W.; Castro, N.J. Independent Evaluation of Medical-Grade Bioresorbable Filaments for Fused Deposition Modelling/Fused Filament Fabrication of Tissue Engineered Constructs. *Polymers (Basel).* **2018**, *10*, doi:10.3390/polym10010040.

181. Jung, S.Y.; Lee, S.J.; Kim, H.Y.; Park, H.S.; Wang, Z.; Kim, H.J.; Yoo, J.J.; Chung, S.M.; Kim, H.S. 3D Printed Polyurethane Prosthesis for Partial Tracheal Reconstruction: A Pilot Animal Study. *Biofabrication* **2016**, *8*, 045015, doi:10.1088/1758-5090/8/4/045015.

182. Hung, K.C.; Tseng, C.S.; Hsu, S.H. Synthesis and 3D Printing of Biodegradable Polyurethane Elastomer by a Water-Based Process for Cartilage Tissue Engineering Applications. *Adv. Healthc. Mater.* **2014**, *3*, 1578–1587, doi:10.1002/adhm.201400018.

183. Hung, K.C.; Tseng, C.S.; Dai, L.G.; Hsu, S. hui Water-Based Polyurethane 3D Printed Scaffolds with Controlled Release Function for Customized Cartilage Tissue Engineering. *Biomaterials* **2016**, *83*, 156–168, doi:10.1016/j.biomaterials.2016.01.019.

184. Chen, Q.; Mangadlao, J.D.; Wallat, J.; De Leon, A.; Pokorski, J.K.; Advincula, R.C. 3D Printing Biocompatible Polyurethane/Poly(Lactic Acid)/Graphene Oxide Nanocomposites: Anisotropic Properties. *ACS Appl. Mater. Interfaces* **2017**, *9*, 4015–4023, doi:10.1021/acsami.6b11793.

185. Tsai, K.J.; Dixon, S.; Hale, L.R.; Darbyshire, A.; Martin, D.; de Mel, A. Biomimetic Heterogenous Elastic Tissue Development. *npj Regen. Med.* **2017**, *2*, 16, doi:10.1038/s41536-017-0021-4.

CHAPTER II

GUIDE TO ARTICLES IN THE DISSERTATION

2. Guide to articles in the dissertation

The basis of the presented doctoral dissertation is a series of six publications, which are described in detail in Chapter IV:

PAPER 1 **Haryńska A.,** Gubanska I., Kucinska-Lipka J., Janik H. Fabrication and Characterization of Flexible Medical-Grade TPU Filament for Fused Deposition Modeling 3DP Technology. *Polymers (Basel).* 2018, *10*, 1304, doi:10.3390/polym10121304.
(Q1 – polymers and plastics, IF_{2018}=3.164, MEiN = 100 pts)

PAPER 2 **Haryńska A.,** Kucinska-Lipka J., Sulowska A., Gubanska I., Kostrzewa M., Janik H. Medical-Grade PCL Based Polyurethane System for FDM 3D Printing—Characterization and Fabrication. *Materials (Basel).* 2019, *12*, 887, doi:10.3390/ma12060887.
(Q2 – material science, IF_{2019}=3.057, MEiN = 140 pts)

PAPER 3 **Haryńska A.,** Carayon I., Kosmela P., Brillowska-Dąbrowska A., Łapiński M., Kucińska-Lipka J., Janik H. Processing of Polyester-Urethane Filament and Characterization of FFF 3D Printed Elastic Porous Structures with Potential in Cancellous Bone Tissue Engineering. *Materials (Basel).* 2020, *13*, 4457, doi:10.3390/ma13194457.
(Q2 – material science, IF_{2019}=3.057, MEiN = 140 pts)

PAPER 4 **Haryńska A.,** Carayon I., Kosmela P., Szeliski K., Łapiński M., Pokrywczyńska M., Kucińska-Lipka J., Janik, H. A comprehensive evaluation of flexible FDM/FFF 3D printing filament as a potential material in medical application. *Eur. Polym. J.* 2020, *138*, doi:10.1016/j.eurpolymj.2020.109958.
(Q1 – polymers and plastics, IF_{2019}=3.862, MEiN = 100 pts)

PAPER 5 **Haryńska A.** (Przybytek A.), Sienkiewicz M., Kucińska-Lipka J., Janik H. Preparation and characterization of biodegradable and compostable PLA/TPS/ESO compositions. *Ind. Crops Prod.* 2018, *122*, doi:10.1016/j.indcrop.2018.06.016.
(Q1 – agronomy and crop science, IF_{2018}=4.244, MEiN = 200 pts)

PAPER 6 **Haryńska A.,** Janik H., Sienkiewicz M,. Mikolaszek B,. Kucińska-Lipka J. PLA–potato thermoplastic starch filament as a sustainable alternative to conventional PLA filament: processing, characterization and FFF 3D printing. *ACS Sustain. Chem. Eng.* 2021, 9(20), 6923-6938, doi.org/10.1021/acssuschemeng.0c09413.
(Q1 – environmental chemistry, IF_{2020}=8.198, MEiN = 140 pts)

The presented series of publications can be ordered and classified according to the type of studied material and the application (as shown in **Figure 7**).

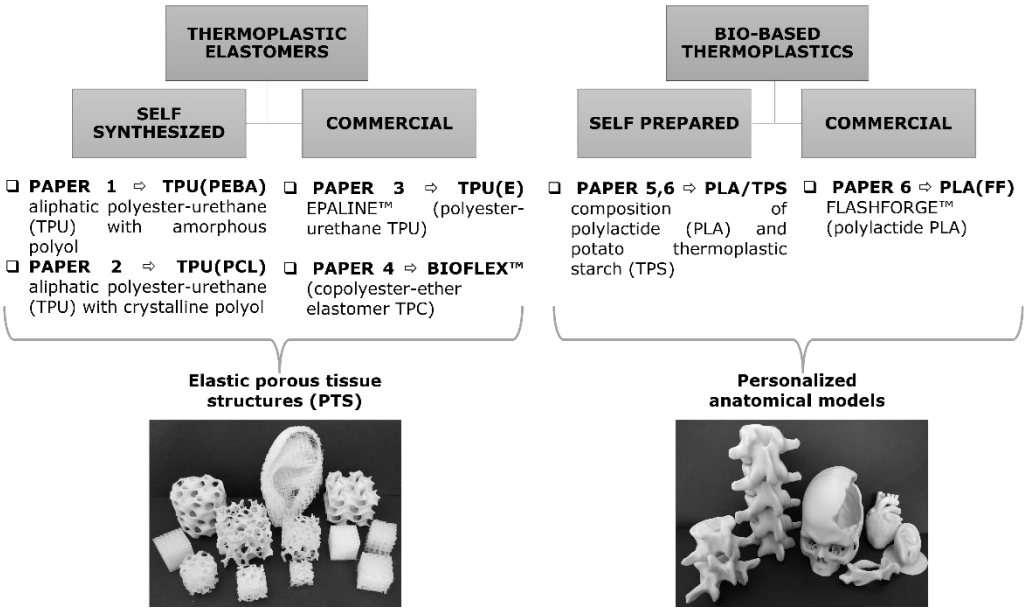

Figure 7 Research design - classification by type of studied material and possible application.

In general, the thesis focuses on the study of new medical-grade materials (filaments) for extrusion-based 3D printers (FDM™/FFF). The literature and market review towards types and limitations of available medical 3D printing filaments indicated the need to develop modern solutions which cover biocompatible materials with enhanced flexibility as well as those obtained from raw materials of plant origin. Consequently, the first four papers **(PAPER 1–4)** are devoted to the study of flexible and biocompatible filaments from the group of thermoplastic elastomers for printing of elastic porous 3D structures. The other two papers **(PAPER 5,6)** present the development of a fully bio-based thermoplastic filament as an alternative biomaterial for 3D printing of personalized anatomical models. The research conducted also includes commercial products in order to compare them with filaments developed during the doctoral studies, as well as to provide a better understating of the process of filament formation and their properties **(PAPER 4,6).**

CHAPTER III

OBJECTIVE AND SCOPE

3.1 Objective of the dissertation

The main objective of the dissertation was the synthesis and/or obtaining by blending new polymeric materials and the formation of 3D-printable medical-grade filaments from them, and then design and 3D printing of structures applicable in medicine.

The intended objective was achieved through:

1) **Elaboration of new thermoplastic polymer materials (a-c),** in which components suitable in biomaterials, were used, namely:

   a) Thermoplastic elastomer **TPU(PEBA)**: uncatalyzed thermoplastic poly(ester urethane) (PEBA/HDI/BDO)

      Components: amorphous polyol [α,ω-dihydroxy(ethylene-butylene adipate) diol (PEBA)], aliphatic di-isocyanate [1,6-hexamethylene di-isocyanate (HDI)], linear chain extender [1,4-butanediol (BDO)]

   b) Thermoplastic elastomer **TPU(PCL)**: uncatalyzed thermoplastic poly(ester urethane) (PCL/HDI/BDO)

      Components: crystalline polyol [(ε-caprolactone) diol (PCL)], aliphatic di-isocyanate [1,6-hexamethylene di-isocyanate (HDI)], linear chain extender [1,4-butanediol (BDO)]

   c) Bio-based thermoplastic **PLA/TPS**: fully plant origin composition (PLA/PS/ESO/pG)

      Components: polylactide (PLA), thermoplastic potato starch (TPS) [potato starch (PS) + plant glycerin (pG)], epoxidized soybean oil (ESO)

2) **Formation of 3D-printable filaments** from elaborated [TPU(PEBA), TPU(PCL), PLA/TPS] and commercial [TPU(E)] materials by melt extrusion and description of the process both on a laboratory (discontinuous manner) and technical (continuous manner) scale.

3) **Design and 3D printing** of the structures with potential in medical applications, namely:

   - elastic porous 3D structures for tissue engineering [TPU(E), Bioflex™]
   - personalized anatomical models for surgical training systems and pre-operative planning procedures [PLA/TPS, PLA(FF)]

3.2 Scope of experimental research

The scope of research work covered six tasks (**Figure 8**), which are described in details in **Table 5**.

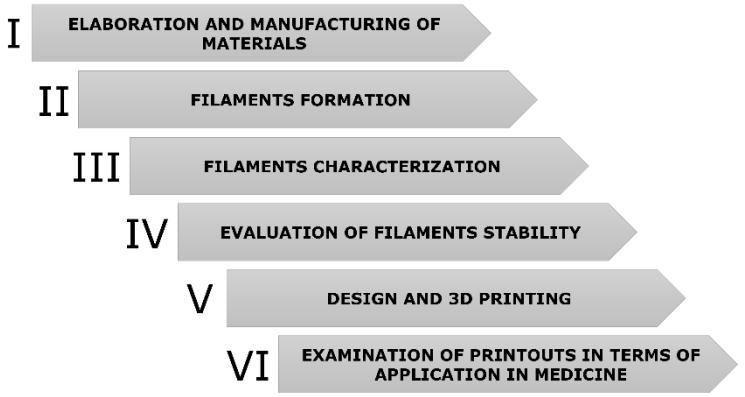

Figure 8 Research tasks of the doctoral dissertation.

Table 5 A detailed description of the research tasks and experimental stages (I, II, III, IV, V, VI).

I. ELABORATION AND MANUFACTURING OF MATERIALS	
Development of raw materials to the production of 3D-printable medical-grade filaments and characterization of the formed materials	
Thermoplastic polyurethanes (TPUs) [PAPER 1,2]	Bio-based thermoplastic blends [PAPER 5]
Scope of research: - elaboration of conditions for uncatalyzed synthesis of aliphatic poly(ester urethanes) differing in the type of polyol i.e. amorphous (PEBA) [PAPER 1], crystalline (PCL) [PAPER 2]. The optimization consisting of selection of the appropriate equipment, temperature, and reaction time, stirring intensity, reagent ratio, as well as gelation and annealing time; - determination of the content of free isocyanate groups by the acidimetric method. In this way, the degree of conversion of the reactants was	**Scope of research:** - preparation of a fully plant origin biodegradable compositions based on polylactide (PLA) and potato thermoplastic starch (TPS) modified with epoxidized soybean oil (ESO). Optimization of processing parameters for melt extrusion procedure to obtain the proper composition, i.e. raw materials ratio, temperature, and speed of extrusion; - determination of the melt flow index using load plastometer - determination of mechanical properties (tensile testing, hardness, impact testing);

controlled, thus determining the required synthesis time; - confirmation of the chemical structure of the TPUs *via* Fourier-transform infrared spectroscopy (FTIR) and Raman spectroscopy; - study of thermal properties of selected TPUs by thermogravimetric analysis (TGA) and differential scanning calorimetry (DSC); - determination of the melt flow rate (MFR) of selected TPUs using load plastometer; - determination of mechanical properties (tensile testing, hardness); - assessment of the wettability by measurement of water contact angle and surface free energy *via* goniometer uses sessile drop technique; - assessment of susceptibility to degradation by long-, and short-term incubation study in PBS, NaOH, and HCl media, as well as water absorption test; - assessment of biological properties *in vitro* of selected TPUs by indirect cytotoxicity test and short-term hemocompatibility test;	- characterization of the blends morphology by analyzing the scanning electron microscope (SEM) micrographs of the fractures surfaces; - study of thermal properties by differential scanning calorimetry (DSC); - analysis of water absorption of the compositions; - preliminary assessment of the compostability with a laboratory-simulated composting test;
II. FILAMENTS FORMATION	
Optimization and description of the filament-forming process	
Discontinuous manner (laboratory scale) [PAPER 1,2]	Continuous manner (technical scale) [PAPER 3,6]
Scope of research: - preparation of the feedstock (granulation, and drying); - optimization of the filament-forming process by adjusting the extrusion parameters (temperature profile, extrusion velocity, and dosing ratio) and the method of collecting the extrudate (filament) as well as	**Scope of research:** - preparation of the feedstock (granulation, and drying); - optimization of the filament-forming process by adjusting the extrusion parameters (temperature profile, head pressure, extrusion velocity), setting parameters of the calibration zones and winding system (type and

selecting the appropriate forming nozzle; - manual and random control of the filament diameter with an electronic caliper.	temperature of cooling medium, calibrators diameter, pulling velocity); - continuous filament diameter control with a laser sensor.

III. FILAMENTS CHARACTERIZATION

A comprehensive characterization of the self-prepared and commercial filaments [PAPER 1,3,4,6]

Scope of research:

The characteristics included the analysis of: (measurement technique)

- chemical structure (FTIR, Raman, H-NMR, XRD);
- thermal properties (DSC, TG);
- thermomechanical properties (DMA);
- rheological properties (MFR);
- contact angle and surface free energy (a goniometer using the sessile drop technique);
- mechanical properties (tensile testing, hardness, Charpy impact test, uniaxial compression test, calculation of brittleness);
- preliminary studies of biocompatibility (cytotoxicity, hemocompatibility);
- estimation of the printability of the filaments by measuring the accuracy of the 3D printouts against the digital models.

IV. EVALUATION OF FILAMENTS STABILITY

Analysis of selected properties of the self-prepared and commercial filaments before and after the 3D printing process [PAPER 3,4,6]

Scope of research:

- comparison of the chemical structure of the filament and the printout based on the obtained FTIR, Raman and H-NMR spectra;
- comparison of the thermal characteristic of the filament and printout based on thermograms obtained from DSC and TG measurements;
- comparison of the rheological properties of the filament and printout based on obtained MFI values

V. DESIGN AND 3D PRINTING

Design of digital models and optimization of the 3D printing parameters [PAPER 3,4,6]

Scope of research:

- creation of digital 3D models of porous structures differing in architecture, shape and dimensions of the pores *via* Autodesk Inventor software [PAPER 3,4,6];
- creation of digital 3D models of personalized anatomical structures directly from CT scans using 3D Slicer platform (segmentation, slicing and modelling) [PAPER 6];

<table>
<tr><td colspan="2">- preparation the models for the 3D printing process using slicer software (selection of 3D printing parameters and modelling of supporting structures) [PAPER 3,4,6];</td></tr>
<tr><th colspan="2">VI. EXAMINATION OF PRINTOUTS IN TERMS OF APPLICATION IN MEDICINE</th></tr>
<tr><td colspan="2">Preliminary evaluation of bio properties, degradability, or compostability of the printed 3D structures</td></tr>
<tr><td>Elastic porous 3D structures (thermoplastics elastomers) [PAPER 3,4]</td><td>Personalized anatomical models (bio-based thermoplastics) [PAPER 6]</td></tr>
<tr><td>Scope of research:
- study of biocompatibility of the elastic porous 3D structures by in vitro cytotoxicity test with MTT assay using fibroblasts-type cells line;
- evaluation of bioactivity of the elastic porous 3D structures in simulated body fluid (SBF) and monitoring of the mineralization process by mass measurements, SEM-EDS, Raman spectroscopy, and compression test
- degradation study of the elastic porous 3D structures through long and short-term incubation in selected media and monitoring of ongoing changes with FTIR spectroscopy, optical microscopy (OM), scanning electron microscopy (SEM), and mass measurement.</td><td>Scope of research:
- assessment of compostability of the printouts by measuring the degree of disintegration under simulated composting conditions and monitoring of outgoing changes with FTIR spectroscopy, optical microscopy, and scanning electron microscopy (SEM);
- study of the printouts degradability by incubation in PBS solution and canola oil, and monitoring of outgoing changes with FTIR spectroscopy, mass, swelling and pH measurements, optical microscopy, and scanning electron microscopy (SEM);
- evaluation of the quality and accuracy of obtained personalized anatomical models, printed from PLA/TPS, by comparing them with virtual models and models obtained using commercial filament.</td></tr>
</table>

To accomplish the above tasks, in the presented doctoral dissertation multidisciplinary research were undertaken, including:

- material synthesis and characterization;
- optimization of technological processes;
- computer modelling of 3D structures;
- 3D printing;
- preliminary biological studies.

In the course of the research, new medical-grade filaments were obtained, and the method of their formation into porous scaffolds with potential for tissue engineering and personalized anatomical models suitable for composting was presented. The results of the performed research tasks have been published in scientific journals indexed in the Journal Citation Reports (JCR) (described below in Chapter IV). Thus, the published papers concerned with the dissertation completed the current state of knowledge regarding the synthesis, processing, and characterization of medical-grade 3D printing filaments.

CHAPTER IV
PUBLICATIONS

4.1 PAPER 1: Fabrication and Characterization of Flexible Medical-Grade TPU Filament for Fused Deposition Modeling 3DP Technology

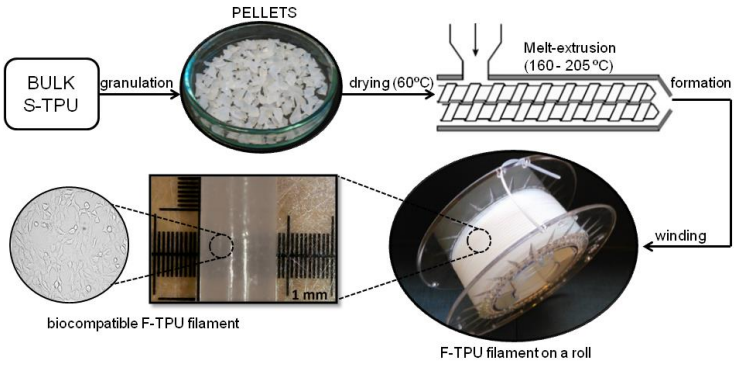

Graphical abstract, source: DOI:10.3390/polym10121304

Authors (contribution): Agnieszka Haryńska (40%), Iga Gubanska (20%), Justyna Kucinska-Lipka (20%), Helena Janik (20%)

Journal: Polymers (Basel)

DOI: 10.3390/polym10121304

Index: Q1, IF_{2018}=3.164, MNSiW = 100 pts

CRediT: Data Curation (lead), Formal Analysis (lead), Investigation (lead: density, melt flow rate (MFR), tensile strength, hardness, optical microscopy, accelerated degradation), Methodology (in part), Project Administration (in part), Visualization (lead), Writing – Original Draft Preparation (lead), Writing – Review & Editing (lead).

Realized doctoral research tasks:
I (material design and characterization) – elaboration of uncatalyzed synthesis of medical-grade poly(ester urethane) (TPU) based on aliphatic di-isocyanate (HDI) and amorphous polyol (PEBA), and characterization of the formed materials;
II (filament formation) – formation of 3D-printable filaments using synthesized TPU on a laboratory scale in a discontinuous manner;
III (filament characterization) – characterization of the formed TPU filaments including preliminary studies of biocompatibility, degradability and wettability;
V (3D printing) – preliminary trials of 3D printing using the TPU filament with most favorable properties.

Material code: TPU(PEBA)

BRIEF DESCRIPTION OF THE PUBLICATION

Discussed topics: the use of additive technologies in medicine; review of available medical-grade filaments for FFF 3D printing; advantages of thermoplastic polyurethanes in medical application.

Scope of the publication: polyurethane uncatalyzed synthesis; filament formation in a laboratory-scale; comparison of material properties before and after the melt-extrusion process.

Novelty of the publication: uncatalyzed synthesis of the thermoplastic poly(ester urethane) based on amorphous polyol (PEBA) and aliphatic di-isocyanate (HDI) for 3D printing technology.

Main scientific achievement: development of non-catalytic synthesis of the thermoplastic poly(ester urethane); fabrication of a novel, elastic filament for FFF 3D printing technology with potential in medical application.

Outline: The article presents the synthesis route, characteristics, and formation process of the medical-grade thermoplastic poly(ester urethane) (TPU) filament for FFF 3D printing. The material was successfully synthesized using amorphous α,ω- dihydroxy(ethylene-butylene adipate) diol (PEBA), aliphatic 1,6-hexamethylene di-isocyanate (HDI), and linear chain extender 1,4-butanediol (BDO). The synthesis was carried out without the use of a catalyst to avoid any possible increase in material toxicity. The chemical structure was analyzed using FTIR spectroscopy whereas mechanical properties by hardness and tensile testing. Rheological properties were studied *via* MFR measurements. Optimum processing parameters and apparatus leading to stable filament were captured and discussed. The stability of the TPU filament was also evaluated by studying selected properties before and after the forming process. Initial studies of the biological properties included indirect cytotoxicity and short-term hemocompatibility tests as well as short-term degradation studies, and water contact angle measurements. By comparing the properties of the filament and the synthesized material, it has been proven that the filament-formation process does not change the properties of the filament which remains biocompatible and hemocompatible. The resulting material exhibits mechanical properties comparable to commercial medical-grade polyurethanes, is hydrophilic and prone to degradation. The conducted research allowed to optimize the reaction conditions of uncatalyzed poly(ester urethanes) and demonstrate significant material properties. In addition, the results indicate that the synthesized TPU can be successfully formed into a filament for extrusion-based 3D printing, and is promising for biomedical application.

DEPARTMENT OF
POLYMER TECHNOLOGY

polymers

MDPI

Article

Fabrication and Characterization of Flexible Medical-Grade TPU Filament for Fused Deposition Modeling 3DP Technology

Agnieszka Haryńska, Iga Gubanska, Justyna Kucinska-Lipka * and Helena Janik

Polymer Technology Department, Chemical Faculty, Gdansk University of Technology, Narutowicza Street 11/12, 80-232 Gdansk, Poland; agnieszka.harynska@pg.edu.pl (A.H.); igaguban@pg.edu.pl (I.G.); heljanik@pg.edu.pl (H.J.)
* Correspondence: juskucin@pg.edu.pl; Tel.: +48-(58)-347-12-14

Received: 23 October 2018; Accepted: 23 November 2018; Published: 25 November 2018

Abstract: The possibility of using additive manufacturing (AM) in the medicine area has created new opportunities in health care. This has contributed to a sharp increase in demand for 3D printers, their systems and materials that are adapted to strict medical requirements. We described herein a medical-grade thermoplastic polyurethane (S-TPU) which was developed and then formed into a filament for Fused Deposition Modeling (FDM) 3D printers during a melt-extrusion process. S-TPU consisting of aliphatic hexamethylene 1,6-diisocyanate (HDI), amorphous α,ω-dihydroxy(ethylene-butylene adipate) (PEBA) and 1,4 butandiol (BDO) as a chain extender, was synthesized without the use of a catalyst. The filament (F-TPU) properties were characterized by rheological, mechanical, physico-chemical and in vitro biological properties. The tests showed biocompatibility of the obtained filament as well as revealed no significant effect of the filament formation process on its properties. This study may contribute to expanding the range of medical-grade flexible filaments for standard low-budget FDM printers.

Keywords: medical-grade filament; thermoplastic polyurethane; fused deposition modeling; filament forming; 3D printing

1. Introduction

Additive manufacturing (AM) technologies have become a very effective and powerful tool in the health care industry [1–3]. Three-dimensional printers (3DP) are no longer the only rapid prototyping devices. The practical applications of an AM technology in medicine are more and more frequent. The use of 3D printers in combination with tools, such as computer-aided design (CAD) and radiographic methods (CT scans, MRI or X-rays), allows for the production of customized implants [4–6], or precise anatomical models for surgical planning [7,8]. Medical products fabricated via 3DP may be divided into five broad categories, i.e., surgical training systems (artificial organs, anatomical models), patient-matched devices (implants and prosthesis), tissue engineering constructs (scaffolds), pharmaceutical systems (drug delivery), as well reproduced tissues and organs. However, these medical products are characterized by different requirements and properties which are associated with the selection of proper material and a 3D printing technology. For example, reproduced temporal bones for drilling surgery training as well as artificial organs for a teaching purpose or preoperative planning should primarily exhibit high dimensional accuracy and organoleptic properties, e.g., texture, tactile sensation and viscoelasticity, which must imitate their biological counterparts [8,9]. Thus, 3D printed medical devices provide enormous assistance for surgeons and medical students. Moreover, tissue scaffolds, which have to provide physical support for new

growing tissues and promote tissue regeneration, primarily should be highly biocompatible and degradable within a given timeframe. They should also have a three-dimensional, highly porous structure, and exhibit appropriate mechanical properties similar to the regenerated tissues [10,11]. These strict medical requirements limit the possibility of using conventional 3D printing materials or systems. Therefore, there is a need to look for and develop more advanced solutions and materials. AM technologies differ in operational principles, used equipment and materials. It is worth mentioning that, according to ASTM F2792-10 [12], AM is the official term but 3D printing (3DP) is a common definition of the family of AM technologies. Several widely used 3D printing technologies in medicine are: selective laser sintering (SLS), PolyJet (PJ), stereolithography (SLA) and fused deposition modeling (FDM) [13]. Bioprinting is a separate branch of AM technologies designed to reproduce functional tissues/organs or create bioactive tissue scaffolds. In this process, biomaterials, different types of living cells/stem cells, nutrients, growths factors or photoinitiators are used, depending on the chosen 3D bioprinting technology. The main 3D bioprinting techniques are: inkjet-based (thermal or acoustic inducted deposition drop by drop materials known as "bioinks" [14]), laser-based (deposition of biomaterial droplets using high energy lasers e.g., laser-inducted forward transfer LIFT [15]), microextrusion-based (pneumatic or mechanical extrusion of the bioinks through a syringe with a piston [16]), cell electrospinning-based (deposition of liquid biomaterial in the form of droplets or fibers using a strong electric field [17]) or stereolithography-based (using the light-induced photo-polymerization process to create 3D bio-structures [18]). In References [14–18], the particular types of bioprinting were explained in more detail.

These innovative solutions, more sophisticated than FDM, require highly advanced machinery, equipment and materials, which are used by collaborating specialists in material engineering, biotechnology and surgery. FDM technology is one of the easiest to use and most cost-effective 3DP technologies, both in terms of purchase and service. According to Oskuti et. al, objects printed with the use of FDM are significantly less toxic than SLA-printed parts for living organisms [19]. FDM has already been successfully used for printing biomedical devices [20,21]. Additionally, a fast-growing open-source community provides access to expert solutions and knowledge in the use of FDM 3DPs, which further reduces costs and facilitates the use of these devices. FDM is based on the layered deposition of plasticized polymeric material on a movable platform. The polymeric material in the form of a filament is fed to the miniature temperature-controlled extruder, where the plasticization takes place. Filament is a thin wire with a strictly defined diameter. One of the filament formation methods is a melt extrusion process [22]. There is a variety of commercially available filament types that exhibit a wide range of properties, however, medical-grade filaments market is still developing. One of the few companies supplying certificated medical-grade filaments dedicated for FDM 3DP is Poly-Med (Anderson, SC, USA). Their series of filaments (Lactoprene® 100M, Caproprene® 100M, Max-Prene® 955, Dioxaprene® 100M) have been recently examined by Mohseni et al. [23] as potential materials for tissue engineering 3D constructs. The mentioned filaments are based on polylactide (PLA), polycaprolactone (PCL), poly(lactic-*co*-glicolic acid) (PLGA), and polydioxanone (PDO). Whereas, Bioflex® supplied by FiloAlfa (Ozzero, Italy) is a highly durable and flexible filament, belonging to the group of so-called thermoplastic elastomers (TPE). Its medical properties are confirmed by USP Class VI and ISO 10993-4/5/10 (cytotoxicity, hemolysis, intracutaneous and injection tests). However, degradation studies performed by our team showed that this material is highly resistant to acidic and alkaline environments (supplementary data 1). This significantly limits its use, for example, in tissue engineering constructs in which the material should degrade and resorb proportionally to the rate of tissue growth [24]. Currently, the most commonly used "medical" filaments for FDM 3D printers are thermoplastic biopolymers based on crystalline PLA or PCL. They provide satisfactory properties required for medical devices and structures such as biodegradability, bioresorbability and adequate/suitable durability [25–27]. However, there is lack of filaments available on the market, which provides properties (texture, flexibility, tactile sensation) that allow for native tissues or organs to mimic. These are important requirements in case of appropriate surgical training systems production

via 3DP technology for the surgeons and medical students [9]. Materials that may be alternative to medical filaments based on PCL and PLA are properly designed thermoplastic polyurethanes (TPUs). According to the literature, they exhibit biocompatibility and hemocompatibility [28]. Moreover, TPU degradation rate can be controlled as well [29]. Biostable TPUs are widely known and used in medicine as prosthetics, implants, artificial blood vessels, or gene carriers [30]. What is more, the TPUs have been already successfully applied as tissue-engineered scaffold [31], nerve guidance channels [32], breast implants, dialysis membranes, or aortic grafts [33]. Additionally, we have not recorded certified medical-grade TPU filaments available on the market. Whereas, studies performed by Jung et al. [34] and Tsai et al. [35] confirm the legitimacy of using appropriately designed TPUs (based on aromatic polyether urethane and Tecoflex®, respectively) as filaments to fabricate advanced structures for the tissue engineering purpose via FDM. Looking for new flexible medical-grade materials for filament fabrication may contribute to the popularization of low-budget FDM printers as a cost-effective tool in health care.

Based on these premises, in this paper, we report our studies on novel flexible and medical-grade filament (F-TPU), dedicated for FDM 3D printing technology. For this purpose, we have synthesized TPU using raw materials suitable for the synthesis of biomedical polyurethanes [36] like aliphatic hexamethylene 1,6-diisocyanate (HDI), amorphous α,ω-dihydroxy(ethylene-butylene adipate) (PEBA) and 1,4 butandiol (BDO) as a chain extender. A discussable subject in terms of polyurethane synthesis is the application of organotin catalysts like dibutyltin dilaurate (DBTDL) and stannous octoate ($Sn(Oct)_2$) [37,38]. To avoid the possible accumulation of these catalysts in the TPU matrix, which may affect the deterioration of biocompatibility and hemocompatibility of the material [39], we did not apply it in the synthesis of TPU described in this paper.

This study is divided into two main sections: The first section focuses on the synthesis in bulk and characterization of cast polyurethane (S-TPU) and filament fabrication (F-TPU) via melt-extrusion. The second part is devoted to impact assessment of the filament forming process on selected physico-chemical and in-vitro biological properties. S-TPU was processed in filament (1.75 mm diameter) via melt-extrusion process. Then, physico-mechanical, chemical and rheological properties (tensile test, hardness, FTIR, contact angle, melt flow rate (MFR)), were characterized. Finally, a series of preliminary biomedical studies, such as hemocompatibility and cytotoxicity tests (NIH 3T3 cells) were performed for both materials S-TPU and F-TPU in order to assess the influence of the processing procedure on their properties.

2. Experimental

2.1. S-TPU Synthesis

S-TPU was synthesized by standard two-step polymerization procedure (Figure 1) [28]. It was derived from amorphous PEBA (in contrary to polyurethanes (PURs) synthesized by using crystalline oligodiols [40,41]), aliphatic HDI and BDO chain extender. No catalysts were used in this synthesis (to avoid possible negative impact of the catalyst on the biocompatibility of the S-TPU [41,42]). In the first step, prepolymerization reaction (8 wt % of free isocyanate groups) was carried out at 90 °C for 6 h under vacuum by using PEBA and HDI. The reaction progress between PEBA and HDI over time was studied by the content of free isocyanate groups (F_{NCO} index) present in the prepolymer.

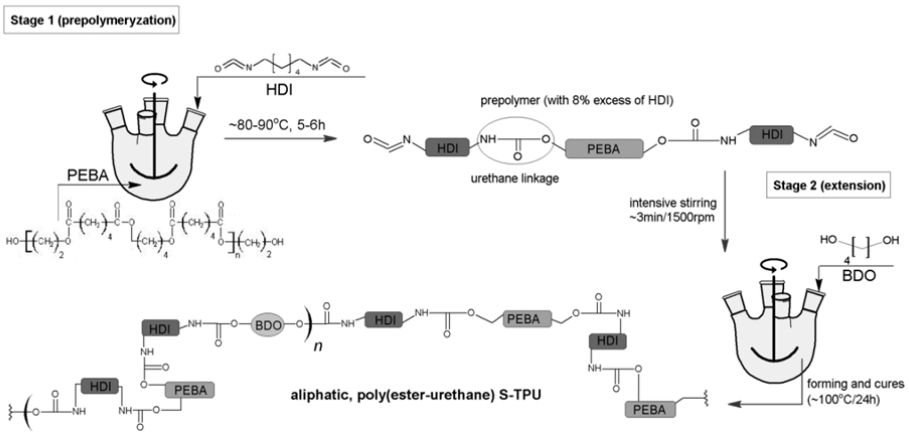

Figure 1. S-TPU synthesis scheme.

In the second step, the BDO was added to the reaction mixture in the molar ratio of unbounded isocyanate groups [NCO] (prepolymer) to hydroxyl groups [OH] (chain extender BDO) equal to 1.1:1. After 3 min of intensive stirring, the mixture was transferred into a mould, set at 80 °C, for 3 h. The gelling time of the reaction mixture in case of S-TPU obtained without the use of a catalyst was twice longer in comparison with TPU processed with 0.5% *w*/*w* of catalyst (dibutyltin dilaurate DBTDL) [36]. Finally, the samples were left in a heating furnace at 100 °C for 48 h to complete the reaction. At the end, obtained solid S-TPU was granulated to the size of 4 mm ± 1 mm (diameter) at room temperatures in a high-speed mill (speed 90 rpm, Wittmann Battenfeld, Grodzisk Mazowiecki, Poland) in order to have the material in the proper state be extruded. The detailed characteristics of used raw materials are given in Table 1.

Table 1. Characteristic and chemical structure of used raw materials for the S-TPUs synthesis.

Compound	Supplier	Description	Structure Formula
BDO	Brenntag, Germany	Low molecular chain extender, Mol mass = 88 g/mol, Physical state–clear liquid, Purity > 95.5%, Tm = 204 °C, Boiling point ~ 230 °C, ϱ (20 °C) = 1020 g/cm^3	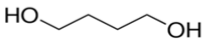
HDI	Sigma-Aldrich, Germany	Aliphatic diisocyanate, colorless liquid. Boiling point = 255 °C, Flash point = 130 °C, ϱ (25 °C) = 1.05 g/cm^3, Purity > 99%, Tm = −67 °C, Soluble in water, LD50 (rat) = 746 mg/kg.	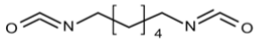
PEBA (POLIOS 55/20)	Purinova, Poland	Ester-based polyol, Mol mass = 2000 g/mol, Hydroxyl number = 54–58, Acid number–max. 0.6.	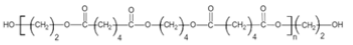

2.2. Identification of Free Isocyanate Groups

The determination of free isocyanate groups (F_{NCO}, %) was performed according to the PN-EN 1242:2006 standard. The percentage of free isocyanate groups was calculated by Formula (1);

$$\%NCO = \frac{(V_0 - V_1) * 0.4}{m} \quad (1)$$

% NCO–percentage of unbound isocyanate groups (% mass)

V_0—volume of HCl solution used for blank probe titration (cm^3)

V_1—volume of HCl solution used for the test sample titration (cm^3)
m—sample mass (g]

2.3. Melt-Extrusion of F-TPU Filament

Double-screw extruder IQLINE (EHP 2 × 20 IQ, Zamak Mercator, Skawina, Poland) with nine heating zones, was used to obtain F-TPU filament. The custom-made molding nozzle diameter was equal to 1.5 mm and the L/D screw ratio was 22. Several parameter combinations were tested in order to obtain F-TPU filament of stable diameter dimension. Filament diameter was controlled by an electronic caliper.

2.4. Material Characterization Techniques

2.4.1. Density

Six S-TPU samples of the 1 cm^2 area were weighed with accuracy to 0.0001 g and then transferred to the analytical balance adjusted to density measurements (RADWAG AS 310/X, Radwag, Radom, Poland). Density was calculated in comparison to distilled water (1.0 g/cm^3) at 20 °C.

2.4.2. Melt Flow Rate (MFR)

S-TPUs MFR determination was carried out by using a load plastometer (ZWICK/Roell, Wrocław, Poland) according to the PN-EN ISO 1133-1:2011 standard. The value of MFR is expressed as a 1 g of material extruded through the standard capillary (2075 mm diameter) placed in a heating nozzle during 10 min (g/10 min). The S-TPU granules used in this study weighted 5 g/measurement. The conditions to perform MFR study for S-TPUs were as follows: 180 °C and 5 kg. Three repetitions were performed and the results were an average.

2.4.3. Mechanical Characterization

Tensile strength and elongation at break were studied by using the universal testing machine Zwick & Roell Z020 (Wrocław, Poland) according to PN-EN ISO 527-2:2012 with a crosshead speed of 500 mm/min and initial force of 1 N. Five samples were studied and the results are an average. Hardness was measured by using Shore method according to PN-EN ISO 868:2005 standard. Obtained data were presented with Shore D degree (°Sh D). The results were an average of 10 measurements.

2.4.4. Fourier Transform Infrared Spectroscopy (FTIR)

The FTIR analysis was performed with the use of Nicolet 8700 Spectrometer (Thermo Fisher Scientific, Waltham, MA, USA) in the spectral range from 4000 to 500 cm^{-1} averaging 256 scans with a resolution of 4 cm^{-1}. The measurement was carried out both for the synthesized S-TPU and filament F-TPU.

2.4.5. Optical Microscopy (OM)

The surface of solid S-TPU and filament F-TPU was studied via reflection microscope. Samples were gold coated in the sputter coater Quorum 150T E. OM (Quorum Technologies Ltd., Laughton, GB) was performed at ×300 magnification.

2.4.6. Contact Angle (CA)

The CA of the solid S-TPU and filament F-TPU surfaces were determined at room temperature by using a Kruss Goniometer G10 (KRÜSS GmbH, Hamburg, Germany) with drop shape analysis software. A droplet of 2 μL volume was deposited on the samples surfaces and images were taken at the static conditions using a video instrument, drop shape analysis software DSA4. The results are an average of five measurement points randomly selected at the samples' surface.

2.5. Biological Characterization

2.5.1. Short-Term Hemocompatibility Test

Hemocompatibility test was conducted in Medical Academy Clinical Centre in Gdansk by using SYSMEX XS–1000i analyzer (Sysmex, Warszawa, Poland), according to the Polish ISO standard (PN-EN ISO 15189). Venous blood, from a healthy women served as a sample, which was placed in a sterile test-tube with an antithrombotic agent (potassium acetate), immediately after sampling. Then, the blood morphology of pure blood was conducted (served as reference parameters). Later, S-TPU and F-TPU samples were cut (8 cm^2 surface) and immersed in 8 mL of blood and then, placed in the sterile test-tubes. All the test specimens (S-TPU and F-TPU) were previously sterilized by using argon plasma generated over H_2O_2. The incubation time of the samples (S-TPU and F-TPU) in blood was 15 min (at room temperature). After this time, the samples were removed and the blood was tested again. The results are an average of six measurements.

2.5.2. Indirect Cytotoxicity Test

Cell Culture Mouse embryonic fibroblast NIH 3T3 cells were cultured in High Glucose Dulbecco's modified Eagle's medium (DMEM HG, Sigma Aldrich, Poznan, Poland) supplemented with 10% fetal bovine serum (FBS) and antibiotics (100 µg/mL each of penicillin and streptomycin) at 37 °C in a humidified atmosphere containing 5% CO_2. The effect of indirect MTT Proliferation Assay of S-TPU or F-TPU exposure on NIH 3T3 cell proliferation was determined by 3-(4,5-dimethylthiazol-2-yl)-2,5-diphenyl tetrazolium bromide (MTT) colorimetric assay using 100% concentrations of samples extract. Sterilization of each side of the samples were conducted in 70% ethanol (30 min) and then by UV (exposure for 1 h). Then, MPLT samples were placed in DMEM HG complemented with 10% FBS and penicillin/streptomycin (24 h, 37 °C). The extraction medium volume was equal to 100 mg/mL. Extraction medium was subsequently filtered (0.2-µM filter) and 100% extracts of S-TPU and F-TPU were obtained. The 24-well plates were used for NIH 3T3 cells (2 × 104) seeding (for 24 h). After this time, the medium was changed to S-TPU/F-TPU extract and the incubation process was carried out for the next 24, 48 and 72 h. A mixture of DMEM HG, FBS and antibiotics was used as a non-toxic control sample. Finally, after the addition of 200 µL of MTT solution (4 mg/mL), the process of cell incubation begun (3 h, 37 °C). After removing the culture medium, the formazan crystals were dissolved in organic solvent (DMSO, Sigma Aldrich, Darmstadt, Germany). Optical density of obtained solutions was measured by iMark Microplate Absorbance Reader (Bio-Rad, Warsaw, Poland) at 570 nm. Results were presented as the percentage of cells proliferating after extract exposure relative to control cells cultured in extract-free medium. Obtained data are a mean of two separate experiments wherein each treatment condition was repeated in two wells.

2.5.3. Statistical Analysis

For each extract, two tests were conducted and the results of the two experiments were averaged. For this purpose, two tests were conducted (ANOVA and Bonferroni) using GraphPad Prism 6 software (San Diago, CA, USA). p values of less than 0.05 were marked as significant (* $p < 0.05$; ** $p < 0.01$; *** $p < 0.001$; **** $p < 0.0001$; ns non-significant).

2.5.4. Analysis Cells Morphology

Cellular morphology was studied using Zeiss inverted microscope with AxioCam digital camera (Zeiss, Göttingen, Germany). The samples placed in the 24-well plate were examined directly under the microscope.

3. Results and Discussions

3.1. S-TPU Synthesis—Identification of Free Isocyanate Groups

The reaction progress between PEBA and HDI over time is presented in Figure 2. After the first hour of the prepolymer synthesis, F_{NCO} index sharply decreased from 11% to ~8%. After the next 4–5 h, the F_{NCO} index stabilized at the level of ~8%, which indicated completion of the reaction between PEBA and HDI reagents. Thus, it can be concluded that PEBA and HDI react in a predictable and repeatable way, which is a significant aspect for further applications of these materials in the biomedical field.

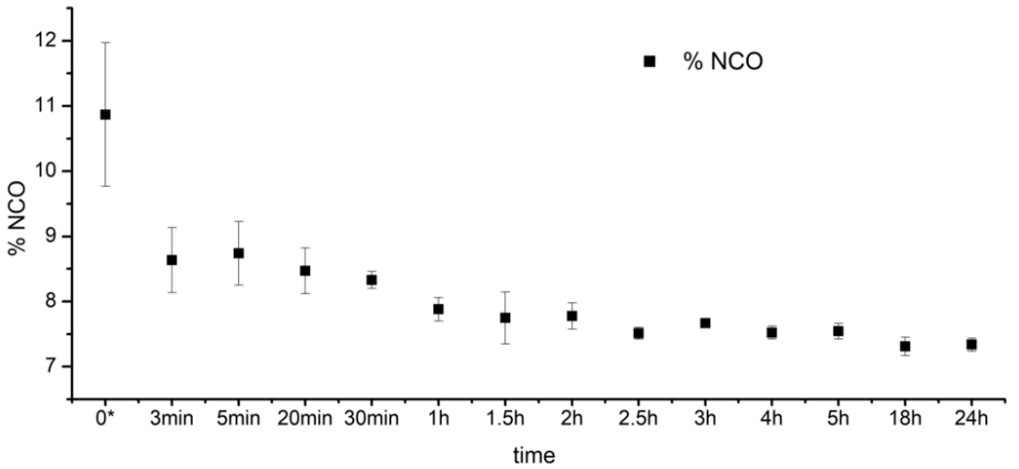

Figure 2. The changes of the isocyanate groups content (F_{NCO}, %) over reaction time between PEBA and HDI (prepolymerization step); * time "0" is related to the moment when the PEBA and HDI were mixed together in a whole volume of the reactive mixture.

3.2. Fabrication of F-TPU Filament from Synthesized S-TPU Granules

In Table 2, the selected melt-extrusion parameters used to fabricate the F-TPU filament, from S-TPU granules is presented. It can be seen that operating parameters are closely related to the temperature profile of S-TPU extrusion. During process 1 and 2 (Table 2), very high head pressure and machine load were noted. When the temperature profile was increased up to 210 °C, the head pressure and machine load dropped significantly, to about 17 bar and 15–18%, respectively. The further increase of the temperature profile (above 215 °C) caused a sharp decrease of head pressure (process 4, Table 2). This might be related to the viscosity of the melt polymer. High melt viscosity hinders the free flow of the polymer through the narrow forming die. Therefore, in process 1 and 2 (Table 2), the temperature profile was not high enough to ensure free flow of the polymer. Additionally, in the case of process 1 and 2, an enormous swelling of the polymer at the die exit (Barus effect) was observed. During process 4 (Table 2), the polymer underwent degradation.

In the process of a filament forming via melt-extrusion process, it is necessary to maintain a constant value of head pressure. In another way, it is not possible to obtain an extrudate with a stable dimension. The combination of the parameters in process 3* provided an appropriate profile which allowed us to obtain stable F-TPU filament with a constant diameter dimension (Table 2—highlighted).

Table 2. Process parameters of F-TPU filament fabrication.

Lp.	Zones Temperature Profile [°C]											Operating Parameters		
	I	II	III	IV	V	VI	VII	VIII	IX	Coupler	Head	Rotation speed [rpm]	Head pressure [bar]	Load [%]
1	160	165	170	175	185	185	190	195	190	190	185	20	37–48	45–50
2	170	175	175	180	190	200	205	200	200	195	195	20	28–30	20–28
3 *	**170**	**175**	**180**	**190**	**200**	**205**	**210**	**210**	**205**	**200**	**200**	**20**	**17–18**	**15–18**
4	170	175	180	190	195	205	210	213	217	215	210	20	3–6	5–7

* Melt-extrusion profile that provide a dimensionally stable F-TPU filament.

3.3. Physico-Mechanical Properties of Synthesized S-TPU

The density of obtained S-TPUs were equal to 1.17 g/cm^3, which is similar to the references, which reports typical PUR density in the range of 0.2–1.2 g/cm^3 [43]. MFR is an important parameter of polymers processing, allowing for an assessment of using thermoplastic materials for further technological procedure. The MFR value is directly related to the melt viscosity at the test temperature as well with the test load. With the increase of sample viscosity, the flow rate decreases. Thermoplastic materials designed for injection molding are characterized by very high MFR value (very high flow-rate and low melt viscosity), in contrast to thermoplasts intended for extrusion. In the FDM process, the material in the form of a filament is plasticized in a mini-extruder and passes through a heated nozzle with a diameter in the range of 0.3–0.8 mm, and settles down at the movable platform. This is associated with a very short duration of heating and plasticizing of material. Therefore, the printed material should be relatively quick and easy to plasticize while maintaining the proper solidification rate, so that it will not flow from the layers built on the printer platform [44]. On the other hand, the strength and quality of the bonds formed between adjacent fibers depends on the growth of the neck formed among them and on the molar diffusion and randomization of the used polymeric filament across the interface [45,46]. Consequently, the degree of flow rate under FDM printing conditions should not be too high and sufficient/adequate for free flow of the filament out of the nozzle. Additionally, it should be added that higher MFR value allows for higher print speed. Thus, at a temperature of 200 °C and test load of 5 kg the MFR value of S-TPU was 40.74 ± 3.16 g/10 min, which might provide the free flow rate of the printed material.

Tensile strength of injection-molded S-TPU samples was 26 ± 2 MPa, which was close to values determined for commercially available medical-grade PURs, like Carbothane® (39–67 MPa) and Desmopan® (25–50 MPa) [47–51], as well in the range of elastic TPU filament NinjaFlex® (26 MPa) [52]. Noted elongation at the break of obtained S-TPUs was of 706 ± 29% and higher than Tecoflex® (365 ± 25%–400 ± 38% [53,54], the medical-grade PUR for biomedical applications and NinjaFlex® filament (660%) [52]. Hardness of the obtained S-TPUs was 37.07 ± 0.80 °ShD and was comparable to the hardness of medical-grade TPU filament Bioflex® (27 °ShD) [55]. It should be noted that as the filament hardness decreases, the difficulty of printing increases. This is particularly related to the folding of the filament on extruder rollers during the printing process. Mechanical properties of S-TPU correspond to those PURs obtained with the use of an organotin catalyst, dibutyltin dilaurate (DBTDL), described in our previous paper [56].

3.4. The Impact Assessment of Filament Formation on Selected S-TPU Properties

3.4.1. Fourier Transform Infrared Spectroscopy (FTIR)

FTIR spectra of obtained S-TPUs and extruded F-TPU filament was presented in Figure 3. The band assignments with a description were given in Table 3. The interpretation of the particular bands was made on the basis of a Silverstein et al. [57] scientific book. The presence of functional groups characteristic for poly(ester urethane)s was confirmed (Table 3) and the results are consistent with the interpretation given by Yiligor et al. [58]. The FTIR spectra of S-TPU and F-TPU are very similar, which might suggest that the extrusion process did not cause any chemical changes in S-TPU structure.

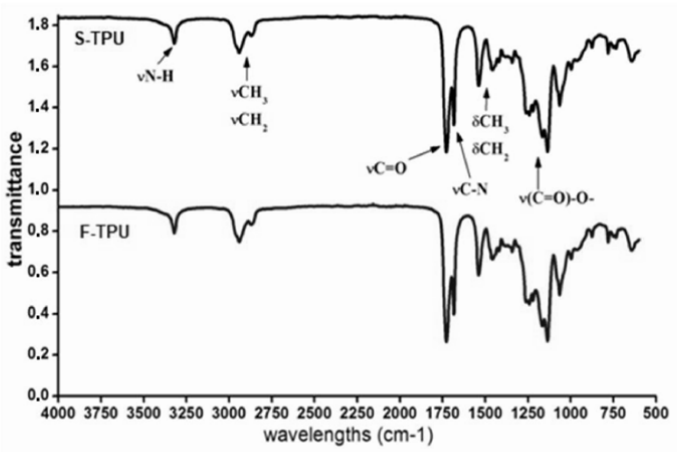

Figure 3. The FTIR spectra of S-TPU and extruded F-TPU filament.

Table 3. Band assignments noted at the FTIR spectra of S-TPU and F-TPU filament.

S-TPU	F-TPU	Band	Description
Wavelength (cm^{-1})			
3324 w	3324 w	νNH	Stretching of NH groups. These groups were hydrogen bonded with C=O of ester groups present in macrodiol.
2941 w, 2863 w	2939 w, 2865 w	νCH_2, νCH_3	Stretching of aliphatic asymmetric and symmetric CH_2 groups present in the S-TPU chain and in the S-TPU filament
1730 vs. −1686 s	1733 vs. −1685 s	νC=O	stretching of C=O in ester groups of macrodiol,(hydrogen bonded and not hydrogen bonded)
1535 s	1535 s	νC–N	Stretching of C–N in urethane group
1459 w–1336 vw	1465 w–1346 w	δCH_2	deformation vibrations of aliphatic CH_2 groups present in the S-TPU and S-TPU filament: bending, wagging, scissoring in plane
1259 m–1219 m	1257 s–1216 m	νC–(C=O)–O	Stretching vibrations of –C–(C=O)–O– (ester group), not hydrogen bonded
1165 s	1165 m	νNH–(C=O)–O	Stretching vibrations of –NH–(C=O)–O– of urethane group
1129 s–994 w	1135 s–947 m	νC–(C=O)–O νC–O	Stretching vibration of hydrogen bonded –C–(C=O)–O–,
873 w–642 w	873 w–638 m	δCH_2, δNH, δOH	out of the plane deformation of CH_2(scissoring/wagging) as well as NH and OH groups (scissoring and wagging).

w (wagging), v(vibrating), s (scissoring).

In both spectra, weak absorption peaks assigned to N–H stretching vibrations are observed at 3324 cm^{-1}, which is related with the presence of hydrogen bonds between NH groups and macrodiol's ester groups (C=O). The peaks, which appeared between 2941–2863 cm^{-1} correspond to the asymmetric and symmetric stretching vibrations of aliphatic CH_2 groups presented in the S-TPU structure. Strong signals registered in the range of 1733–1685 cm^{-1} are related to stretching of C=O (both, hydrogen bonded and not hydrogen bonded in ester groups of macrodiol). Polyurethanes characteristic peak from C–N stretching are seen at 1535 cm^{-1}. Peaks observed at 1465–1336 cm^{-1} correspond to deformation vibrations of aliphatic CH_2 groups present in the S-TPU. Stretching

vibrations of –NH–(C=O)–O– (urethane group), were registered at 1165 cm^{-1}. In turn, stretching vibration of hydrogen bonded –C–(C=O)–O–, is presented between 1135–947 cm^{-1}. Finally, peaks in the range of 873–863 are associated with out of plane bonding vibrations of C–H bending, CH_2, NH, OH wagging and scissoring. According to physicochemical tables [57], absorbance in the range of 2250–2270 cm^{-1} is assigned to free NCO groups. The absence of those peaks indicates the complete reaction between reagents (HDI, PEBA, BDO) until the –NCO groups are completely converted into urethanes functional groups. This is also in accordance with the identification of free isocyanate groups during the pre-polymerization stage. FTIR analysis confirmed that F-TPU has the same chemical bonding type as bulk S-TPU and the filament formation process did not affect its chemical structure.

3.4.2. Optical Microscopy (OM)

The optical microscopy of S-TPU and F-TPU filament was presented in Figure 4.

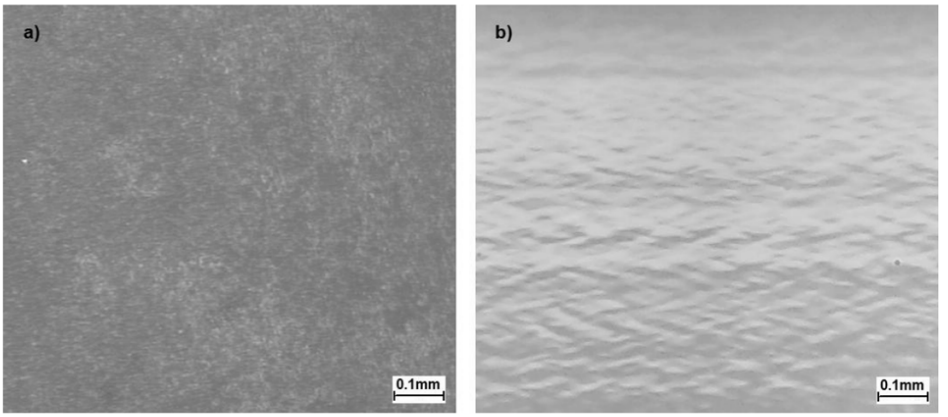

Figure 4. Optical microscopy of (**a**) bulk S-TPU and (**b**) F-TPU filament.

The surface of S-TPU (Figure 4a) is very rough and it does not reflect much of the light, so the particular patterns of the image are not clearly visible contrary to the image of extruded F-TPU (Figure 4b) surface. F-TPU surface is very smooth and very well reflects the light. A characteristic image of mound-depression nature for un-crosslinked TPUs [59] was observed (Figure 4b). The pattern in the image is oriented, which is obvious as the sample was extruded.

3.4.3. Water Contact Angle (CA)

Water contact angle studies allow to specify the hydrophilicity/hydrophobicity of the material surface. However, CA is not a sufficient indicator to determine the biocompatibility of the material. Notwithstanding, hydrophilicity is an important biomedical parameter that favors the adherence and interaction of cells with material surfaces, thus CA studies provide preliminary biomedical characterization [60].

Results of CA measurements of S-TPU and F-TPU were presented in Figure 5. The analysis of CA revealed that the extrusion process slightly increased the CA from 64° for S-TPU to 73° for F-TPU filament. Thus, the material became more hydrophobic after processing, which can be explained by the smoother surface presented by F-TPU filament. However, obtained values are still within the range of 55–75° that ensures proper adhesion of human cells to the surface of the selected material [50].

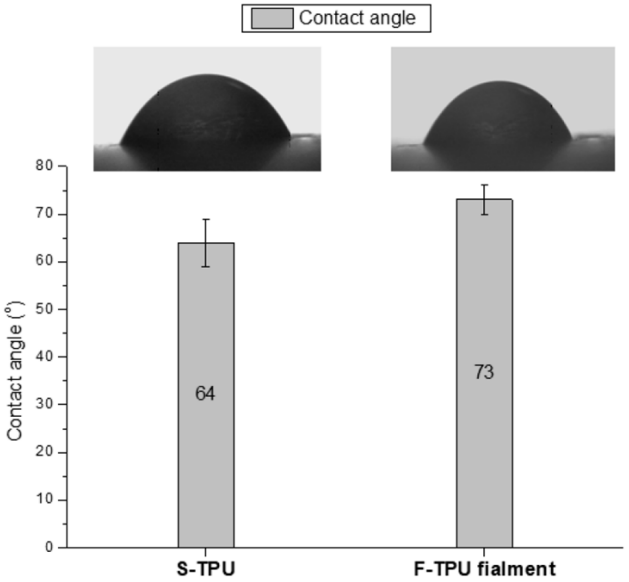

Figure 5. Contact angle of pure S-TPU and of extruded F-TPU filament.

3.5. Biological Studies

3.5.1. Short-Term Hemocompatibility Test

One of the test methods to evaluate biological properties in vitro is the study of blood response. Synthetic materials marked as medical-grade are intended for direct or indirect contact with body tissues, such as blood. Therefore, the study of the interaction of material with blood which is the fluid tissue present in every part of the body, seems to be important. It is a known fact that all of the biomaterials which are in contact with body tissues, cause the initiation of an inflammatory reaction (foreign body response FBR) [61]. Occurrence of acute or chronic reactions for a long time, disqualifies the material in medical applications. An initial interaction of cellular blood components with the artificial/synthetic surface occurs after the first few minutes of contact. Consequently, short-term studies of the interaction material—blood, can provide preliminary information about the biocompatibility of the material.

Analysis of the obtained data (Figure 6) showed that both synthesized S-TPU and extruded F-TPU filament can be pre-classified as biocompatible materials, under the specified conditions. Thus, the extrusion process did not influence this parameter and obtained materials may find a potential application in blood-contacting medical devices. This is consistent with the references related to the fact that PURs are one of the most hemocompatible synthetic polymers dedicated to medical applications [62].

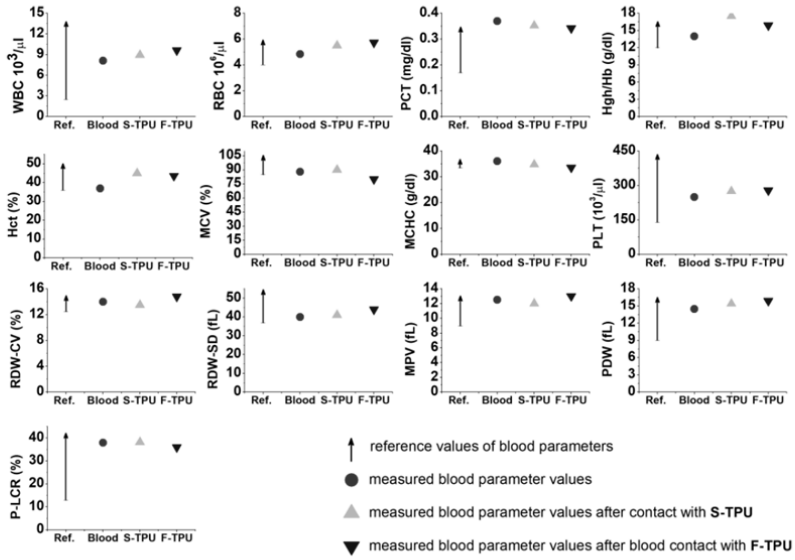

Figure 6. Short-term biocompatibility of S-TPU and extruded F-TPU filament with human blood. WBC—white blood cells (leucocytes); RBC—red blood cells (erythrocytes); PCT—percentage of platelets in whole blood volume; Hgh/Hb—hemoglobin; Hct—hematocrit; MCV mean corpuscular volume; MCHC—mean concentration of hemoglobin in blood cells; PLT—platelet amount (thrombocytes); RDW-CV/RDW-SD—distribution volume of red blood cells; MPV—mean platelet volume; PDW—indicator of platelet volume distribution; P-LCR—platelet larger cell ratio.

It should be noted that all of the studied blood parameters are in the references range and they do not differ significantly from the values obtained for pure blood. Hemocompatibility test indicated that both S-TPU and F-TPU did not change the cell count of MCV, MCHC, PLT, RDW-CV, RDW-SD, MPV, PDW, and P-LCR. On the contrary to WBC, RBC, PCT, Hgh/Hb, Hct, which changed slightly. A slight decrease in the PCT value corresponding to the platelet count was observed. It can be related to aggregation and activation of platelets on the S-TPU surface [63]. This is an undesirable phenomenon that can lead to thrombosis [64]. Nevertheless, this value is still the norm. An increase of white blood cell (WBC) number was noticed, which is related to an initial inflammatory reaction that always takes place when in contact with an artificial organism. In turn, blood parameter associated with erythrocytes (RBC, Hgh/Hb, Hct) slightly increased to the maximum reference value, after contact with S-TPU and extruded F-TPU. Eventually, a significant reduction in RBC and Hct values could indicate the adhesion to the surfaces of erythrocytes, which in turn have a tendency to aggregate and form the so-called blood clots [65].

3.5.2. Cytotoxicity

The cytotoxicity of obtained S-TPU and F-TPU filament was shown in Figure 7. As it can be observed, both materials indicated biocompatibility towards NIH 3T3 cells. For S-TPU after 24 h and 48 h of incubation, the proliferation of cells was noted (over 100% of cells viability), while for F-TPU it was 95%, 86% and 79% after 24 h, 48 h, and 72 h, respectively. Slight differences in biocompatibility can be directly related to the higher hydrophilicity of the S-TPU surface than the extruded F-TPU. Moreover, the greater roughness and the more irregular the surface, the better adhesion of cells to the substrate, was noted [66], hence the possible difference in cell proliferation in the differentiation to F-TPU filament.

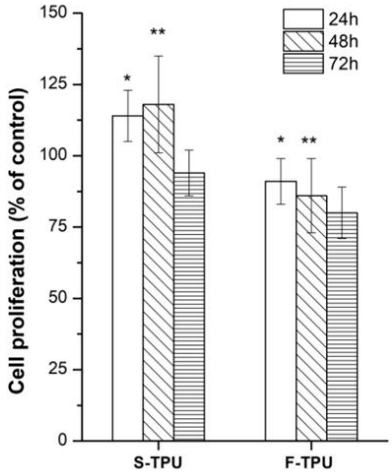

Figure 7. The effect of S-TPU and extruded F-TPU extracts on the in vitro growth of mouse embryonic fibroblast NIH 3T3 cells measured using MTT assay. Cell proliferation is represented as a percentage of control cell growth in cultures containing no S-TPU or extruded S-TPU filament extracts. Results are a mean ± SD of two separate experiments wherein each treatment condition was repeated in two wells. * $p < 0.05$; ** $p < 0.001$ vs. control.

Morphology of cells was observed for 72 h and the images are presented in Figure 8. As it can be seen, S-TPU and F-TPU filament extracts did not significantly change the morphology of the NIH 3T3 cells.

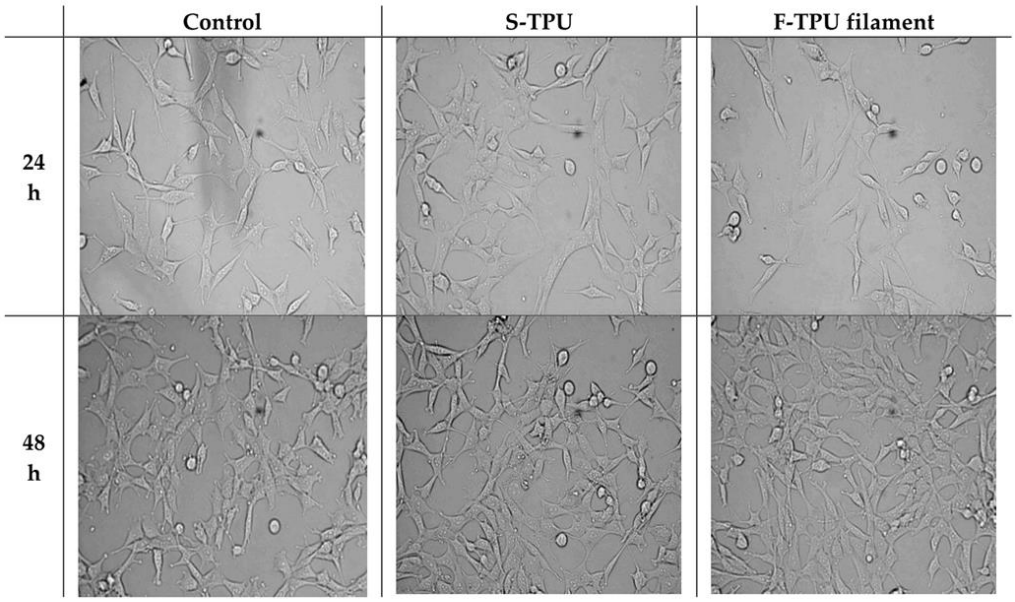

Figure 8. *Cont.*

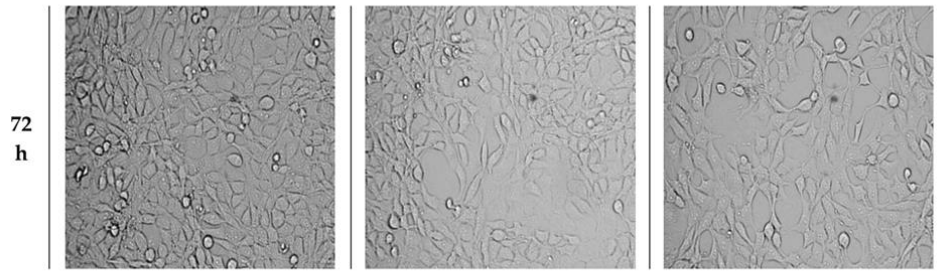

Figure 8. The effect of S-TPU and F-TPU filament extracts on the cellular morphology of mouse embryonic fibroblast NIH 3T3 cells.

The morphology of NIH 3T3 cells did not change and was comparable to the control up to 72 h of incubation. Shape and cells dimensions were not impaired. It should be noted that there was a slight decrease in cell number when they had contact with the F-TPU filament, in comparison to the control sample. However, no cells degeneration or apoptosis was noticed during the incubation of both S-TPU and F-TPU. This might be explained by hindered cell adhesion to the F-TPU substrate, which exhibits a higher contact angle and smother surface than bulk S-TPU. Thus, these materials may be considered as suitable for biomedical applications.

4. Conclusions

In this work, we reported the synthesis, processing, physico-mechanical characterization and biological studies of new uncatalyzed aliphatic, amorphous polyurethane, as a potential medical-grade filament for using in FDM 3D printing technology.

For this purpose, bulk S-TPU with 1.1:1 NCO:OH molar ratio was synthesized and efforts have been made to adjust the temperature profile and operating parameters of S-TPU melt-extrusion. Established extrusion processing temperature for S-TPU was in the range of 160–205 °C, respectively. As a result, a stable F-TPU filament with 1.75 mm diameter was received. The mechanical characteristic and MFR of S-TPU is satisfactory, which has reference to FDM 3D printing, where the ease of processing, stability in print conditions and the proper flow, viscosity and hardness of the filament are responsible for the print quality. The summary of the obtained S-TPU mechanical properties and its comparison to the commercial medical-grade PURs in terms of mechanical efficiency is given in Table 4.

Table 4. Comparison of available medical-grade polyurethanes properties with the synthesized uncatalyzed S-TPU system. (The data were taken from the material safety data sheets available on the manufacturers' websites).

Value Range	MilaMed®	Desmopan® AU	Texin®RxT50	S-TPU
TSb [MPa]	15–30	25–50	25–52	26
Eb [%]	540–565	470–880	320–770	705
HS [°Sh A/D]	no data found	60A–75D	70A–65D	26D
Chemical composition	Aliphatic polyether	Aromatic polyester	Aromatic polyether	Aliphatic polyester

It can be seen that the mechanical properties of synthesized S-TPU are within the range of values suitable for medical-grade polyurethanes such as MillaMed®, Desmopan® or Texin®. Thus, obtained uncatalysed aliphatic S-TPUs seems to be a promising candidate as a filament material for FDM 3D printer for medical purposes. Preliminary biological studies showed biocompatibility and hemocompatibility of F-TPU filament provided that this material may find application as a novel medical-grade, flexible filament for FDM 3DP. To confirm the validity of the presented studies, a test print of anatomical flexible heart using F-TPU filament and FDM type 3D printer, was made. Results

are presented in supplementary data 2. The initial evaluation of FDM print with the use of obtained F-TPU filament allows to conclude that obtained F-TPU filament is suitable for 3D printing in the FDM type technology. Fabrication of F-TPU filament combined with 3DP technology allows for fabrication of customized and repeatable products without the use of toxic substances during printing. Moreover, the 3D printing technology in combination with elastomeric filament led to design cost-efficient and achievable patient-customized products.

Supplementary Materials: The following are available online at http://www.mdpi.com/2073-4360/10/12/1304/s1. Supplementary data 1 provides the results and methodology of accelerated degradation studies on Bioflex® and F-TPU filaments as well microscopic analysis of degraded samples. Supplementary data 2 presents trial of FDM 3D printing process using obtained F-TPU filament.

Author Contributions: Writing-original draft and Investigation A.H., Writing-review & editing, I.G., Funding and Supervision, J.K.-L., H.J.

Funding: Part of the research (Supplementary Materials) was founded by Gdansk University of Technology—Centre for Knowledge and Technology Transfer, grant number [26].

Acknowledgments: The work was supported by the Gdansk University of Technology, Narutowicza St. 11/12, 80-233 Gdansk, Poland.

Conflicts of Interest: The authors declare no conflict of interest.

References

1. Javaid, M.; Haleem, A. Additive manufacturing applications in medical cases: A literature based review. *Alexandria J. Med.* **2017**. [CrossRef]
2. Schubert, C.; Van Langeveld, M.C.; Donoso, L.A. Innovations in 3D printing: A 3D overview from optics to organs. *Br. J. Ophthalmol.* **2014**, *98*, 159–161. [CrossRef] [PubMed]
3. Ventola, C.L. Medical Applications for 3D Printing: Current and Projected Uses. *Pharm. Ther.* **2014**, *39*, 704–711. [CrossRef]
4. Klammert, U.; Gbureck, U.; Vorndran, E.; Rödiger, J.; Meyer-Marcotty, P.; Kübler, A.C. 3D powder printed calcium phosphate implants for reconstruction of cranial and maxillofacial defects. *J. Cranio-Maxillofacial Surg.* **2010**, *38*, 565–570. [CrossRef] [PubMed]
5. Bergmann, C.; Lindner, M.; Zhang, W.; Koczur, K.; Kirsten, A.; Telle, R.; Fischer, H. 3D printing of bone substitute implants using calcium phosphate and bioactive glasses. *J. Eur. Ceram. Soc.* **2010**, *30*, 2563–2567. [CrossRef]
6. Lee, M.-Y.; Chang, C.-C.; Ku, Y.C. New layer-based imaging and rapid prototyping techniques for computer-aided design and manufacture of custom dental restoration. *J. Med. Eng. Technol.* **2008**, *32*, 83–90. [CrossRef] [PubMed]
7. O'reilly, M.K.; Reese, S.; Herlihy, T.; Geoghegan, T.; Cantwell, C.P.; Feeney, R.N.M.; Jones, J.F.X. Fabrication and Assessment of 3D Printed Anatomical Models of the Lower Limb for Anatomical Teaching and Femoral Vessel Access Training in Medicine. *Anat. Sci. Educ.* 2015. [CrossRef] [PubMed]
8. Qiu, K.; Zhao, Z.; Haghiashtiani, G.; Guo, S.-Z.; He, M.; Su, R.; Zhu, Z.; Bhuiyan, D.B.; Murugan, P.; Meng, F.; et al. 3D Printed Organ Models with Physical Properties of Tissue and Integrated Sensors. *Adv. Mater. Technol.* **2017**, *1700235*, 1–9. [CrossRef] [PubMed]
9. Garcia, J.; Yang, Z.; Mongrain, R.; Leask, R.L.; Lachapelle, K. 3D printing materials and their use in medical education: a review of current technology and trends for the future. *BMJ Simul. Technol. Enhanc. Learn.* **2017**. bmjstel-2017-000234. [CrossRef] [PubMed]
10. Ikada, Y. Challenges in tissue engineering. *J. R. Soc. Interface* **2006**, *3*, 589–601. [CrossRef] [PubMed]
11. Hutmacher, D.W. Scaffolds in tissue engineering bone and cartilage. *Biomaterials* **2000**, *21*, 2529–2543. [CrossRef]
12. *ASTM F2792-10, Standard Terminology for Additive Manufacturing Technologies*; ASTM International: West Conshohocken, PA, USA, 2010.
13. Kim, G.B.; Lee, S.; Kim, H.; Yang, D.H.; Kim, Y.-H.; Kyung, Y.S.; Kim, C.-S.; Choi, S.H.; Kim, B.J.; Ha, H.; et al. Three-Dimensional Printing: Basic Principles and Applications in Medicine and Radiology. *Korean J. Radiol.* **2016**, *17*, 182–197. [CrossRef] [PubMed]

14. Cui, X.; Boland, T. Human microvasculature fabrication using thermal inkjet printing technology. *Biomaterials* **2009**, *30*, 6221–6227. [CrossRef] [PubMed]
15. Gaebel, R.; Ma, N.; Liu, J.; Guan, J.; Koch, L.; Klopsch, C.; Gruene, M.; Toelk, A.; Wang, W.; Mark, P.; et al. Patterning human stem cells and endothelial cells with laser printing for cardiac regeneration. *Biomaterials* **2011**, *32*, 9218–9230. [CrossRef] [PubMed]
16. Merceron, T.K.; Burt, M.; Seol, Y.J.; Kang, H.W.; Lee, S.J.; Yoo, J.J.; Atala, A. A 3D bioprinted complex structure for engineering the muscle-tendon unit. *Biofabrication* **2015**, *7*, 35003. [CrossRef] [PubMed]
17. Palareti, G.; Legnani, C.; Cosmi, B.; Antonucci, E.; Erba, N.; Poli, D.; Testa, S.; Tosetto, A. Comparison between different D-Dimer cutoff values to assess the individual risk of recurrent venous thromboembolism: analysis of results obtained in the DULCIS study. *Int. J. Lab. Hematol.* **2016**, *38*, 42–49. [CrossRef] [PubMed]
18. Miri, A.K.; Nieto, D.; Iglesias, L.; Goodarzi Hosseinabadi, H.; Maharjan, S.; Ruiz-Esparza, G.U.; Khoshakhlagh, P.; Manbachi, A.; Dokmeci, M.R.; Chen, S.; et al. Microfluidics-Enabled Multimaterial Maskless Stereolithographic Bioprinting. *Adv. Mater.* **2018**, *30*, 1–9. [CrossRef] [PubMed]
19. Oskui, S.M.; Diamante, G.; Liao, C.; Shi, W.; Gan, J.; Schlenk, D.; Grover, W.H. Assessing and Reducing the Toxicity of 3D-Printed Parts. *Environ. Sci. Technol. Lett.* **2016**, *3*, 1–6. [CrossRef]
20. Xu, N.; Ye, X.; Wei, D.; Zhong, J.; Chen, Y.; Xu, G.; He, D. 3D artificial bones for bone repair prepared by computed tomography-guided fused deposition modeling for bone repair. *ACS Appl. Mater. Interfaces* **2014**, *6*, 14952–14963. [CrossRef] [PubMed]
21. Vargas-Alfredo, N.; Dorronsoro, A.; Cortajarena, A.L.; Rodríguez-Hernández, J. Antimicrobial 3D Porous Scaffolds Prepared by Additive Manufacturing and Breath Figures. *ACS Appl. Mater. Interfaces* **2017**, *9*, 37454–37462. [CrossRef] [PubMed]
22. Melocchi, A.; Parietti, F.; Maroni, A.; Foppoli, A.; Gazzaniga, A.; Zema, L. Hot-melt extruded filaments based on pharmaceutical grade polymers for 3D printing by fused deposition modeling. *Int. J. Pharm.* **2016**, *509*, 255–263. [CrossRef] [PubMed]
23. Mohseni, M.; Hutmacher, D.W.; Castro, N.J. Independent evaluation of medical-grade bioresorbable filaments for fused deposition modelling/fused filament fabrication of tissue engineered constructs. *Polymers (Basel).* **2018**, *10*, 40. [CrossRef]
24. O'Brien, F.J. Biomaterials & scaffolds for tissue engineering. *Mater. Today* **2011**, *14*, 88–95. [CrossRef]
25. Patrício, T.; Domingos, M.; Gloria, A.; Bártolo, P. Characterisation of PCL and PCL/PLA scaffolds for tissue engineering. *Procedia CIRP* **2013**, *5*, 110–114. [CrossRef]
26. Zein, I.; Hutmacher, D.W.; Tan, K.C.; Teoh, S.H. Fused deposition modeling of novel scaffold architectures for tissue engineering applications. *Biomaterials* **2002**, *23*, 1169–1185. [CrossRef]
27. Hutmacher, D.W.; Schantz, T.; Zein, I.; Ng, K.W.; Teoh, S.H.; Tan, K.C. Mechanical properties and cell cultural response of polycaprolactone scaffolds designed and fabricated via fused deposition modeling. *J. Biomed. Mater. Res.* **2001**, *55*, 203–216. [CrossRef]
28. Kucinska-Lipka, J.; Gubanska, I.; Strankowski, M.; Cieśliński, H.; Filipowicz, N.; Janik, H. Synthesis and characterization of cycloaliphatic hydrophilic polyurethanes, modified with L-ascorbic acid, as materials for soft tissue regeneration. *Mater. Sci. Eng. C* **2017**, *75*, 671–681. [CrossRef] [PubMed]
29. Cauich-rodríguez, J.V.; Chan-Chan, L.H.; Hernandez-Sánchez, F.; Cervantes-Uc, J.M. Degradation of Polyurethanes for Cardiovascular Applications. In *Advances in Biomaterials Science and Biomedical Applications*; Pignatello, R., Ed.; InTechOpen: Rijeka, Croatia, 2012; pp. 51–82, ISBN 978-953-51-1051-4.
30. Davis, F.J.; Mitchell, G.R. Polyurethane Based Materials with Applications in Medical Devices. In *Bio-Materials and Prototyping Applications in Medicine*; CRC press: Washington, DC, USA, 2008; pp. 27–48.
31. Kucińska-Lipka, J.; Gubanska, I.; Pokrywczynska, M.; Ciesliński, H.; Filipowicz, N.; Drewa, T.; Janik, H. Polyurethane porous scaffolds (PPS) for soft tissue regenerative medicine applications. *Polym. Bull.* **2017**, 1–23. [CrossRef]
32. Borkenhagen, M.; Stoll, R.C.; Neuenschwander, P.; Suter, U.W.; Aebischer, P. In vivo performance of a new biodegradable polyester urethane system used as a nerve guidance channel. *Biomaterials* **1998**, *19*, 2155–2165. [CrossRef]
33. Lamba, N.M.K.; Woodhouse, K.A.; Cooper, S.L.; Lelah, M.D. *Polyurethanes in biomedical applications*; CRC press: Washington, DC, 1998; ISBN 9780849345173.

34. Jung, S.Y.; Lee, S.J.; Kim, H.Y.; Park, H.S.; Wang, Z.; Kim, H.J.; Yoo, J.J.; Chung, S.M.; Kim, H.S. 3D printed polyurethane prosthesis for partial tracheal reconstruction: A pilot animal study. *Biofabrication* **2016**, *8*, 045015. [CrossRef] [PubMed]
35. Tsai, K.J.; Dixon, S.; Hale, L.R.; Darbyshire, A.; Martin, D.; de Mel, A. Biomimetic heterogenous elastic tissue development. *npj Regen. Med.* **2017**, *2*, 16. [CrossRef] [PubMed]
36. Kucińska-Lipka, J.; Gubanska, I.; Skwarska, A. Microporous Polyurethane Thin Layer as a Promising Scaffold for Tissue Engineering. *Polymers (Basel).* **2017**, *9*, 277. [CrossRef]
37. Park, H.; Gong, M.-S.; Knowles, J.C. Catalyst-free synthesis of high elongation degradable polyurethanes containing varying ratios of isosorbide and polycaprolactone: physical properties and biocompatibility. *J. Mater. Sci. Mater. Med.* **2013**, *24*, 281–294. [CrossRef] [PubMed]
38. Kim, H.-J.; Kang, M.-S.; Knowles, J.C.; Gong, M.-S. Synthesis of highly elastic biocompatible polyurethanes based on bio-based isosorbide and poly(tetramethylene glycol) and their properties. *J. Biomater. Appl.* **2014**, *29*, 454–464. [CrossRef] [PubMed]
39. Tanzi, M.C.; Verderio, P.; Lampugnani, M.G.; Resnati, M.; Dejana, E.; Sturani, E. Cytotoxicity of some catalysts commonly used in the synthesis of copolymers for biomedical use. *J. Mater. Sci. Mater. Med.* **1994**, *5*, 393–396. [CrossRef]
40. Hassan, M.; Mauritz, K.; Storey, R.; Wiggins, J. Biodegradable Aliphatic Thermoplastic Polyurethane Based on Poly(e-caprolactone) and L-Lysine Diisocyanate. *J. Polym. Sci. Part A Polym. Chem.* **2006**, *44*, 2990–3000. [CrossRef]
41. Heijkants, R.G.J.C.; Van Calck, R.V.; Van Tienen, T.G.; De Groot, J.H.; Buma, P.; Pennings, A.J.; Veth, R.P.H.; Schouten, A.J. Uncatalyzed synthesis, thermal and mechanical properties of polyurethanes based on poly(ε-caprolactone) and 1,4-butane diisocyanate with uniform hard segment. *Biomaterials* **2005**, *26*, 4219–4228. [CrossRef] [PubMed]
42. Barrioni, B.R.; De Carvalho, S.M.; Oréfice, R.L.; De Oliveira, A.A.R.; Pereira, M.D.M. Synthesis and characterization of biodegradable polyurethane films based on HDI with hydrolyzable crosslinked bonds and a homogeneous structure for biomedical applications. *Mater. Sci. Eng. C* **2015**, *52*, 22–30. [CrossRef] [PubMed]
43. Janik, H.Z. Struktury nadcząsteczkowe i wybrane właściwości rozgałęzionych i usieciowanych poli(estro-uretanów), poli(etero-uretanów) i poli(uretano-biuretów) formowanych reaktywnie. *Zesz. Nauk. Politech. Gdańskiej. Chem.* **2005**, *Nr 53(599)*, 3–141.
44. Pietrzak, K.; Isreb, A.; Alhnan, M.A. A flexible-dose dispenser for immediate and extended release 3D printed tablets. *Eur. J. Pharm. Biopharm.* **2015**, *96*, 380–387. [CrossRef] [PubMed]
45. Sun, Q.; Rizvi, G.M.; Bellehumeur, C.T.; Gu, P. Effect of processing conditions on the bonding quality of FDM polymer filaments. *Rapid Prototyp. J.* **2008**, *14*, 72–80. [CrossRef]
46. Gkartzou, E.; Koumoulos, E.P.; Charitidis, C.A. Production and 3D printing processing of bio-based thermoplastic filament. *Manuf. Rev.* **2017**, *4*, 1. [CrossRef]
47. Nezarati, R.M.; Eifert, M.B.; Dempsey, D.K.; Cosgriff-Hernandez, E. Electrospun vascular grafts with improved compliance matching to native vessels. *J. Biomed. Mater. Res. Part B Appl. Biomater.* **2015**, *103*, 313–323. [CrossRef] [PubMed]
48. Qin, Y.; Liu, R.; Zhao, Y.; Hu, Z.; Li, X. Preparation of Dipyridamole/Polyurethane Core–Shell Nanofibers by Coaxial Electrospinning for Controlled-Release Antiplatelet Application. *J. Nanosci. Nanotechnol.* **2016**, *16*, 6860–6866. [CrossRef]
49. Wang, H.; Feng, Y.; Fang, Z.; Yuan, W.; Khan, M. Co-electrospun blends of PU and PEG as potential biocompatible scaffolds for small-diameter vascular tissue engineering. *Mater. Sci. Eng. C* **2012**, *32*, 2306–2315. [CrossRef]
50. Wang, H.; Feng, Y.; An, B.; Zhang, W.; Sun, M.; Fang, Z.; Yuan, W.; Khan, M. Fabrication of PU/PEGMA crosslinked hybrid scaffolds by in situ UV photopolymerization favoring human endothelial cells growth for vascular tissue engineering. *J. Mater. Sci. Mater. Med.* **2012**, *23*, 1499–1510. [CrossRef] [PubMed]
51. Yuan, W.; Feng, Y.; Wang, H.; Yang, D.; An, B.; Zhang, W.; Khan, M.; Guo, J. Hemocompatible surface of electrospun nanofibrous scaffolds by ATRP modification. *Mater. Sci. Eng. C* **2013**, *33*, 3644–3651. [CrossRef] [PubMed]
52. NinjaTek Technical Sepcification of NinjaFlex 3D Printing Filament. Available online: https://ninjatek.com/wp-content/uploads/2016/05/NinjaFlex-TDS.pdf (accessed on 4 March 2018).

53. Chen, R.; Huang, C.; Ke, Q.; He, C.; Wang, H.; Mo, X. Preparation and characterization of coaxial electrospun thermoplastic polyurethane/collagen compound nanofibers for tissue engineering applications. *Colloids Surfaces B Biointerfaces* **2010**, *79*, 315–325. [CrossRef] [PubMed]
54. Detta, N.; Errico, C.; Dinucci, D.; Puppi, D.; Clarke, D.A.; Reilly, G.C.; Chiellini, F. Novel electrospun polyurethane/gelatin composite meshes for vascular grafts. *J. Mater. Sci. Mater. Med.* **2010**, *21*, 1761–1769. [CrossRef] [PubMed]
55. Filoalfa–Bioflex Filament. Available online: https://www.filoalfa3d.com/en/filaments-175mm/296-bioflex-pla-shore-27d-white-o-175-mm-8050327032385.html (accessed on 4 March 2018).
56. Kucinska-Lipka, J.; Gubanska, I.; Sienkiewicz, M. Thermal and mechanical properties of polyurethanes modified with L-ascorbic acid. *J. Therm. Anal. Calorim.* **2017**, *127*, 1631–1638. [CrossRef]
57. Socrates, G. *Infrared and Raman Characteristic Group Frequencies: Tables and Charts*; third; John Wiley & Sons, Ltd.: Hoboken, NJ, USA, 2004; ISBN 978-0-470-09307-8.
58. Yilgor, I.; Yilgor, E.; Guler, I.G.; Ward, T.C.; Wilkes, G.L. FTIR investigation of the influence of diisocyanate symmetry on the morphology development in model segmented polyurethanes. *Polymer (Guildf).* **2006**, *47*, 4105–4114. [CrossRef]
59. Janik, H. Progress in the studies of the supermolecular structure of segmented polyurethanes. *Polimery* **2010**, *55*, 419–500.
60. Menzies, K.L.; Jones, L. The impact of contact angle on the biocompatibility of biomaterials. *Optom. Vis. Sci.* **2010**, *87*, 387–399. [CrossRef] [PubMed]
61. Anderson, J.; Rodrigues, A.; Chang, D. Ferogin Body Reaction To Biometerials. *Semin. Immunol.* **2008**, *20*, 86–100. [CrossRef] [PubMed]
62. Fromstein, J.D.; Woodhouse, K.A. Elastomeric biodegradable polyurethane blends for soft tissue applications. *J. Biomater. Sci. Polym. Ed.* **2002**, *13*, 391–406. [CrossRef] [PubMed]
63. Xin, Z.; Du, B.; Wang, Y.; Qian, S.; Li, W.; Gao, Y.; Sun, M.; Luan, S.; Yin, J. Hemocompatibility Evaluation of Polyurethane Film with Surface-Grafted Sugar- Based Amphipathic Compounds. *J. Anal. Bioanal. Tech.* **2017**, *8*, 1–6. [CrossRef]
64. Williams, D.F. On the mechanisms of biocompatibility. *Biomaterials* **2008**, *29*, 2941–2953. [CrossRef] [PubMed]
65. Tahara, D.; Oikawa, N.; Kurita, R. Mobility enhancement of red blood cells with biopolymers. *J. Phys. Soc. Japan* **2016**, *85*, 10–12. [CrossRef]
66. Keshel, S.H.; Azhdadi, S.N.K.; Asefnejad, A.; Sadraeian, M.; Montazeri, M.; Biazar, E. The relationship between cellular adhesion and surface roughness for polyurethane modified by microwave plasma radiation. *Int. J. Nanomedicine* **2011**, *6*, 641–647. [CrossRef] [PubMed]

Supplementary materials

Supplementary data 1

Degradation study

Accelerated degradation was performed for filaments Bioflex® (Filoalfa, Italy) and F-TPU, using 5M KOH and 2M HCl media. Cut samples (1,5 cm length) were immersed in the respective dilutions and incubated at 37°C for 30 days. At each respective time point (7, 14, 2 and 30 days), degradated samples were carefully rinsed out with deionizer water and dried in laboratory oven at 40°C for 48h. Mass loss was calculated as following;

$$Ms\ (\%) = \frac{m_0 - m_1}{m_0} * 100\ \% \qquad (1)$$

Where, (m_0) is initial mass of sample and (m_1) is residual mass.

The test result is shown in the graph below.

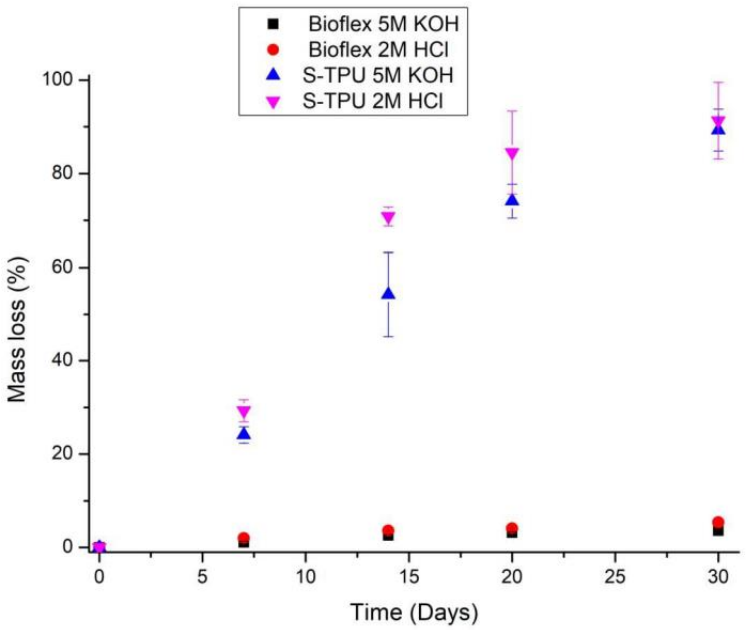

Figure S1 Accelerated degradation of Bioflex® and F-TPU filaments in 5M KOH and 2M HCl medium. Results are represented as mean ± SD (n = 4)

Optical microscopy

The surfaces of pristine and degraded filaments were analyzed by using optical microscope (OM) Delta Optical Genetic Pro (at x80 magnification).

Table S1 OM images of pristine and degradated filaments in KOH medium (x80).

Sample	0 days	7 days	20 days
Bioflex®	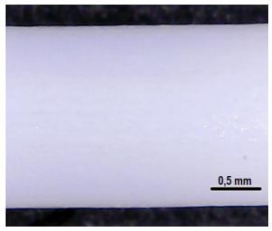		
F-TPU	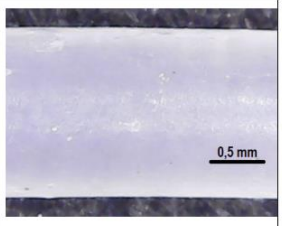	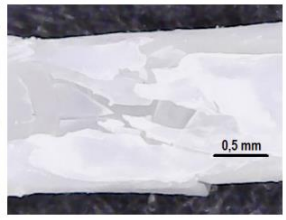	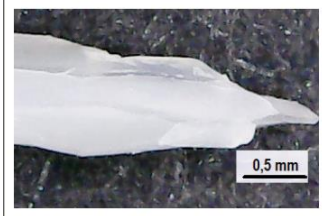

Table S2 OM images of pristine and degradated filaments in HCl medium (x80).

Sample	0 days	7 days	20 days
Bioflex®	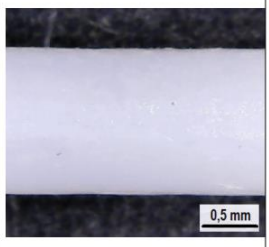	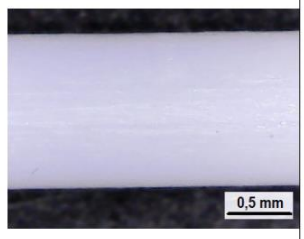	

F-TPU	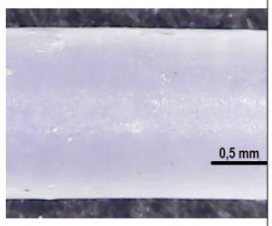		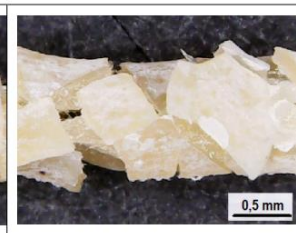

Table S3 Comparison of Bioflex and F-TPU after 20 days of incubation in KOH and HCl medium (x80)

20 days in KOH	20days in HCl
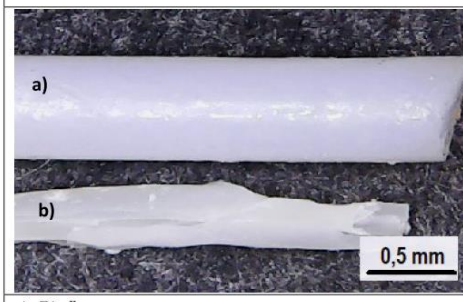	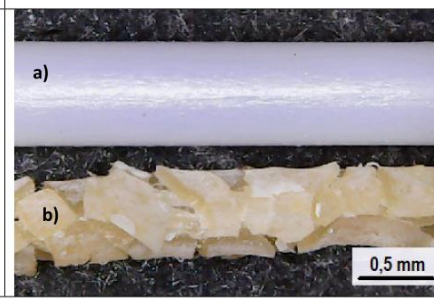
a) Bioflex b) F-TPU	

Supplementary data 2

Initial FDM 3D printing of F-TPU filament

For preliminary evaluation of F-TPU filament potential use in FDM 3D printers, the test of printing was performed. For this purpose, we used ready-made SLT. format file of anatomical heart, available on 3dprint.nih.gov website (NIH 3D Print Exchange – an open-source community). This STL. file was converted into the printer control code "g-code" using an open-source program (Slic3r 1.2.9). The model was printed using single-head FDM-type 3D printer (self-made printer, Gdansk, Poland) (Figure S2.). The proper parameters of printing were as follow; printing speed, 25mm/s; printing temperature, 205-210°C; bed temperature, 55°C, fill density, 80%; layer thickness, 0.4mm. The printing time was about 8 hours.

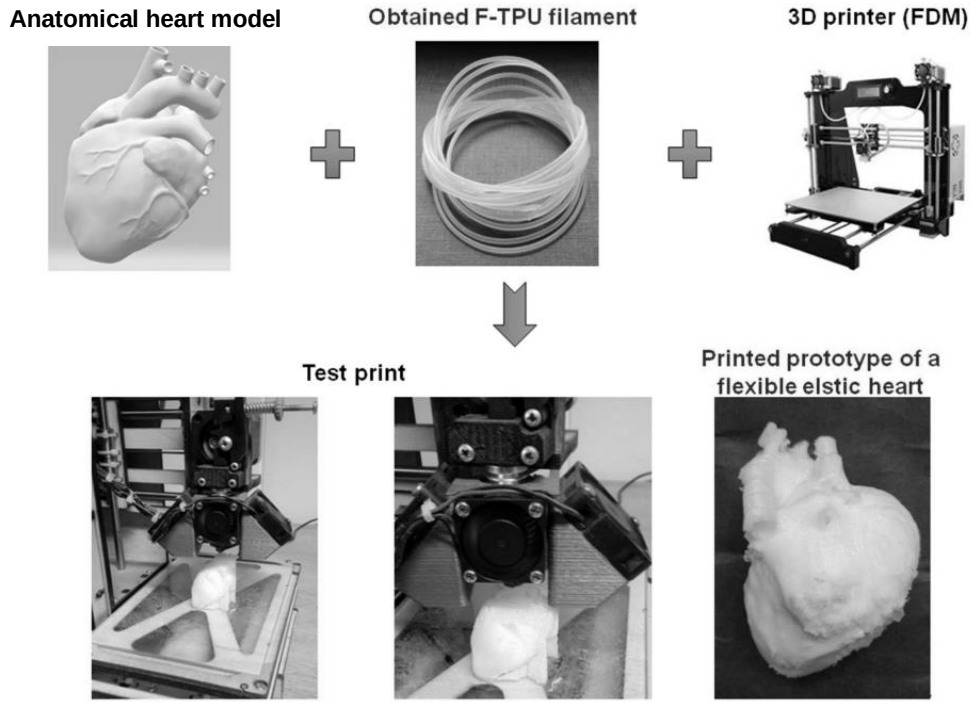

Figure S2 Scheme of the initial FDM 3D printing of heart by using F-TPU.

The initial evaluation of FDM print with the use of obtained F-TPU filament allows to conclude that obtained F-TPU filament is suitable for 3D printing in the FDM type technology.

4.2 PAPER 2: Medical-Grade PCL Based Polyurethane System for FDM 3D Printing—Characterization and Fabrication

Authors (percentage share): Agnieszka Haryńska (50%), Justyna Kucinska-Lipka (15%), Agnieszka Sulowska (10%), Iga Gubanska (10%), Marcin Kostrzewa (5%), Helena Janik (10%)

Journal: Materials (Basel)

DOI: 10.3390/ma12060887

Index: Q2, IF_{2019}=3.057, MNSiW = 140 pts

CRediT: Conceptualization (in part), Data Curation (lead), Formal Analysis (lead), Investigation (lead: FTIR, Raman, tensile test, hardness, DSC, TGA, contact angle, surface free energy, long-and short-term degradation, melt-extrusion) Methodology (in part), Project Administration (in part), Visualization (lead), Writing – Original Draft Preparation (lead), Writing – Review & Editing (lead).

Realized doctoral research tasks:
I (material design and characterization) – elaboration of uncatalyzed synthesis of medical-grade poly(ester urethane) (TPU) based on aliphatic diisocyanate (HDI) and crystalline polyol (PCL), and characterization of the formed materials;
II (filament formation) – formation of 3D-printable filaments using synthesized TPU on a laboratory scale in a discontinuous manner.

Material code: TPU(PCL)

BRIEF DESCRIPTION OF THE PUBLICATION

Discussed topics: review of biomaterials with suitable softness and flexibility for FFF 3D printing; pros of PCL-systems in the medical application; review of contemporary medical-grade PCL-based polyurethane systems

Scope of the publication: polyurethane uncatalyzed synthesis; comparison of material properties synthesized with two different isocyanate index (NCO to OH group ratios); filament formation in a laboratory scale

Novelty of the publication: the use of biodegradable and crystalline polyol (PCL) in the uncatalyzed synthesis of the thermoplastic poly(ester urethane) for 3D printing technology.

Main scientific achievement: synthesis of a novel, medical-grade poly(ester urethane) that is suitable for the formation of the filament for FFF 3D printing technology.

Outline: In this article, novel PCL-based medical-grade thermoplastic poly(ester urethanes) was obtained using the previously developed method described in PAPER 1. The material was synthesized using biodegradable poly (ε-caprolactone) diol (PCL), aliphatic 1,6-hexamethylene di-isocyanate (HDI), and 1,4-butanediol (BDO). The successful synthesis of the uncatalyzed PCL-based poly(ester urethane) was confirmed by FTIR and Raman spectra. The influence of the isocyanate index (molar ratio of NCO to OH groups) on the chemical structure and material properties was investigated. Thermal properties studied *via* differential scanning calorimetry (DSC) and thermogravimetry (TG) revealed thermal transitions and stability,

respectively. Surface properties were examined by water contact angle (wCA) and surface free energy (SFE) measurements. The initial assessment of biological properties *in vitro* included both short- and long-term degradation, water absorption, and cytotoxicity test. Finally, the material with more favorable properties was processed into a 3D-printable filament *via* the melt-extrusion process. However, the process was carried out on a laboratory scale in a discontinuous manner, yielding only small fragments of the filament. Nevertheless, the obtained results indicate that the fabricated filament exhibit promising properties for medical applications, especially where high flexibility, durability, and long-term degradability are required.

GDAŃSK UNIVERSITY OF TECHNOLOGY

materials

MDPI

Article

Medical-Grade PCL Based Polyurethane System for FDM 3D Printing—Characterization and Fabrication

Agnieszka Haryńska [1], Justyna Kucinska-Lipka [1,*], Agnieszka Sulowska [1], Iga Gubanska [1], Marcin Kostrzewa [2] and Helena Janik [1]

[1] Department of Polymer Technology, Faculty of Chemistry, Gdansk University of Technology, 80-232 Gdansk, Poland; agnieszka.harynska@pg.edu.pl (A.H.); agnsulow@student.pg.edu.pl (A.S.); igaguban@pg.edu.pl (I.G.); heljanik@pg.edu.pl (H.J.)

[2] Department of Organic Materials Technology, Technical University of Radom, 26-600 Radom, Poland; m.kostrzewa@uthrad.pl

* Correspondence: juskucin@pg.edu.pl; Tel.: +48-(58)-347-12-14

Received: 28 February 2019; Accepted: 13 March 2019; Published: 16 March 2019

Abstract: The widespread use of three-dimensional (3D) printing technologies in medicine has contributed to the increased demand for 3D printing materials. In addition, new printing materials that are appearing in the industry do not provide a detailed material characterization. In this paper, we present the synthesis and characterization of polycaprolactone (PCL) based medical-grade thermoplastic polyurethanes, which are suitable for forming in a filament that is dedicated to Fused Deposition Modeling 3D (FDM 3D)printers. For this purpose, we synthesized polyurethane that is based on PCL and 1,6-hexamethylene diisocyanate (HDI) with a different isocyanate index NCO:OH (0.9:1, 1.1:1). Particular characteristics of synthesized materials included, structural properties (FTIR, Raman), thermal (differential scanning calorimetry (DSC), thermogravimetric analysis (TGA)), mechanical and surfaces (contact angle) properties. Moreover, pre-biological tests in vitro and degradation studies were also performed. On the basis of the conducted tests, a material with more desirable properties S-TPU(PCL)0.9 was selected and the optimization of filament forming via melt-extrusion process was described. The initial biological test showed the biocompatibility of synthesized S-TPU(PCL)0.9 with respect to C2C12 cells. It was noticed that the process of thermoplastic polyurethanes (TPU) filaments forming by extrusion was significantly influenced by the appropriate ratio between the temperature profile, rotation speed, and dosage ratio.

Keywords: PCL based TPU; material characterization; fused-filament fabrication; fused deposition modeling; 3D printing; polyurethane filament

1. Introduction

Global interest in three-dimensional (3D) printable biopolymers for applications, such as drug delivery devices, scaffolds in tissue engineering, as well as artificial organs for surgery trainings, are constantly growing [1–3]. While there are more and more modifications of 3D printers for medical purposes [4–6], new material solutions are also needed.

Synthetic polymers, including polylactonesthat were obtained from L- or DL-lactide monomers, glycolide, ε-caprolactone, or p-dioxanone have found wide clinical application [7,8]. Parts of polylactones, especially those with a high content of L-lactide or glycolide, are materials with increased stiffness. For implanted parts in the areas of soft body tissues, such as the skin [9], adipose tissue [10], cardiovascular area [11], or for anatomical models [12], more soft and elastic biopolymers are needed than rigid ones. There is a constant need for biomaterials that can be modified both in terms of

biodegradability and mechanical properties. In this context, polyurethanes are a very promising group of synthetic polymers.

Thermoplastic polyurethanes (TPUs) consist of alternating rigid (hard) and flexible (soft) blocks, which, under appropriate conditions, can undergo the separation phenomenon of the blocks, leading to nanodomain morphology, which acts as a physical crosslinking of the system and the materials, called thermoplastic elastomers (TPEs), are then created. TPEs behave like elastomers, but they can be processed like thermoplastic materials. The latter properties are very important in making filaments from TPU. Flexible segments consist of the reaction products between polyols (polyesters, polyethers, or polycarbonates) and diisocyanates, while rigid segments are the result of the reaction between diisocyanates and small molecular chain extenders [13]. The flexible segments provide elastomeric character, while rigid segments usually provide additional strength due to hydrogen bonding between urethane groups [14]. The use of different starting substrates, change of their molecular mass, and the ratio of rigid and flexible segments may lead to polyurethanes with different physical and physicochemical properties, or biodegradability, tailored for the intended use [15]. Moreover, properly designed thermoplastic polyurethanes (TPUs) are suitable materials for use in 3D printing by the Fused Deposition Modeling (FDM) method [16,17]. FDM uses materials that are based on a thermoplastic polymer matrix in the form of a thin filament of a given diameter. Using computer software and 3D models with the STL. Format, the FDM printer creates ready-made 3D structures layer by layer.

Polycaprolactone (PCL) is a one of the most commonly used biopolymers in medical application. Ease of processing and high flexibility characterizes PCL. It is also a material that is thoroughly examined by scientists in the context of biological interactions in vivo and in vitro, thanks to which the FDA approves many medical devices that are based on PCL polymer. Due to these features, PCL is successfully used as a polyol in the synthesis of medical polyester urethanes (Table 1).

Table 1. Review of medical-grade polyurethane systems in which polycaprolactone (PCL) is used as a polyol part of the chain.

Polyurethane System	Short Description	Year	Reference
(SF/LDI/PCLdiol/BDA) Silk fibroin poly(ester-urethane) urea	Tissue scaffolds with the structure of nanofibers for the regeneration of the heart valves obtained via electrospinning.	2018	[18]
(HDI/PCLtriol/PEG/glycerol) Crosslinked aliphatic poly(ester urethane)	Biodegradable polyurethane films with cross-linked hydrolysable bonds and a homogeneous structure for biomedical applications. PU with hydrogel behavior and susceptibility to hydrolytic degradation.	2015	[19]
(LDI-ε-caprolactone)block/LDI) Polyurethane block copolymer	Biodegradable PU with potential application in soft tissue engineering. A synthesis of a poly (L-lactide-ε-caprolactone) block copolymer was carried out, which was then used to react with L-lysine diisocyanate(LDI). The PU obtained can be used as a viscous injection which is cured in situ.	2017	[20]
(BDI/PCLdiol/L-Lysine ethyl ester dihydrochloride) Poly(ester-urethane)	Poly(ester-urethane) tissue scaffolds were obtained using the melt-extrusion additive manufacturing technique. The obtained scaffolds were cytocompatible and tested for use in the regeneration of myocardial tissue.	2014	[21]
(HDI/PCLdiol/BDO/Fe_2O_3 nanoparticles) Magnetic poly(ester-urethane) nanocmposite	A poly(ester-urethane) material of potential application for the regeneration of nerve tissue was obtained. The addition of nanoparticles improved the electrical conductivity, hydrophilicity and roughness of the obtained material. Biological tests show that nanocomposite was biocompatible and has suitable cell viability (in vitro cytotoxicity).	2014	[22]
(HDI/PCLdiol/PEG) Aliphatic poly(ester-urethane)	Electrospunednanofiberpoly(ester-urethane) membranes dedicated for guided bone regeneration. Obtained membranes had mechanical properties slightly higher than commercially available collagen or PTFE membrane.	2018	[23]

Taking into account the literature overview on medical grade TPUs, which is shortly presented in Table 1, we found that there are only a few systems of PCL/based TPUs that are dedicated

as filaments for 3D printing technology. In most of the presented works (Table 1), the obtained polyester-urethanes for medical application were processed by electrospining or hydrogels were formed or thin films were produced. Guney et al. [24] paper is one of rare examples, in which the synthesis, characterization, and formation of a medical filament for 3D printing in FDM technology are presented. They synthesized thermoplastic tough polyurethane hydrogels from triblock copolymers (PCL-PEG-PCL) and HDI diisocyanate. They described the synthesis, characterization, and formation of filament by the melt-extrusion process. They also successfully tested the filament on a 3D FDM printer. Another paper in which new 3D FDM filaments were obtained with the use of holt-melt extrusion is that one of Fuenmayor et al. [25]. Designed filaments that were based on PCL and PVP were dedicated to solid dosage forms. Researchers characterized the process and problems occurring during the formation of filaments for FDM 3D printing via melt-extrusion.

In our previous work [16], we examined the effect of TPU filament formation on its selected properties. The results showed no significant changes on the chosen properties of the obtained filament after the melt-extrusion extrusion process. Notwithstanding, the final characteristic of the printed 3D object (mechanical characteristic [26,27] or biological properties [28,29]) also depends on the 3D printing parameters and the design of 3D object. Therefore, we decided to prepare polyurethane filament for the use in Fused Filament Fabrication 3D printing with potential to be used as a medical-grade material and characterize solid material before its formation into filament.

2. Materials and Methods

In order to receive the intended results, the following steps were taken:

- Synthesis of aliphatic polyester-urethane S-TPU(PCL) with PCL diol as a polyol,
- Material (S-TPU(PCL) characterization, which included:
    - structure studies (FTIR, Raman);
    - mechanical properties (static tensile test, hardness);
    - thermal characterization(differential scanning calorimetry (DSC), thermogravimetric analysis (TGA));
    - surface properties (surface free energy, contact angle);
    - interaction with media (short-, and long-term degradation tests, water absorption test); and,
    - initial biological test (cytotoxicity).
- Formation of filament F-TPU(PCL) for FDM 3D printing via melt-extrusion process

2.1. S-TPU(PCL) Synthesis

In accordance with previous works [16,30] a two-stage (prepolymer method) synthesis of polyester urethanes (S-TPU(PCL)) was carried out. The first stage of the synthesis was the reaction of the polyol (PCL diol), with an excess of diisocyanate (HDI) resulting in a prepolymer mixture containing an isocyanate terminated prepolymer (building soft segments) and an excess of unreacted diisocyanate. The next step was the chain extension reaction, by adding a small molecular weight chain extender (BDO) to the prepolymer mixture. The description of raw materials that were used in polyurethane synthesis is described in Table 2. No catalysts were used for the synthesis of polymeric materials, which seems reasonable for medical application. What is more, the lack of catalyst can help to improve the biocompatibility of materials. Tanzi et al. [31] demonstrated that the catalysts commonly used in the synthesis of polyurethanes (such as tin octoate, dibutyltindilaurate, 1,4-diazabicyclooctane, tetramethylbutanediamine) increase the cytotoxicity of the polymer with respect to human endothelial cells. Hence, the synthesis of polyurethanes for medical applications are more often carried out without the use of the above catalysts [19,32].

Before the synthesis, PCL, diol, and BDO were dried in a vacuum for four hours at 100 °C, while stirring. HDI was used without prior treatment. The dried PCL diol, was placed in the reactor and

then heated to melt. After reaching a temperature of 40 °C, HDI was added in portions (to obtain a prepolymerwith an 8% excess of unbound isocyanate groups -NCO). After the prepolymerization stage was carried out at 80 °C for 3 h, the reaction mixture was left for 12 h at room temperature to complete the reaction. Subsequently, the chain extension process was conducted by adding the BDO to preheated (60 °C) prepolymer mixture (mechanical stirring, 3 min, 1050 rpm). The chain extender was added in two different molar ratio of NCO groups to OH groups equal to 0.9:1 and 1.1:1, respectively. After that, the mixture was degassed and then poured into a preheated mould (100 °C). Finally, the material in the mold was put into the dryer for 24 h.

Table 2. Description of raw materials used in polyurethane synthesis.

Compound	Supplier	Short Description	Structure Formula
PCL diol (Capa^{TM} 2200)	Perstrop, Malmo, Sweden	Linear polyestrodiol, terminated with hydroxyl groups; Appearance: white, waxy solid; Average molecular weight: 2000 g/mol; Melting temp: 40–50 °C; Density: 1.05 g/cm^3; Viscosity at 60 °C: 480 mPa s; Purity> 99%.	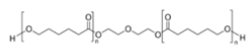
HDI	Sigma-Aldrich, Taufkirchen, Germany	Aliphatic diisocyanate; Appearance: colorless liquid; Molar mass = 168.2 g/mol; Boiling point: 255 °C; Melting point: −67 °C; Density (25 °C) = 1.05 g/cm^3; Purity> 99%; LD50 (rat) = 746 mg/kg.	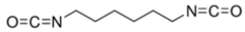
BDO	Brenntag, Essen, Germany	Low molecular weight chain extender Molar mass = 90.12 g/mol; Appearance: colorless liquid; Purity> 95.5%; Melting point: 20.4 °C; Density (20 °C) = 1.02 g/cm^3	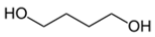

2.2. S-TPU(PCL) Characterization

The chemical structure of samples was tested using an FTIR Nicolet 8700 (Thermo Fisher Scientific, Waltham, MA, USA) spectrometer at room temperature. The equipment included a Specac's Golden Gate module and a single reflective ATR (Attenuated Total Reflectance) diamond, used to attenuate the total infrared reflection. The range of recorded spectra was 4000–500 cm^{-1}. Each sample was scanned 254 times at a resolution of 4 cm^{-1}. Additionally, the chosen samples from short-term degradation test were tested with FTIR.

Raman spectroscopy was also applied to study a chemical composition of the sample. It uses monochromatic light and its phenomenon of inelastic scattering with molecules. Measurements were performed using micro-Raman system (InVia, Renishaw, Wotton-under-Edge, UK). The spectra were collected at randomly selected locations (50x magnification) over the 100–3200 cm^{-1} range, at room temperature. The used wavelength was of 785 nm (red laser) and the power of laser was of 15 mW. Each sample was scanned five times.

The hardness of the samples was measured using the Shore type (A and D) electronic hardness tester (Zwick/Roell), in accordance with the PN-EN ISO 868:2004 standard. Flat samples of solid polymer materials with a thickness of about 8 mm were used. The results were averaged from 10 measurements. A density measurement of samples was carried out using the analytical balance (AS 110/C/2, Radwag, Radom, Poland) equipped with a density set. The mass of samples was determined in the air and then in water. The results were the arithmetic mean of eight measurements. The static tensile strength test of the samples was conducted using Zwick/Roell Z020 table resistance machine (Wrocław, Poland) integrated with the testXpert® I program in accordance with the PN-EN ISO 527-2:2012 standard (dumbbell shaped samples). The test was conducted at room temperature with a crosshead speed of 500 mm/min and initial force of 1 N. The results are the arithmetic mean of eight measurements.

Differential scanning calorimetry (DSC) measurements were conducted using a heat-fluxNetzsch DSC 204F1machine (Netzsch, Selb, Germany). The thermal properties of samples with the mass of 7–8 mg were investigated at the temperature range of −85 °C to 220 °C (heating rate 10 °C/min, cooling rate 20 °C/min), under nitrogen atmosphere (N_2 flow rate 20 mL/min).

The thermal stability of the obtained polyurethanes was tested with thermogravimetric analysis (TGA) using a Q1000 TAInstruments (New Castle, DE, USA). Samples of 3–6 mg mass were heated under a nitrogen atmosphere from 20 °C to 700 °C, with a heating rate of 10 °C/min.

To determine the wettability of the surface layer and surface free energy (SFE) of synthesized polyurethanes, the contact angle test by the sessile drop technique was carried out. The analysis was performed while using Kruss Goniometer G10 (KRÜSS GmbH, Hamburg, Germany) with drop shape analysis software DSA4.1 (5.5.3 version). On purified with n-hexane samples surface, a 2 µL droplet of liquid was placed and the images were taken. The SFE was determined by two methods, the Owens-Wendt method and Acid-base approach. The first method requires the use of polar and dispersion liquids, therefore the distilled water and diiodomethanewere used. In turn, acid-base method needs the use of three polar liquids (formamide, ethylene glycol, water) and one dispersive/non-polar (diiodomethane) to calculate the SFE. The results of contact angle for each of the four liquids were an average of six measurements taken on randomly selected surface points.

2.3. Cytocompatibility (In Vitro)

The cytotoxicity evaluation was performed according to the ISO 10993-5:2009 standard. The cell metabolic activity was estimated by using MTT assay. Extract: prior the extract preparation, polyesterurethanes were sterilized with ice-cold 70% EtOH overnight and then exposed to UV for 15 min at each side. The sterile samples of S-TPU(PCL)0.9/1.1 were incubated for 24 h in culture medium: Dulbecco's Modified Eagle's Medium (High glucose DMEM, Sigma Aldrich, Poznań Poland) containing 10% Fetal Bovine Serum (FBS, HyClone, Pittsburgh, PA, USA) and 1% penicillin/streptomycin (P/S, Sigma Aldrich, Poznań, Poland). After this, the time extracts were added to the cells. Cell culture: C2C12 murine myoblasts (ATCC) were expanded and maintained in DMEM, containing 10% FBS and 1% P/S. C2C12 myoblasts were seeded at a cell density of 10^5 cells per well in a 24-well tissue culture plate (BD) and then incubated. After 24 h in culture, the media was changed, and the 100% extract of polyester urethanes was added. Following 72 h incubation, the experimental materials were removed and the cytotoxicity was assessed by MTT assay kit (Sigma Aldrich, Poznań, Poland). A plate reader was used to measure the conversion of the tetrazolium salt to its colorimetric indicator at a wavelength of 490 nm.

The statistical analysis was performed with the use of the Origin Pro 8.5 (Washington, DC, USA). To evaluate statistical differences, the two-way ANOVA ($\alpha = 0.05$) and post hock Tukey test ($\alpha = 0.05$) were used.

2.4. Degradation Study and Water Absorption Test

Standard, from medical point of view [3], degradation tests of prepared polyurethanes were conducted to estimate the interaction of polymer with different media. For this purpose, long-term degradation studies (84 days, 37 °C) in phosphate buffer (PBS) and short-term degradation (32 days, 37 °C) in 2M HCl and 5M NaOH were performed [3,33]. Round samples (diameter 7 mm) were cut before testing and then dried to a constant weight (4 h, 60 °C). Six samples were taken for each of the tests. The samples were placed in 3 mL wells test plate, immersed with 2 mL of the appropriate solution (PBS, HCl, or NaOH), and then incubated at 37 °C. During the short-term degradation test (HCl/NaOH), sample's weight loss was measured after one, two, three weeks, and 32 days. In turn, for the long-term degradation process (PBS), the weight of the samples was measured afterone week, one month, and three months. After specified time intervals, the samples were rinsed several times in distilled water, then dried (three days, 37 °C), and weighed again using an analytical balance (Radwag, Poland). The degree of degradation was determined by the percentage loss of mass of the sample

over time. Additionally, after short-term degradation (in 2 M HCl and 5 M NaOH), the samples were observed under the optical microscope (Bresser, Rhede, Germany) camera integrated with VidCap 5.1 program (Microsoft, Washington, DC, USA), mag. 40x and 400x).

The water absorption (WA) test was carried out on circular samples with a diameter of 7mm. The dried samples (4 h, 60 °C) were weighed and placed in the wells of the test plate, and then flooded with 2 mL of distilled water. The incubation time of samples was as follows: 0.5 h; 1 h; 5 h; 24 h; 48 h; and, 72 h. After removing the samples from the test plates, the excess of water was gently removed with tissue paper, and the samples were re-weighed. Water absorption was calculated based on the amount of water absorbed according to Equation (1). The obtained results constituted the arithmetic mean of four measurements.

$$WA = \frac{m_i - m_0}{m_0} \cdot 100\% \quad (1)$$

where: *WA*—water absorption [%], m_0—initial mass of dry sample [g], and m_i—mass of sample after incubation in water [g].

2.5. Filament Formation

Synthesized bulk S-TPU was granulated while using high-speed mill (WittmannBattenfeld, Grodzisk Mazowiecki, Poland) and dried in laboratory oven (60 °C, 24 h) before the melt-extrusion process. Single screw extruder (Brabender, Duisburg, Germany) with two heating zones was used toconvert the synthesized polyurethane (S-TPU) into polyurethane filament (F-TPU). The custom-made molding nozzle diameter was equal to 1.9 mm. The processing parameters, like temperature profile, dosage rate, and rotation speed were tested to obtain a dimensionally stable extrudate. Electronic caliper was used to control the filament diameter.

3. Results and Discussion

3.1. Material Characterization S-TPU(PCL)

Chemical Characterization (FTIR, Raman)

Based on the FTIR spectra (Figure 1), the chemical structure of the synthesized materials was analyzed. Both FTIR spectra were similar. The presence of the main peaks that are characteristic of polyurethanes was observed, which confirmed the positive reaction of polyester urethanes synthesis. The absorption bands at 3318 cm^{-1}, 1686–1660 cm^{-1}, and 1223 cm^{-1} described the vibrations of amide bonds, N–H, C=O, and C–N, respectively, suggesting the formation of urethane bonds. The characteristic peaks at 2917 cm^{-1} and 2850 cm^{-1} corresponded to the asymmetric and symmetric vibrations of the –CH2– groups. Two strong and high intensity peaks at 1717 cm^{-1} and 1160 cm^{-1} were the stretching vibrations of C=O and C–O bonds of the ester groups of the soft PCL segment. Table 3 presenteda detailed description of the FTIR spectra. No intensive peak with a wavenumber around 2280 cm^{-1} indicated the complete reaction of isocyanate groups (lack of –NCO groups).

Raman spectroscopy was performed to complete the FTIR study (Figure 2). The results proved to be complementary. Thus, it confirmed the presence of hydrogen bonded C=O band in the structure of synthesized polyester urethanes [33]. However, it seems thata more complementary technique to describe polyurethanes structure is the FTIR study. A visible change between samples intensity of the Raman spectrum was noted. This is related to the phenomenon of fluorescence of the studied materials. It can be seen that S-TPU(PCL)1.1 exhibited a noticeably higher degree of illumination as a result of interaction with the laser light (785 nm). The obtained Raman spectrum was complementary and it confirmed the FTIR studies well.

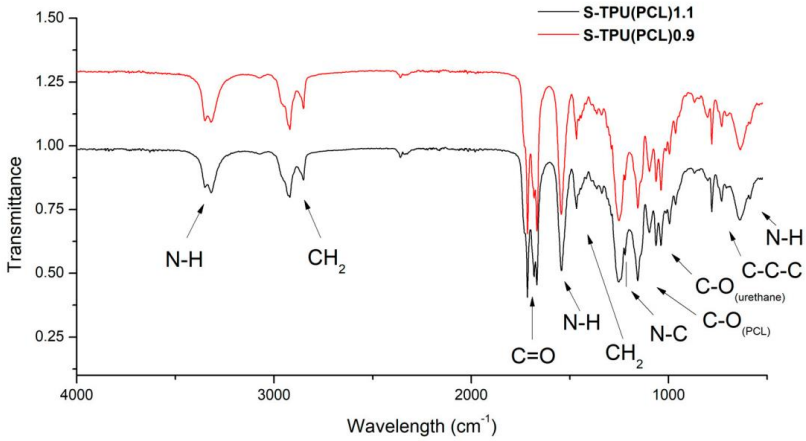

Figure 1. FTIR spectra of synthesized S-TPU(PCL)0.9/1.1.

Table 3. Description of vibrations in FTIR spectra of S-TPU(PCL)0.9/1.1.

Wavelength [cm^{-1}]	Band	Description
3330–3318w	νNH	N-H stretching of urethane bond. Free and hydrogen bonded NH.
2917w, 2850w	νCH_2	Asymmetric and symmetric stretching C-H vibrations occurring in the aliphatic chains.
1717s	νC=O	Stretching vibration of carbonyl group of PCL part.
1686vs, 1660w	νC=O	Stretching vibration of carbonyl group occurring in the urethane bond; non-hydrogen bonded and strongly hydrogen bonded urethane group.
1542m	δNH	N-H deformation of urethane bond (bending vibration).
1464m	δCH_2	C-H deformation (scissoring in plane).
1223s	νN–C	Stretching vibration (urethane bonding).
1160s	νC–O	Stretching vibration of ester (PCL part).
1065m, 1038m	νC–O	Stretching vibration of C-O occurring in the urethane bond.
730v	γC–C	Skeletal vibrations of alkaline carbon chain (-C-C_n-, n>4) present in HDI/ or PCL structure.
640m	δN–H	Wide spectrum of N-H wagging, out of plane.

vw—very weak, w—weak, m—medium, s—strong, vs—very strong, v—variable.

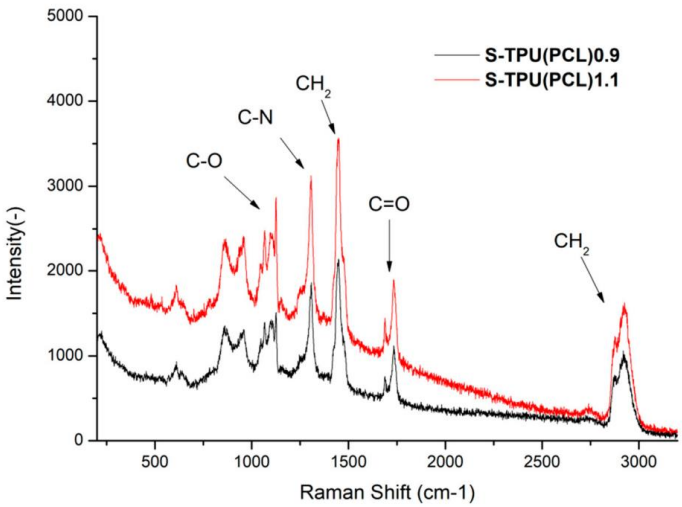

Figure 2. Raman spectroscopy of synthesized S-TPU(PCL)0.9/1.1.

Thermal Characterization (DSC, TGA)

Figure 3 presents the results of DSC study. The measurements were used to determine the glass transition temperature (T_g), melting temperature (T_m), and heat enthalpy (ΔH_m). The first heating run showed the glass transition (T_g) at the temperature of −54.8 °C for S-TPU(PCL)1.1 and around −56.5 °C for S-TPU(PCL)0.9. This corresponds to the glass transition temperature of soft segments having PCL in their structure. The glass transition temperature for neat PCL, according to the literature, is around −60 °C [34]. Moreover, first heating run showed three melting temperatures. The first melting point was observed in the range of around 20 °C and the second ones at around 57 °C. They can both be attributed to the melting of soft segments, in which homo and heterogenous nucleation, according to the literature, can take place for neat PCL [35–37]. The third melting point with the highest heat enthalpy occurred at over 130 °C. This endothermictransition is due to the melting of strong hydrogen bonded chains of hard segments in both materials (T_{m3} = 131 °C, ΔH_m = 8.2 J/g for S-TPU(PCL)0.9 and T_{m3} = 137 °C, ΔH_m = 12.5 J/g for S-TPU(PCL)1.1). In turn, the first cooling run showed crystallization temperatures of soft segments (T_{c1}) and hard segments (T_{c2}). The crystallization of both regions in S-TPU(PCL)1.1 occurred at noticeablyhigher temperatures than in the case of S-TPU(PCL)0.9.

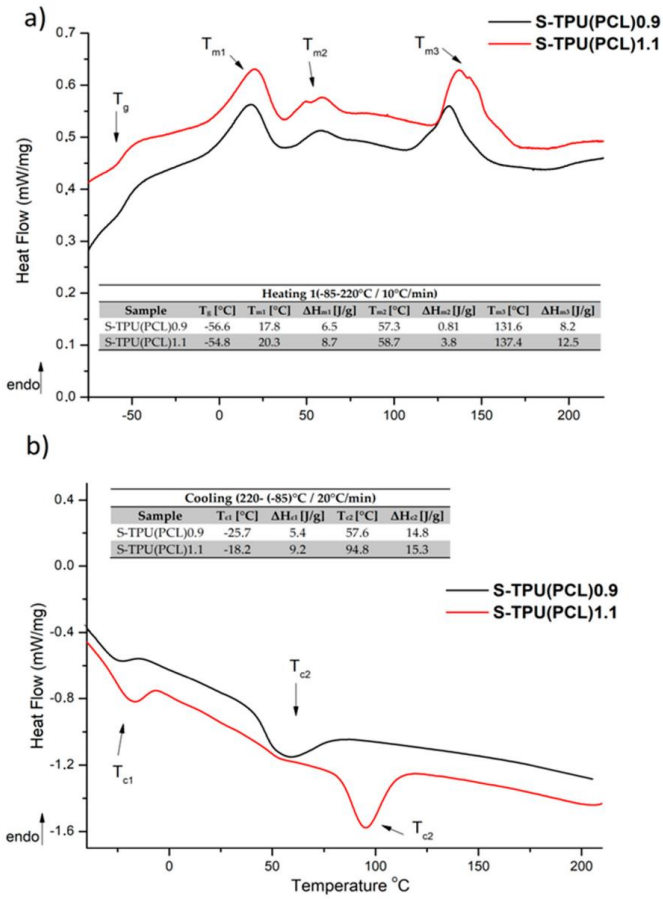

Figure 3. Differential scanning calorimetry (DSC) curves of S-TPU(PCL)0.9/1.1 with designated values; (**a**) first heating run, (**b**) first cooling run.

Figure 4 and Table 4 present the results of the thermogravimetricanalysis. The thermal stability of both synthesized polyester urethanes is above 260 °C (which shows that they can be processed for filaments until up that temperature), whilethe complete degradation occurs between 455–490 °C. Both thermo grams of the obtained materials have a similar shape. The determined derivative curves (DTG) (Figure 4) allowed forobservinga two-stage decomposition process that might indicate the presence of micro-phase separation in synthesized polyester-urethanes [38]. Thermal degradation begins with the thermal dissociation of urethane bonds (the weakest against the temperature) and it occurs at 351 °C for S-TPU(PCL)0.9 and at 393 °C for S-TPU(PCL)1.1(I stage of decomposition, T_{maxI}). The observedsmall peak of the second stage of decomposition (T_{maxII})is related to the thermal decomposition of soft segments that are present in polyesterurethanes (PCL part of chain). The results in Table 4 indicate adifferent path of degradation S-TPU(PCL)1.1 and S-TPU(PCL)0.9. It can be explained by the possibility of creating some cross-linking for the sample with 1.1:1 isocyanate index. For comparison, the decomposition temperatures of PCL tested by [39] is around 350 °C.

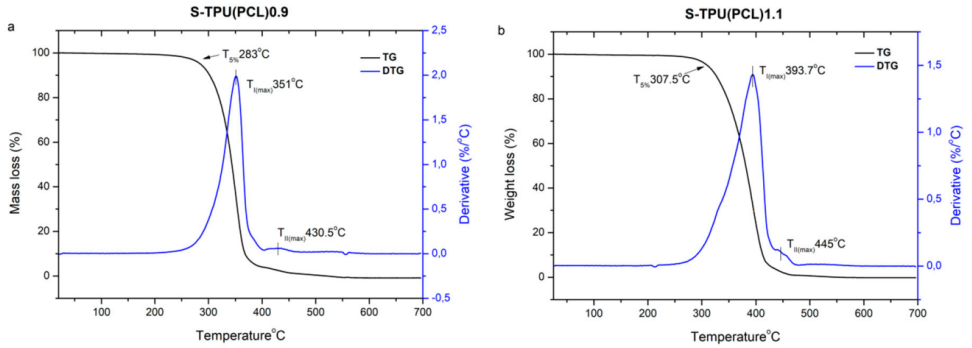

Figure 4. TGA graph of S-TPU(PCL)0.9/1.1 with a derivative curve (DTG).

Table 4. Thermogravimetric analysis (TGA) and DTG results for obtained polyurethanes.

Sample	TS[a] (°C)	T_{max}[b] (°C)		$T_{5\%}$[c] (°C)	$T_{30\%}$[d] (°C)	$T_{50\%}$[e] (°C)	T_{offset}[f] (°C)
		I	II				
S-TPU(PCL)0.9	~260	351	430.6	283.8	330.3	344.8	455
S-TPU(PCL)1.1	~275	393.7	445	307.5	358.6	381.5	493

[a] Thermal stability (up to 1% mass loss temperature), [b] First I/second II stage maximum rate of degradation temperature, [c,d,e]5,30,50% mass loss temperature, [f] complete degradation temperature.

Physico-Mechanical Poperties

Table 5 presents the results of hardness, density, and static tensile tests of the synthesized polyurethane materials. The density value was slightly different for both of the samples and equaled to 1.118 g/cm^3 for S-TPU(PCL)0.9 and 1.021 g/cm^3 for S-TPU(PCL)1.1, respectively. However, significant differences in strength properties between materials were noticed. The static tensile test showed that S-TPU(PCL)1.1 had almost three times higher tensile strength (~21 MPa) and elongation at break (~720%) than S-TPU(PCL)0.9 (~8MPa, ~200%), which was closely related with changes in structure of both materials. Isocyanate index NCO:OH=1.1:1 in S-TPU(PCL)1.1 might have contributed to the partial cross-linking of polymer chains, which is manifested by better mechanical properties, significantly higher elongation at break, and higher (~91°ShA) hardness than S-TPU(PCL)0.9 sample (~84°ShA). These observations were consistent with the research that was carried out by Kasprzyk et al. [40], in which, among others, the influence of the isocyanate index on selected mechanical properties of polyesterurethanes was examined.

Table 5. Hardness, density, and tensile properties of synthesized materials.

Material Properties		S-TPU(PCL)0.9	S-TPU(PCL)1.1
Shore Hardness [°Sh]	A	84.36 ± 1.12	91.05 ± 4.86
	D	30.30 ± 1.27	36.97 ± 6.21
Density [g/cm^3]		1.118 ± 0.007	1.021 ± 0.029
T_{SB} [MPa]		8.55 ± 0.49	21.40 ± 3.26
ε_b[%]		204.85 ± 13.74	726.32 ± 58.55
HS[%]		29	28

HS—theoretical content of hard segments.

The mechanical properties of polyurethanes depend among others on: degree of crystallinity, concentration and structure of rigid segments, or ability of soft segments to crystallize [41]. By changing the weight ratio of hard and soft segments, the mechanical properties of polyurethanes can be modified. With an increasing ratio of NCO groups to OH (0.9 to 1.1), the tensile strength increased and then reached a maximum value of 21.4 MPa for S-TPU(PCL)1.1.

Surface Properties (Contact Angle and Surface Free Energy)

Tables 6 and 7 present the results of study on surfaces properties of S-TPU(PCL)0.9/1.1. The obtained materials had water contact angle in the range from 104° (S-TPU(PCL)0.9) and 107° (S-TPU(PCL)1.1). The contacts anglesthat were studied in diiodomethanewere the lowest, ~63° and 59° for S-TP(PCL)0.9 and S-TPU(PCL)1.1, respectively. In turn, the values of contact angle that were obtained using formamide and ethylene glycol were similar and were around 81–88° (S-TPU(PCL)0.9) and 83–90° (S-TPU(PCL)1.1).

Contact angle and surface energy are important parameters, especially inmaterials that are used in biomedicine. These parameters affect the interaction of the material with the cells and allow them to adhere. The common definition says that biocompatible polymers should have a water contact angle between (55–75°), which ensures adequate adhesion of the cells to the substrate [42]. However, according to Menzies et al. [43], low values of contact angle do not provide biocompatible properties of the tested polymer. In some medical applications (e.g., dental implants), the hydrophobicity of the surface is favored to prevent excessive intervention and adhesion of live cells or organs (bacteria) that can cause the erosion of the polymeric material.

Table 6. Contact angle measurements of S-TPU(PCL)0.9/1.1 with respect to various liquids.

Sample	Contact Angle Measurements			
	Diiodomethane [°]	Formamide [°]	Water [°]	Ethylene Glycol [°]
S-TPU(PCL)0.9	63.22 ± 1.08	88.91 ± 2.08	104.43 ± 2.07	81.62 ± 0.82
S-TPU(PCL)1.1	59.86 ± 1.28	90.10 ± 1.99	107.86 ± 0.88	83.15 ± 2.73

An increase in the isocyanate index (up to 1.1) resulted in an increase in contact angles towards polar liquids, and thus the total surface energy of S-TPU(PCL)1.1 (~23 and 27 mN/m) was lower

than for S-TPU(PCL)0.9 (~25 and 28 mN/m), as calculated by Owens–Wendt and acid–base theory, respectively. It should be point out that too high surface energy (high hydrophilicity of the surface) can even causedisruption ofcell-cell interactions and reduce biocompatibility [43]. Therefore, depending on the application, biomaterials with both hydrophilic and hydrophobic properties should be developed.

Table 7. Surface energy of S-TPU(PCL)0.9/1.1 calculated using the Owens–Wendt and acid-base method.

Sample	Owens-Wendt Method			Acid-Base Method				
	Total Surface Energy	Diperse Part	Polar Part	Total Surface Energy	L-W Part	Acid-Base Part	Acid Part	Base Part
	mN/m	mN/m	mN/m	mN/m	mN/m	mN/m	mN/m	mN/m
S-TPU(PCL)0.9	25.87	25.87	0.00	28.69	28.14	0.55	0.24	0.31
S-TPU(PCL)1.1	23.52	23.30	0.21	27.68	26.46	1.21	0.27	1.35

Interactions with Media (Water Absorption Test, Short-, and Long-Term Degradation Tests)

Figure 5 summarizes the results of absorption test of S-TPU(PCL)0.9 and 1.1 samples during incubation in distilled water. These data show the percentage of water that was absorbed by polyester-urethane materials during the measurement. At the first hour of incubation, the largest increase in both samples mass was observed. After this time, the rate of water absorption remained at a relatively constant level (between 1.8–2.1%). After 72 hours, the water absorption of both samples was approximately 2.2%.

Data from the graph showed that the S-TPU(PCL)0.9 sample wasslightly more susceptible to water absorption in the initial stage of the study. These observations coincided with the results of the water contact angle measurements: S-TPU (PCL)0.9 (~104°), S-TPU (PCL)1.1 (~107°), therefore less hydrophobic material absorbs more water. Slower water absorption of S-TPU(PCL)1.1 might also be connected with difficult access of water molecules between partially cross-linked chains.

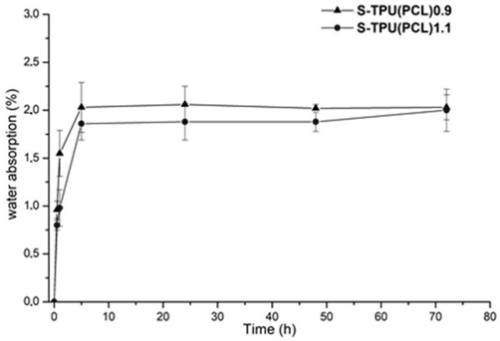

Figure 5. Graph of percentage water absorption change over time of S-TPU(PCL)0.9/1.1 samples.

Table 8 summarizes the results of a sample incubation test in phosphate buffer (PBS) at 37 °C. PBS buffer (pH~7.4) provides a hydrolytic degradation environment. After one week of incubation, a very slight weight loss was observed. However, after 12 weeks of incubation, the mass of the samples increased slightly, which could be caused by the precipitation of salt on the samples surface or bywater absorption. There was no significant weight loss after 12 weeks of incubation, thus the polyester urethanesthat were tested in this work proved to be stable during long-term degradation in the PBS environment.

Table 8. Mass change of S-TPU(PCL) samples 0.9/1.1 during incubation in PBS at 37 °C.

Sample	Time of Incubation [Weeks]		
	1	4	12
	Mass Change [%]		
S-TPU(PCL)0.9	99.575 ± 0.062	99.887 ± 0.080	100.168 ± 0.069
S-TPU(PCL)1.1	99.972± 0.039	99.973 ± 0.039	100.182 ± 0.075

Short-term degradation (in concentrated aqueous solutions of 2 M HCl and 5 M NaOH) included microscopic studies of the degradation progress (Figure 6a), measurements of the percentage loss of mass of the tested samples (Figure 6b), and FTIR spectra analysis from degradation progress (Figure 6c,d). The accelerated degradation results clearly illustrate thatthe degradation of polyester-urethanes was highly dependent on the environment in which the process was carried out. The tested materials were more susceptible to degradation in an acidic than the basic environment. In 2 M HCl, the mass of samples after 32 days decreased by 57 and 56%, respectively, for S-TPU(PCL)0.9 and S-TPU(PCL)1.1. After the same time, the mass of samples in 5 M NaOH decreased by 37% and 26%, respectively, for S-TPU(PCL)0.9 and S-TPU(PCL)1.1.

Microscopic photos showed that, after 32 days of incubation in the acidic environment, the structure of both samples was destroyed, while the erosion of the material in the alkaline medium progressed surface (the material did not disintegrate by volume, Figure 6a). It was also noted that, in the initial stages of incubation in both media, the samples with an isocyanate index NCO: OH 1.1:1 were more resistant to erosion (14 days incubation in HCl, S-TPU(PCL)1.1 weight loss equal to 26%, when for S-TPU(PCL)0.9 was 42%). The mechanism and degradation progress of synthesized materials werealso observed by FTIR spectra analysis (Figure 6c,d). The obtained FTIR spectra showed that, during incubation in aqueous HCl and NaOH solutions, the band at 1720 cm^{-1}, corresponding to the stretching vibration of carbonyl group (PCL part), disappeared (Figure 6c,d). However, it should be noted that this effect was more noticeable in the case of the alkaline environment and the sample with a lower isocyanate index (NCO: OH = 0.9:1). It can be seen that erosion at the beginning of the test occurred through the destruction of ester bonds in soft segments and the degradation of hydrogen bonded urethane bonds (visible disappearance of the N–H stretching vibration around 3340 cm^{-1}). The intensity of the peak originating from N–H deformation (~1542 cm^{-1}) decreased, which suggested the breakdown of urethane bonds. Peaks originating from νC–O occurring in the urethane bond (at 1065, 1038 cm^{-1}) were also deformed. An appearance of peak around 1220–1200 cm^{-1} might be associated with C–O stretching vibration that originated from alcohols formed as a result of urethane bond degradation.

A rapid rate of degradation of polyester-urethanes (both S-TPU(PCL)0.9 and S-TPU(PCL)1.1) can be observed in the acidic environment after five days, until about 21 days. After 21 days, the degradation rate remained relatively stable. In turn, a completely different rate of mass changes over time, as compared to degradation in the acid environment, characterizes the degradation in the alkaline environment. In 5 M aqueous NaOH solution, the rate of degradation had a relatively linear character. The hydrolysis of polyesters depends on the pH of the environment. The environment containing the acidic proton is significantly more aggressive to the obtained polyester-urethanes. A similar course of short-term degradation behind concentrated aqueous solutions was observed in our earlier works [33].

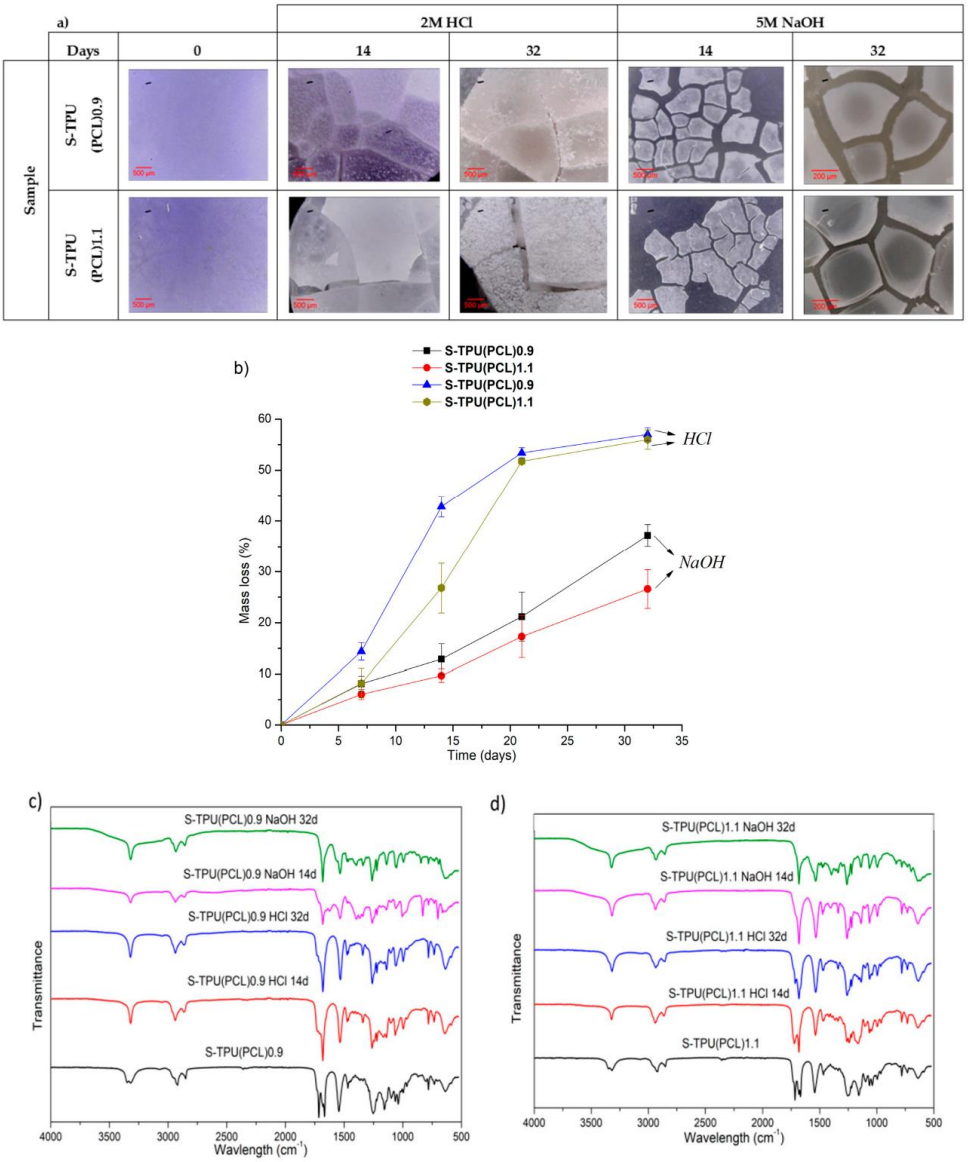

Figure 6. Results of study on short-term degradation in 2M HCl and 5M NaOH of S-TPU(PCL)0.9/1.1, (**a**) optical microscopy, (**b**) graph of percentage mass loss during degradation process, (**c**,**d**) FTIR spectrum measured at different time of degradation of S-TPU(PCL)0.9.

Cytotoxicity (In Vitro)

Figure 7 presents the effect of synthesized materials extracts on the growth of C2C12 cells that were studied by MTT assay. The cytotoxicity examination is one of the tests to determine whetherthe material is biocompatible and suitable for medical application.

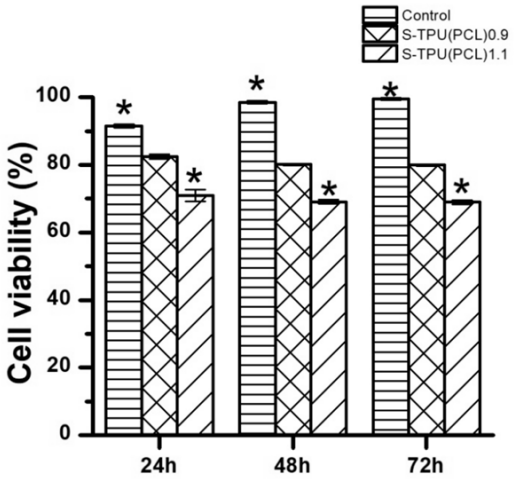

Figure 7. The effect of S-TPU(PCL)0.9/1.1 extracts on the growth of C2C12 cells tested via MTT assay after 24, 48, and 72 h of incubation.

Figure 7 shows that C2C12 cells viability was above 80% for the obtained S-TPU(PCL)0.9, and this difference was not statistically significant ($p < 0.05$) in comparison to the control, which represents 100% of cell viability. On the other hand, S-TPU(PCL)1.1 represents lower cell viability (~70%) in comparison to the S-TPU(PCL)0.9, but the results were not statistically different between each other. The statistical difference was observed between S-TPU(PCL)1.1 and the control, which means that the biocompatibility significantly decreased for S-TPU(PCL).1.1 ($p < 0.05$). The cytotoxicity test showed that S-TPU(PCL)0.9 that was obtained with medical-grade PCL macrodiol may be suitable for medical applications of such filaments.

3.2. Melt-Extrusion of F-TPU(PCL)0.9 Filament

It was necessary to choose the appropriate temperature profile, extrusion speed, and the degree of granulate dosage in order to obtain a stable dimensional filament. Table 9 presents the results of the melt-extrusion process. In process number 1, the temperature profile between 165–175 °C was too low and the inclusions in the material causing discontinuity of the filament were observed. It was a non-plasticized polymer granulate, therefore, in process 2, both the temperature and the extrusion speed were increased in order to increase the pressure in the extruder barrel, which could improve the degree of plasticization. It was noted that the changes introduced led to degradation of the material, the temperature turned out to be too high, and a material with many visible blisters of a yellowing color was obtained. In process 3, the temperature was again lowered, and plasticized material was obtained, however with too large diameter (too much material in the cylinder and the insufficient temperature of the zone 2 (T2) caused a large swelling of the extruded wire). The above observations allowed for the selection of appropriate parameters, which ensured obtaining a stable filament F-TPU(PCL)0.9 (process 4).

Table 9. Melt-extrusion parameters of F-TPU(PCL)0.9 * filament formation.

Process	T1 [°C]	T2 [°C]	Rotation Speed [rpm]	Dose Rate (g/min)	Filament Appearance
1	165	175	40	50	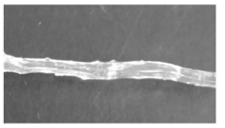
2	185	200	80	50	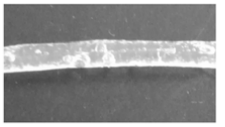
3	185	190	80	50	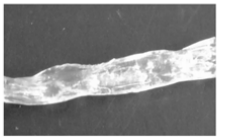
4	175	185	50	30	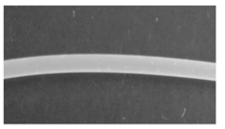

* For the filament formation stage the S-TPU(PCL)0.9 was selected due to, cytotoxicity results, higher swelling ratio, as well as lower water contact angle than S-TPU(PCL)1.1 sample.

4. Conclusions

The purpose of this work in the first step was the synthesis and detailed characterization of polyester-urethanes that are based on biodegradable PCL and aliphatic HDI, differing by the isocyanateindex (NCO:OH = 0.9: 1 and 1.1:1, respectively) and in the second step processing of thus obtained TPU into filament for use in 3D FDM printers. On the basis of the mechanical, physic-chemical, and thermal characteristics, it was found that, with the increase of NCO:OH index, the Shore hardness, tensile strength, and thermal stability of solid polyurethanes increased. With the increase of the NCO:OH ratio, the water absorption decreases, which is adequate to the result of contact angle studies and the higher hydrophobicity of the S-TPU(PCL)1.1 sample. The above relationships were probably due to the partial cross-linking of S-TPU(PCL)1.1 polymer chains. Both of the materials were stable in the PBS environment. On the basis of the conducted short-term degradation study, it was observed that the obtained materials were more susceptible to degradation in acidic than alkaline, and in both cases degradation begun with the cracking of strongly hydrogen bonded urethane bonds and the destruction of ester bonds that originatedfrom PCL. The S-TPU(PCL)0.9 was characterized by the satisfactory biocompatibility with respect to C2C12 cells in comparison to the S-TPU(PCL)1.1, thus it may be suggested for further development in the medical field. When selecting the appropriate extrusion parameters, it is possible to obtain a stable filament. However, it is the production of small sections of the filament. In order to be able to receive the filament in a larger scale, the melt-extrusion system should be complemented with at least a cooling system (with a cooling tub), a laser measure of the diameter, and a system of the filament winding.

As a result of the studies, a 3D printing filament with well-characterized properties was obtained, which in the forthcoming tests will be evaluated for the printability of 3D structures while using the FDM 3D printer.

Author Contributions: Conceptualization, J.K.-L. and I.G.; methodology, A.H. and I.G.; investigation, A.H., M.K. and A.S.; data curation, M.K., A.S.; formal analysis, A.H. and H.J.; Writing—Original Draft preparation, A.H.; Writing—Review and Editing, A.H. and H.J.; supervision, J.K.-L. and H.J.; funding acquisition, J.K.-L. and H.J.

Funding: Part of the research was founded by Gdansk University of Technology—Centre for Knowledge and Technology Transfer, grant number [26].

Acknowledgments: Authors would like to thank to Michał Strankowski who conducted DSC measurements (Polymer Technology Department, Gdansk University of Technology).

Conflicts of Interest: The authors declare no conflict of interest.

References

1. Salentijn, G.I.J.; Oomen, P.E.; Grajewski, M.; Verpoorte, E. Fused Deposition Modeling 3D Printing for (Bio)analytical Device Fabrication: Procedures, Materials, and Applications. *Anal. Chem.* **2017**, *89*, 7053–7061. [CrossRef] [PubMed]
2. Skowyra, J.; Pietrzak, K.; Alhnan, M.A. Fabrication of extended-release patient-tailored prednisolone tablets via fused deposition modelling (FDM) 3D printing. *Eur. J. Pharm. Sci.* **2015**, *68*, 11–17. [CrossRef]
3. Mohseni, M.; Hutmacher, D.W.; Castro, N.J. Independent evaluation of medical-grade bioresorbable filaments for fused deposition modelling/fused filament fabrication of tissue engineered constructs. *Polymers* **2018**, *10*, 40. [CrossRef]
4. Okwuosa, T.C.; Stefaniak, D.; Arafat, B.; Isreb, A.; Wan, K.-W.; Alhnan, M.A. A Lower Temperature FDM 3D Printing for the Manufacture of Patient-Specific Immediate Release Tablets. *Pharm. Res.* **2016**, *33*, 2704–2712. [CrossRef] [PubMed]
5. Jung, S.Y.; Lee, S.J.; Kim, H.Y.; Park, H.S.; Wang, Z.; Kim, H.J.; Yoo, J.J.; Chung, S.M.; Kim, H.S. 3D printed polyurethane prosthesis for partial tracheal reconstruction: A pilot animal study. *Biofabrication* **2016**, *8*, 045015. [CrossRef]
6. Hung, K.C.; Tseng, C.S.; Hsu, S.H. Synthesis and 3D Printing of biodegradable polyurethane elastomer by a water-based process for cartilage tissue engineering applications. *Adv. Healthc. Mater.* **2014**, *3*, 1578–1587. [CrossRef]
7. Armentano, I.; Bitinis, N.; Fortunati, E.; Mattioli, S.; Rescignano, N.; Verdejo, R.; Lopez-Manchado, M.A.; Kenny, J.M. Multifunctional nanostructured PLA materials for packaging and tissue engineering. *Prog. Polym. Sci.* **2013**, *38*, 1720–1747. [CrossRef]
8. Seyednejad, H.; Ghassemi, A.H.; van Nostrum, C.F.; Vermonden, T. Functional aliphatic polyesters for biomedical and pharmaceutical applications. *J. Control. Release* **2011**, *152*, 168–176. [CrossRef]
9. Gogolewski, S.; Pennings, A.J. An artificial skin based on biodegradable mixtures of polylactides and polyurethanes for full-thickness skin wound covering. *Die Makromol. Chemie Rapid Commun.* **1983**, *4*, 675–680. [CrossRef]
10. Gogolewski, S.; Walpoth, B.; Rheiner, P. Polyurethane microporous membranes as pericardial substitutes. *Colloid Polym. Sci.* **1987**, *265*, 971–977. [CrossRef]
11. Gogolewski, S.; Galletti, G.; Ussia, G. Polyurethane vascular prostheses in pigs. *Colloid Polym. Sci.* **1987**, *265*, 774–778. [CrossRef]
12. Qiu, K.; Zhao, Z.; Haghiashtiani, G.; Guo, S.-Z.; He, M.; Su, R.; Zhu, Z.; Bhuiyan, D.B.; Murugan, P.; Meng, F.; et al. 3D Printed Organ Models with Physical Properties of Tissue and Integrated Sensors. *Adv. Mater. Technol.* **2017**, *3*, 1700235. [CrossRef] [PubMed]
13. Guelcher, S.A.; Gallagher, K.M.; Didier, J.E.; Klinedinst, D.B.; Doctor, J.S.; Goldstein, A.S.; Wilkes, G.L.; Beckman, E.J.; Hollinger, J.O. Synthesis of biocompatible segmented polyurethanes from aliphatic diisocyanates and diurea diol chain extenders. *Acta Biomater.* **2005**, *1*, 471–484. [CrossRef] [PubMed]
14. Tatai, L.; Moore, T.G.; Adhikari, R.; Malherbe, F.; Jayasekara, R.; Griffiths, I.; Gunatillake, P.A. Thermoplastic biodegradable polyurethanes: The effect of chain extender structure on properties and in-vitro degradation. *Biomaterials* **2007**, *28*, 5407–5417. [CrossRef] [PubMed]
15. Da Silva, G.R.; da Silva-Cunha, A.; Behar-Cohen, F.; Ayres, E.; Oréfice, R.L. Biodegradation of polyurethanes and nanocomposites to non-cytotoxic degradation products. *Polym. Degrad. Stab.* **2010**, *95*, 491–499. [CrossRef]

16. Haryńska, A.; Gubanska, I.; Kucinska-Lipka, J.; Janik, H. Fabrication and Characterization of Flexible Medical-Grade TPU Filament for Fused Deposition Modeling 3DP Technology. *Polymers* **2018**, *10*, 1304. [CrossRef]
17. Xiao, J.; Gao, Y. The manufacture of 3D printing of medical grade TPU. *Prog. Addit. Manuf.* **2017**, *2*, 117–123. [CrossRef]
18. Du, J.; Zhu, T.; Yu, H.; Zhu, J.; Sun, C.; Wang, J.; Chen, S.; Wang, J.; Guo, X. Potential applications of three-dimensional structure of silk fibroin/poly(ester-urethane) urea nanofibrous scaffold in heart valve tissue engineering. *Appl. Surf. Sci.* **2018**, *447*, 269–278. [CrossRef]
19. Barrioni, B.R.; De Carvalho, S.M.; Oréfice, R.L.; De Oliveira, A.A.R.; Pereira, M.D.M. Synthesis and characterization of biodegradable polyurethane films based on HDI with hydrolyzable crosslinked bonds and a homogeneous structure for biomedical applications. *Mater. Sci. Eng. C* **2015**, *52*, 22–30. [CrossRef]
20. Laube, T.; Weisser, J.; Berger, S.; Börner, S.; Bischoff, S.; Schubert, H.; Gajda, M.; Bräuer, R.; Schnabelrauch, M. In situ foamable, degradable polyurethane as biomaterial for soft tissue repair. *Mater. Sci. Eng. C* **2017**, *78*, 163–174. [CrossRef]
21. Chiono, V.; Mozetic, P.; Boffito, M.; Sartori, S.; Gioffredi, E.; Silvestri, A.; Rainer, A.; Giannitelli, S.M.; Trombetta, M.; Nurzynska, D.; et al. Polyurethane-based scaffolds for myocardial tissue engineering. *Interface Focus* **2014**, *4*, 1–11. [CrossRef] [PubMed]
22. Shahrousvand, M.; Hoseinian, M.S.; Ghollasi, M.; Karbalaeimahdi, A.; Salimi, A.; Tabar, F.A. Flexible magnetic polyurethane/Fe2O3 nanoparticles as organicinorganic nanocomposites for biomedical applications: Properties and cell behavior. *Mater. Sci. Eng. C* **2017**, *74*, 556–567. [CrossRef] [PubMed]
23. Lee, S.-Y.; Wu, S.-C.; Chen, H.; Tsai, L.-L.; Tzeng, J.-J.; Lin, C.-H.; Lin, Y.-M. Synthesis and Characterization of Polycaprolactone-Based Polyurethanes for the Fabrication of Elastic Guided Bone Regeneration Membrane. *Biomed Res. Int.* **2018**, *2018*, 1–13. [CrossRef] [PubMed]
24. Güney, A.; Gardiner, C.; McCormack, A.; Malda, J.; Grijpma, D. Thermoplastic PCL-b-PEG-b-PCL and HDI Polyurethanes for Extrusion-Based 3D-Printing of Tough Hydrogels. *Bioengineering* **2018**, *5*, 99. [CrossRef] [PubMed]
25. Fuenmayor, E.; Forde, M.; Healy, A.V.; Devine, D.M.; Lyons, J.G.; McConville, C.; Major, I. Material Considerations for Fused-Filament Fabrication of Solid Dosage Forms. *Pharmaceutics* **2018**, *10*, 44. [CrossRef] [PubMed]
26. Belter, J.T.; Dollar, A.M. Strengthening of 3D printed fused deposition manufactured parts using the fill compositing technique. *PLoS ONE* **2015**, *10*, e0122915. [CrossRef] [PubMed]
27. Zein, I.; Hutmacher, D.W.; Tan, K.C.; Teoh, S.H. Fused deposition modeling of novel scaffold architectures for tissue engineering applications. *Biomaterials* **2002**, *23*, 1169–1185. [CrossRef]
28. Puig, T.; Martin, J.; Polonio, E.; Guerra, A.; Rabionet, M.; Ciurana, J. Design of a Scaffold Parameter Selection System with Additive Manufacturing for a Biomedical Cell Culture. *Materials* **2018**, *11*, 1427.
29. Ariadna, G.-P.; Marc, R.; Teresa, P.; Joaquim, C. Optimization of Poli(ε-caprolactone) Scaffolds Suitable for 3D Cancer Cell Culture. *Procedia CIRP* **2016**, *49*, 61–66. [CrossRef]
30. Kucinska-Lipka, J.; Marzec, M.; Gubanska, I.; Janik, H. Porosity and swelling properties of novel polyurethane–ascorbic acid scaffolds prepared by different procedures for potential use in bone tissue engineering. *J. Elastomers Plast.* **2017**, *49*, 440–456. [CrossRef]
31. Tanzi, M.C.; Verderio, P.; Lampugnani, M.G.; Resnati, M.; Dejana, E.; Sturani, E. Cytotoxicity of some catalysts commonly used in the synthesis of copolymers for biomedical use. *J. Mater. Sci. Mater. Med.* **1994**, *5*, 393–396. [CrossRef]
32. Heijkants, R.G.J.C.; Van Calck, R.V.; Van Tienen, T.G.; De Groot, J.H.; Buma, P.; Pennings, A.J.; Veth, R.P.H.; Schouten, A.J. Uncatalyzed synthesis, thermal and mechanical properties of polyurethanes based on poly(ε-caprolactone) and 1,4-butane diisocyanate with uniform hard segment. *Biomaterials* **2005**, *26*, 4219–4228. [CrossRef]
33. Kucińska-Lipka, J.; Malysheva, K.; Włodarczyk, D.; Korchynskyi, O.; Karczewski, J.; Kostrzewa, M.; Gubanska, I.; Janik, H. The Influence of Calcium Glycerophosphate (GPCa) Modifier on Physicochemical, Mechanical, and Biological Performance of Polyurethanes Applicable as Biomaterials for Bone Tissue Scaffolds Fabrication. *Polymers* **2017**, *9*, 329. [CrossRef]
34. Król, P.; Król, B.; Pielichowska, K.; Szałański, P.; Kobylarz, D. Polyurethanes modified by hydroxyapatite as biomaterials. *Polimery* **2015**, *60*, 559–571. [CrossRef]

35. Mucha, M.; Tylman, M.; Mucha, J. Crystallization kinetics of polycaprolactone in nanocomposites. *Polimery* **2015**, *60*, 686–692. [CrossRef]
36. Wurm, A.; Zhuravlev, E.; Eckstein, K.; Jehnichen, D.; Pospiech, D.; Androsch, R.; Wunderlich, B.; Schick, C. Crystallization and Homogeneous Nucleation Kinetics of Poly(ε-caprolactone) (PCL) with Different Molar Masses. *Macromolecules* **2012**, *45*, 3816–3828. [CrossRef]
37. Zhuravlev, E.; Schmelzer, J.W.P.; Wunderlich, B.; Schick, C. Kinetics of nucleation and crystallization in poly(ε-caprolactone) (PCL). *Polymer* **2011**, *52*, 1983–1997. [CrossRef]
38. Datta, J.; Kasprzyk, P.; Błażek, K.; Włoch, M. Synthesis, structure and properties of poly(ester-urethane)s obtained using bio-based and petrochemical 1,3-propanediol and 1,4-butanediol. *J. Therm. Anal. Calorim.* **2017**, *130*, 261–276. [CrossRef]
39. Suggs, L.J.; Moore, S.A.; Mikos, A.G. Synthetic Biodegradable Polymers for Medical Applications. In *Physical Properties of Polymers Handbook*; Springer: New York, NY, USA, 2007; pp. 939–950.
40. Kasprzyk, P.; Datta, J. Effect of molar ratio [NCO]/[OH] groups during prepolymer chains extending step on the morphology and selected mechanical properties of final bio-based thermoplastic poly(ether-urethane) materials. *Polym. Eng. Sci.* **2018**, *58*, E199–E206. [CrossRef]
41. Lee, D.-K.; Tsai, H.-B. Properties of segmented polyurethanes derived from different diisocyanates. *J. Appl. Polym. Sci.* **2000**, *75*, 167–174. [CrossRef]
42. Guelcher, S.A.; Srinivasan, A.; Dumas, J.E.; Didier, J.E.; McBride, S.; Hollinger, J.O. Synthesis, mechanical properties, biocompatibility, and biodegradation of polyurethane networks from lysine polyisocyanates. *Biomaterials* **2008**, *29*, 1762–1775. [CrossRef] [PubMed]
43. Menzies, K.L.; Jones, L. The impact of contact angle on the biocompatibility of biomaterials. *Optom. Vis. Sci.* **2010**, *87*, 387–399. [CrossRef] [PubMed]

4.3 PAPER 3: Processing of Polyester-Urethane Filament and Characterization of FFF 3D Printed Elastic Porous Structures with Potential in Cancellous Bone Tissue Engineering

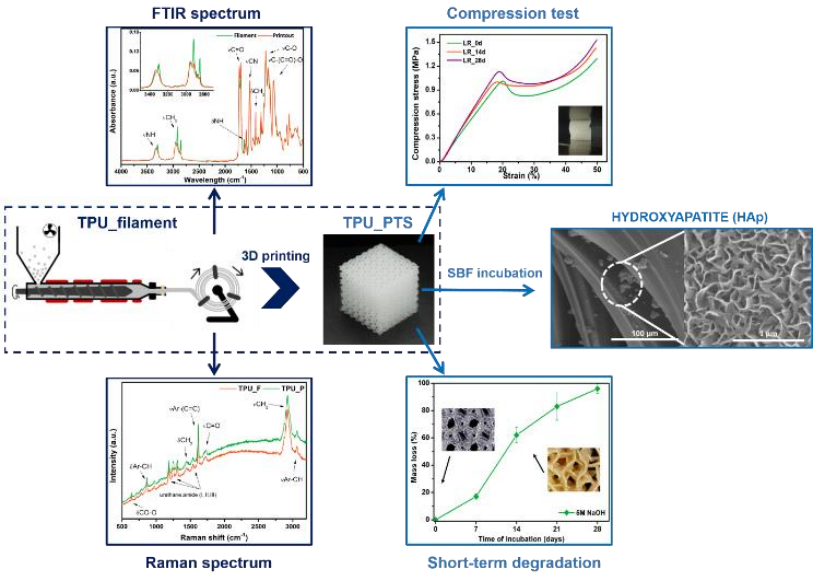

Graphical abstract, source: DOI: 10.3390/ma13194457

Authors (percentage share): Agnieszka Haryńska(corresponding author) (50%), Iga Carayon (10%), Paulina Kosmela (5%), Anna Brillowska-Dąbrowska (10%), Marcin Łapiński (5%), Justyna Kucińska-Lipka (10%), Helena Janik (10%)
Journal: Materials (Basel)
DOI: 10.3390/ma13194457
Index: Q2, IF_{2019}=3.057, MNSiW = 140 pts
CRediT: Conceptualization (in part), Data Curation (lead), Formal Analysis (lead), Investigation (FTIR, Raman, H-NMR, MFR, tensile and compression tests, hardness, contact angle, surface free energy, long and short-term degradation studies, SBF incubation, optical microscopy), Methodology (lead), Project Administration (in part), Visualization (lead), Writing – Original Draft Preparation (lead), Writing – Review & Editing (lead).
Realized doctoral research tasks: **II (filament formation)** – formation of 3D-printable filament using commercial TPU granules on a technical scale in a continuous manner; description of a filament-formation process, parameters, and critical points influencing the formation of a stable elastic filament; **III (filament characterization)** – a comprehensive characterization of the formed TPU(E) filament; **IV (evaluation of the filament stability)** – analysis of structural, thermal and rheological properties of the TPU(E) filament before and after the 3D printing process;

V (3D printing) – design of digital 3D models of test samples and porous structures (scaffolds) with diverse architecture *via* Autodesk Inventor software; optimization of the 3D printing parameters;
VI (examination of the printouts in terms of their application in medicine) – preliminary evaluation of the printed TPU elastic porous structures as scaffolds in cancellous tissue engineering (study of degradability, biocompatibility, bioactivity, mechanical, and surface properties).

Material code: TPU(E)

BRIEF DESCRIPTION OF THE PUBLICATION

Discussed topics: literature review of filament formation by melt-extrusion in a continuous manner.

Scope of the publication: filament formation in a continuous manner; comparison of material properties before and after FFF 3D printing; design and printing of porous 3D structures; preliminary evaluation of biological properties as cancellous bone porous tissue scaffolds.

Novelty of the publication: description of filament-formation line, including all the necessary processing parameters and apparatus to obtain high-quality flexible filament in a continuous manner.

Main scientific achievement: manufacture of medical-grade poly(ester urethane) filament TPU(E) exhibiting remarkable printability; design and 3D printing of porous structures that meet the prerequisites of cancellous bone porous tissue scaffolds.

Outline: The article covers three main issues: (1) description of the filament-formation process in a continuous system (technical scale), (2) examination of the filament stability over 3D printing time, and (3) evaluation (*in vitro*) of the printed porous structures as candidates for cancellous bone tissue scaffolds, yielding the entire cycle from filament manufacture to functional end-product. The first part of the article describes in detail the production line and the parameters necessary to obtain high-quality TPU(E) filament in a continuous extrusion system. In the second part, TPU(E) filament was characterized in terms of structural (FTIR, Raman), thermal (DSC, TGA), mechanical and rheological tests (tensile testing, hardness, MFR). In the third part, several *in vitro* studies including long-term incubation in phosphate-buffered saline (PBS), cytotoxicity test, contact angle (CA), and surface free energy (SFE) measurements, were performed. The results classified the filament as a biomaterial, therefore, a series of porous 3D structures with diverse architecture were designed and printed. Then, they were incubated in simulated body fluid (SBF) to assess bioactivity. The effect of exposure to the SBF on the printouts morphology, stability, and mechanical properties was investigated by SEM, EDS, mass measurements, and compression test, respectively. Finally, the effect of short-term degradation on porous structures was monitored *via* mass measurements and microscopy observation. As a result, the highly flexible poly(ester urethane) filament in a continuous manner was manufactured. The filament was stable under 3D printing conditions and possessed remarkable

printability characterized by high dimensional stability of the obtained printouts and repeatability. The *in vitro* studies showed that the TPU printouts are stable for up to 6 months during PBS incubation, biocompatible, and hydrophilic. A study in SBF revealed that porous structures were susceptible to mineralization and that hydroxyapatite (HAp) released on the surface significantly increased their compressive strength. The determined strength values of TPU printouts were within the ranges appropriate for human cancellous bone, which pre-qualified them for bone tissue engineering applications. The filament-formation system presented in the article was applied in subsequent stages of the doctoral dissertation to form a bio-filament (PLA/TPS).

materials

MDPI

Article

Processing of Polyester-Urethane Filament and Characterization of FFF 3D Printed Elastic Porous Structures with Potential in Cancellous Bone Tissue Engineering

Agnieszka Haryńska [1,*], Iga Carayon [1], Paulina Kosmela [1], Anna Brillowska-Dąbrowska [2,*], Marcin Łapiński [3], Justyna Kucińska-Lipka [1] and Helena Janik [1]

1 Department of Polymers Technology, Faculty of Chemistry, Gdansk University of Technology (GUT), Narutowicza Street 11/12, 80-233 Gdansk, Poland; iga.carayon@pg.edu.pl (I.C.); paulina.kosmela@pg.edu.pl (P.K.); juskucin@pg.edu.pl (J.K.-L.); heljanik@pg.edu.pl (H.J.)
2 Department of Molecular Biotechnology and Microbiology, Faculty of Chemistry, Gdansk University of Technology (GUT), Narutowicza Street 11/12, 80-233 Gdansk, Poland
3 Institute of Nanotechnology and Materials Science, Faculty of Applied Physics and Mathematics, Gdansk University of Technology (GUT), Narutowicza Street 11/12, 80-233 Gdansk, Poland; marcin.lapinski@pg.edu.pl
* Correspondence: agnieszka.harynska@pg.edu.pl (A.H.); annbrill@pg.edu.pl (A.B.-D.)

Received: 14 September 2020; Accepted: 5 October 2020; Published: 8 October 2020

Abstract: This paper addresses the potential of self-made polyester-urethane filament as a candidate for Fused Filament Fabrication (FFF)-based 3D printing (3DP) in medical applications. Since the industry does not provide many ready-made solutions of medical-grade polyurethane filaments, we undertook research aimed at presenting the process of thermoplastic polyurethane (TPU) filament formation, detailed characteristics, and 3DP of specially designed elastic porous structures as candidates in cancellous tissue engineering. Additionally, we examined whether 3D printing affects the structure and thermal stability of the filament. According to the obtained results, the processing parameters leading to the formation of high-quality TPU filament (TPU_F) were captured. The results showed that TPU_F remains stable under the FFF 3DP conditions. The series of in vitro studies involving long- and short-term degradation (0.1 M phosphate-buffered saline (PBS); 5 M sodium hydroxide (NaOH)), cytotoxicity (ISO 10993:5) and bioactivity (simulated body fluid (SBF) incubation), showed that TPU printouts possessing degradability of long-term degradable tissue constructs, are biocompatible and susceptible to mineralization in terms of hydroxyapatite (HAp) formation during SBF exposure. The formation of HAp on the surface of the specially designed porous tissue structures (PTS) was confirmed by scanning electron microscope (SEM) and energy-dispersive X-ray spectroscopy (EDS) studies. The compression test of PTS showed that the samples were strengthened due to SBF exposure and deposited HAp on their surface. Moreover, the determined values of the tensile strength (~30 MPa), Young's modulus (~0.2 GPa), and compression strength (~1.1 MPa) allowed pre-consideration of TPU_F for FFF 3DP of cancellous bone tissue structures.

Keywords: filament formation; Fused Filament Fabrication; 3D printing; thermoplastic polyurethane; tissue scaffolds; material characterization

1. Introduction

For years, polyurethanes have been successfully used as materials in biomedical applications. Their complex chemical structure and possibility of modification enable the properties to be adjusted

to the desired needs. Polyurethanes are widely utilized in drug delivery systems, vascular and cardiac surgery or tissue engineering, thus novel and advanced methods of their processing are being constantly developed. Recently, 3D printing (3DP) has become one of the most desired methods of product fabrication for some medical applications [1]. This is most likely due to the design freedom combined with the possible direct use of DICOM (Digital Imaging and Communications in Medicine) files, which allows for the production of patient-matched and complex 3D medical structures [2,3]. Medicine uses many different techniques of 3DP, including SLS (Selective Laser Sintering), bioprinting or PJ (PolyJet). However, polyurethanes are most often applied with SLA (Stereolithography), bioplotting or FFF (Fused Filament Fabrication) 3DP techniques [4]. FFF is one of the most common 3D printer types due to its relatively low purchase, maintenance, and feedstock costs and high availability. It uses thermoplastic-based materials in the form of fiber with a constant diameter (filament) and operates a mini-heated extruder where plastification of the polymer takes place. Such plasticized material is deposited on the platform following the loaded design path, forming the desired object.

The unique properties of polyurethanes, including flexibility, biocompatibility, hemocompatibility or degradability are highly desirable features in tissue engineering applications. Therefore, research has been undertaken on the use of thermoplastic polyurethanes (TPU) in FFF 3DP of porous tissue structures [5–7]. A review of works related to the polyurethane-based elastic tissue constructs formed via FFF 3DP is presented for example in Przybytek et al. [8]. Nevertheless, none of these works describes in detail the TPU filament formation process and its characteristics. They focus on comprehensive in vitro and in vivo research of the ready-made printed structures. Therefore, we undertook complex research starting from filament formation to characterization, the assessment of filament stability and the FFF 3DP process, as well as preliminary in vitro evaluation of the obtained porous structures as tissue scaffolds.

Forming of starting materials for FDM/FFF 3D printing (filaments) is a complex process which is based on the melt extrusion of polymer in the form of granules/pellets. In the literature, the process is briefly described and uses micro-scale lines, which are based on extruders equipped with a nozzle of the appropriate diameter and a manual system of diameter control [9–11]. There are few reports that extensively describe the processing line and parameters of the continuous filament forming process. Carneiro et al. [12] noticed that in order to obtain a dimensionally stable and defect-free filament, attention should be paid not only to the extrusion processing window but also to the appropriate equipment of the production line. Hence, the filament-forming system should also be equipped with a pulling unit, cooling/heating reservoirs, calibration zones, direct diameter measurement system or winding set. Korte at el. [13] points to the need for studies on continuous filament formation in a larger-scale production. In their research, they paid attention to selection and optimization of several extrusion parameters (pressure on the extruder head, feed rate or extrusion temperature), but also the production line itself (pulling velocity on a conveyor belt, direct laser diameter measurements, calibration zones). Thus, with the results of a full factor design of experiments (DoE), they received a pharmaceutical-grade FFF 3D printable filament in a continuous melt extrusion process. The filament-forming process is particularly challenging when the used polymers are highly flexible and possess hygroscopic nature, such as polyurethanes. Therefore, special attention should be paid to the drying process, the selection of the winding parameters and the type of cooling reservoirs, to minimize the defects of extrudate (foaming, voids, irregular diameter or generation of internal stresses).

Conducting tests, from filament formation through product application tests, ensures full control of the process and precise characteristics of the medical device printed with the FFF 3D method. Hence, in this study, polyester-urethane filament (TPU_F) was fabricated using a complex filament-forming system and the structure (FTIR, Raman, H-NMR), thermal stability (DSC, TGA), rheological (MFR) and mechanical properties, characterized. We also captured and presented line and processing parameters leading to the manufacture of high-quality TPU filament in a continuous extrusion process. Further, to find out the impact of FFF 3D printing processing on TPU_F stability, researches

were carried out for both the filament and the printout (TPU_P). Then, series of in vitro studies including the evaluation of TPU_P degradability (long-term degradation in 0.1M PBS, up to six months), biocompatibility (cytotoxicity test ISO 10993:5), and determination of their surface properties (contact angle) were performed. Once the in vitro results confirmed the potential application of printouts as tissue-engineered constructs, the incubation of specially designed porous tissue structures (TPS) in simulated body fluid (SBF; 37 °C/28 days) was performed. The effect of incubation on morphology, stability, and mechanical properties of TPSs was investigated by SEM, EDS, mass measurements, and compression test. Finally, the mass loss measurements and microscopy observation during the short-term degradation (5 M NaOH; 37 °C/28 days) were also conducted. Thus, the presented paper comprehensively describes the cycle from filament production to the FFF 3DP of porous structures with various architectures and their in vitro evaluation as potential tissue scaffolds, thereby providing technological and process aspects as well as physico- chemical tests of filament stability under 3D printing conditions.

2. Materials and Methods

2.1. Materials

Epaline® (390 A series) granules were purchased from Epaflex Polyurethanes (Italy). It is an extrusion grade thermoplastic polyester urethane (TPU) with a hardness of 90 Shore A, a density of 1.20 g cm^{-3}, a tensile strength of 44 MPa, and elongation at break equal to 514%. Melt flow rate (MFR) is assessed as 24 g 10 min^{-1} at 5 kg load and 205 °C.

2.2. Filament (TPU_F) Formation

The filament-forming system was based on the melt extrusion process. Single-screw extruder with the following parameters was used, L/D ratio of 32; working length 33 mm; three-barrel heating zones; two heads heating zones; nozzle diameter of 2 mm. Several processing parameters were tested to obtain TPU_F filament with a stable diameter dimension. The scheme of the filament-forming system line with a precise description and the processing parameters is presented in Section 3.1.

2.3. 3D printer, Test Sample, and Porous Tissue Structure Design and Formation

Flash Forge Inventor I® (FlashForge, Jinhua, China) FFF-based 3D printer with FlashPrint slicer (4.2.0 version) (FlashForge, Jinhua, China) was used to prepare testing samples. Formed TPU_F filament was used as a feedstock. Samples for the tensile test were made according to the ISO 37:2017 standard by using Autodesk Inventor software (Autodesk, Warszawa, Poland) (Table S1). Two different infill raster angles were given (0/90° and ±45°). In turn, samples for long-term degradation and cytotoxicity studies were cut out from the printed porous matrix–mesh with triangular infill of 85% and thicknesses of 3 mm (Table S2), by using brass corkscrew (Ø 8 mm). The porous mesh design was made directly in slicer software. Specimens for tensile test, long-term degradation in phosphate-buffered saline (PBS) and cytotoxicity studies (marked as TPU_P) were printed maintaining the parameters given in Table S3. Finally, three types of porous tissue structures (PTS), marked as LR, G25, and G3D and dimensions of 15 × 15 × 15 mm^3, were designed in Autodesk Inventor software and printed with parameters given in Table S4. To increase the resolution and accuracy of printing porous structures, a 3D printer with nozzle 0.2 mm in diameter was used (Prusa MK3S, Josef Prusa, Prague, Czech Republic). PTSs differ in architecture, shape, and dimensions of the pores (Table 1). The porosity of the obtained PTSs was calculated using the following Formula (1):

$$P\,(\%) = \left(1 - \frac{m}{V \times g}\right) \times 100 \quad (1)$$

where (P%) represents porosity, m—sample mass (g), V—the volume of the structure (cm^3), g—density of the filament TPU_F, g = 1.12 g cm^{-1} (n = 5). 3D print accuracy was estimated according to actual dimensions of the printed PTSs (n = 5). Percentage values, presented in the supplementary data (Table S5), were calculated with respect to the 3D model (15 × 15 × 15 mm^3—represents 100% accuracy).

Table 1. Preview of prepared porous tissue structures (PTS) (model, printout, pores pattern).

Type of PTS	LR	G25	G3D
Side view of the project	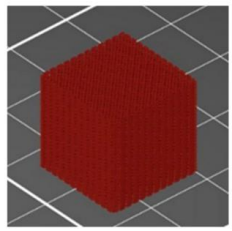	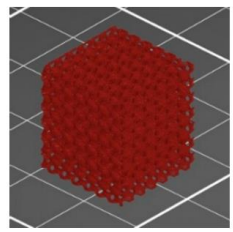	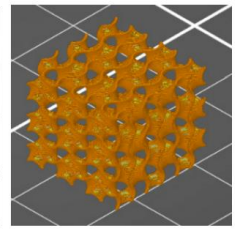
Top view of the project	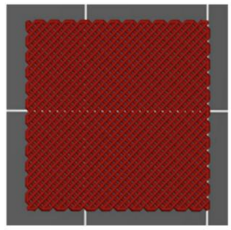	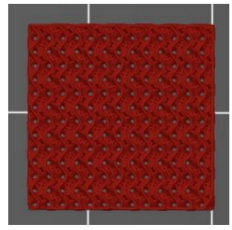	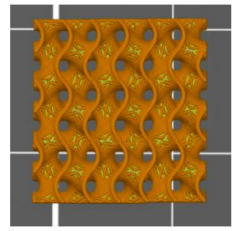
Printout	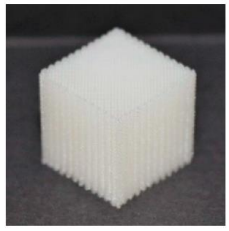	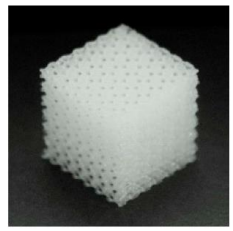	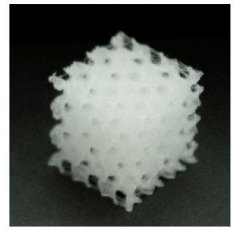
Pores pattern	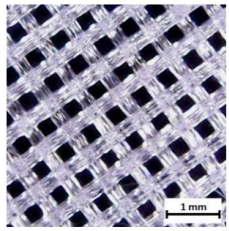	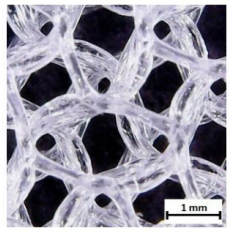	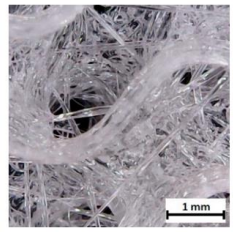
Porosity (%)	58.4 ± 1.2	76.6 ± 0.4	78.8 ± 0.6
Print accuracy (%)	x – 98.95 ± 0.18 y – 98.87 ± 0.16 z – 98.77 ± 0.15	x – 98.77 ± 0.10 y – 98.73 ± 0.16 z – 98.84 ± 0.22	x – 97.17 ± 0.33 y – 97.45 ± 0.26 z – 98.67 ± 0.08

2.4. Characterization Methods of Filament (TPU_F) and 3D Printouts (TPU_P)

Series of the following studies, spectroscopic (FTIR, Raman); thermal studies (DSC, TGA); gel permeation chromatography (GPC), and melt flow rate (MFR) measurements were conducted on both, filament (TPU_F) and printout (TPU_P) to characterize the obtained filament and to assess whether the printing process causes changes in the printout properties compared to the used filament.

2.4.1. Spectroscopic Studies

Attenuated total reflectance (ATR) FTIR Nicolet 8700 spectrometer (Thermo Fisher Scientific, Waltham, MA, USA) was used to examine the chemical functional groups of the obtained TPU samples. The spectral range was 4000–500 cm^{-1} with 4 cm^{-1} resolution (64 scans). Measurements were taken at room temperature. In turn, Raman spectra were collected by a confocal micro-Raman system (InVia, Renishaw, New Mills, UK). Green laser (514 nm) operating at 50% of its total power (50 mW) was used. Measurements were taken at randomly selected locations on the sample surface (50× magnification).

2.4.2. Thermal Properties

Thermal behavior and stability of filament and printout were studied by differential scanning calorimetry (DSC) and thermogravimetry (TG). Netzsch 204F1 Phoenix apparatus (Netzsch, Selb, Germany) was used for DSC measurements (5 mg of sample, under nitrogen atmosphere). First, the sample was heated to 220 °C, then cooled to −80 °C and finally reheated to 220 °C. The heating/cooling rate was 5 °C min^{-1}. Thermogravimetric analysis was performed using a Netzsch TG 209 instrument (Netzsch, Selb, Germany) at a temperature range from 35 °C to 700 °C under nitrogen atmosphere (sample weight ~5 mg). The heating rate was 10 °C min^{-1}.

2.4.3. Dynamic Mechanical Analysis (DMA)

DMA Q800 analyzer (TA Instruments, New Castle, DE, USA) was used to perform dynamical mechanical tests. The measurements were carried out in the single cantilever bending mode with 1 Hz frequency of an oscillatory deformation on printed TPU samples ($40 \times 10 \times 2$ mm^3 dimension), at the temperature range of −100 °C to 150 °C (heating rate 4 °C min^{-1}). The storage modulus (G'), loss modulus (G''), and damping factor (tangent δ) were determined as a function of temperature.

2.4.4. Melt Flow Rate (MFR)

The melt flow rate (MFR) and melt volume rate (MVR) of the obtained TPU filament and printout were measured using load plastometer (Zwick/Roell, Ulm, Germany) according to ISO 1133 standard at a temperature of 200 °C and 210 °C with a load of 5 kg. Five repetitions were performed for each sample and the results were averaged (n = 5).

2.4.5. Hardness and Tensile Strength

The hardness measurements and tensile test were performed on printed dumbbell shaped TPU specimens. The mechanical properties of TPU_P were evaluated depending on the infill raster orientation (0/90° and ±45°). A Shore A type durometer (Zwick/Roell, Ulm Germany) was used to measure the hardness of samples (ISO 868 standard). Fifteen measurements per sample were made and the results averaged. The tensile test was conducted using a Zwick/Roell Z020 universal tensile machine (Zwick/Roell, Ulm, Germany), according to the ISO 527 standard. The study was carried out at room temperature. The crosshead speed was 100 mm min^{-1} and the initial force was 1 N. At least eight of the printed dumbbell shaped TPU series samples were tested and results were averaged (n = 8).

2.4.6. Contact Angle (CA)

The contact angle and surface free energy (SFE) of TPU printouts were determined using a ramé-hart 90-U3 goniometer with a DROPimage Pro software (ramé-hart, Succasunna, NJ, USA). The printed surface was degreased, then 2 μL droplet of selected solvent was deposited and the images were collected. Measurements were taken over two different solvents—water and diiodomethane. The Fowkes method [14] was used to calculate SFE (based on CA results for polar (water) and non-polar (diiodomethane) liquids).

2.4.7. Long-Term Degradation

The TPU printed porous meshes were subjected to long-term degradation studies to evaluate their susceptibility to degradation. Incubation was carried out in 0.1 M phosphate-buffered saline (PBS, Sigma-Aldrich) for 6 months at 37 °C. The medium was replenished every month. Porous discs with a diameter of 8 mm and a thickness of 3 mm were dried, weighed (m_0), placed in 6 mL wells test plates, and immersed with 3.5 mL of PBS solution. At each respective time points, samples were carefully removed, rinsed out with DI water and dried in a laboratory oven at 40 °C for at least 48 h. Mass loss (Ms) was calculated as follows (2):

$$Ms(\%) = \frac{m_0 - m_1}{m_0} \times 100\%, \quad (2)$$

where (m_0) is an initial mass of the sample and (m_1) is residual mass. In the case of a mass increase due to incubation in 0.1 M PBS, the mass change (Mc) was calculated based on the following formula (3):

$$Mc(\%) = \frac{m_1 - m_0}{m_1} \times 100\%, \quad (3)$$

Incubation in PBS was monitored by FTIR spectra, SEM images (SEM, FEI Quanta FEG 250, accelerating voltage 10 kV), optical microscope photos of the sample surface (Delta Optical Generic Pro, Mińsk Mazowiecki, Poland), and mass measurements. Three samples were tested and the results were averaged (n = 3).

2.4.8. Cytotoxicity Studies

Cytotoxicity of TPU printouts was studied based on ISO 10993-5 standard using fibroblast CCL-136 cell line, which was provided by ATCC, Manassas, VA, USA (BALB/3T3 clone A31, ATCC® CCL-163™). Before the test, samples were sterilized under a UV lamp (Binovo, Legnica, Poland) for 30 min. Sample extracts (four different concentrations, i.e., 100, 50, 25, and 12.5%, respectively) were prepared in culture medium DMEM/F-12 with fetal bovine serum (FBS) and 5 μg mL^{-1} of penicillin with streptomycin with 5 μg mL^{-1} amphotericin B(all Corning). Solution was placed in an incubator for 24 h at 37 °C and 5% CO_2. Next, CCL-163 cells were prepared by seeding on 96-well plates (1000 cells/well, Nunc) and incubated for 24 h in the previously prepared extract. Then, the MTT assay was conducted. The absorbance of extracts was examined via Varioskan at λ = 570 nm (ThermoFisher Scientific, Waltham, MA, USA). The statistical differences were calculated via a one-way ANOVA (α = 0.05) test (OriginPro 8.5, Washington, DC, USA).

2.5. Studies of Elastic Porous Tissue Structures (PTS)

In the second part of the work, printed PTSs were incubated for 28 days in simulated body fluid (SBF) solution to estimate their potential in cartilage/bone tissue engineering. Bioactivity was assessed by examination of the hydroxyapatite (HAp) crystal formulation on the sample surface via scanning electron microscopy (SEM, FEI Quanta FEG 250, accelerating voltage 10 kV, FEI, Eindhoven, Netherlands and EDS (EDAX, Mahwah, NJ, USA) (Energy Dispersive Spectrometer) spectroscopy. Further, the impact of the incubation in SBF on the mechanical properties (static uniaxial compression test, initial force 1 N, the compression rate of 20 mm min^{-1} up to 50% of the initial height, Zwick/Roell Z020, Ulm, Germany) and water contact angle of the PTS were studied. Printed PTSs were also tested in strong alkaline media. Short-term degradation was conducted for 28 days at (37 °C) in 5 M NaOH. The medium was not changed during incubation, (n = 5).

3. Results and Discussion

3.1. Filament (TPU_F) Formation

The scheme of the used filament forming system is shown in Figure 1a. The system consisted of a single-screw extruder equipped with a granulate dryer; calibration zones with four diameter calibrators and two cooling tubs; a diameter laser sensor and the system of pulling and spool winding.

a)

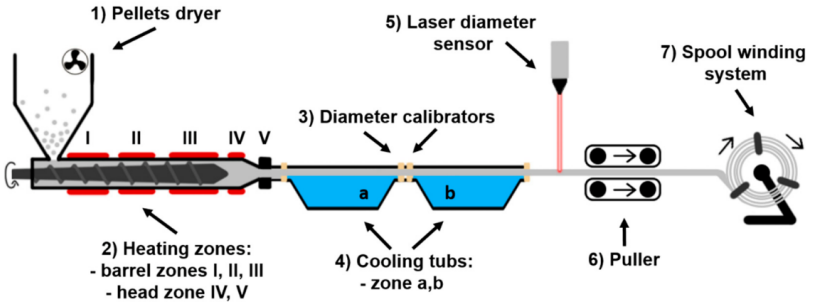

b)

ZONES TEMEPERATURE PROFILE (°C)						OPERATING PARAMETERS	
I	II	III	IV	V	Melt temperature	Head pressure (bar)	Extrusion velocity (rpm)
155	185	190	193	192	200	62 ± 2	50

Figure 1. Scheme of thermoplastic polyurethane TPU filament (TPU_F) forming system (**a**), extrusion parameters of TPU_F formation (**b**).

Extrusion parameters of TPU_F are shown in Figure 1b; adjusted filament forming system parameters were as follow:

(1) Pellets drying −10 h, 60 °C
(2) Hot melt extrusion parameters—Figure 1b
(3) Calibration zone (a)

Water temperature −40 °C
Calibrators diameter −2 mm
Tube length ~ 2.5 m

(4) Calibration zone (b)

Water temperature −23 °C
Calibrators diameter −1.8 mm
Tube length ~ 2.0 m

(5) Laser sensor accuracy −0.01 mm
(6) Pulling velocity ~ 180 rpm

First, polymer pellets were dried for 10 h at 60 °C (with airflow). Then, based on the melt flow rate (MFR) value (MFR of Epaline pellets is 24 g 10 min^{-1}) the temperatures and velocity of extrusion were adapted. With the set parameters, the melt temperature was 200 °C and the head pressure was kept at a constant level of 62 bar. Cooling bathtubs were refilled with water, which gradually cooled down extrudate, (40 °C and 23 °C), thus preventing the generation of thermal stress of the extrudate. This, in combination with the diameter calibrators (located at the inlet and outlet of the bathtubs), ensures that the filament is of the correct dimension and shape. The pulling velocity was adjusted in the final stage of the filament forming process (during the regulation of collecting and winding onto the

spool) and was equal to 180 rpm. The mechanism controlling the diameter of a filament is most often a laser sensor or manual measurement. Herein, the filament diameter was constantly measured by a laser sensor with an accuracy of 0.01 mm. The combination of described and presented parameters resulted in the formation of polyester urethane (TPU_F) defect-free filament with a constant diameter of (1.75 ± 0.01 mm), suitable for the use in the FDM/FFF 3D printers (Figure 2).

Figure 2. View of obtained TPU_F filament.

The first step defining the success of the filament forming process is the correct preparation of the granulate (feedstock) by thorough drying. This is particularly important in the case of hygroscopic polymers such as thermoplastic polyurethanes. If water or moisture is present during extrusion, process instability may occur resulting in pressure fluctuation. This leads to the dimensional instability of the extrudate, defects in the filament (voids, bubbles), or even degradation of polymer chains. This may be manifested by a reduction in viscosity and molecular weight of the resulting filament. Hence, drying of TPU pellets is especially important. Another step of the filament forming process is adjusting the temperatures and operating parameters of melt extruding. The selection of an adequate temperature profile ensures proper plasticization of the polymer as well as affecting the head pressure in the extruder which determines the stable flow of the melt [15]. This is crucial when a specified stable diameter (filament Ø 1.75 mm) of an extruded profile is necessary. A further essential element of the process is the calibration zone. As we noted when molding highly flexible thermoplastics, it should consist of water-filled bathtubs with gradually lowering temperature. In this way, the stretching effect of the elastic extrudate, which occurs when using conventional conveyor belts, is limited. This effect disrupts the diameter stability but can also lead to buckling of the spool with the finished filament. Therefore, an incorrectly selected calibration and the winding system can lead to permanent damage to the spool with the highly flexible filament (see Figure S1).

3.2. *Chemical Analysis of TPU Filament and Printout*

The results of the spectroscopic studies of formed TPU_F and its printout (TPU_P) are shown in Figure 3. The presence of functional groups characteristic for polyester urethanes was noted, based on the FTIR spectrum (Figure 3a). The absorption peak visible in the range of 3300 cm^{-1} corresponds to –NH group stretching vibrations of the urethane blocks. Bending vibration of –NH and stretching vibration of C–N of urethane blocks are seen at 1594 and 1525 cm^{-1}, respectively. The range of 2950 cm^{-1} is associated with symmetrical and asymmetrical stretching vibration of aliphatic $–CH_2$ groups. The signal observed at 1750 cm^{-1} is associated with C=O stretching vibration (both, hydrogen and non-hydrogen bonded) in polyester and urethane groups. Peaks noticed between 1170–1070 cm^{-1} correspond to vibration of urethane units; stretching vibration of C–O and C–(C=O)–O.

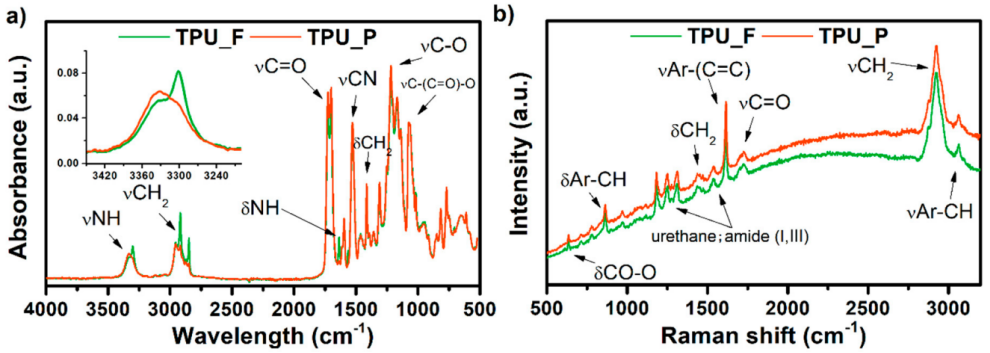

Figure 3. FTIR (**a**) and Raman (**b**) spectra of obtained TPU filament and printout.

In the case of the TPU_F sample, two bands appear in this region. The peak at 3330 cm^{-1} corresponds to free –NH groups while at 3300 cm^{-1} the –NH groups are hydrogen-bonded [16]. After the FDM 3D printing process (TPU_P), the band slightly shifts towards higher values, and the peak representing the hydrogen-bonded –NH group decreases significantly. Thus, the printing process reduced the number of hydrogen-bonded –NH groups occurring in the TPU structure. Nevertheless, material degradation due to the 3D printing process cannot be stated.

The Raman spectrum confirmed the structure of the obtained TPU filament. Amide bands (I, III) were detected. The presence of peaks corresponding to the vibrations of aromatic carbons was also observed (stretching vibration of aromatic CH at 3064 cm^{-1} and C=C of benzene ring at 1620 cm^{-1}) which is most likely derived from the aromatic diisocyanate used for polyester urethane synthesis. The above considerations are consistent with the ^{1}H-NMR measurements which showed the presence of methylene diphenyl diisocyanate (MDI) in the TPU_F structure (see supplementary data, Figure S2).

3.3. Thermal and Thermomechanical Properties of TPU Filament and Printout

The obtained filament (TPU_F) and printout (TPU_P) samples were subjected to a series of thermal and thermo-mechanical tests. Thermoplastic polyurethanes built with hard and soft segments show the ability for micro-phase separation and formulation of the microstructure [17]. Crystallizable phases of TPU microstructures can be studied by differential scanning calorimetry (DSC) measurements. DSC thermograms (Figure 4) enabled the determination of the glass transition temperature (T_g), melting temperature (T_m), heat enthalpy (ΔH_m), and crystallization temperature (T_c). The first heating scans of both samples reveal T_g to be in a very similar range of ~40 °C. Therefore, it can be assumed that the 3DP process did not affect the soft phase transition of TPU. Two melting points were observed. T_{m1} corresponds to the endothermic transition of soft segments, while T_{m2} is connected with the melting of crystalline hard segments present in the TPU structure. The heat enthalpy value of both transitions is relatively low, which suggests a low crystallinity degree of the studied samples. It is worth noting that the T_{m1} of TPU_P was about 5 °C lower than TPU_F (25.8 °C) whilst the melting temperature of hard segments did not change. The crystallization temperature of hard segments was noticed between 164–168 °C. A possible cause of the T_{m1} shift may be a change in the mobility of the soft segment chains due to the 3DP process. Nevertheless, the variations are inconsiderable and do not indicate TPU_P degradation.

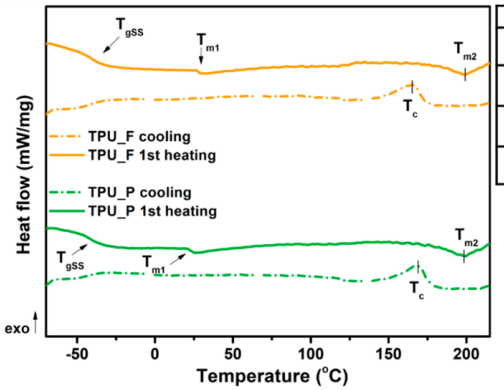

	TPU_F	TPU_P
T_g (°C)	−40.8	−40.5
T_{m1} (°C) / ΔH_m (J g^{-1})	30.4 / 1.73	25.8 / 1.93
T_{m2} (°C) / ΔH_m (J g^{-1})	199.1 / 4.09	198.9 / 3.78
T_c (°C)	164.2	168.3

Figure 4. Differential scanning calorimetry DSC curves of obtained TPU filament and printout (1st heating and cooling cycle).

Thermogravimetric analysis (TGA) allowed the determination of the thermal stability of the prepared samples. The results are presented in Table 2 and Figure 5. The thermal stability of both samples was similar, around 300 °C (T_{onset}). The complete decomposition of material occurred at 475 °C (T_{offset}). Since thermoplastic polyurethanes have a segmented structure, the degradation of these polymers takes place in two stages. Additional information on the phase separation of TPU can be provided by the first derivative of the TGA curve (DTG) diagrams in which clearly separated peaks indicate the decomposition of subsequent polyurethane phases. The determination of DTG curves indicates a two-stage material decomposition, which confirms the segmental structure of the tested polyurethanes [18]. The first peak on the DTG curves corresponds to the decomposition of the urethane bonds that build hard segments (at ~350 °C), while the destruction of the soft segments (ester bonds), present in long-chain polyester-part of TPUs, begins at 390 °C. Such minor changes in thermal properties between TPU filament and printout allow it to be stated that the formed filament is thermally stable under FFF 3D printing conditions.

Table 2. Thermal decomposition characteristics of the TPU filament and printout.

Sample	$T_{5\%}$ (°C)	$T_{50\%}$ (°C)	T_{max} (°C) Step I/Step II	Residual Mass at 700 °C (%)
TPU_F	307.3	375.1	351.8/390.3	6.15
TPU_P	308.8	377.9	347.0/394.6	6.34

For further characterization of the obtained material, dynamic mechanical analysis (DMA) was performed. DMA analysis is used to determine the mechanical and viscoelastic properties of materials as a function of temperature, time, and frequency.

Based on the curves shown in Figure 6, different viscoelastic states of the sample can be distinguished, i.e., at minus temperature range—glassy state; a broad glass transition region (−40 to 40 °C); a rubbery plateau region (over 50 °C). The value of the storage modulus (E′) in the glassy state region was over 1450 MPa and decreased by about 1.2 times after exceeding −40 °C. The α-relaxation temperatures, determined as the values of the glass transition region start, a maximum value of E″, and loss factor (tag δ) peak, were −39 °C, −21 °C and −3.7 °C, respectively. In this temperature range, the long-rate intermolecular movements of the macromolecule polymer chains take place. The maximum amplitude of loss factor (so-called damping factor) reached 0.3 which indicates scanty damping properties of the formed sample. According to the literature, polyurethanes designed to dampen vibration (with excellent energy dissipation) exhibit a loss factor value (tag δ) greater than 0.6 [19,20].

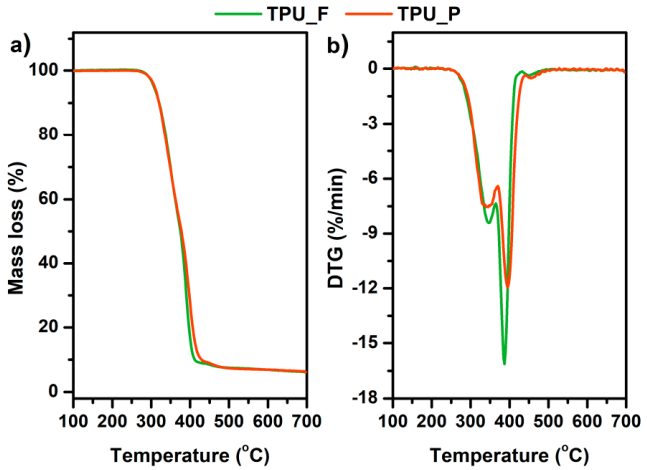

Figure 5. Mass loss (**a**) and derivative thermogravimetric DTG curves (**b**) vs. temperature of TPU filament and printout.

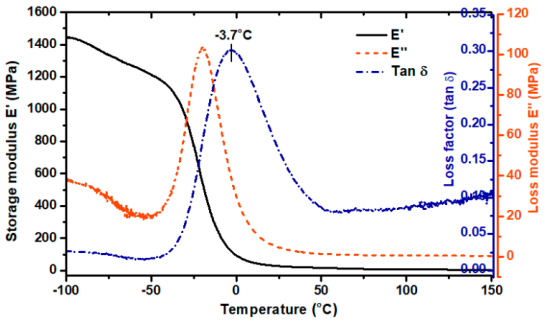

Figure 6. Dynamic mechanical analysis DMA results of TPU printout. Storage modulus (E′), loss modulus (E″), loss factor (Tan δ).

3.4. Melt Flow Rate (MFR) Results

The melt flow is a parameter determining the polymer's ability to melt and flow under the influence of temperature and pressure. It can be expressed in units of mass (MFR) or volume (MVR) of the material flowing from the plastometer nozzle under a given load over a period of 10 min. The conditions during the MFR measurement can be compared with those in the print head during FFF 3D printing. MFR is also related to the dynamic viscosity of the polymer melt, so it can be useful in assessing the printing speed at which the filament can be successfully printed. The studies conducted by Ramanath et al. [21] showed that MFR is closely related to the interlayer adhesion between formed layers and therefore affects the quality of the printed part. Therefore, the melt flow rate is a very helpful parameter in evaluating the suitability of a filament for FFF 3DP [22].

The results of the melt flow measurements are listed in Table 3. The study showed an increase in the MFR value after the 3DP process. Hence, the rheological properties of the formed TPU filament changed slightly. This is related to the reprocessing of the material during 3D printing in which changes in the polyurethane microstructure occur. It is in line with the thermal characteristics as well as with results of the FTIR examination, wherein a small reduction in the number of hydrogen bonds, through which the domain structure in polyurethanes is formed, was noticed. However, taking into account the standard deviation of the results, this difference is insignificant.

Table 3. The results of melt flow measurements of the TPU filament and printout.

Sample	Temperature 200 °C, Load 5 kg		Temperature 210 °C, Load 5 kg	
	MFR (g 10 min^{-1})	MVR (cm^3 10 min^{-1})	MFR (g 10 min^{-1})	MVR (cm^3 10 min^{-1})
TPU_F	21.8 ± 0.4	20.3 ± 0.3	29.7 ± 0.7	27.9 ± 0.8
TPU_P	23.9 ± 1.1	22.5 ± 1.4	32.1 ± 0.9	30.3 ± 1.1

The MFR measurement for the TPU_F sample proceeded smoothly. The material-flow from the plastometer nozzle was continuous, without any swelling effect. No defects of extrudate (bubbles, foaming) were observed. The MFR value of the TPU_F was around 22 g 10 min^{-1} at 200 °C and a load of 5 kg and increased by ~8 g 10 min^{-1} with increasing test temperature by 10 °C. The melt flow of commercial TPU filaments is around 16 g 10 min^{-1} (Ultimaker®, TPU 95A, 225 °C/1.2 kg), 15 cm^3 10 min^{-1} (Basf®, Ultrafuse TPU 85A, 190°C/3.8 kg). However, it is difficult to compare these values because they strictly depend on the measurement conditions which were variable in each case.

During the stage of adjusting the 3D printing parameters of TPU_F, it was noticed that the printing temperature of 210 °C ensures the correct course of the process with the best ratio of time to printout quality. Hence, it can be concluded that the MFR values of the order of ~20–30 g 10min^{-1} (at a temperature range of 200–210 °C and 5 kg load) allow to pre-qualify the studied TPU filaments as suitable for 3D printing with the FFF/FDM method. However, it should be remembered that to fully assess the suitability of the filament for 3D printing, the results of tests such as thermal, rheological or mechanical should be taken into account [23–25].

3.5. Hardness and Tensile Test of TPU_P

Further analysis concerns only the printed samples (TPU_P) to demonstrate the practical application of the formed filament (TPU_F). Series of conducted mechanical studies have shown that the change in printing parameters (infill orientation) did not significantly affect the hardness and tensile strength profile of the samples (Table 4). Although the mean values for the samples marked as ± 45° are higher, the standard deviation indicates that the mechanical properties are not strictly related to the infill orientation. It allows the assumption that the printouts showed good interlayer adhesion, and therefore the orientation of the sequentially arranged/placed fibers did not affect the obtained results.

Table 4. Results of hardness and tensile strength test. The conditions of test sample printing are shown in the supplementary appendix.

Infill Orientation	HS (Sh A)	Tensile Strength (MPa)	Elongation at Break (%)	Relative Elongation (%)	Young's Modulus (GPa)
± 45°	86 ± 2	31.1 ± 6.5	412.6 ± 53.4	39.1 ± 7	0.21 ± 0.10
0/90°	85 ± 1	29.0 ± 3.2	392.3 ± 42.8	32.2 ± 2	0.19 ± 0.05

The hardness of printed structures was in the range of 85 ShA (~33 ShD) which corresponds to a type of hard rubber. Tested samples showed a comparatively low value of the relative elongation parameter (~30–40%), which indicates a small permanent deformation formed after loading the printouts. It is worth paying attention to the decrease in mechanical properties in relation to the raw-material (Epaline® granules) from which the filament was formed. The tensile strength, elongation at break and hardness of Epaline® was 44 MPa, 514%, and 90 ShA, respectively. This corresponds to a decrease in mechanical properties of 30, 20, and 5% concerning the starting material. It is related to the imperfections of FFF 3D printing technology in which defects in the print structure, such as voids, warping deformations or insufficient interlayer bonding (i.e. raster-raster, contour raster bonding) caused by uneven temperature distribution, cannot be overcome [26–28].

3.6. Results of in vitro Studies on TPU_P

3.6.1. Long-Term Degradation in PBS

Since TPU filament was to be considered as a material for medical applications a series of in vitro studies was performed. Initially, long-term degradation in the phosphate-buffered saline (PBS) environment, to verify the stability of the material under simulated conditions, was performed [29,30]. The long-term degradation was monitored by mass measurements, optical microscopy, SEM images, and FTIR study (Figure 7, Table 5 and Table S6).

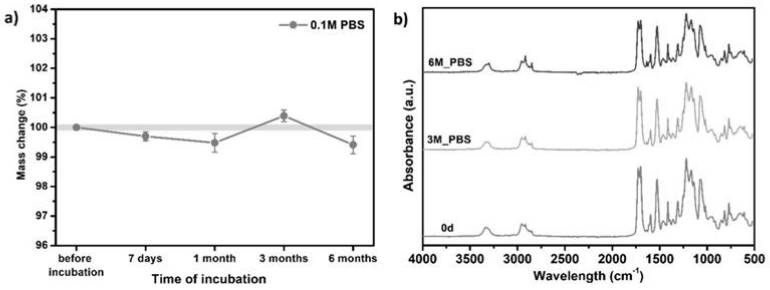

Figure 7. The results of long-term degradation studies on TPU_P samples in 0.1 M phosphate-buffered saline PBS solution (37 °C), (**a**) mass change measurements, (**b**) FTIR spectra. Optical images can be found in supplementary data Table S6.

Table 5. Scanning electron microscope SEM images of long-term degradation of TPU_P (day 0, 3 and 6 months of study).

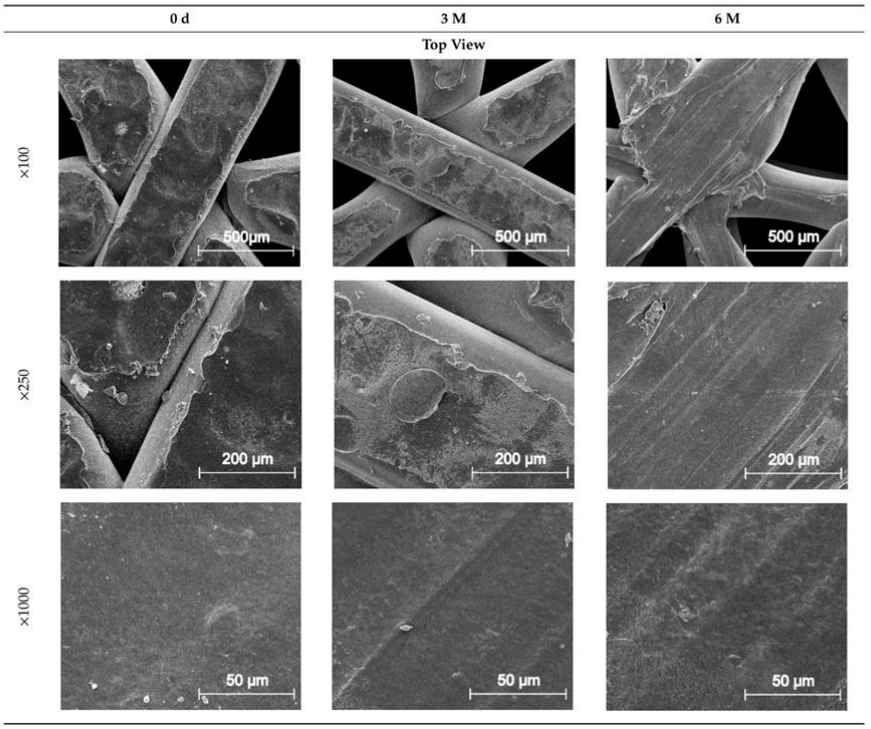

Table 5. *Cont.*

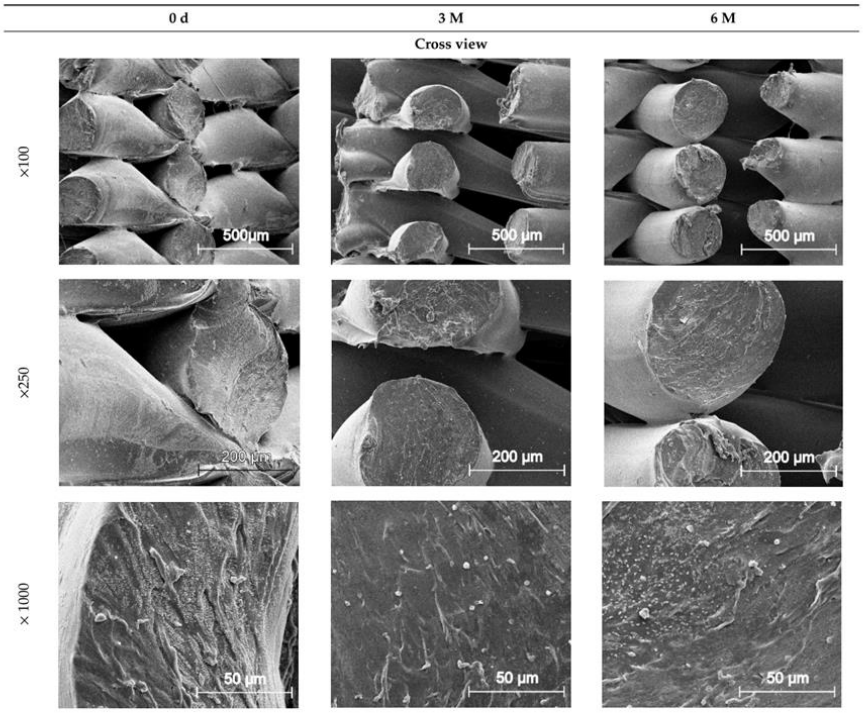

The mass measurements showed that the TPU_P samples are stable for up to six months of incubation in PBS. Weight changes did not exceed 1% throughout the study. The stability of the printouts was confirmed by FTIR study. The spectrum of the sample remained unchanged after six months of incubation. SEM images showed that the morphology of TPU_P did not change during incubation, no surface erosion or cracking was observed. At the end of the study, however, yellowing of the sample was noticed (Table S6), most likely due to accumulation on the sample surface of salt deposits. Nevertheless, the stability of TPU_P, under PBS incubation conditions, corresponds to the requirements set for structures intended, for instance for tissue engineering application [31].

3.6.2. Biocompatibility and Surface Properties

Further in vitro studies included the evaluation of printout biocompatibility and examination of their surface properties. One of the basic tests evaluating the suitability of materials intended for medical applications is the cytotoxicity test [32]. It uses tissue cells in vitro and monitors their response to contact with foreign material (cell growth, viability, and morphological effect).

The cytotoxicity test results are displayed in Figure 8. Noted cell viability after 24 h of exposure against all prepared TPU_P extract was greater than 100%, indicating cell proliferation. The prepared TPU_P extracts did not show a toxic effect against the fibroblast cells. The images of CCL-163 cells after 24 h contact with TPU_P extracts—show no morphological changes in relation to the control. Consequently, the TPU_P can be pre-defined as biocompatible and non-toxic [33]. The obtained results are in common with the in vitro cytotoxicity studies on polyurethanes materials, performed by Calvo-Correas et al. or Uscátegui et al. [34,35]. Thus, the statement, common in the literature, that polyurethanes are widely used in medical applications due to their exceptional biocompatibility and non-toxicity was confirmed [36].

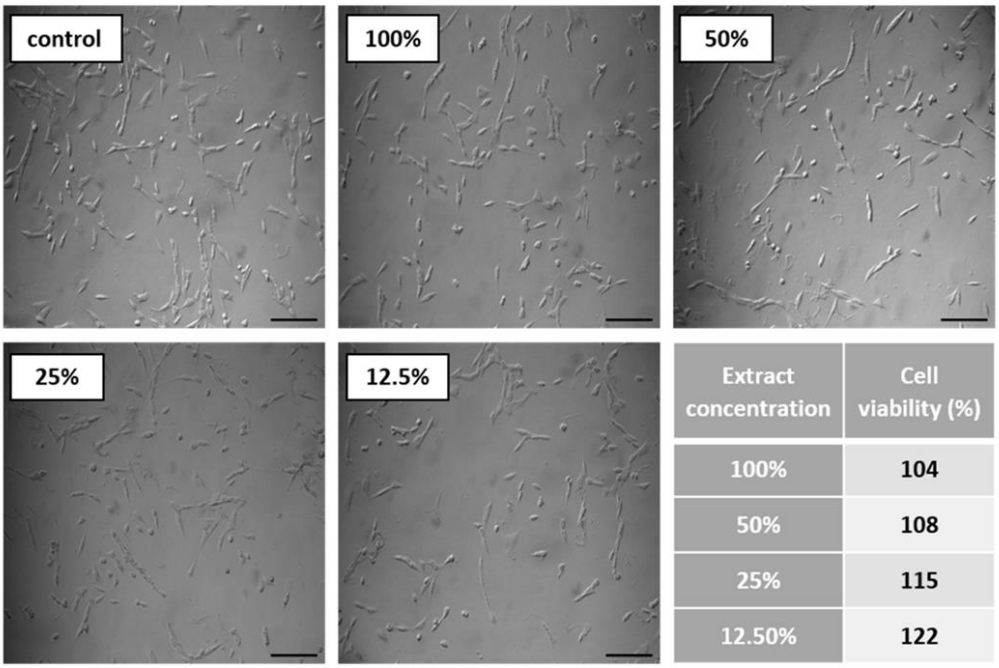

Extract concentration	Cell viability (%)
100%	104
50%	108
25%	115
12.50%	122

Figure 8. Results of cytotoxicity test. Images show CCL-163 cells morphology after 24 h contact with TPU_P extracts of specified concentrations (100–12.5%). Scale bar = 50 μm. The table present percentage of cell viability towards control (100%). SD were negligibly small, there were no statistical differences between the obtained results.

The biocompatibility and thus the adhesion, proliferation, and differentiation of cells, are reflected in the surface properties of a biomaterial [37]. The surface properties, among others, can be defined by measuring the contact angle (CA) and surface free energy (SFE). The generally accepted definition says that hydrophilic materials exhibit a water contact angle of less than 90°, while hydrophobic materials have CA>90° [38]. Medical-grade polyurethanes show a wide range of CA depending on the designed chemical structure and desired application. For example, the polyurethane microporous thin layers (MPTL) intended for soft tissue engineering, obtained by Kucinska-Lipka et al., possessed CA of 55° [39], whereas electrospun PUR bone scaffolds exhibited strongly hydrophobic properties (CA over 100°) [40]. Therefore, when considering the use of the obtained samples in tissue engineering, it should be taken into account that an excessively hydrophilic surface can disrupt the interaction between seeded cells, while too high hydrophobicity may lead to a reduction in biocompatibility due to hindered cells' adhesion [37].

The water contact angle of TPU_P was of 76° while SFE was of 42 mN m^{-1}, which indicates a quite hydrophilic nature with moderate wettability (Table 6). Taking into account the results of performed in vitro tests on TPU_P samples, it can be stated that the studied printouts meet the initial requirements for materials distorted for tissue engineering, i.e., they are stable for up to six months in PBS incubation conditions; they are non-toxic towards CCL-163 cells line, and show promising surface properties. Therefore, in the next step, specially designed porous structures were printed using TPU_F and tested to determine their potential as tissue scaffolds.

Table 6. Result of contact angle measurements of TPU_P.

Water Contact Angle (°)	Diiodomethane Contact Angle (°)	Surface Free Energy (mN m^{-1})		
75.9 ± 3.5	43.7 ± 2.7	Dispersive part 37.6 ± 0.2	Polar part 5.0 ± 0.1	Total 42.6 ± 0.2

3.7. Porous Tissue Structures (PTS) after Exposure in Simulated Body Fluid (SBF) and Their Susceptibility to Accelerated Degradation (5 M NaOH)

SBF incubation is a well-known method for the preliminary determination of the in vitro bioactivity of materials [41]. Since the SBF solution possesses ion concentration nearly equal to those of human blood plasma, the formulation of bonelike apatite on a material surface can be monitored. While the mineralization effect of bone-like implants is highly desirable [42], in the case of soft tissue structures (e.g., heart valve, coronary stents, urinary implants) the process can be disastrous [43].

The printed porous tissue structures (PTS) with different architecture (LR, G25, G3D, Table 1) were subjected to incubation in simulated body fluid (SBF) for 28 days. The SEM examination revealed the appearance of spherical particles on the surface of the PTS, already after 14 days of soaking in SFB solution (Figure 9). They were randomly located on the entire surface area of the studied porous structures, creating spherical agglomerates. The particle morphology resembled a micro lath-like network, with a structure typical for hydroxyapatite (HAp) minerals [44,45]. EDS study of the crystals revealed a high content of the elements Ca, P, O, and C, respectively, which correspond to the chemical formula of hydroxyapatite ($Ca_{10}(PO_4)_6(OH)_2$). The calcium to phosphate (Ca/P) atomic ratio of that phase was equal to 1.45. The Ca/P value of stoichiometric HAp was 1.67, thus the formed minerals seem to be deficient in calcium. The reason might be the presence of Mg^+ and Na^+ ions, which distort the structure of HAp. However, it is worth noting the relatively high content of the carbon and oxygen elements in the crystal structure, which suggest the presence of CO_3^- ions. Thus, on the PTS surface, so-called carbonated-hydroxyapatite (C-HAp) was formed. According to the literature, C-HAp corresponds more to natural-occurring hydroxyapatite and therefore possesses enhanced biocompatibility compared to the synthetic one [45,46].

Further, SBF-incubated PTS samples were subjected to a compression test and the results were compared with the values before incubation (Figure 10a–c). The LR-PTS structure proved to have the most compressive strength (~1.05 MPa) while the G3D type - the lowest one (~0.12 MPa). It was also observed that with the change of the porous structure architecture (porosity and pore shape/size), the course of the compression curve changes. The LR and G25 samples show a clear yield point and a sharp increase in stress, while the G3D structure (most irregular) shows a mild increase in stress over compression. Moreover, in all type of PTS, an evident increase in compressive strength with the incubation time in SBF was observed. This increase was the highest for the G3D and G25 samples, by around 0.08 MPa and 0.07 MPa, respectively after 28 days of the incubation period. Thus, the mineral particles of hydroxyapatite formed during SBF soaking significantly strengthened the elastic porous structures. The addition of hydroxyapatite (synthetic or natural) to the polymeric tissue scaffolds most likely increases their compressive strength [47,48]. However, the process of isolation HAp from the SBF solution involves simultaneous hydrolytic degradation, thus a mass loss of the sample. Therefore, in many cases, a decrease (or no change) in the mechanical properties of polymeric tissue scaffolds is observed as a result of their incubation in SBF solution [49,50]. The mass loss of printed PTS after 28 days of SBD soaking did not exceed 1% (Figure 10d), so an intense strengthening effect of the secreted C-HAp was observed. This study confirmed the previous results of degradation in 0.1 M PBS and hence the PTSs can be considered as long-term scaffolds for bone tissue engineering.

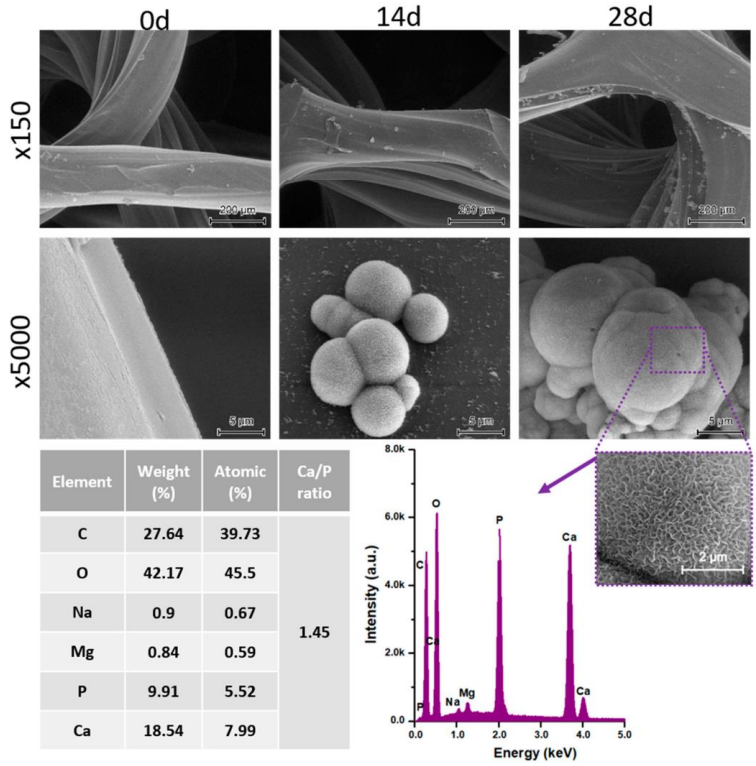

Element	Weight (%)	Atomic (%)	Ca/P ratio
C	27.64	39.73	1.45
O	42.17	45.5	
Na	0.9	0.67	
Mg	0.84	0.59	
P	9.91	5.52	
Ca	18.54	7.99	

Figure 9. SEM images and EDS spectrum of G25 PTS after incubation in SBF.

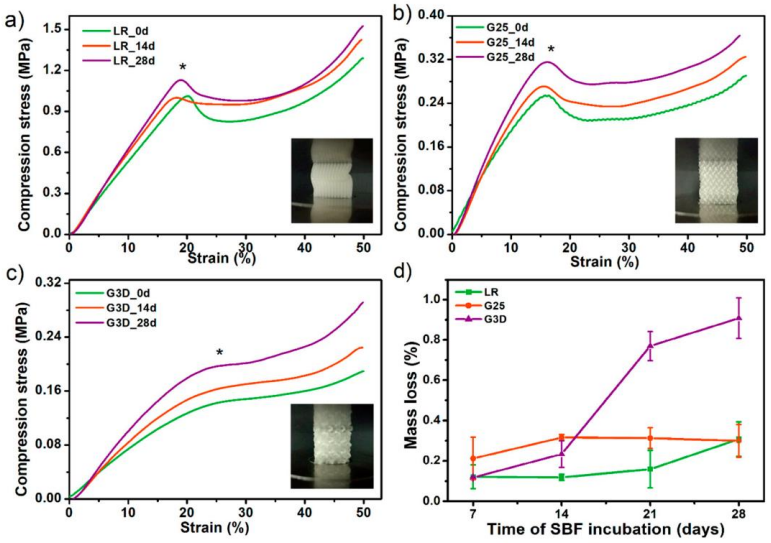

Figure 10. The influence of incubation in simulated body fluid SBF solution on compressive strength (**a**–**c**) and mass loss (**d**) of selected porous tissue structures PTS. * The inflexion point of the stress-strain curves (the so-called Yield point) was assumed as the compressive strength values of studied PTS.

Finally, the selected PTS sample (G25) was subjected to accelerated degradation study in 5 M NaOH for 28 days. It is a widely used method for short-term in vitro evaluation of the degradability of medical-grade materials [51]. Together with testing in PBS and SBF solutions, this completes the material degradation profile. The results of the study in terms of mass loss and FTIR measurements are presented in Figure 11. Already after 7 days of incubation, a weight loss of the G25 sample by 18% was noted. Whereas on the 14th day of the test, the sample structure was destroyed and the material was fully degraded (mass loss ~ 60%). The FTIR spectra showed that degradation proceeds mostly by destruction of the ester (C=O 1750 cm^{-1}) and urethane (–NH 1594 cm^{-1}, –CN 1525 cm^{-1}) bonds. Aliphatic $–CH_2$ groups presented in long-chain hydrocarbon chains were also destroyed (2950, 1320 cm^{-1}). Thus, the G25 PTS is very susceptible to erosion in a highly alkaline environment which is in the line with polyester polyurethanes as they are susceptible to hydrolysis in an alkaline media [52,53]. Some of the materials dedicated to tissue engineering applications exhibit mass loss around 80–90% during a month of accelerated degradation (or ~50% up to 15 days of alkaline incubation), thus the obtained PTSs might find such application as long-term degradable and elastic tissue scaffolds [51,54,55].

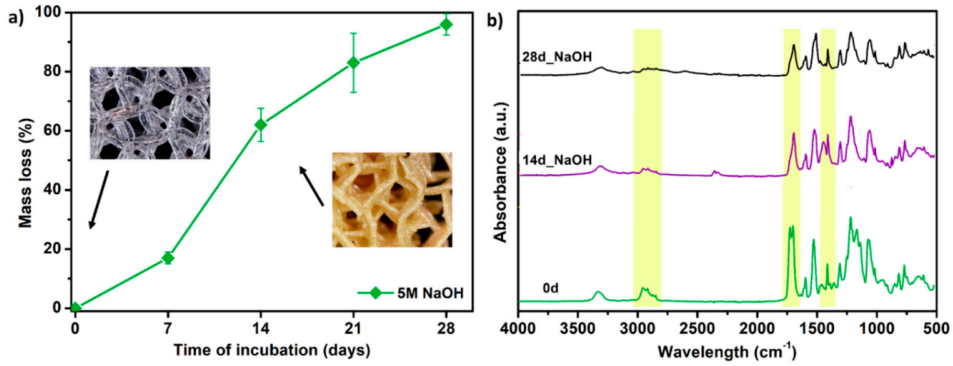

Figure 11. The results of accelerated degradation studies on G25 PTS in 5 M sodium hydroxide NaOH, (**a**) mass loss measurements, (**b**) FTIR spectra. SEM images showing the accelerated degradation process are presented in supplementary data (Table S7).

4. Conclusions

In this work, filament processing, its comprehensive characterization, and the FFF 3D printing of elastic porous tissue structures were presented and described extensively. Since FFF 3DP in medical applications is widely applied, studies of novel filament solutions are desirable. Polyurethanes, as proven materials used in the medical industry with a wide range of properties, among others are attractive in bone-tissue engineering application. Therefore, here we presented fully characterized polyester-urethane filament with potential in 3D printing of elastic porous structures for cartilage tissue engineering.

The most important conclusions of the study are as follows:

- The full list of filament-forming parameters which ensures the formation of a stable flexible filament was presented. Besides, the critical points of the process occurring during the formation of filament for FDM/FFF 3D printing were described.
- Spectroscopic studies (FTIR, Raman) confirmed the structure of the obtained TPU filament. Moreover, the analysis of spectra confirmed that the FFF 3D printing process does not cause significant structural changes in the formed filament.
- The series of thermal and thermomechanical tests showed that the TPU_F is stable under the FFF 3DP process.

- By analyzing the MFR results, the range of values that allows prediction of the suitability of the tested flexible filament for 3D printing in FFF technology was determined. The MFR range is 20–30 g 10 min^{-1} (at 200–210 °C and 5 kg load).
- A series of in vitro tests showed that TPU_P printouts are stable for up to 6 months under PBS incubation conditions, meet the cytocompatibility requirements (ISO 10993:5), and have a water contact angle of ~76°. Thus, the studied material can be considered in medical applications, including tissue engineering.
- The results of accelerated degradation point out that the formed PTSs exhibit degradability suitable for long-term tissue engineering structures.
- Incubation of PTSs in SBF solution showed the susceptibility to mineralization and formation of hydroxyapatite (HAp) crystals on their surface. This effect is desired in the case of bone-like systems. Nevertheless, to confirm the bioactivity of PTS, further, more advanced biological studies must be carried out.
- HAp released on the surface of the samples significantly strengthened the examined structures. There was up to 55% increase in compressive strength after incubation in SBF for 28 days (for the G3D sample).
- The scaffold architecture (pore shape, porosity) significantly affects the mechanical properties. The LR-type architecture with the highest degree of pore ordering exhibited the highest compressive strength of 1.1 MPa.
- The tensile strength and Young's modulus values of the obtained printouts and compression strength of the formed PTSs, enable pre-consideration of TPU_F for FFF 3DP for application in cancellous bone tissue engineering (Table 7).

Table 7. Summary of the properties of TPU_F printed structures vs cancellous human bone.

	Young's Modulus (GPa)	Tensile Strength (MPa)	Compressive Strength (MPa)
TPU_F FFF printouts	0.19–0.21	29–31	0.16–1.20
Cancellous boneReference	0.1–0.5 [56]	1–5 [56]	4–12 [56] 0.1–16 [57]

Supplementary Materials: The following are available online at http://www.mdpi.com/1996-1944/13/19/4457/s1, Figure S1: Damaged spool of TPU filament due to excessively high extrudate stresses generated during the forming and winding process, Figure S2: ^{1}H-NMR spectra of TPU_F and TPU_P, Table S1: Design of prepared dumbbell shaped TPU samples for tensile test, Table S2: Design of porous matrix for degradation studies of TPU, Table S3: 3D printing settings of test samples TPU_P (dumbbell shaped tensile test specimens, porous matrix for long term degradation in PBS and samples for cytotoxicity study), Table S4: 3D printing settings of porous tissue structures with different architecture (LR, G25 and G3D), Table S5: Analysis of PTSs print accuracy, Table S6: Optical microscopy images of TPU_P samples obtained during long-term degradation study in 0.1 M PBS solution, Table S7: SEM images from the accelerated degradation studies of G25 porous tissue structure.

Author Contributions: Conceptualization, A.H.; methodology, A.H., I.C.; software, A.H.; validation, A.H.; formal analysis, I.C., A.B.-D., J.K.-L. and H.J.; investigation, A.H., P.K., M.Ł. and I.C.; resources, J.K.-L. and H.J.; data curation, A.H.; writing—original draft preparation, A.H.; writing—review and editing, A.H., I.C., A.B.-D., J.K.-L. and H.J.; visualization, A.H.; supervision, J.K.-L. and H.J.; project administration, A.H.; funding acquisition, J.K.-L. and H.J. All authors have read and agreed to the published version of the manuscript.

Funding: The APC was funded by Gdańsk University of Technology (University program "Publications 2020").

Acknowledgments: We acknowledge Miriam Pacler for conducting compression tests and optical microscopy.

Conflicts of Interest: The authors declare no conflict of interest.

Data Availability: The raw/processed data required to reproduce these findings cannot be shared at this time due to technical or time limitations. Nevertheless, they can be made available on request.

References

1. Yan, Q.; Dong, H.; Su, J.; Han, J.; Song, B.; Wei, Q.; Shi, Y. A Review of 3D Printing Technology for Medical Applications. *Engineering* **2018**, *4*, 729–742. [CrossRef]
2. Liaw, C.Y.; Guvendiren, M. Current and emerging applications of 3D printing in medicine. *Biofabrication* **2017**, *9*, 024102. [CrossRef] [PubMed]
3. Rengier, F.; Mehndiratta, A.; von Tengg-Kobligk, H.; Zechmann, C.M.; Unterhinninghofen, R.; Kauczor, H.U.; Giesel, F.L. 3D printing based on imaging data: Review of medical applications. *Int. J. Comput. Assist. Radiol. Surg.* **2010**, *5*, 335–341. [CrossRef] [PubMed]
4. Griffin, M.; Castro, N.; Bas, O.; Saifzadeh, S.; Butler, P.; Hutmacher, D.W. The Current Versatility of Polyurethane Three-Dimensional Printing for Biomedical Applications. *Tissue Eng. Part B Rev.* **2020**, *26*, 272–283. [CrossRef] [PubMed]
5. Tsai, K.J.; Dixon, S.; Hale, L.R.; Darbyshire, A.; Martin, D.; de Mel, A. Biomimetic heterogenous elastic tissue development. *NPJ Regen. Med.* **2017**, *2*, 16. [CrossRef]
6. Chen, Q.; Mangadlao, J.D.; Wallat, J.; de Leon, A.; Pokorski, J.K.; Advincula, R.C. 3D printing biocompatible polyurethane/poly(lactic acid)/graphene oxide nanocomposites: Anisotropic properties. *ACS Appl. Mater. Interfaces* **2017**, *9*, 4015–4023. [CrossRef]
7. Jung, S.Y.; Lee, S.J.; Kim, H.Y.; Park, H.S.; Wang, Z.; Kim, H.J.; Yoo, J.J.; Chung, S.M.; Kim, H.S. 3D printed polyurethane prosthesis for partial tracheal reconstruction: A pilot animal study. *Biofabrication* **2016**, *8*, 045015. [CrossRef]
8. Przybytek, A.; Gubańska, I.; Kucińska-Lipka, J.; Janik, H. Polyurethanes as a potential medical–grade filament for use in fused deposition modeling 3d printers—A brief review. *Fibers Text. East. Eur.* **2018**, *26*, 120–125. [CrossRef]
9. Xiao, J.; Gao, Y. The manufacture of 3D printing of medical grade TPU. *Prog. Addit. Manuf.* **2017**, *2*, 117–123. [CrossRef]
10. Bachtiar, E.O.; Erol, O.; Millrod, M.; Tao, R.; Gracias, D.H.; Romer, L.H.; Kang, S.H. 3D printing and characterization of a soft and biostable elastomer with high flexibility and strength for biomedical applications. *J. Mech. Behav. Biomed. Mater.* **2020**, *104*, 103649. [CrossRef]
11. Alhijjaj, M.; Nasereddin, J.; Belton, P.; Qi, S. Impact of processing parameters on the quality of pharmaceutical solid dosage forms produced by fused deposition modeling (FDM). *Pharmaceutics* **2019**, *11*, 633. [CrossRef] [PubMed]
12. Carneiro, O.S.; Silva, A.F.; Gomes, R. Fused deposition modeling with polypropylene. *Mater. Des.* **2015**, *83*, 768–776. [CrossRef]
13. Korte, C.; Quodbach, J. Formulation Development and Process Analysis of Drug-loaded Filaments manufactured via Hot-Melt Extrusion for 3D-Printing of Medicines. *Pharm. Dev. Technol.* **2018**, *23*, 1117–1127. [CrossRef] [PubMed]
14. Fowkes, F.M. Attractive Forces AT Interfaces. *Ind. Eng. Chem.* **1964**, *56*, 40–52. [CrossRef]
15. Haryńska, A.; Gubanska, I.; Kucinska-Lipka, J.; Janik, H. Fabrication and Characterization of Flexible Medical-Grade TPU Filament for Fused Deposition Modeling 3DP Technology. *Polymers* **2018**, *10*, 1304. [CrossRef]
16. Rueda-Larraz, L.; d'Arlas, B.F.; Tercjak, A.; Ribes, A.; Mondragon, I.; Eceiza, A. Synthesis and microstructure-mechanical property relationships of segmented polyurethanes based on a PCL-PTHF-PCL block copolymer as soft segment. *Eur. Polym. J.* **2009**, *45*, 2096–2109. [CrossRef]
17. Sahebi Jouibari, I.; Haddadi-Asl, V.; Mirhosseini, M.M. A novel investigation on micro-phase separation of thermoplastic polyurethanes: Simulation, theoretical, and experimental approaches. *Iran. Polym. J. Engl. Ed.* **2019**, *28*, 237–250. [CrossRef]
18. Datta, J.; Kasprzyk, P.; Błażek, K.; Włoch, M. Synthesis, structure and properties of poly(ester-urethane)s obtained using bio-based and petrochemical 1,3-propanediol and 1,4-butanediol. *J. Therm. Anal. Calorim.* **2017**, *130*, 261–276. [CrossRef]
19. Wei, W.; Zhang, Y.; Liu, M.; Zhang, Y.; Yin, Y.; Gutowski, W.S.; Deng, P.; Zheng, C. Improving the damping properties of nanocomposites by monodispersed hybrid POSS nanoparticles: Preparation and mechanisms. *Polymers* **2019**, *11*, 647. [CrossRef]

20. Yoon, K.H.; Yoon, S.T.; Park, O.O. Damping properties and transmission loss of polyurethane. I. Effect of soft and hard segment compositions. *J. Appl. Polym. Sci.* **2000**, *75*, 604–611. [CrossRef]
21. Ramanath, H.S.; Chua, C.K.; Leong, K.F.; Shah, K.D. Melt flow behaviour of poly-ε-caprolactone in fused deposition modelling. *J. Mater. Sci. Mater. Med.* **2008**, *19*, 2541–2550. [CrossRef] [PubMed]
22. Wang, S.; Capoen, L.; D'hooge, D.R.; Cardon, L. Can the melt flow index be used to predict the success of fused deposition modelling of commercial poly(lactic acid) filaments into 3D printed materials? *Plast. Rubber Compos.* **2018**, *47*, 9–16. [CrossRef]
23. Feuerbach, T.; Callau-Mendoza, S.; Thommes, M. Development of filaments for fused deposition modeling 3D printing with medical grade poly(lactic-co-glycolic acid) copolymers. *Pharm. Dev. Technol.* **2019**, *24*, 487–493. [CrossRef] [PubMed]
24. Coogan, T.J.; Kazmer, D.O. In-line rheological monitoring of fused deposition modeling. *J. Rheol.* **2019**, *63*, 141–155. [CrossRef]
25. Cicala, G.; Giordano, D.; Tosto, C.; Filippone, G.; Recca, A.; Blanco, I. Polylactide (PLA) filaments a biobased solution for additive manufacturing: Correlating rheology and thermomechanical properties with printing quality. *Materials* **2018**, *11*, 1191. [CrossRef] [PubMed]
26. Tronvoll, S.A.; Welo, T.; Elverum, C.W. The effects of voids on structural properties of fused deposition modelled parts: A probabilistic approach. *Int. J. Adv. Manuf. Technol.* **2018**, *97*, 3607–3618. [CrossRef]
27. Alsoufi, M.S.; Elsayed, A.E. Warping deformation of desktop 3D printed parts manufactured by open source fused deposition modeling (FDM) system. *Int. J. Mech. Mechatron. Eng.* **2017**, *17*, 7–16.
28. Sun, Q.; Rizvi, G.M.; Bellehumeur, C.T.; Gu, P. Effect of processing conditions on the bonding quality of FDM polymer filaments. *Rapid Prototyp. J.* **2008**, *14*, 72–80. [CrossRef]
29. Mishra, A.; Seethamraju, K.; Delaney, J.; Willoughby, P.; Faust, R. Long-term in vitro hydrolytic stability of thermoplastic polyurethanes. *J. Biomed. Mater. Res. Part A* **2015**, *103*, 3798–3806. [CrossRef]
30. Domingos, M.; Chiellini, F.; Cometa, S.; de Giglio, E.; Grillo-Fernandes, E.; Bártolo, P.; Chiellini, E. Evaluation of in vitro degradation of pcl scaffolds fabricated via bioextrusion. part 1: Influence of the degradation environment. *Virtual Phys. Prototyp.* **2010**, *5*, 65–73. [CrossRef]
31. Kucinska-Lipka, J.; Gubanska, I.; Strankowski, M.; Cieśliński, H.; Filipowicz, N.; Janik, H. Synthesis and characterization of cycloaliphatic hydrophilic polyurethanes, modified with L-ascorbic acid, as materials for soft tissue regeneration. *Mater. Sci. Eng. C* **2017**, *75*, 671–681. [CrossRef] [PubMed]
32. Li, W.; Zhou, J.; Xu, Y. Study of the in vitro cytotoxicity testing of medical devices. *Biomed. Rep.* **2015**, *3*, 617–620. [CrossRef] [PubMed]
33. ISO/EN10993-5. *Biological Evaluation of Medical Devices—Part 5: Tests for in Vitro Cytotoxicity*, 3rd ed.; International Organization for Standardization: Geneva, Switzerland, 2009.
34. Uscátegui, Y.L.; Díaz, L.E.; Gómez-Tejedor, J.A.; Vallés-Lluch, A.; Vilariño-Feltrer, G.; Serrano, M.A.; Valero, M.F. Candidate polyurethanes based on castor oil (ricinus communis), with polycaprolactone diol and chitosan additions, for use in biomedical applications. *Molecules* **2019**, *24*, 237. [CrossRef] [PubMed]
35. Calvo-Correas, T.; Santamaria-Echart, A.; Saralegi, A.; Martin, L.; Valea, Á.; Corcuera, M.A.; Eceiza, A. Thermally-responsive biopolyurethanes from a biobased diisocyanate. *Eur. Polym. J.* **2015**, *70*, 173–185. [CrossRef]
36. Zdrahala, R.J.; Zdrahala, I.J. Biomedical applications of polyurethanes: A review of past promises, present realities, and a vibrant future. *J. Biomater. Appl.* **1999**, *14*, 67–90. [CrossRef] [PubMed]
37. Menzies, K.L.; Jones, L. The impact of contact angle on the biocompatibility of biomaterials. *Optom. Vis. Sci.* **2010**, *87*, 387–399. [CrossRef]
38. Law, K.-Y. Definitions for Hydrophilicity, Hydrophobicity, and Superhydrophobicity: Getting the Basics Right. *J. Phys. Chem. Lett.* **2014**, *5*, 686–688. [CrossRef]
39. Kucinska-Lipka, J.; Gubanska, I.; Lewandowska, A.; Terebieniec, A.; Przybytek, A.; Cieśliński, H. Antibacterial polyurethanes, modified with cinnamaldehyde, as potential materials for fabrication of wound dressings. *Polym. Bull.* **2018**, *76*, 2725–2742. [CrossRef]
40. Chao, C.Y.; Mani, M.P.; Jaganathan, S.K. Engineering electrospun multicomponent polyurethane scaffolding platform comprising grapeseed oil and honey/propolis for bone tissue regeneration. *PLoS ONE* **2018**, *13*, e0205699. [CrossRef]
41. Kokubo, T.; Takadama, H. Simulated Body Fluid (SBF) as a Standard Tool to Test the Bioactivity of Implants. In *Handbook of Biomineralization*; Wiley-VCH Verlag GmbH: Weinheim, Germany, 2008; Volume 3, pp. 97–109.

42. Shin, K.; Acri, T.; Geary, S.; Salem, A.K. Biomimetic Mineralization of Biomaterials Using Simulated Body Fluids for Bone Tissue Engineering and Regenerative Medicine. *Tissue Eng. Part A* **2017**, *23*, 1169–1180. [CrossRef]
43. Mosier, J.; Nguyen, N.; Parker, K.; Simpson, C.L. Calcification of Biomaterials and Diseased States. In *Biomaterials—Physics and Chemistry, New ed.*; InTech: London, UK, 2018.
44. Sooksaen, P.; Pengsuwan, N.; Karawatthanaworrakul, S.; Pianpraditkul, S. Formation of porous apatite layer during in vitro study of hydroxyapatite-AW based glass composites. *Adv. Condens. Matter Phys.* **2015**, *2015*, 1–9. [CrossRef]
45. Kim, S.; Park, C.B. Mussel-inspired transformation of CaCO3 to bone minerals. *Biomaterials* **2010**, *31*, 6628–6634. [CrossRef] [PubMed]
46. Landi, E.; Celotti, G.; Logroscino, G.; Tampieri, A. Carbonated hydroxyapatite as bone substitute. *J. Eur. Ceram. Soc.* **2003**, *23*, 2931–2937. [CrossRef]
47. Shuai, C.; Shuai, C.; Wu, P.; Yuan, F.; Feng, P.; Yang, Y.; Guo, W.; Fan, X.; Su, T.; Peng, S.; et al. Characterization and bioactivity evaluation of (polyetheretherketone/polyglycolicacid)-hydroyapatite scaffolds for tissue regeneration. *Materials* **2016**, *9*, 934. [CrossRef]
48. El-Meliegy, E.; Abu-Elsaad, N.I.; El-Kady, A.M.; Ibrahim, M.A. Improvement of physico-chemical properties of dextran-chitosan composite scaffolds by addition of nano-hydroxyapatite. *Sci. Rep.* **2018**, *8*, 1–10. [CrossRef]
49. Chen, L.; Tang, Y.; Tsui, C.P.; Chen, D.Z. Mechanical properties and in vitro evaluation of bioactivity and degradation of dexamethasone-releasing poly-D-L-lactide/nano-hydroxyapatite composite scaffolds. *J. Mech. Behav. Biomed. Mater.* **2013**, *22*, 41–50. [CrossRef]
50. Singh, D.; Babbar, A.; Jain, V.; Gupta, D.; Saxena, S.; Dwibedi, V. Synthesis, characterization, and bioactivity investigation of biomimetic biodegradable PLA scaffold fabricated by fused filament fabrication process. *J. Braz. Soc. Mech. Sci. Eng.* **2019**, *41*, 121. [CrossRef]
51. Lam, C.X.F.; Savalani, M.M.; Teoh, S.H.; Hutmacher, D.W. Dynamics of in vitro polymer degradation of polycaprolactone-based scaffolds: Accelerated versus simulated physiological conditions. *Biomed. Mater.* **2008**, *3*, 034108. [CrossRef]
52. Kucińska-Lipka, J.; Malysheva, K.; Włodarczyk, D.; Korchynskyi, O.; Karczewski, J.; Kostrzewa, M.; Gubanska, I.; Janik, H. The Influence of Calcium Glycerophosphate (GPCa) Modifier on Physicochemical, Mechanical, and Biological Performance of Polyurethanes Applicable as Biomaterials for Bone Tissue Scaffolds Fabrication. *Polymers* **2017**, *9*, 329. [CrossRef]
53. Haryńska, A.; Kucinska-Lipka, J.; Sulowska, A.; Gubanska, I.; Kostrzewa, M.; Janik, H. Medical-Grade PCL Based Polyurethane System for FDM 3D Printing—Characterization and Fabrication. *Materials* **2019**, *12*, 887. [CrossRef]
54. Mohseni, M.; Hutmacher, D.W.; Castro, N.J. Independent evaluation of medical-grade bioresorbable filaments for fused deposition modelling/fused filament fabrication of tissue engineered constructs. *Polymers* **2018**, *10*, 40. [CrossRef] [PubMed]
55. Gubanska, I.; Kucinska-Lipka, J.; Janik, H. The influence of amorphous macrodiol, diisocyanate type and L-ascorbic acid modifier on chemical structure, morphology and degradation behavior of polyurethanes for tissue scaffolds fabrication. *Polym. Degrad. Stable* **2019**, *163*, 52–67. [CrossRef]
56. Wagoner Johnson, A.J.; Herschler, B.A. A review of the mechanical behavior of CaP and CaP/polymer composites for applications in bone replacement and repair. *Acta Biomater.* **2011**, *7*, 16–30. [CrossRef]
57. Feng, P.; Wei, P.; Shuai, C.; Peng, S. Characterization of Mechanical and Biological Properties of 3-D Scaffolds Reinforced with Zinc Oxide for Bone Tissue Engineering. *PLoS ONE* **2014**, *9*, e87755. [CrossRef] [PubMed]

materials

MDPI

Supplementary

Processing of Polyester-Urethane Filament and Characterization of FFF 3D Printed Elastic Porous Structures with Potential in Cancellous Bone Tissue Engineering

Agnieszka Haryńska *, Iga Carayon, Paulina Kosmela, Anna Brillowska-Dąbrowska *, Marcin Łapiński, Justyna Kucińska-Lipka and Helena Janik

Supplementary data

Dumbbell-shaped specimens for the tensile test (Table S1)

Table S1. Design of prepared dumbbell-shaped TPU samples for tensile test.

Specimen Dimensions	Raster Angle	Printout
➢ A =115 ➢ B=25 ➢ C=33 ➢ D=6 ➢ E=14 ➢ F=25 ➢ G=2	±45 45° -45°	
View of STL file	0/90 0° 90°	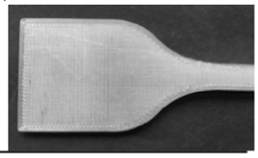

Porous matrix for long-term degradation in PBS and cytotoxicity studies (Table S2)

Table S2. Design of porous matrix for degradation studies of TPU.

View of STL file	Printout
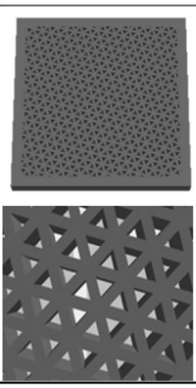	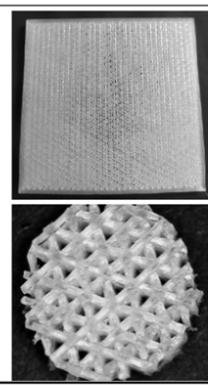

3D printing parameters (Tables S3 and S4)

Table S3. 3D printing settings of test samples TPU_P (dumbbell shaped tensile test specimens, porous matrix for long term degradation in PBS and samples for cytotoxicity study).

3D Printing Parameter	Value
Extrusion temperature (°C)	210
Bed temperature (°C)	65
Cooling	Fan on (start from the second layer)
Printing speed (mm s^{-1})	20
Layer height (mm)	0.18
Infill (%)	100
Nozzle diameter (mm)	0.4
Extrusion ratio (-)	1.05

Table S4. 3D printing settings of porous tissue structures with different architecture (LR, G25 and G3D).

3D Printing parameter	LR	G25	G3D
Extrusion temperature (°C)		225	
Bed temperature (°C)		60	
Cooling		Fan on (start from the second layer)	
Printing speed (mm s^{-1})		20	
Layer height (mm)		0.15	
Extrusion ratio (-)		1.00	
Nozzle diameter (mm)		0.2	
Print time (min)	46	31	49
Used filament (m)	0.73	0.36	0.32

3D print accuracy measurements of printed TPSs

Table S5. Analysis of PTSs print accuracy.

PTS Symbol	3D Model Dimensions (mm)	Actual Dimensions of Printouts (mm) x, y, z (Directions)	Print Accuracy (%) x, y, z (directions)	Average Value of Print Accuracy (%)
LR	15 × 15 × 15	14.82 × 14.77 × 14.80	98.80 × 98.47 × 98.67	
		14.81 × 14.82 × 14.79	98.73 × 98.80 × 98.60	x—98.95 ± 0.18
		14.85 × 14.84 × 14.87	99.00 × 98.93 × 99.13	y—98.87 ± 0.16
		14.90 × 14.87 × 14.82	99.33 × 99.13 × 98.80	z—98.77 ± 0.15
		14.83 × 14.85 × 14.80	98.87 × 99.00 × 98.67	
G25		14.81 × 14.85 × 14.87	98.73 × 99.00 × 99.13	
		14.80 × 14.78 × 14.80	98.67 × 98.53 × 98.67	x—98.77 ± 0.10
		14.80 × 14.79 × 14.77	98.67 × 98.60 × 98.47	y—98.73 ± 0.16
		14.85 × 14.80 × 14.84	99.00 × 98.67 × 98.93	z—98.84 ± 0.22
		14.82 × 14.83 × 14.85	98.80 × 98.87 × 99.00	
G3D		14.59 × 14.63 × 14.81	97.27 × 97.53 × 98.73	
		14.52 × 14.57 × 14.81	96.80 × 97.13 × 98.73	x—97.17 ± 0.33
		14.64 × 14.67 × 14.77	97.60 × 97.80 × 98.47	y—97.45 ± 0.26
		14.51 × 14.57 × 14.81	96.73 × 97.13 × 98.73	z—98.67 ± 0.08
		14.62 × 14.65 × 14.80	97.47 × 97.67 × 98.67	

The effect of the buckled spool.

Figure S1. Damaged spool of TPU filament due to excessively high extrudate stresses generated during forming and winding process.

Nuclear magnetic resonance ^{1}H-NMR

Proton nuclear magnetic resonance (^{1}H-NMR) spectra were obtained using Bruker Avance III HD spectrometer (400 MHz). 10 mg of samples were dissolved in 1 mL of deuterated dimethylsulfoxide (DMSO-d6, Sigma-Aldrich). The TopSpin® software (Bruker) was used to process the obtained data.

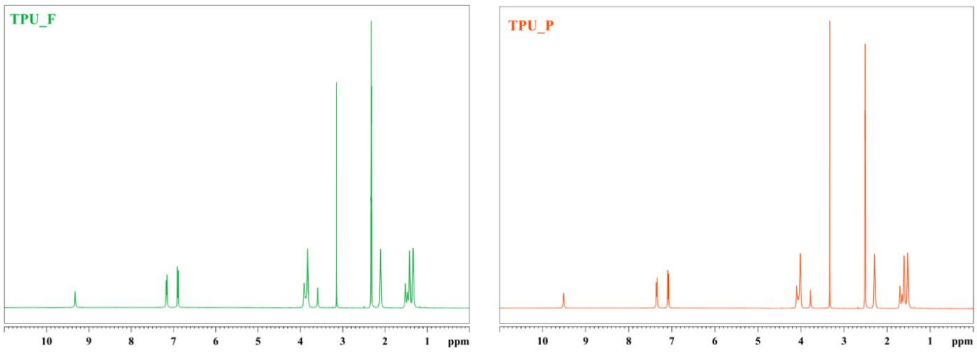

Figure S2. ^{1}H-NMR spectra of TPU_F and TPU_P.

Figure S2 shows the results of H-NMR measurements of TPU_F and TPU_P samples. H-NMR spectra allow the analysis of the chemical structure of the material based on the chemical shifts of the protons. According to literature studies on TPUs, a single peak above 9 ppm most likely corresponds to the protons derived from the urethane bond in the rigid TPU segments. While dublets present around 6.90 to 7.40 ppm correspond to methylene protons placed in aromatic rings of methylene diphenyl diisocyanate (MDI) used for TPU synthesis [1,2].

Long-term degradation in PBS

Table S6. Optical microscopy images of TPU_P samples obtained during long-term degradation study in 0.1 M PBS solution.

	Time of Degradation			
	Day 0	1 month	3 months	6 months
0.1M PBS	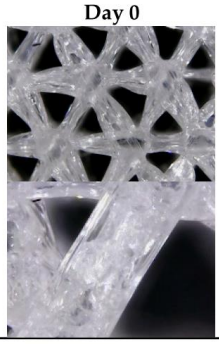	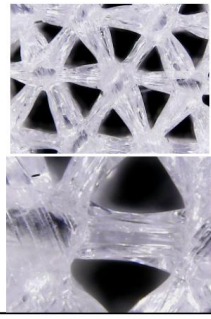	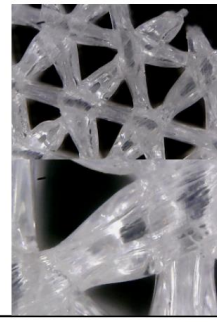	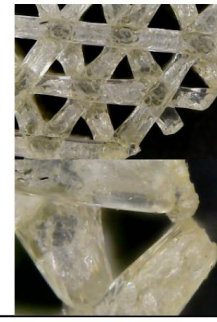

Studies of porous tissue structures (PTS)

Table S7. SEM images from the accelerated degradation studies of G25 porous tissue structure.

× 150	× 1000	× 5000
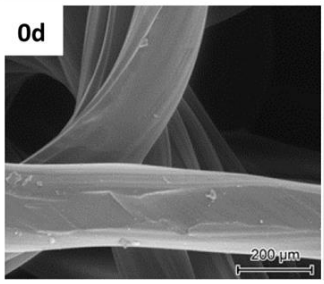	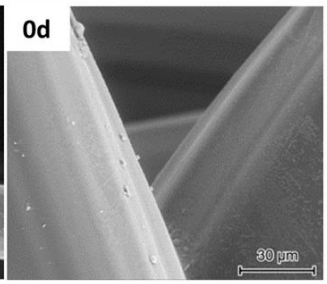	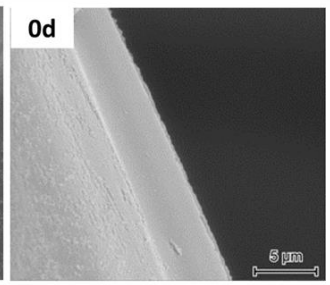
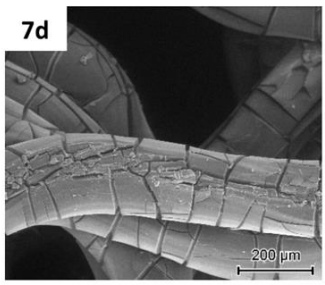	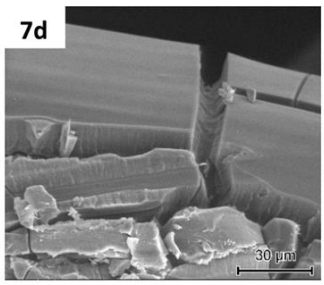	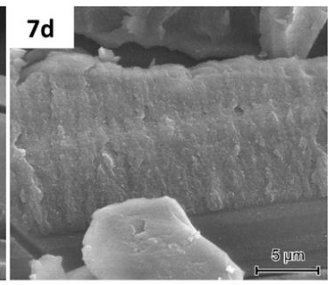
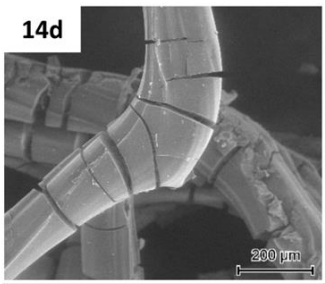	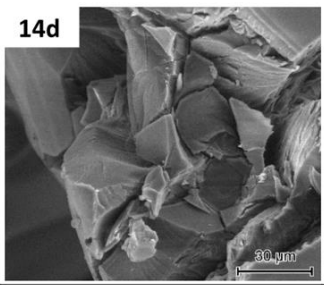	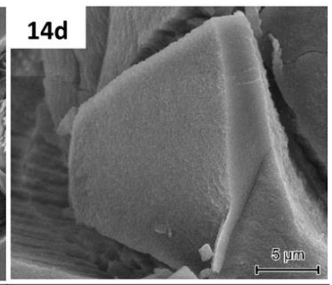

References

1. Parcheta, P.; Głowińska, E.; Datta, J. Effect of bio-based components on the chemical structure, thermal stability and mechanical properties of green thermoplastic polyurethane elastomers. *Eur. Polym. J.* **2020**, *123*, 109422, doi:10.1016/j.eurpolymj.2019.109422.
2. Choi, J.; Moon, D.S.; Jang, J.U.; Yin, W. Bin; Lee, B.; Lee, K.J. Synthesis of highly functionalized thermoplastic polyurethanes and their potential applications. *Polymer (Guildf).* **2017**, *116*, 287–294, doi:10.1016/j.polymer.2017.03.083.

4.4 PAPER 4: A Comprehensive Evaluation of Flexible FDM/FFF 3D Printing Filament as a Potential Material in Medical Application

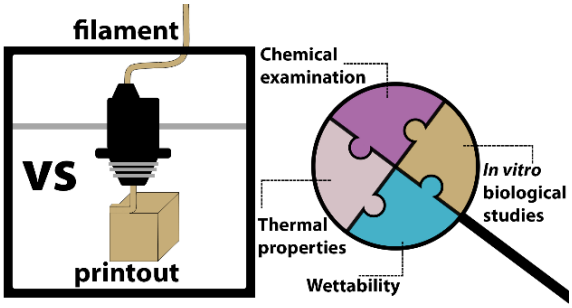

Graphical abstract, source: DOI:10.1016/j.eurpolymj.2020.109958

Authors (percentage share): Agnieszka Haryńska(corresponding author) (50%), Iga Carayon (10%), Paulina Kosmela (5%), Kamil Szeliski (5%), Marcin Łapiński (5%), Marta Pokrywczyńska (5%), Justyna Kucińska-Lipka (10%), Helena Janik (10%)

Journal: European Polymer Journal

DOI: 10.1016/j.eurpolymj.2020.109958

Index: Q1, IF_{2019}=3.862, MNSiW = 100 pts

Author's contribution: Conceptualization (lead), Data Curation (lead), Formal Analysis (in part), Investigation (lead: FTIR, Raman, MFR, tensile and compression tests, hardness, contact angle, surface free energy, short-term degradation studies, SBF incubation), Methodology (lead), Project Administration (in part), Visualization (lead), Writing – Original Draft Preparation (lead), Writing – Review & Editing (lead).

Realized doctoral research tasks:

III (filament characterization) – a comprehensive characteristic of the commercial elastic filament (Bioflex™) and verification of medical-grade features;

IV (evaluation of the filament stability) – analysis of structural and thermal properties of the commercial flexible filament before and after the 3D printing process;

V (3D printing) – design of digital 3D models of test samples and porous structures (scaffolds) *via* Autodesk Inventor software; optimization of the 3D printing parameters;

VI (examination of the printouts in terms of their application in medicine) – preliminary evaluation of the printed elastic porous structures as scaffolds in cancellous tissue engineering (study of degradability, biocompatibility, bioactivity, mechanical, and surface properties).

Material code: Bioflex

BRIEF DESCRIPTION OF THE PUBLICATION

Discussed topics: a brief review of commercial medical-grade filaments; a short discussion about the lack of standards for medical-grade filaments testing and material data presented in Technical Data Sheed (TDS).

Scope of the publication: material characterization; comparison of filament properties before and after FFF 3D printing; 3D printing of porous structures; preliminary evaluation of biological properties.

Novelty of the publication: comprehensive examination one of the few medical-grade flexible filaments commercially available in terms of suitability for 3D printing of medical devices.

Main scientific achievement: it has been proven that the FFF 3D printing process does not change the filament properties (structural, thermal, rheological) and the resulted printouts remain biocompatible.

Outline: The article covers a comprehensive material characterization as well as investigates the effect of FFF 3D printing on structural, thermal, and rheological properties of the medical-grade elastic filament - Bioflex™. In addition to that, a series of the *in vitro* tests were conducted to assess its potential to 3D print structures applicable in medicine. According to the literature and market review, at the time of commencement of doctoral studies, only three companies (Poly-Med, Taulman3D, and Filoalfa) were supplying commercially certified medical-grade filaments for FFF 3D printing, of which only Bioflex™ (Filoalfa) represented a group of flexible filament (thermoplastic elastomer). This product was the benchmark for my research on polyurethane filaments as I could not provide a commercial equivalent of PUR filament for FFF 3D printing.

The results showed that the 3D printing does not change structural and thermal properties of the filament, and thus, it is stable during the process. In turn, it was noted that the mechanical properties of the printouts significantly differ from the Bioflex™ technical data sheet and strongly depend on the 3D printing parameters. The cytotoxicity test showed that the 3D printing process does not change the biological properties and the printouts remain biocompatible. Accelerated degradation studies revealed that Bioflex™ printouts are highly resistant to hydrolysis, which excludes their application as degradable structures, whereas a preliminary bioactivity test showed that the printouts are susceptible to the mineralization by the formation of carbonate hydroxyapatite (C-HAp) on the surface. The tested material appears to be suitable for FFF 3D printing of medical devices or internal long-term bone-type implants due to the outstanding resistance to hydrolysis in aggressive media, biocompatibility, and susceptibility to mineralization. The presented work enables a comparison of the filaments developed in the dissertation with commercial products as well as provides relevant information and data for investigators looking for modern solutions in extrusion-based 3D printing for medical applications.

European Polymer Journal 138 (2020) 109958

Contents lists available at ScienceDirect

European Polymer Journal

journal homepage: www.elsevier.com/locate/europolj

A comprehensive evaluation of flexible FDM/FFF 3D printing filament as a potential material in medical application

Agnieszka Haryńska[a,*], Iga Carayon[a], Paulina Kosmela[a], Kamil Szeliski[c], Marcin Łapiński[b], Marta Pokrywczyńska[c], Justyna Kucińska-Lipka[a], Helena Janik[a]

[a] Department of Polymers Technology, Faculty of Chemistry, Gdansk University of Technology (GUT), Narutowicza Street 11/12, 80-233 Gdansk, Poland
[b] Department of Solid State Physics, Faculty of Applied Physics and Mathematics, Gdansk University of Technology (GUT), Narutowicza Street 11/12, 80-233 Gdansk, Poland
[c] Department of Regenerative Medicine, Cell and Tissue Bank, Nicolaus Copernicus University, Collegium Medicum, M.Sklodowskiej-Curie 9, 85-094 Bydgoszcz, Poland

ARTICLE INFO

Keywords:
Material characterization
Fused deposition modelling
3D printing
Medical-grade filament
Bioactivity
Simulated body fluid (SBF)

ABSTRACT

The use of FDM/FFF in 3D printing for medical sciences is becoming common. This is due to the high availability and decent price of both 3D printers and filaments useful for FDM/FFF. Currently, researchers' attention is focused mainly on the study of medical filaments based on PLA, PCL or their modifications. This contributes to insufficient diversity of medical-grade filaments on the market. Moreover, due to the lack of specified standards for filaments testing, manufacturers often provide merely the characteristics of the raw materials, which were used for filaments fabrication. This lack of comprehensive data can be problematic when viewed as medical-grade material. As a consequence of this overview, we have performed a comprehensive evaluation of a flexible medical-grade filament for FDM/FFF 3DP - Bioflex® (Filoalfa). We have performed complex characterization through a variety of methods and techniques including spectroscopic analysis (FTIR, Raman), dynamic mechanical analysis (DMA), thermal properties (DSC, TGA), rheological characteristic (MFR). In the next step, printed Bioflex® samples were utilized to characterize the material behaviour after the 3D printing process. The mechanical analysis allowed to estimate how the material strength decreases after the printing process according to the values given in the technical data sheet. The contact angle measurements determined wettability of the Bioflex® printouts. Performed series of *in vitro* studies were carried out to assess its potential as as implantable structures. In conclusion, 3D printing process did not affect the printouts biocompatibility (ISO 10993:5). Accelerated degradation studies indicated elevated hydrolysis resistance of printed samples. In turn, performed incubation in simulated body fluid (SBF) solution, revealed carbonated hydroxyapatite (HAp) deposition on printouts surface indicating their bioactive properties. Thus, studied filament seems to be a suitable candidate for further development of FDM/FFF 3DP structures for advanced biological and medical application.

1. Introduction

Biopolymers, both natural and synthetic, have been known in medicine for centuries. Due to the simplicity of their formation, biocompatible or biostable nature and a wide range of the properties that can be adapted to the desired needs, they constantly attract the interest of scientists and the medical industry [1]. Progress in the field of polymers is, among others, associated with the research on modern and advanced methods of their processing technologies. Although the basic thermoplastics forming methods such as extrusion, thermoforming or injection moulding are still used in the medical industry, improved processes for the formation of personalized complex structures in a time-saving and efficient way are desirable. These methods include additive manufacturing technologies AM (so-called 3D printing). The use of AM technologies created wide opportunities especially in the field of personalized medicine and drug delivery [2–4]. Fused deposition modelling (FDM, Stratasys, USA) / Fused Filament Formation (FFF, non-trademark) are 3DP technologies that form objects by extrusion of thermoplastic-based material supplied in the form of the filament. Here, molten material is deposited layer by layer on the build table following the loaded computer data. The FDM/FFF technologies belong to the group of extrusion-based 3D printers. They have gained particular attention in medicine, pharmaceutical industry as well as various branches of science due to the high accessibility, relatively low production

* Corresponding author.
E-mail address: agnieszka.harynska@pg.edu.pl (A. Haryńska).

https://doi.org/10.1016/j.eurpolymj.2020.109958
Received 9 July 2020; Received in revised form 11 August 2020; Accepted 16 August 2020
Available online 25 August 2020

Table 1
Review of selected commercial medical-grade filaments for FDM/FFF 3D printing. Presented data are taken from TDS available on the manufacturers' websites.

Trade name (company)		Bioflex® (Filoalfa)	Arnitel® ID 2045 (DSM)	FibreTuff® II (IPM)	guidel!ne® (taulman3D)
Chemical family/product description		TPC (thermoplastic copolyester elastomer)	TPC (thermoplastic copolyester elastomer)	PMC (composite based on polyamide, polyolefin and cellulose fibres)	PETG based (glycol-modified polyethene terephthalate)
Mechanical properties	Tensile modulus (MPa)	35 (ASTM D790)	29 / 29* (ISO 527)	850 (ISO 527)	1940 (ASTM D412)
	Tensile strength (MPa)	16 (ASTM D638)	8 / 7.6* (ISO 527)	23 (ISO 527)	47 (ASTM D412)
	Elongation at break (%)	800 (ASTM D638)	350 / 390* (ISO 527)	4 (ISO 527)	5.9 (ASTM D412)
	Hardness	27 Sh D (ASTM D2240)	34 Sh D (ISO 868)	–	–
Thermal properties	Melting point (°C)	185 (ASTM D3417)	158 (ISO 11357)	–	220
	Glass transition temperature (°C)	–70	–35 (ISO 11357)	–	77
Biological evaluation of medical devices		USP Class VI ISO 10993-4/5/10	USP Class VI ISO 10993-5/10	USP Class VI	USP Class VI ISO 10993-3/4/5/6/10/11 ISO 11607-1 DMF (type III)

– tests conducted on printed specimens.
* – infill raster orientation 0/90° and ± 45°, respectively.

or equipment costs [5]. Thereby, advanced products such as anatomical models and surgical training systems [6–8], drug delivery systems [9–11], dialysis catheters [12,13], customized laboratory equipment [14,15] or tissue engineering scaffolds [16–18] are successfully formed using FDM/FFF 3D printers. Since the selection of an appropriate material for the production of medical prototypes (objects that do not interact with biological matter) is not an issue, the 3DP of objects having permanent or short-term contact with tissues should utilize medical-grade materials. Considering filament market, the number of the certified, medical-grade materials is constantly increasing, however, the choice is still limited. Some of them are briefly described in Table 1.

In general, filament manufacturers provide comprehensive material characteristics, but most of the data concerns to a raw material from which filament was formed. So far, there are no specified requirements or standards describing how the material data related to filament should be presented. This leads to inconsistencies in the developed research with their use. FDM/FFF 3DP is based on a combination of high-temperature extrusion process and application of mechanical stress. Thus, we can expect changes in polymer properties and the general characteristic is no longer comparable to data provided by a manufacturer [19]. Moreover, this issue is becoming even more complex when factors affecting the FDM/FFF 3D printout properties are taken under consideration. The list of factors affecting the quality and mechanical properties of the FDM/FFF printouts has been reliably presented by Goh et al. [20]. They include the print orientation on build table, temperature parameters, print speed, extrusion ratio, nozzle diameter, infill properties, layer thickness, flow rate or cooling factors.

The extensive material characterization seems particularly important when we consider using FDM/FFF printed structures for medical purposes [21]. The characterization should include biological and degradation tests. Besides *in vitro* cytotoxicity, cell adhesion, long and short-term degradation studies [21–23], the incubation in simulated body fluid (SBF) is desirable since it is a very effective method to assess material bioactivity in terms of apatite formation ability [24]. It is worth noting, that SBF solution is characterized by ion concentration nearly the same to those of human blood plasma. Most of the bone-bonding materials subjected to SBF solution form on their surface a mineral structure (apatite) by which they bond and adapt to living bone tissues [25].

Material data provided by the Bioflex® manufacturer refer to the properties of the raw material used for its fabrication, hence it seems reasonable to extend the product characteristic with the properties of the filament and printouts obtained from it. Therefore, we conducted a series of studies to assess whether and how the FFF 3D printing process affects filament and printout properties compared to the source material. For this purpose, we analyzed a chemical structure and determined thermal, thermomechanical, mechanical, rheological and surface properties. Bioflex® filament is marked as suitable for medical certifications (USP Class VI and ISO 10993-4/5/10), thus we carried out preliminary tests to evaluate its potential application for structures, which can interact with a human body. Printouts in the form of porous meshes were subjected to cytotoxicity test, short-term degradation studies as well as incubation in simulated body fluid (SBF) for *in vitro* biomineralization evaluation. Cytotoxicity test was carried out with the use of CCl163 cell line according to requirements given by ISO 10993-5 standard. The degradation process was monitored via FTIR spectroscopy and mass change measurement. The apatite deposition on the printout's surface after SBF incubation was examined by SEM supplemented by EDS and Raman spectroscopy.

2. Material and methods

2.1. Material

Bioflex® filament was purchased from Filoalfa, Italy. It is a flexible fibre marked as a copolyester with USP VI class and ISO 10993-4/5/10 medical certifications. Filament has a milky white colour and a diameter of 1.75 mm. Table 1 shows the extended product characteristics. Recommended print settings are as follows, extruder temperature 210–230 °C, bed temperature 0–70 °C and printing speed 40–60 mm s^{-1}.

2.2. 3D printer and test sample preparation

Inventor I series FFF 3D printer (FlashForge, China) in conjunction with FlashPrint slicer (4.2.0 version, FlashForge, China) was used to form test printouts. The following basic print settings were maintained: extruder temperature 220 °C, bed temperature 50 °C, printing speed 20–40 mm s^{-1} and nozzle diameter 0.4 mm. For detailed information on test samples design and printing parameters please see Supplementary data. The filament was examined as received.

2.3. Filament characterization methods

2.3.1. Spectroscopic studies

Spectroscopic studies were carried out to examine the chemical functional groups of Bioflex® filament to evaluate the impact of the printing process on its stability. Thus, the filament and printouts were investigated. Attenuated total reflectance (ATR) FTIR analysis was conducted with a Nicolet 8700 spectrometer (Thermo Fisher Scientific, Waltham, USA) at spectral range of 4000–500 cm^{-1} (64 scans, resolution 4 cm^{-1}) under room temperature. Raman spectra were collected using a confocal micro-Raman system (InVia, Renishaw, UK) at randomly selected locations (50x magnification) with a green laser (514 nm) operating at 50% of its total power (50 mW).

2.3.2. Thermal properties

To determine thermal behaviour and stability of the filament and printouts, differential scanning calorimetry (DSC) and thermogravimetry (TG) were applied. DSC measurements were performed using a Netzsch 204F1 Phoenix apparatus (Netzsch, Germany) under nitrogen atmosphere (flow rate 20 mm min^{-1}). Approximately 5 mg samples were placed in aluminium crucibles. Heating/cooling cycle was performed as follows; Initially, the sample was heated to 250 °C. Once the temperature was reached, it was cooled to –80 °C and reheated to 250 °C. The heating/colling rate was 10 °C min^{-1}. In turn, thermogravimetric analysis was carried out using a Netzsch TG 209 instrument (Netzsch, Germany). Samples of ~5 mg were studied at a heating rate of 10 °C min^{-1} in the temperature range from 35 °C to 700 °C under nitrogen atmosphere.

2.3.3. Dynamic mechanical analysis (DMA)

The dynamic mechanical test was performed using DMA Q800 analyzer (TA Instruments, USA). Printouts having dimensions of 40 × 10 × 2 mm were measured in the single cantilever bending mode with 1 Hz frequency of an oscillatory deformation. The study was conducted at the temperature range from –100 °C to 150 °C; the heating rate was 4 °C min^{-1}. Thereby the storage modulus (G'), loss modulus (G'') and damping factor (tangent δ) were recorded as a function of temperature. The specimen printing conditions were presented in Table S4.

2.3.4. Melt flow rate (MFR)

A Zwick/Roell load plastometer was used to measure melt flow rate (MFR) and melt volume rate (MVR) of filament before and after printing. The study was conducted according to ISO 1133 standard at the temperature of 200 °C and load of 5 kg (n = 5).

2.3.5. Mechanical properties

The parameters provided by the manufacturer of Bioflex® refer to the properties of the solid polymer. Therefore, all the mechanical properties of the filament were studied on printed samples. Furthermore, the influence of raster angle on hardness and tensile properties were investigated, as shown in Table S1. The hardness was measured with a Shore type A durometer (Zwick/Roell, Germany) according to ISO 868 standard. The results are the arithmetic mean of ten measurements. A Zwick/Roell Z020 universal tensile machine was used for tensile testing according to ISO 527 standard. Measurements were carried out at room temperature; crosshead speed was set to 100 mm min^{-1} and initial force was 1 N. Reported results are the average calculated from eight measured dumbbell-shaped specimens. Uniaxial compression test was conducted on solid and porous cubic samples with the dimension of 15 × 15 × 15 mm using a Zwick/Roell Z020 machine. Samples were compressed at a rate of 20 mm min^{-1} until 50% strain was reached (n = 5). Detailed information on design and printing conditions were presented in Table S3 and S4.

2.3.6. Surface properties

The contact angle test by the sessile drop technique was applied to determine the wettability and surface free energy (SFE) of Bioflex® printouts. Measurements were performed using ramé-hart 90-U3 goniometer with a DROPimage Pro software (ramé-hart, USA). A 2 μL droplet of selected solvent was deposited on the degreased sample surface and the images were taken. The contact angle was measured for four different solvents, i.e. water, diiodomethane, formamide and ethylene glycol. At least six randomly selected points on the sample surface were tested. In turn, SFE was determined via the Fowkes method in which concept is based on acid-base interactions. Therefore, the contact angle measurements for polar (water) and non-polar (diiodomethane) liquids were used to calculate SFE.

2.4. In vitro studies of Bioflex® printed porous structures

2.4.1. Cytotoxicity assay

Cytotoxicity of Bioflex® printouts was studied according to the ISO 10993-5 standard. Firstly, the sample was sterilized 30 min each side under UV radiation. Then, an extract of studies sample was prepared in culturing medium DMEM/F-12 supplemented with FBS; 5 μg ml^{-1} penicillin with streptomycin; 5 μg ml^{-1} amphotericin B (all Coring). The extract thus obtained was incubated for 24 h (37 °C, 5% CO_2), filtrated and given to the CCl163 cells which were prepared as follows; cells were seeded on 96-well culture plates with a density of 1000 cells per well (Nunc) and cultured for 24 h (37 °C, 5% CO2) in the supplemented DMEM/F-12 culturing medium. After 24 h of cells incubation with extract, the MTT assay was performed. The absorbance of prepared solutions was scanned by Varioskan at λ = 570 nm (Thermo Scientific, USA). The results were presented as a cells viability towards control (100% of survival). The statistical analysis was performed with the use of the Origin Pro 8.5 (Washington, DC, USA). Statistical differences were evaluated by the one-way ANOVA (α = 0.05) and post hock Tukey test (α = 0.05).

2.4.2. Degradation studies

The printouts were subjected to an *in vitro* short-term degradation study to estimate degradation susceptibility [26]. Firstly, samples in the shape of disks (ϕ = 8 mm, h = 3 mm) were cut out from the printed matrix. Then samples were degreased, weighed and placed in 12-well plates. Short-term degradation was conducted for 28 days in strongly alkaline and acidic solutions, 5 M NaOH and 2 M HCl, respectively. 3 ml of selected media was added to each well and incubated at 37 °C. Medium was replenished every 2 weeks. After specified time intervals, samples were taken out, rinsed with DI water and dried. The degradation process was monitored by FTIR spectrum and mass measurements. For each time intervals, three replicates were investigated (n = 3).

2.4.3. Bioactivity evaluation in simulated body fluid (SBF)

The *in vitro* bioactivity was tested in an SBF solution prepared according to the procedure developed by Kokubo et al. [24]. Samples for testing were prepared in the same manner as for short-term degradation (n = 3). Incubation was conducted in 6-well plates at 37 °C within periods of 7 days, 1 and 3 months. The SBF solution was refreshed every 2 weeks. Incubated samples were removed from the test solution, rinsed with DI water and left to dry at room temperature. The surface

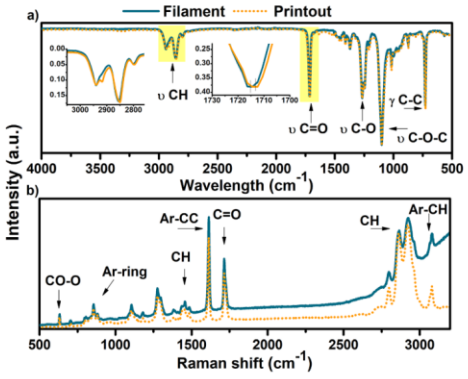

Fig. 1. FTIR (a) and Raman (b) spectra of Bioflex® filament and selected printout.

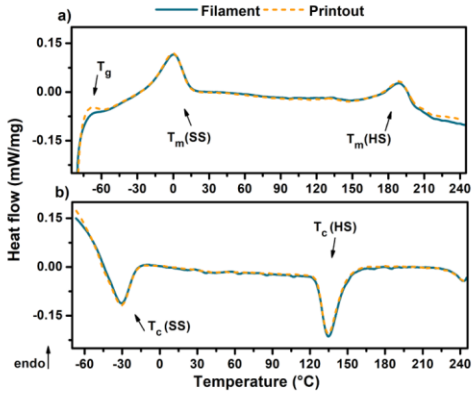

Fig. 2. DSC thermograms of filament and Bioflex® printouts. (a) second heating run, (b) cooling run.

morphology of the samples was observed by Scanning Electron Microscope (SEM) (FE-SEM, FEI Quanta FEG 250, accelerating voltage 10 kV) while formed crystals were characterized using EDS and Raman spectroscopy.

3. Results and discussion

3.1. Characterization of chemical structure (ATR-FTIR, Raman)

The chemical structure analysis of the filament and printouts was conducted based on FTIR and Raman spectra (Fig. 1a,b). According to the information provided by the producer, Bioflex® is a thermoplastic copolyester elastomer (TPC) which suggests the presence of a segmented structure based on a long soft polyester/ether segments (SS) and a short rigid hard segments (HS) [27]. In both samples, absorption peaks at the range of wavenumbers from 3000 to 2795 cm^{-1} indicate the presence of methylene groups. Double peaks at 2929 and 2917 cm^{-1} might be attributed to the stretching vibrations of −CH in the aromatic ring. While signal at 2852 cm^{-1} corresponds to the symmetric and asymmetric −CH stretching vibration of aliphatic methylene groups. A slight peak at 2799 cm^{-1} may belong to the methylene group that is adjacent to oxygen. Typical TPCs polyester blocks are represented by the vibration of the carbonyl (C═O) group at ~1713 cm^{-1} and a double absorption peak at 1267 and 1250 cm^{-1} related to the asymmetric and symmetric ν(C−O) vibration of ester groups. In turn, a sharp band at 1100 cm^{-1} is most likely associated with the presence of the ether oxygen ν(C−O−C). Bands corresponding to the bending vibrations are visible around 1445 cm^{-1} (−CH_2) and ~1015 cm^{-1} (C═O). Strong signal around 724 cm^{-1} correspond to carbon-carbon bonds γ(C−C). Additionally, peaks in the range of 1500–1447 cm^{-1} and 874 cm^{-1} might be attributed to the stretching vibration and bending vibration (out of plane) of C═C and −CH of an aromatic ring, respectively [28–30]. The FTIR spectra of the filament and print are very similar, no significant changes in intensity or band shifts were noted. Nevertheless, analyzing the carbonyl band an upshift of the printout relative to the filament by ~4 cm^{-1} was noted. According to Chen et al. [31], this shift is related to the weakening of hydrogen bonds occurring in the structure. However, the peak is not split thus the presence of H-bonding is rather unlikely or their participation is insignificant. To confirm the above considerations, the Raman spectroscopy was performed. It showed the presence of the following functional groups in the Bioflex® structure; C═O carbonyl groups (single peak at 1714 cm^{-1}); ether oxygen (1104 cm^{-1}), CO−O in-plane deformation of ester groups (632 cm^{-1}); CH_2 deformation vibration at the range of 1434–1488 cm^{-1}; symmetric and asymmetric stretching vibration of −CH (2864, 2924 cm^{-1}). In addition, the Raman spectra confirmed the presence of aromatic rings; Ar−CH stretch at 3065, 3081 cm^{-1}; Ar-CC ring vibration at 1614 cm^{-1}; bending vibration of Ar-ring at the range of 830–880 cm^{-1} [32–35]. In this case, no differences between the filament and printout spectra were observed, also no hydrogen bonded functional groups were found. Thus, it can be concluded that the structure of Bioflex® is based on aromatic polyester-ether compounds connected by ester linkages in which there are no suitable protons that can form H-bonding.

3.2. Thermal properties

Segmented structure of thermoplastic copolyester elastomers (TPC) and their ability to phase separation respond for their dual nature. TPCs act as a crosslinked elastomer at room temperature while after heating they exhibit thermoplastic properties [27]. Bioflex® belongs to the TPC group, thus to confirm its segmented structure we examined its phase transitions by DSC. Based on the obtained thermograms glass transition temperature (T_g), melting temperature (T_m), heat enthalpy (ΔH_m) and crystallisation temperature (T_c) were determined. The second heating run (Fig. 2a) revealed the presence of two melting points at 0.36 °C (ΔH_m 14.82 J g^{-1}) and 189.4 °C(ΔH_m 4.87 J g^{-1}). The first endothermic transition corresponds to the melting of soft segment crystallites (T_mSS) while the second peak is due to the melting of crystalline hard segments (T_mHS). Relatively low heat enthalpy of T_m(HS) transition could indicate a low crystallinity degree of the hard phase. In turn, the appearance of the T_mSS peak around 0 °C points out the presence of relatively long soft segments or/and their high concentration comparing to HS building blocks [36]. The glass transition for both samples occurs around –68.7 °C and its slightly higher than the T_g value given in the Bioflex® technical data sheet (–70 °C). This value is associated with the soft phase transition. The T_g of TPCs, which according to the literature reveals at about –70 °C, corresponds to the systems based on PTMO (polytetramethylene oxide) soft phase [36–39]. The cooling run (Fig. 2b) showed the crystallization temperature of HS at 134.6 °C and for SS phase around –30.8 °C. The obtained thermograms for the filament and printout overlaps. It can be assumed that the 3D printing process did not cause changes at the microstructure level of Bioflex®.

TGA measures the amount and rate of change in weight of a sample as temperature function and gives information on its thermal stability. Obtained TG curves and their derivatives are shown in Fig. 3. Both thermograms indicate one-step degradation process in the temperature

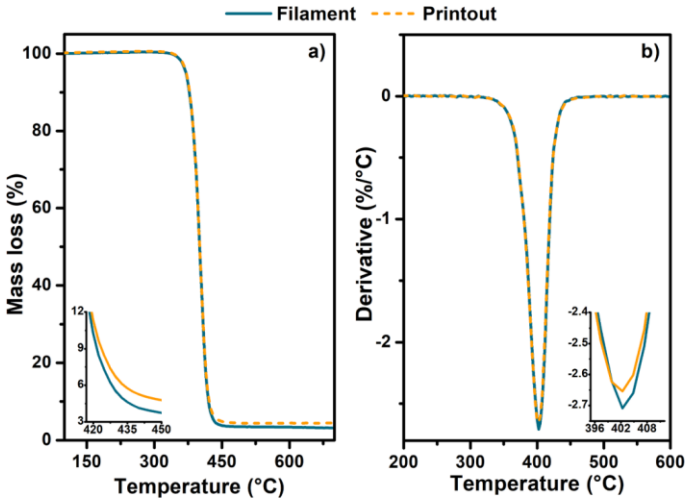

Fig. 3. TG (a) and DTG (b) curves of Bioflex® filament and printout.

Table 2
TGA data: temperature of 5, 10, 30, 50, 90% weight loss and residual mass.

	$T_{5\%}$,°C	$T_{10\%}$,°C	$T_{30\%}$,°C	$T_{50\%}$,°C	$T_{90\%}$,°C	Residual mass
Filament	369.8	377.6	392.3	400.7	420.3	3.21% at 697.8°C
Printout	370.8	378.3	392.4	400.7	421.8	4.37% at 697.9°C

range of 370–470 °C. The average thermal stability of filament and printout is around 368 °C (T_{onset}). Decomposition process starts at 355 °C with a backbone degradation of the material matrix which progresses very rapidly. The printouts exhibited a slightly higher temperature of 90% weight loss and residual mass compared to the filament as given in Table 2. However, such insignificant differences could be due to the little difference in the masses of the tested samples. Thus, conducted thermal studies showed that the Biolex® filament is a thermally stable material that retains its properties after the 3D printing process.

3.3. Physico-mechanical properties (DMA)

For further characterization of Bioflex® material, DMA study was performed. DMA can provide additional information on TPC phase behaviour including thermal transitions (T_g, T_m) and mechanical features. For this measurement, a sample with a standardized size is required, hence the results presented in Fig. 4 refer only to the printout sample. Based on the storage modulus curve viscoelastic behaviour regions can be distinguished, a glassy state (at a low-temperature range) with the highest storage modulus value; a glass transition area and region of a rubbery plateau characteristic for thermoplastic elastomers [38]. Tangents delta curve exposes the region of glass transition at the temperature of –75 to 25 °C in which the relaxation and transition of soft amorphous phase take place. The maximum of this peak is around –46 °C which confirms the presence of PTMO as a soft phase in the structure of Bioflex®, which is consistent with the literature [40]. It is known that amorphous phase in TPCs containing not only the soft

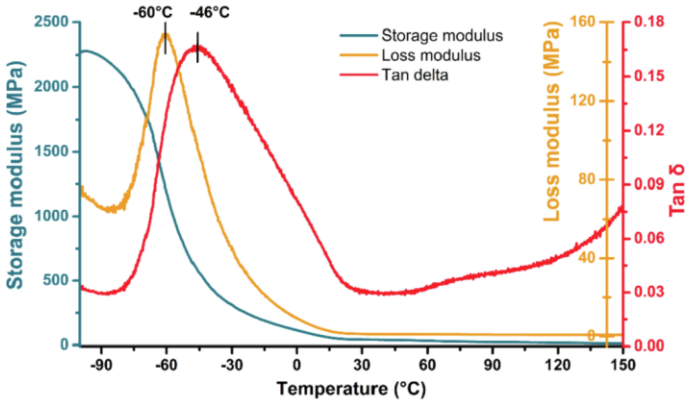

Fig. 4. DMA curves of Bioflex® printout - storage, loss modulus and damping parameter.

segments (e.i PTMO) but it is a mixture of amorphous SS-rich and some noncrystalline hard segments phases [36,40]. Consequently, it can be assumed that a very broad and slight peak around 73 °C (Tan δ curve) corresponds to the T_g of the amorphous HS phase.

The research carried out so far indicates the segmented, heterophase structure of the Bioflex® material which belongs to the group of poly(ester ether) copolymers and contains PTMO as a soft segment. Additionally, the filament exhibits outstanding thermal stability and its chemical structure which does not change after the 3D printing process.

3.4. Melt flow rate (MFR)

The melt flow rate (MFR) is an important parameter of thermoplastic materials intended for processing. This parameter represents the rheological properties and is closely associated with a melt viscosity of thermoplastics. FDM/FFF 3DP is based on the extrusion process in which the filament is plasticized in a mini-heating block and deposited on a platform by a heated nozzle with a diameter of 0.15–0.6 mm. Unlike the conventional extrusion process, this operation is devoid of a screw and thus occurring mechanical shear forces are much lower. Therefore, thermoplastic materials for extrusion-based 3DP should be easily plasticized in a relatively short time. Furthermore, such material should be capable of properly solidification (toughening) rate which allows for appropriate interlayer bonding and shape stabilization [41]. The melt rate value is represented as a mass (g, MFR) or volume (cm^3, MVR) of material extruded through the standardized die under constant load and temperature per 10 min. The melt rate of commercial TPC filaments is in the range of MVR = 45 cm^3 10 min^{-1} (Arnitel®, 230 °C/2.16 kg), MFR = 28 g 10 min^{-1} (Z-Flex®, 225 °C/2.16 kg), MVR = 39 cm^3 10 min^{-1} (FlexiFil®, 230 °C/2.16 kg). The data comes from TDS available on the manufacturers' websites.

The results of MFR measurements are presented in Table 3. It was noted that the change in the flow rate of the filament relative to the printout is insignificant. Thus, the printing process did not change the rheological properties of the Bioflex®. Unfortunately, due to the different MFR measurement conditions (temperature/load), these values cannot be directly compared with the values of commercial products.. Is known that, as the MFR increases the print speed of the object can be higher [42]. In turn, to high MFR value might cause uncontrolled leakage of material from the printer nozzle, thereby causing significant defects of the printouts [43].

3.5. Mechanical characterization

Further characteristics of the Bioflex® filament included mechanical tests such as hardness, tensile and compression strength. All printing parameters of the test samples were provided in Supplementary data. Several studies have shown that the design and printing parameters significantly affect the printout features [44]. Table 4 presents the results of tensile strength and hardness depending on the applied infill raster orientation as well as compression test data. The hardness of printouts was in the range of 76–78 Sh A, which corresponds to about 22 Sh D. This value is much lower than that given in the Bioflex® TDS (27 ShD) which is probably related to the uneven surface of the printouts formed by successive layers of the oval filament streams. Tensile strength and elongation at break were slightly higher for samples with infill raster orientation ± 45° (14 MPa, 760%) than those with raster orientation 0/90°. This is probably due to the higher tension of the layers arranged perpendicular to the stretching direction of the sample [45]. In turn, the tensile strength of raw material from which Bioflex® was formed is 16 MPa thus there is no significant loss of tensile strength after the 3DP process. This may indicate exceptionally good adhesion between successive layers of the printouts. The stress-strain curves (see Fig. 5a) of both samples are characteristic of elastomeric materials and their appearance notably resembles curves for TPC with the content of soft segments (SS) exceeding 50 wt% [38].

Table 3
MFR of Bioflex® filament and printout.

(200 °C/5 kg)	MFR (g 10 min^{-1})	MVR (cm^3 10 min^{-1})
Filament	9.14 ± 0.48	9.50 ± 0.50
Printout	9.70 ± 0.63	10.54 ± 0.71

Table 4
Summary of mechanical tests of printed samples. In the compression test section (P) and (A) mean orientation of cubic specimens during the compression test. P - perpendicular and A- along to plane of the printed layers.

Infill raster orientation	0/90°	± 45°
Hardness (Shore A)	76 ± 1	78 ± 1
Young modulus (MPa)	0.16 ± 0.1	0.19 ± 0.1
Tensile strength (MPa)	12.6 ± 1.8	14.1 ± 0.9
Elongation at break (%)	646.7 ± 37.5	757.3 ± 35.7
Relative elongation (%)	318.3 ± 45.2	275.6 ± 42.6
Compression test	Yield point (MPa)	Maximum registered compressive strength (MPa)
Solid_A	0.80 ± 0.12	4.11 ± 0.19
Porous_A	0.61 ± 0.10	2.43 ± 0.15
Solid_P	0.46 ± 0.10	2.54 ± 0.22
Porous_P	0.52 ± 0.11	1.88 ± 0.17

The compressive strength test was carried out perpendicular (P) and along (A) to the plane of the printed layers (Fig. 5b). Solid and porous cubic specimens were tested. Based on the compression curves, three areas distinguished, at low strain narrow elastic region with the yield strength was defined; wide stress plateau where plastic deformation occurs; densification of sample evident by a sharp stress increase. It was noted that the samples tested in the along direction (A) showed markedly higher values of compressive strength (Table 4). These observations confirm the anisotropic behaviour of the FFF 3D printed samples compared to the solid ones. Similar observations were reported in the Sung-Hoon et al. [46] work, where the compressive strength of ABS samples tested perpendicular to the plane of printed layers was above 20% lower than for specimens tested in the opposite direction. It is worth noting that during the compression test none of the cubic samples was permanently damaged.

3.6. Contact angle (CA) and surface free energy (SFE)

Contact angle (CA) and surface free energy (SFE) studies provide important information about surface properties, especially when considering Bioflex® as a medical-grade filament. CA results are presented in Fig. 6. The water contact angle of 69.0° ± 1.1° indicates a hydrophilic surface with average wettability. Surface free energy was calculated (Fowkes method) using the contact angle against water (polar) and diiodomethane (apolar) liquids. SFE was 52.69 ± 0.16 mN m^{-1} (dispersive part 46.64 ± 0.11 mN m^{-1}, polar part 6.04 ± 0.14 mN m^{-1}). Hydrophilicity (CA around 50-70°) and relatively high surface energy have a beneficial effect on the cells/protein adsorption hence integration between implants and tissues [47,48]. Thus, Bioflex® printouts might be initially considered as elastic implantable products.

3.7. In vitro studies of porous structures

This part of the research focuses on *in vitro* studies of an elastic porous matrix printed by using Bioflex® filament to initially examine its potential as a product suitable for short/long-term implantation in the human body. For detail information on printed porous structures, please see Table S3-4 (supplementary data).

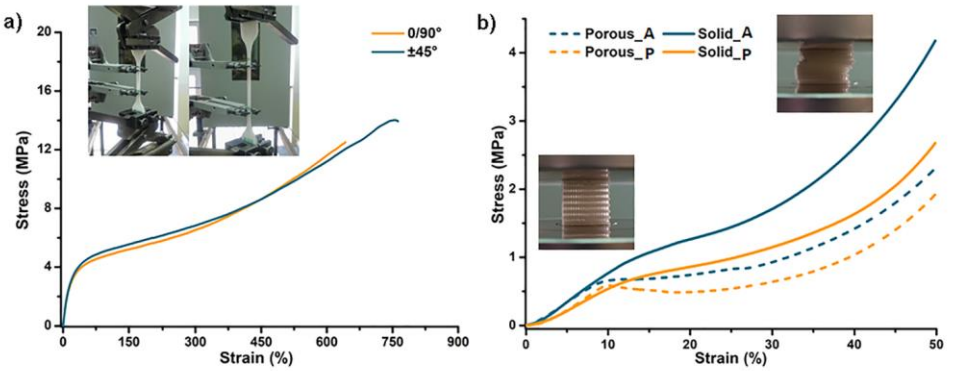

Fig. 5. Representative stress–strain curves (a) tensile test (b) compression test.

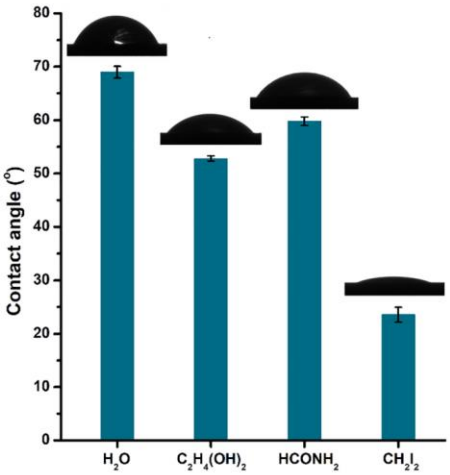

Fig. 6. Contact angle of Bioflex® printouts with respect to various liquids.

3.7.1. Cytotoxicity

The cytotoxicity assay was performed to determine the cytocompatibility of printed structures. The results of cell viability are expressed as the percentage of a control group. The study was performed with the use of established fibroblast cell line CCL-163. Cell viability for all prepared extract concentrations (12.5–100%) was above 100% in comparison to the control (Table 5). According to the regulation given in the ISO 10993:5 standard, material which exhibits cell viability higher than 70% (compared to 100% control) can be considered as cytocompatible and non-toxic [49]. Therefore, obtained printouts are qualified as biocompatible. What further confirms that the 3D printing process does not cause loss of biocompatibility features relative to the Bioflex® raw material.

The morphology of CCL-163 cells was observed after 24 h (Table 5). The distribution and shape of cells were comparable to the control. The number of cells markedly increased as the concentration of prepared extract decreased. Nevertheless, Bioflex-exposed cells remain viability even after exposure to 100% extract.

3.7.2. Accelerated degradation studies

One of the method to *in vitro* study degradation susceptibility of polymer materials is so-called accelerated degradation studies. It is a very effective and time-saving method to assess changes occurring in the material during exposure in environments imitating a human body. High solution concentration allows to markedly reduce the time of examination, which in media such as phosphate-buffered saline (PBS) can last even within a year [21,50].

Accelerated degradation (in 2 M HCl and 5 M NaOH media) included microscopic studies (Table S5), mass loss measurements (Fig. 7a) and FTIR examination (Fig. 7b) were performed. The results showed that susceptibility to degradation was depended on the solution used. Samples were more sensitive to strongly alkaline medium. After 7 days of incubation, a 3% mass loss was noted while for the 2 M HCl solution mass loss of samples did not exceed 0.5%. In the acid environment, Bioflex® samples remained practically untouched (mass loss after 28 days around 1.5%). In turn, in alkaline medium, 10% weight loss was noticed at the end of the study. The analysis of FTIR spectra confirmed that degradation proceeded primarily as a result of the destruction of the ester bonds present in the Bioflex® structure (Fig. 7b). Changes in the peak intensity of ester (νC—O at 1250, 1267 cm^{-1}) and carbonyl (νC═O at 1714 cm^{-1} and δC═O at 1015 cm^{-1}) groups are noticeable in samples incubated in 5 M NaOH medium Those minor changes might indicate a significant concentration of resistant to hydrolysis long hydrocarbon chains, i.e. the advantage of high molecular weight soft segments (SS) in the Bioflex® structure.

PCL is a biodegradable polymer widely used in regenerative medicine application. However, it belongs to the long-term degradable material with the degradation rate event up to 4 years in the implementation environment. FDM 3D printed porous scaffolds based on PCL during accelerated degradation show a weight loss of 80–90% after about 4 weeks of incubation [21,50]. In turn, polyurethane (TPU) materials dedicated to regenerative purpose in such degradation conditions show a weight loss of 80% (2 M HCl) and 20% (5 M KOH) after just 15 days of incubation [51]. Thus, the results obtained for porous Bioflex® printouts indicate its high resistance to hydrolysis in such aggressive environments and might be considered as biostable.

This feature may exclude Bioflex® filament for application as degradable tissue-engineered constructs, which should gradually degrade after implantation at the tissue defect site [21,52]. Nonetheless, this does not eliminate the use of this filament for 3D printing of medical equipment, devices and biostable long-term implants representing high resistance to aggressive environments and superb elasticity.

Table 5
CCL-163 cells morphology and viability after 24 h of contact with extracts obtained by using printed Bioflex®. The results of cell viability were presented towards control (100%). No statistical differences between the obtained results were noticed, SD were negligibly small.

Extract concentration	100%	50%	25%	12.5%	control
Cell morphology	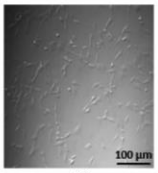	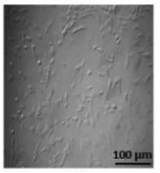	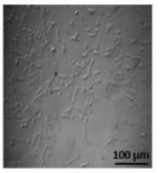	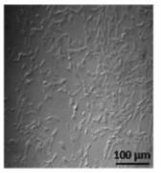	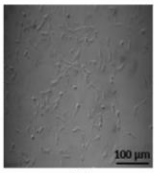
Cell viability (%)	103	108	106	111	100

3.7.3. Incubation in simulation body fluid (SBF)

The *in vitro* bioactivity of the printed porous structures was tested in simulated body fluid (SBF) solution over 3 months period. SEM images revealed the crystals deposition on the surface of printouts (Fig. 8 a,b). These were observed after 1 month of incubation (Table S6). The crystals presented plate-like morphology, typical for hydroxyapatite (HAp) minerals [53,54], and they were forming agglomerates growing one on another on the printout's surface. The elements of formed crystals were further characterized by EDS measurements (Fig. 8 c). EDS analysis revealed the presence of P, Ca, C and O elements which correspond to the chemical formula of HAp ($Ca_{10}(PO_4)_6(OH)_2$). Noticeable signals of carbon and oxygen might also be related to the presence of carbonate in the HAp structure. Trace amounts of magnesium and sodium chloride from the SBF solution have also been noted. The Ca/P atomic ratio was 1.55. It is a lower value than the corresponding to the stoichiometric HAp (Ca/P = 1.67), thus formed HAp assumed to be calcium-deficient. It is probably due to the presence of other ions (Mg, Na, CO_3^{-}) which disturbed the HAp structure. Nevertheless, this dependence is common when biological hydroxyapatite is formed [55].

To support those considerations Raman spectroscopy of deposited crystals was conducted. The spectra show three distinct peaks. The signals at 425 and 588 cm^{-1} correspond to P—O and O—P—O vibrations, respectively. In turn, a sharp peak at 960 cm^{-1} is assigned to stretching vibration of the phosphate group. The presence of a slight signal at the range of 1071 cm^{-1} is attributed to the carbonate groups [56,57]. This explains the registered carbon and oxygen elements in the EDS spectrum. Obtained results indicate the formulation of carbonated-type hydroxyapatites (C-HAp) on the surface of printed structures. According to Kim et al. [54], the existence of carbonate ions in the HAp structure provides enhanced biocompatibility and resorption features compared to synthetic HAp. It has also been shown that such C-HAp is more like natural apatite minerals found in living hard tissues [58].

4. Conclusions

In the presented work, extensive characteristics of the commercial FDM/FFF 3D printing medical-grade filament under the trade name Bioflex® by Filoalfa (Italy) were conducted. Due to the many benefits of using FDM/FFF type 3DP in medicine, there is a need to look for new materials that meet strict medical criteria. The filament market is growing rapidly, however, both in the market and in the literature, attention is mainly devoted to thermoplastic materials such as PLA or PCL and their modifications. Therefore, attention should be paid to materials from the group of thermoplastic elastomers (TPC) that can fill the gap of high-flexibility medical filaments.

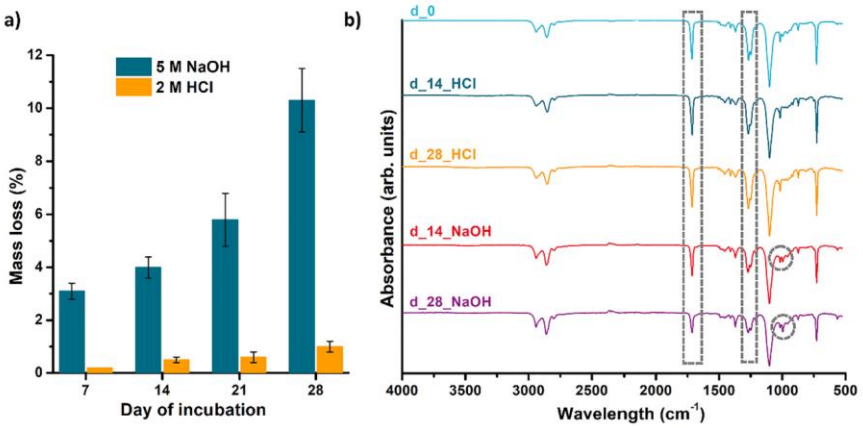

Fig. 7. Results of accelerated degradation study performed in 5 M NaOH and 2 M HCl solutions of porous matrix printed using Bioflex® filament, (a) percentage mass loss during degradation, (b) FTIR spectrum collected at a different time of degradation.

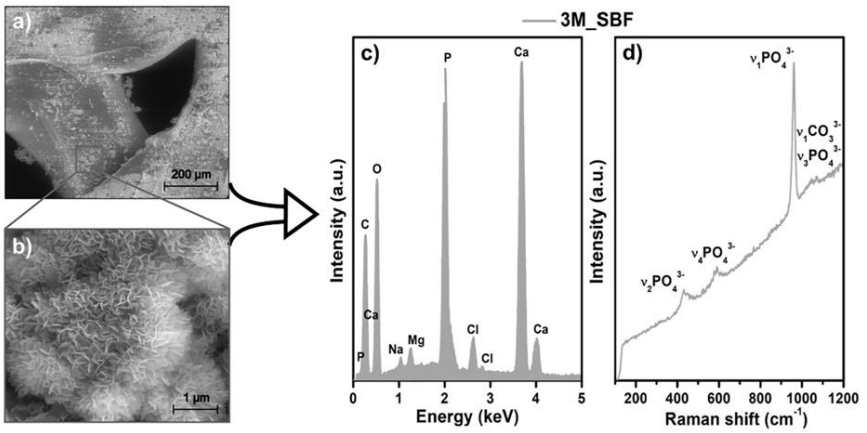

Fig. 8. Selected SEM images of Bioflex® printouts after 3 months of incubation in SBF (a,b), and corresponding EDS (c) and Raman (d) spectra of formed crystals. Ca/P ratio is equal to 1.57. SEM images after 1 week and 1 month of incubation can be found in Table S6 (supplementary data).

The partial conclusions of the study are as follows:

1. Performed spectroscopic, thermal, thermomechanical and rheological analysis showed that 3D printing does not cause changes in the filament structure. No signs of degradation or changes in thermal properties of resulted printouts were noted. Thus, the Bioflex® filament is highly stable under 3D printing conditions.
2. Based on the performed studies and literature overview it was found out that Bioflex® belongs to the thermoplastic copolyester-ether elastomer (TPC) polymer group with the polythtramethylne oxide (PTMO) as a soft segment (SS). The results of thermal studies, hardness and tensile stress-strain curves also suggest that it is a material with an advantage of SS phase in the structure.
3. It has been observed that the infill orientation and build orientation affects the mechanical properties of printouts.
4. Contact angle study revealed hydrophilic properties of Bioflex® printouts surface.
5. *In vitro* cytotoxicity studies confirmed that the Bioflex® printouts meet the criteria of biocompatibility, according to the ISO 10993:5 standard.
6. Accelerated degradation studies showed outstanding resistance to hydrolysis of Bioflex® printouts which exclude its application as degradable medical constructs.
7. Incubation of Bioflex® printouts in SBF solution revealed deposition of carbonate hydroxyapatite (C-HAp) at their surface. Therefore, its application can be considered in the field of bone or cartilage engineering.

In this article, we wanted to pay attention of filament manufacturers to provide extended material characterization in their technical datasheet. In the case of this study, Bioflex® occurred to be suitable for FDM/FFF 3D printing of medical equipment, devices and internal long-term implants. This is due to its sufficient biocompatibility and outstanding resistance to hydrolysis and aggressive environments. With all of the data provided in this article further development of FDM/FFF 3DP with the use of Bioflex® will be continued. In summary, this work provides relevant information in both material and application as well as creates a strong basis for further more advanced biological and medical researches.

CRediT authorship contribution statement

Agnieszka Haryńska: Conceptualization, Methodology, Software, Validation, Investigation, Writing - original draft, Writing - review & editing, Visualization, Project administration. **Iga Carayon:** Formal analysis, Investigation, Resources, Writing - review & editing. **Paulina Kosmela:** Investigation. **Kamil Szeliski:** Investigation. **Marcin Łapiński:** Investigation. **Marta Pokrywczyńska:** Investigation. **Justyna Kucińska-Lipka:** Resources, Writing - review & editing. **Helena Janik:** Resources, Writing - review & editing.

Declaration of Competing Interest

The authors declare that they have no known competing financial interests or personal relationships that could have appeared to influence the work reported in this paper.

Acknowledgements

We acknowledge MSc Dawid Zakrzewski for conducting tensile strength test.

Data availability

The raw/processed data required to reproduce these findings cannot be shared at this time due to technical or time limitations. However, they may be made available on request.

Appendix A. Supplementary data

Supplementary data to this article can be found online at https://doi.org/10.1016/j.eurpolymj.2020.109958.

References

[1] A.J.T. Teo, A. Mishra, I. Park, Y.J. Kim, W.T. Park, Y.J. Yoon, Polymeric Biomaterials for Medical Implants and Devices, ACS Biomater. Sci. Eng. 2 (2016) 454–472, https://doi.org/10.1021/acsbiomaterials.5b00429.
[2] A. Aimar, A. Palermo, B. Innocenti, The Role of 3D Printing in Medical Applications: A State of the Art, J. Healthc. Eng. (2019), https://doi.org/10.1155/2019/

5340616.
[3] C. Lee Ventola, Medical applications for 3D printing: Current and projected uses, Pharm. Ther. 39 (2014) 704–711.
[4] V. Afsana, N. Jain, K. Haider, Jain, 3D Printing in Personalized Drug Delivery, Curr. Pharm. Des. 24 (2019) 5062–5071, https://doi.org/10.2174/1381612825666190215122208.
[5] J. Garcia, Z. Yang, R. Mongrain, R.L. Leask, K. Lachapelle, 3D printing materials and their use in medical education: a review of current technology and trends for the future, bmjstel-2017-000234, BMJ Simul. Technol. Enhanc. Learn. (2017), https://doi.org/10.1136/bmjstel-2017-000234.
[6] F. Govsa, T. Yagdi, M.A. Ozer, C. Eraslan, A.K. Alagoz, Building 3D anatomical model of coiling of the internal carotid artery derived from CT angiographic data, Eur. Arch. Oto-Rhino-Laryngology. 274 (2017) 1097–1102, https://doi.org/10.1007/s00405-016-4355-0.
[7] M. Chung, N. Radacsi, C. Robert, E.D. McCarthy, A. Callanan, N. Conlisk, P.R. Hoskins, V. Koutsos, On the optimization of low-cost FDM 3D printers for accurate replication of patient-specific abdominal aortic aneurysm geometry, 3D Print, Med. 4 (2018) 2, https://doi.org/10.1186/s41205-017-0023-2.
[8] M.C. Luque, A. Calleja-Hortelano, P.E. Romero, Use of 3D printing in model manufacturing for minor surgery training of general practitioners in primary care, Appl. Sci. 9 (2019), https://doi.org/10.3390/app9235212.
[9] G. Verstraete, A. Samaro, W. Grymonpré, V. Vanhoorne, B. Van Snick, M.N. Boone, T. Hellemans, L. Van Hoorebeke, J.P. Remon, C. Vervaet, 3D printing of high drug loaded dosage forms using thermoplastic polyurethanes, Int. J. Pharm. 536 (2018) 318–325, https://doi.org/10.1016/j.ijpharm.2017.12.002.
[10] T.C. Okwuosa, C. Soares, V. Gollwitzer, R. Habashy, P. Timmins, M.A. Alhnan, On demand manufacturing of patient-specific liquid capsules via co-ordinated 3D printing and liquid dispensing, Eur. J. Pharm. Sci. 118 (2018) 134–143, https://doi.org/10.1016/j.ejps.2018.03.010.
[11] A. Goyanes, A.B.M. Buanz, A.W. Basit, S. Gaisford, Fused-filament 3D printing (3DP) for fabrication of tablets, Int. J. Pharm. 476 (2014) 88–92, https://doi.org/10.1016/j.ijpharm.2014.09.044.
[12] J.A. Weisman, D.H. Ballard, U. Jammalamadaka, K. Tappa, J. Sumerel, H.B. D'Agostino, D.K. Mills, P.K. Woodard, 3D Printed Antibiotic and Chemotherapeutic Eluting Catheters for Potential Use in Interventional Radiology. In Vitro Proof of Concept Study, Acad. Radiol. 26 (2019) 270–274, https://doi.org/10.1016/j.acra.2018.03.022.
[13] E. Mathew, J. Domínguez-Robles, S.A. Stewart, E. Mancuso, K. O'Donnell, E. Larrañeta, D.A. Lamprou, Fused Deposition Modeling as an Effective Tool for Anti-Infective Dialysis Catheter Fabrication, ACS Biomater. Sci. Eng. 5 (2019) 6300–6310, https://doi.org/10.1021/acsbiomaterials.9b01185.
[14] A.L. Tyson, S.T. Hilton, L.C. Andreae, Rapid, simple and inexpensive production of custom 3D printed equipment for large-volume fluorescence microscopy, Int. J. Pharm. 494 (2015) 651–656, https://doi.org/10.1016/j.ijpharm.2015.03.042.
[15] G.I.J. Salentijn, P.E. Oomen, M. Grajewski, E. Verpoorte, Fused Deposition Modeling 3D Printing for (Bio)analytical Device Fabrication: Procedures, Materials, and Applications, Anal. Chem. 89 (2017) 7053–7061, https://doi.org/10.1021/acs.analchem.7b00828.
[16] I. Buj-Corral, A. Bagheri, O. Petit-Rojo, 3D Printing of Porous Scaffolds with Controlled Porosity and Pore Size Values, Materials (Basel). 11 (2018) 1532, https://doi.org/10.3390/ma11091532.
[17] C. Esposito Corcione, F. Gervaso, F. Scalera, S.K. Padmanabhan, M. Madaghiele, F. Montagna, A. Sannino, A. Licciulli, A. Maffezzoli, Highly loaded hydroxyapatite microsphere/ PLA porous scaffolds obtained by fused deposition modelling, Ceram. Int. 45 (2019) 2803–2810, https://doi.org/10.1016/j.ceramint.2018.07.297.
[18] S. Chen, L. Zhu, W. Wen, L. Lu, C. Zhou, B. Luo, Fabrication and Evaluation of 3D Printed Poly(l -lactide) Scaffold Functionalized with Quercetin-Polydopamine for Bone Tissue Engineering, ACS Biomater. Sci. Eng. 5 (2019) 2506–2518, https://doi.org/10.1021/acsbiomaterials.9b00254.
[19] C. Capone, L. Di Landro, F. Inzoli, M. Penco, L. Sartore, Thermal and Mechanical Degradation During Polymer Extrusion Processing, Polym. Eng. Sci. 47 (2007) 1813–1819, https://doi.org/10.1002/pen.20882.
[20] G.D. Goh, Y.L. Yap, H.K.J. Tan, S.L. Sing, G.L. Goh, W.Y. Yeong, Process–Structure–Properties in Polymer Additive Manufacturing via Material Extrusion: A Review, Crit. Rev. Solid State Mater. Sci. 45 (2020) 113–133, https://doi.org/10.1080/10408436.2018.1549977.
[21] M. Mohseni, D.W. Hutmacher, N.J. Castro, Independent evaluation of medical-grade bioresorbable filaments for fused deposition modelling/fused filament fabrication of tissue engineered constructs, Polymers (Basel). 10 (2018), https://doi.org/10.3390/polym10010040.
[22] C.G. Liu, Y.T. Zeng, R.K. Kankala, S.S. Zhang, A.Z. Chen, S. Bin Wang, Characterization and preliminary biological evaluation of 3D-printed porous scaffolds for engineering bone tissues, Materials (Basel) 11 (2018), https://doi.org/10.3390/ma11101832.
[23] D.W. Hutmacher, T. Schantz, I. Zein, K.W. Ng, S.H. Teoh, K.C. Tan, Mechanical properties and cell cultural response of polycaprolactone scaffolds designed and fabricated via fused deposition modeling, J. Biomed. Mater. Res. 55 (2001) 203–216, https://doi.org/10.1002/1097-4636(200105)55:2<203::AID-JBM1007>3.0.CO;2-7.
[24] T. Kokubo, H. Takadama, How useful is SBF in predicting in vivo bone bioactivity? Biomaterials. 27 (2006) 2907–2915, https://doi.org/10.1016/j.biomaterials.2006.01.017.
[25] T. Kokubo, H. Takadama, Simulated Body Fluid (SBF) as a Standard Tool to Test the Bioactivity of Implants, in: Handb. Biominer., Wiley-VCH Verlag GmbH, Weinheim, Germany, 2008: pp. 97–109. https://doi.org/10.1002/9783527619443.ch51.
[26] S.M. Cetina-Díaz, L.H. Chan-Chan, R.F. Vargas-Coronado, J.M. Cervantes-Uc, P. Quintana-Owen, K. Paakinaho, M. Kellomaki, L. Di Silvio, S. Deb, J.V. Cauich-Rodríguez, Physicochemical characterization of segmented polyurethanes prepared with glutamine or ascorbic acid as chain extenders and their hydroxyapatite composites, J. Mater. Chem. B. 2 (2014) 1966–1976, https://doi.org/10.1039/c3tb21500h.
[27] J. Djonlagic, M.S. Nikolic, Thermoplastic Copolyester Elastomers, in: Handb. Eng. Spec. Thermoplast. Polyethers Polyesters, John Wiley and Sons, Hoboken, NJ, USA, 2011: pp. 377–427. https://doi.org/10.1002/9781118104729.ch10.
[28] G. Socrates, Infrared and Raman Characteristic Group Frequencies: Tables and Charts, third, John Wiley & Sons Ltd (2004), https://doi.org/10.1002/jrs.1238.
[29] Y. Davies, J. Davies, M.J. Forrest, Infrared Spectra of Rubbers, Plastics and Thermoplastic Elastomers, De Gruyter, Berlin, Boston (2019), https://doi.org/10.1515/9783110645750.
[30] V. Nagarajan, A.K. Mohanty, M. Misra, Blends of polylactic acid with thermoplastic copolyester elastomer: Effect of functionalized terpolymer type on reactive toughening, Polym. Eng. Sci. 58 (2018) 280–290, https://doi.org/10.1002/pen.24566.
[31] J. Chen, Q. Lv, D. Wu, X. Yao, J. Wang, Z. Li, Nucleation of a Thermoplastic Polyester Elastomer Controlled by Silica Nanoparticles, Ind. Eng. Chem. Res. 55 (2016) 5279–5286, https://doi.org/10.1021/acs.iecr.5b04464.
[32] E. Rebollar, S. Pérez, M. Hernández, C. Domingo, M. Martín, T.A. Ezquerra, J.P. García-Ruiz, M. Castillejo, Physicochemical modifications accompanying UV laser induced surface structures on poly(ethylene terephthalate) and their effect on adhesion of mesenchymal cells, Phys. Chem. Chem. Phys. 16 (2014) 17551–17559, https://doi.org/10.1039/c4cp02434f.
[33] S. Betelu, I. Tijunelyte, L. Boubekeur-Lecaque, I. Ignatiadis, A. Schnepf, E. Guenin, N. Bouchemal, N. Felidj, E. Rinnert, M. Lamy de la Chapelle, Raman Characterization of Phenyl-Derivatives: From Primary Amine to Diazonium Salts, J. Org. Inorg. Chem. 3 (2017) 1–10, https://doi.org/10.21767/2472-1123.100021.
[34] J. James, G.V. Thomas, K. Pramoda, N. Kalarikkal, S. Thomas, Thermoplastic-elastomer composition based on an interpenetrating polymeric network of styrene butadiene rubber-poly(methyl methacrylate) as an efficient vibrational damper, New J. Chem. 42 (2018) 1939–1951, https://doi.org/10.1039/c7nj03998k.
[35] F. Adar, Introduction to Interpretation of Raman Spectra Using Database Searching and Functional Group Detection and Identification, Spectroscopy. 31 (2016) 16–23.
[36] W. Gabriëlse, M. Soliman, K. Dijkstra, Microstructure and phase behavior of block copoly(ether ester) thermoplastic elastomers, Macromolecules. 34 (2001) 1685–1693, https://doi.org/10.1021/ma0012696.
[37] J. Krijgsman, D. Husken, R.J. Gaymans, Synthesis and properties of thermoplastic elastomers based on PTMO and tetra-amide, Polymer (Guildf). 44 (2003) 7573–7588, https://doi.org/10.1016/j.polymer.2003.09.043.
[38] A. Szymczyk, E. Senderek, J. Nastalczyk, Z. Roslaniec, New multiblock poly(ether-ester)s based on poly(trimethylene terephthalate) as rigid segments, Eur. Polym. J. 44 (2008) 436–443, https://doi.org/10.1016/j.eurpolymj.2007.11.005.
[39] S. Paszkiewicz, A. Szymczyk, Z. Špitalský, J. Mosnáček, K. Kwiatkowski, Z. Rosłaniec, Structure and properties of nanocomposites based on PTT-block-PTMO copolymer and graphene oxide prepared by in situ polymerization, Eur. Polym. J. 50 (2014) 69–77, https://doi.org/10.1016/j.eurpolymj.2013.10.031.
[40] R.J. Zhou, T. Burkhart, Thermal and mechanical properties of poly(ether ester)-based thermoplastic elastomer composites filled with TiO2 nanoparticles, J. Mater. Sci. 46 (2011) 2281–2287, https://doi.org/10.1007/s10853-010-5068-1.
[41] J. Yin, C. Lu, J. Fu, Y. Huang, Y. Zheng, Interfacial bonding during multi-material fused deposition modeling (FDM) process due to inter-molecular diffusion, Mater. Des. 150 (2018) 104–112, https://doi.org/10.1016/j.matdes.2018.04.029.
[42] M.H. Khaliq, R. Gomes, C. Fernandes, J. Nóbrega, O.S. Carneiro, L.L. Ferrás, On the use of high viscosity polymers in the fused filament fabrication process, Rapid Prototyp. J. 23 (2017) 727–735, https://doi.org/10.1108/RPJ-02-2016-0027.
[43] D. Hua, X. Zhang, Z. Ji, C. Yan, B. Yu, Y. Li, X. Wang, F. Zhou, 3D printing of shape changing composites for constructing flexible paper-based photothermal bilayer actuators, J. Mater. Chem. C. 6 (2018) 2123–2131, https://doi.org/10.1039/c7tc05710e.
[44] D. Popescu, A. Zapciu, C. Amza, F. Baciu, R. Marinescu, FDM process parameters influence over the mechanical properties of polymer specimens: A review, Polym. Test. 69 (2018) 157–166, https://doi.org/10.1016/j.polymertesting.2018.05.020.
[45] A.K. Sood, R.K. Ohdar, S.S. Mahapatra, Parametric appraisal of mechanical property of fused deposition modelling processed parts, Mater. Des. 31 (2010) 287–295, https://doi.org/10.1016/j.matdes.2009.06.016.
[46] S.H. Ahn, M. Montero, D. Odell, S. Roundy, P.K. Wright, Anisotropic material properties of fused deposition modeling ABS (2002), https://doi.org/10.1108/13552540210441166.
[47] M.M. Gentleman, E. Gentleman, The role of surface free energy in osteoblast-biomaterial interactions, Int. Mater. Rev. 59 (2014) 417–429, https://doi.org/10.1179/1743280414Y.0000000038.
[48] S.H. Kim, H.J. Ha, Y.K. Ko, S.J. Yoon, J.M. Rhee, M.S. Kim, H.B. Lee, G. Khang, Correlation of proliferation, morphology and biological responses of fibroblasts on LDPE with different surface wettability, J. Biomater. Sci. Polym. Ed. 18 (2007) 609–622, https://doi.org/10.1163/156856207780852514.
[49] ISO/EN10993-5, Biological Evaluation of Medical Devices—Part 5: Tests for in Vitro Cytotoxicity, 3rd ed., Int. Organ. Stand. Geneva, Switz. (2009).
[50] C.X.F. Lam, M.M. Savalani, S.H. Teoh, D.W. Hutmacher, Dynamics of in vitro polymer degradation of polycaprolactone-based scaffolds: Accelerated versus simulated physiological conditions, Biomed. Mater. 3 (2008), https://doi.org/10.1088/1748-6041/3/3/034108.
[51] I. Gubanska, J. Kucinska-Lipka, H. Janik, The influence of amorphous macrodiol, diisocyanate type and L-ascorbic acid modifier on chemical structure, morphology and degradation behavior of polyurethanes for tissue scaffolds fabrication, Polym. Degrad. Stab. 163 (2019) 52–67, https://doi.org/10.1016/j.polymdegradstab.

2019.02.025.
[52] J. Kucińska-Lipka, I. Gubanska, A. Skwarska, Microporous polyurethane thin layer as a promising scaffold for tissue engineering, Polymers (Basel). 9 (2017), https://doi.org/10.3390/polym9070277.
[53] Z. Gou, J. Chang, J. Gao, Z. Wang, In vitro bioactivity and dissolution of Ca2(SiO3)(OH)2 and β-Ca2SiO4 fibers, J. Eur. Ceram. Soc. 24 (2004) 3491–3497, https://doi.org/10.1016/j.jeurceramsoc.2003.11.023.
[54] S. Kim, C.B. Park, Mussel-inspired transformation of CaCO3 to bone minerals, Biomaterials. 31 (2010) 6628–6634, https://doi.org/10.1016/j.biomaterials.2010.05.004.
[55] B. Wopenka, J.D. Pasteris, A mineralogical perspective on the apatite in bone, in: Mater. Sci. Eng. C, Elsevier, 2005: pp. 131–143. https://doi.org/10.1016/j.msec.2005.01.008.
[56] A. Awonusi, M.D. Morris, M.M.J. Tecklenburg, Carbonate assignment and calibration in the Raman spectrum of apatite, Calcif. Tissue Int. 81 (2007) 46–52, https://doi.org/10.1007/s00223-007-9034-0.
[57] D. Bellucci, G. Bolelli, V. Cannillo, A. Cattini, A. Sola, In situ Raman spectroscopy investigation of bioactive glass reactivity: Simulated body fluid solution vs TRIS-buffered solution, Mater. Charact. 62 (2011) 1021–1028, https://doi.org/10.1016/j.matchar.2011.07.008.
[58] E. Landi, G. Celotti, G. Logroscino, A. Tampieri, Carbonated hydroxyapatite as bone substitute, J. Eur. Ceram. Soc. 23 (2003) 2931–2937, https://doi.org/10.1016/S0955-2219(03)00304-2.

A comprehensive examination of flexible FDM/FFF 3D printing filament as a potential material in medical application

Agnieszka Haryńska[1,*], Iga Carayon[1], Paulina Kosmela[1], Kamil Szeliski[3], Marcin Łapiński[2], Marta Pokrywczyńska[3], Justyna Kucińska-Lipka[1], Helena Janik[1]

[1] Department of Polymers Technology, Faculty of Chemistry, Gdansk University of Technology (GUT), Narutowicza Street 11/12, 80-233 Gdansk, Poland

[2] Department of Solid State Physics, Faculty of Applied Physics and Mathematics, Gdansk University of Technology (GUT), Narutowicza Street 11/12, 80-233 Gdansk, Poland

[3] Department of Regenerative Medicine, Cell and Tissue Bank, Nicolaus Copernicus University, Collegium Medicum, M.Sklodowskiej-Curie 9, 85-094 Bydgoszcz, Poland

Supplementary data: Appendix 1

1. Sample preparation – design and 3D printing settings.

   - Dumbbell-shaped specimens for the tensile test (Table S1)

Samples for the tensile test were made according to the ISO 37:2017 standard by using Autodesk Inventor software. Two different infill raster orientation were adapted (0/90° and 45/135°).

Table S1 Dimensions and design of prepared dumbbell-shaped samples.

Specimen dimensions	Raster angle	Printout
➢ A =115 ➢ B=25 ➢ C=33 ➢ D=6 ➢ E=14 ➢ F=25 ➢ G=2 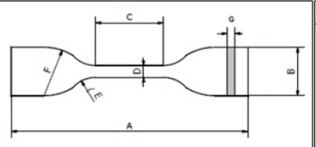	±45 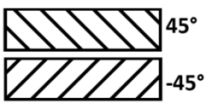	
View of STL file 	0/90 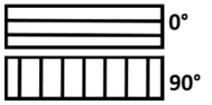	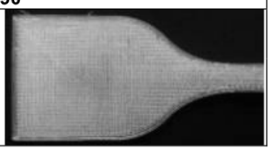

   - Porous matrix for degradation/incubation and cytotoxicity studies (Table S2)

Samples for degradation tests were cut out from the printed porous matrix (mesh with 85% of triangular infill) by using brass cork borer (⌀ 8mm).

Table S2 Porous specimens for degradation and cytotoxicity studies.

View of STL file	Printout	Dimensions [mm]	Porosity [%]
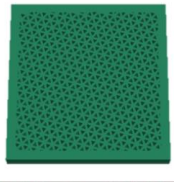		80x80x3	53.81 ± 1.47
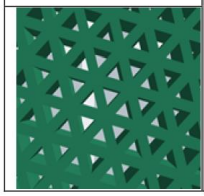	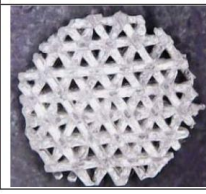	⌀ 8 h=3	

- Cubic structures for compressive strength test (Table S3)

Two types of cubic specimens (15x15x15mm) were prepared in Autodesk Inventor software (based on own concept). Detailed 3D printing parameters are presented below (Table S4).

Table S3 Cubic samples for the compressive strength test.

	Model	Lay pattern	Printout	Porosity
Porous	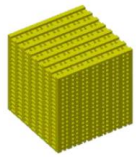	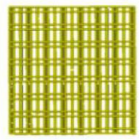	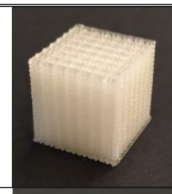	63.21 ± 0.72
Solid	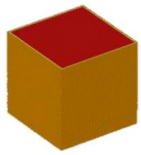		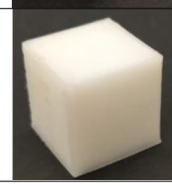	-

Table S4 3D printing settings.

	Dumbbell shaped specimens for tensile test	DMA specimen	Porous matrix for degradation	Cubes structures for compressive strength test	
				Solid	Porous
Filament	Bioflex (Filoalfa, Italy)				
Extrusion temperature [°C]	220				

Bed temperature [°C]	50				
Printing speed [mm/s]	40				20
Printing time	42 min	12 min	2h 20min	19min	2h 13min
Layer height [mm]	0.18			0.10	
Shell number	2		5	2	
Infill [%] (raster angle)	100 (line ±45°, 0/90°)	100 (line ±45°)	85 (triangular)	100 (line ±45°)	
Extrusion ratio [-]	1.05				0.95
Cooling	Fan on (start form second layer)				
Nozzle diameter [mm]	0.4				
Slicer	FlashPrint 4.2.0				

2. Short-term degradation studies

Table S5 Optical images of Bioflex matrix during short-term degradation studies.

Day of incubation	0	7	14	21	28
5 M NaOH	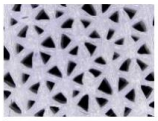	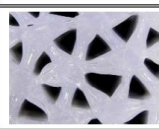 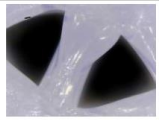	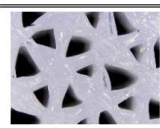 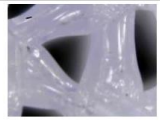	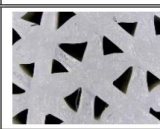 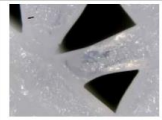	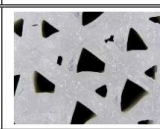 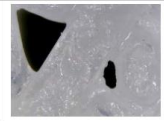
Mass loss (%)		3.1 ±0.3	4.6 ±0.4	5.8 ±1.0	10.3 ±1.2
2 M HCl	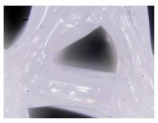	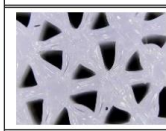 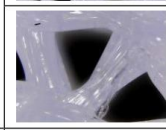	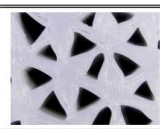 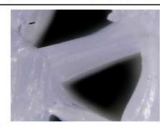	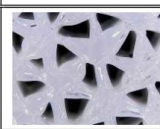 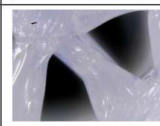	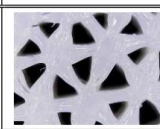 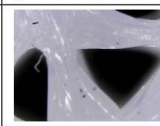
Mass loss (%)	-	0.2 ± 0.0	0.5 ±0.1	0.6 ±0.2	1.0 ±0.2

3. Incubation in simulated body fluid (SBF)

Table S6 SEM micrographs of Bioflex matrix during incubation in SBF.

Time of incubation	7 days	1 month	3 months
150x	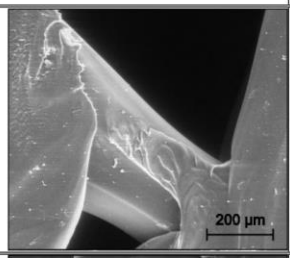	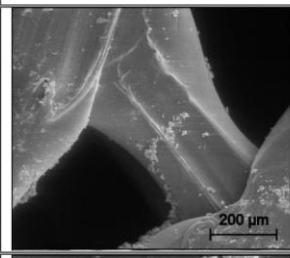	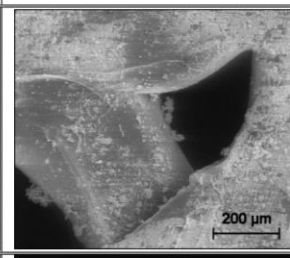
1 000x	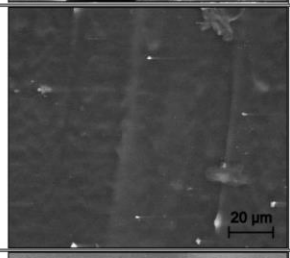	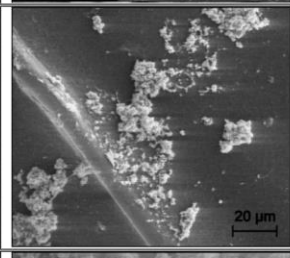	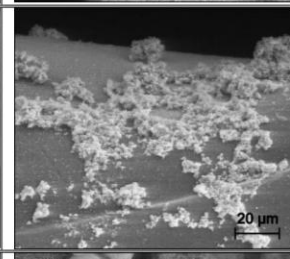
10 000x	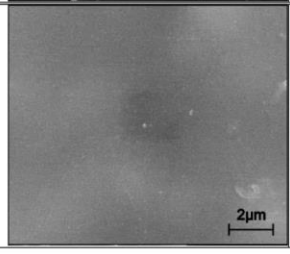	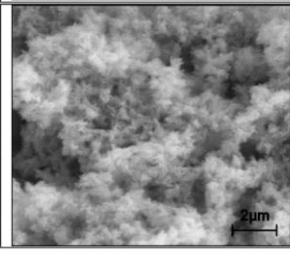	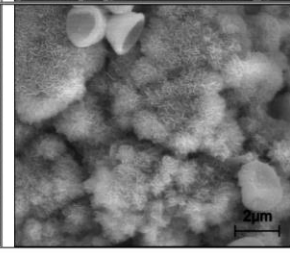

4.5 PAPER 5: Preparation And Characterization Of Biodegradable And Compostable PLA/TPS/ESO Compositions

Authors (percentage share): Agnieszka Haryńska (30%), Maciej Sienkiewicz (40%), Justyna Kucińska-Lipka (10%), Helena Janik (20%)

Journal: Industrial Crops and Products

DOI: 10.1016/j.indcrop.2018.06.016.

Index: Q1, IF_{2018}=4.244, MNSiW = 200 pts

CRediT: Data Curation (lead), Formal Analysis (in part), Investigation (lead: MFR, tensile tests, impact strength, hardness, water resistance), Methodology (lead), Project Administration (in part), Visualization (lead), Writing – Original Draft Preparation (lead), Writing – Review & Editing (lead).

Realized doctoral research tasks:

I (material design and characterization) – development of a fully plant origin compositions based on polylactide (PLA) and potato thermoplastic starch (TPS) modified with epoxidized soybean oil (ESO) and testing depending on the ratio of the components used (amount of ESO and TPS to PLA); study of mechanical, thermal, and rheological properties, as well as compostability test under laboratory conditions.

Material code: PLA/TPS

BRIEF DESCRIPTION OF THE PUBLICATION

Scope of the publication: preparation of a biodegradable and compostable polymer composition; material characterization; laboratory simulated composting.

Novelty of the publication: utilization of epoxidized soybean oil (ESO) as a green compatibilizer of the polylactide (PLA)/thermoplastic potato starch (TPS) blends; preparation of bio-blends exclusively from renewable sources.

Main scientific achievement: improved ductility, and impact strength of the developed PLA/TPS/ESO blend comparing to the pure PLA.

Outline: The article describes the preparation route and characterization of the composition based on polylactide (PLA) and thermoplastic potato starch (TPS) modified with epoxidized soybean oil (ESO). The bio-blend was optimized by altering the amount of TPS and ESO against PLA. Then, the mechanical, thermal, rheological, and morphological properties of the compositions were studied. In addition, water resistance and compostability were determined. The results indicated that ESO acts as a green plasticizer and compatibilizer of the PLA/TPS blends improving the interfacial adhesion between PLA and TPS molecules. An increase in impact strength and elongation at break compared to pure PLA was noted. The developed compositions completely disintegrate within 57 days in laboratory composting. Melt flow rate (MFR) values of the studied blends correspond to the extrudable thermoplastics. Basing on the obtained results, it has been noticed that the developed composition can be utilized in various branches of technologies including 3D printing. Therefore, the elaborated PLA/TPS/ESO composition was further investigated as a candidate for a novel sustainable bio-filament for extrusion-based 3D printing.

Industrial Crops & Products 122 (2018) 375–383

Contents lists available at ScienceDirect

Industrial Crops & Products

journal homepage: www.elsevier.com/locate/indcrop

Preparation and characterization of biodegradable and compostable PLA/TPS/ESO compositions

A. Przybytek, M. Sienkiewicz, J. Kucińska-Lipka*, H. Janik

Gdansk University of Technology, Chemical Faculty, Polymer Technology Department, Narutowicza Street 11/12, Gdansk 80-232, Poland

ARTICLE INFO

Keywords:
Potato thermoplastic starch
Biodegradable/composting polymers
Polylactide
Epoxydized soybean oil
Renewable raw resources

ABSTRACT

In this study, biodegradable and compostable compositions, derived from totally natural feedstock/raw materials, namely polylactide (PLA), potato thermoplastic starch (TPS) and plant glycerin have been made by melt extrusion with epoxydized soybean oil (ESO) as reactive modifier in order to improve PLAs ductility and reduce the products cost without compromising biodegradation. The obtained PLA/mTPS(0,5ESO)[75/25] and PLA/mTPS(2ESO)[75/25] compositions provides satisfactory.mechanical properties comparable to native PLA. Addition of 25% TPS and 0,5-2% ESO to PLA, improved impact strength from 13,70 kJ/m2 to 16,69 kJ/m2 70 kJ/m2 to 16,69 kJ/m2 compared to neat PLA and increase elongation at break from 2,6% to 8,8%. The addition of ESO into PLA/TPS composition enhanced water resistance and improved impact strength to over 16 kJ/m2 for PLA/TPS(2%ESO)[75/25] composition. The thermal, rheological and morphology of fractured surface were also studied. Finally, biodegradability and compostability of prepared samples was specified by stimulated composting process (according to PN-EN 14806:2010 standard). Possibility of replacing up to 25% of PLA by TPS and ESO, allows to reduces the costs of the product as well as maintain quite similar properties and ability to composting relative to native PLA.

1. Introduction

In Europe, packaging applications are the largest application sector for the plastics industry and represent 39,6% of the total plastics demand (PlasticsEurope, 2016). Conventional plastic packages are post-consumer wastes which are difficult for disposal and constitute a burden to the environment, due to their large volume and inability to biodegrade or to compost (Gregory, 2009; Imre and Pukánszky, 2013; Kale et al., 2007; Siracusa et al., 2008). Mainly, municipal solid wastes (MSW) consist of a containers and packaging wastes (Kale et al., 2007). The continuous increase in the amount of packaging wastes contributed to significant growing interest in raw materials derived from renewable sources. The current environmental protection requirements necessitate withdrawal commonly used petroleum based polymers. This has led to an enormous development of innovative bio-polymers and biotechnologies (Luckachan and Pillai, 2011).

Currently, the most common biodegradable polymers are polylactide (PLA), poly(hydroxybutyrate) (PHB), poly(glycolic acid) (PGA) and natural-based polymers like starch and cellulose (Kale et al., 2007; Mohanty et al., 2000; Shen et al., 2009). Each of these polymers has many different advantages and disadvantages. One of the ways of extracting the positive features of these materials is their mutual blending. The benefit of this approach is the possibility of using already known manufacturing methods and conventional machinery. PLA or PHB are very universal but also expensive polymers, therefore their modification via blending with a naturally occurring polymers may cause reduction of material costs, without compromising biodegradation (Martin and Avérous, 2001; Parulekar and Mohanty, 2007; Zhang and Sun, 2004). On the other hand, in most cases biopolymer pairs are thermodynamically immiscible - this prevents to mix them at the molecular level (Teixeira et al., 2012; Wang et al., 2008). In order to enhance the interfacial adhesion and improve compatibility between the polymers matrix a number of different agents, may be added. There are many reports which indicates that an incorporation of enhancing additives, such as: acrylic acid (AA) (Wu, 2005), maleic anhydrite (MA) (Clasen et al., 2015; Huneault and Li, 2007; Leadprathom et al., 2010; Zhang and Sun, 2004), methylene-diphenyldiisocyanate (MDI) (Carmona et al., 2015; Wang et al., 2001), fillers, e.g. montmorillonite (MMT) (Guarás et al., 2016; Jalalvandi et al., 2015), or phenyl diisocyanate (PDI) (Karagoz and Ozkoc, 2013), might contributed to a significant improvement of miscibility biodegradable blends. Consequently, the production of bio-blends containing solely of fully natural raw materials is a challenging.

Polylactide (PLA) is obtained by the condensation of lactic acid or

* Corresponding author.
E-mail address: juskucin@pg.gda.pl (J. Kucińska-Lipka).

https://doi.org/10.1016/j.indcrop.2018.06.016
Received 12 September 2017; Received in revised form 26 April 2018; Accepted 4 June 2018

ring opening polymerization of cyclic-lactides and has one of the most advantageous properties for the fabrication of high-quality, eco-friendly packaging materials (Lim et al., 2008). PLA possesses good mechanical properties (high Young's modulus and tensile strength), high degree of transparency and is easily processable same as conventional petro-based plastics (Auras et al., 2004). Unfortunately due to the high price and some drawbacks (brittleness, low flexibility), PLA still cannot completely replace a conventional plastics from a widespread use. One of a simple solution to reduce the costs of PLA, seems to be blending with thermoplastic starch (TPS) - a polymer obtained by mechanical and thermal processing of native starch with a plasticizer (Zhang et al., 2014). TPS is a highly biodegradable, inexpensive and abundantly available biopolymer, capable of serve as a PLA filler. The main function of a plasticizer is to decrease the melting point of native starch, thereby allowing use of traditional plastic processing techniques, such as extrusion and injection molding. Furthermore, the plasticizer lowers the glass transition temperature (T_g) and increases flexibility. In turn, the major drawbacks of starch are: unsatisfactory mechanical properties, migration of plasticizers from the matrix – retrogradation and hydrophilic character (Kaseem et al., 2012; Khan et al., 2016; Nafchi et al., 2013). However, the literature shows that in the most cases PLA/TPS blends exhibited very poor interfacial adhesion (Ayana et al., 2014; Müller et al., 2012; Wootthikanokkhan et al., 2012; Yang et al., 2015). On the other hand improving properties of PLA/TPS blends could be achieved by incorporation of reactive modifier.

Epoxidized soybean oil (ESO) belongs to a wide group of vegetable oils (Khoo and Chow, 2015), natural resources-based substance, commonly used as a polymer plasticizer (Vijayarajan et al., 2014; Xiong et al., 2013). There are some data on the addition of epoxidized vegetable oils as a plasticizer and modifiers to improve the brittleness and low flexibility of PLA (Ali et al., 2009; Xing and Matuana, 2016; Yu-Qiong Xu, 2009), what is mainly manifested by an increase in elongation at break with the simultaneous reduction in tensile strength properties. There are another paper in which the addition ESO to TPS presents different trend. Belhassen et al. (Belhassen et al., 2014), modified in situ thermoplastic starch (pre-plasticized with glycerol) with epoxidized soybean oil (ESO) using reactive blending. It was found the condensation reaction between the oxirane rings of ESO and the hydroxyl groups (starch and glycerol) by FTIR spectra. It led to an increase in tensile strength, modulus of elasticity and hydrophobicity of the resulting materials. The enormous potential of ESO is likely due to the molecule construction, i.e. high molecular weight, occurrence of reactive oxirane rings and long carbon chains. Moreover, biodegradability and non-toxicity encourages further research on this unconventional polymers modifier.

The aim of our research is to prepare fully biodegradable polymer compositions using materials originating solely from renewable resources. For this purpose, polylactide (PLA) was blended with modified by epoxidized soybean oil (ESO) thermoplastic starch (TPS) using melt extruding. The present study also aimed to receive the less expensive biodegradable blends for the use in packaging industry, that will have similar properties to PLA. The mechanical, thermal and rheological properties of the obtained materials were characterized by the static tensile test, impact strength, hardness, the melt flow rate (MFR) and DSC analysis. Morphology of fractured surface and resistant to water were also studied. Finally, biodegradability and compostability of prepared samples were specified by stimulated composting process.

2. Materials and methods

2.1. Materials

Each formulation was prepared with the use of biodegradable and compostable materials made from renewable resource of plant origin. Native potato starch was purchased from ZetPezet, Poland (humidity max. 16%, pH = 5.5–7.5). PLA (7032D, MFR = 7 g/10 min at 210 °C, 2.16 kg, density 1.25 g/cm^3, humidity 3%) was supplied by NatureWorks LLC (USA), as a transparent injection grade. Plant pharmaceutical grade glycerin (TechlandLab, Poland, density$_{20°C}$ 1.26 g/cm^3, purity 99.5%), was used as a starch plasticizer. Epoxidized soybean oil (ESO) (Brenntag, Germany) with oxirane oxygen about 6–10 gO_2/100 g and iodine number approximately 3 gI_2/100 g, served as a starch reactive modifier.

Table 1
Composition of TPS mixtures used in the study.

Formulation	Starch (%)	Glycerol (%)	ESO (%)
TPS	75	25	–
mTPS(0,5ESO)	74,5	25	0,5
mTPS(1ESO)	74	25	1
mTPS(2ESO)	73	25	2

2.2. Preparation and modification of TPS

At preliminary stage, native potato starch and glycerol (contents 25 wt%), were manually mixed and stored at ambient conditions for 24 h. The resulting blends were placed into co-rotating twin-screw extruder (Laboratory extruder IQLINE EHP 2 × 20 IQ, ZAMAK, Poland). The temperature was in the range of 120–170 °C in nine heating zones. The screw speed was between 60 and 80 rpm. The extruded material was granulated after air-cooling. Modified thermoplastic starch (mTPS) was obtained by adding ESO (0.5, 1 or 2 wt%) and the same processing as previously described. The final composition of prepared compound was shown in Table 1.

2.3. PLA/TPS compositions fabrication

The PLA/TPS blends were prepared by using twin-screw extrusion process. PLA was mixed with a varying amounts of unmodified or modified thermoplastic starch (12.5 or 25 wt% TPS) granulates. Then, prepared PLA/TPS blends were extruded. The processing conditions were similar to those described previously, i.e. 130–180 °C and 40–60 rpm (Fig. 1). PLA/TPS blends, in form of strands, were cooled in air, granulated and stored in sealed aluminum tins at room temperature.

Obtained PLA/TPS blends were injection molded (hydraulic injection molding machine HM 45/130, BATTENFELD, Poland), into normalized molds. Prepared PLA/TPS blends were used for further static tensile test study. All samples were pre-conditioned at room temperature for at least 48 h prior to testing. Symbols of the prepared PLA/TPS blends, with their brief explanation, were given in Table 2.

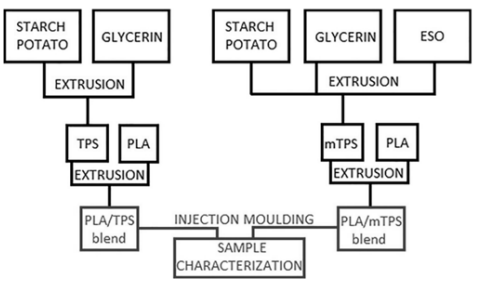

Fig. 1. Representative scheme for processing stages.

Table 2
Composition and description of obtained PLA/TPS samples.

Formulation	PLA (%)	Starch (%)	Glycerol (%)	ESO (%)
PLA/TPS [87.5/12.5]	87.5	9.375	3.125	–
PLA/TPS [75/25]	75	18.75	6.25	–
PLA/mTPS(0.5ESO) [87.5/12.5]	87.5	8.875	3.125	0.5
PLA/mTPS(1ESO) [87.5/12.5]	87.5	8.375	3.125	1
PLA/mTPS(2ESO) [87.5/12.5]	87.5	7.375	3.125	2
PLA/mTPS(0.5ESO) [75/25]	75	18.25	6.25	0.5
PLA/mTPS(1ESO) [75/25]	75	17.75	6.25	1
PLA/mTPS(2 ESO) [75/25]	75	16.75	6.25	2

2.4. Melt flow rate (MFR)

MFR was performed by using plastometer (M-Flow BFN-001, ZWICK, Poland), according to the PN-EN ISO 1133:2005 standard (180 °C, load of 2.16 kg). The value of MFR is expressed as a X g of material extruded through the standard capillary placed in a heating nozzle during 10 min [g/10 min].

2.5. Mechanical characterization

The static tensile test was performed on Zwick/Roell Z020 testing machine according to the PN-EN ISO 527:2004 standard (dumb-bell-shaped test specimen, type A). The crosshead speed was of 5 mm/min and the initial force was equal to 2 N. For each PLA/TPS blend 5 samples were examined and the results were averaged.

The impact strength test was performed on Zwick/Roell HIT5.5 P according to the PN-EN ISO 180:2004 standard. A 5.5 J pendulum was used and U-shaped hammer was taken. Bar-shaped specimens (10 × 80 x 4 mm) without notch were tested. For each PLA/TPS blend 5 samples were examined and the results were averaged.

Hardness was measured by using Shore method according to PN-EN ISO 868:2004. Obtained data were presented with Shore D degree (°Sh D). For each PLA/TPS blend 10 samples were examined and the results were averaged.

2.6. Morphology characterization

The morphology of obtained blends was investigated using scanning electron microscope Phenom TM with a magnification range: 80–100.000 ×, digital zoom: 12 × (ProX/Pro), at 5 kV voltage. The samples were prepared from cryogenically fractured surface of injection molded parts under liquid nitrogen. The surface was sputter coated with gold prior to observation.

2.7. Thermal properties

The thermal properties of prepared blends were characterized by differential scanning calorimetry (DSC) on a TA Instrument (model Q100). Firstly, the samples were conditioned at 30 °C for 2 min. Then, measurements were carried out from -50 to 190 °C, at a heating rate of 10 °C/min, under a nitrogen atmosphere.

2.8. Water resistance

Water resistance was studied as follows; Samples of PLA/TPS blends of 20 × 10 x 4 mm were dried in a laboratory oven at 60 °C until constant weight was achieved (m_0). Samples cooled down to the room temperature. Immediately afterwards, specimens were immersed in the containers filled with 25 ml of tap water. The incubation process was carried out for 1 month and the control time points were after 1 h, 8 h, 24 h, 48 h, respectively. Water resistance was calculated according to the formula 1 and formula 2. Formula 1 express the swelling ratio (i_{tx}) of the samples, which was determined by the mass of adsorbed solvent (m_1) in storage period (t_x). Formula 2 is associated with the samples mass loss *(ml%)* after each time point, where samples were removed out of container, dried to the constant mass and weighted (m_z).

$$i_{t_x} = \frac{(m_1 - m_0)^* 100}{m_0} \quad (1)$$

$$ml = \frac{(m_0 - m_z)^* 100}{m_0} \quad (2)$$

2.9. Stimulated composting

Preliminary evaluation of the disintegration of packaging materials under simulated composting conditions in a laboratory scale test was commissioned to carry by COBRO - Polish Packaging Research Institute, according to PN-EN 14806:2010 standard. As a compost was used organic fertilizer obtained by the biodegradability of the mixture consisting essentially of plant residues. The initial pH of compost was equal to 5.95. Material for the study was provided in the form of sheets with dimensions of 25 × 25 x 2 mm. Three samples were made for each prepared material. Prior to study, samples were dried in a laboratory dryer (60 °C, 24 h) and weighted. The samples were then put into polypropylene (PP) reactors and placed in a bioreactor. The incubation process was carried out for 64 days maintaining constant temperature of 58 °C. The degree of degradation was determined after composting cycle (64 days) by sieving through a sieve of 2 mm. The material that passed through the sieve is treated as totally biodegradable.

3. Results and discussion

3.1. Melt flow rate (MFR)

MFR as an important parameter of the plastics processing was investigated. It facilitates the selection of the factors of the technological process which shortens the time and reduces the cost of production preparation. To be able to determine the influence of ESO to MFR of different compositions, starting materials (PLA, TPS, mTPS) and finished blends (PLA/TPS, PLA/mTPS) were examined. It was observed that in all cases the values of MFR were higher than those of pure PLA (2.34 g/10 min). The results in Fig. 2 show influence of incorporation ESO to TPS. For the content of 0.5% ESO in TPS, no significant change in MFR value was noted. Increasing the ESO content to 1% caused a rapid increase in the MFR value to 30,23 g/10 min. This indicates the

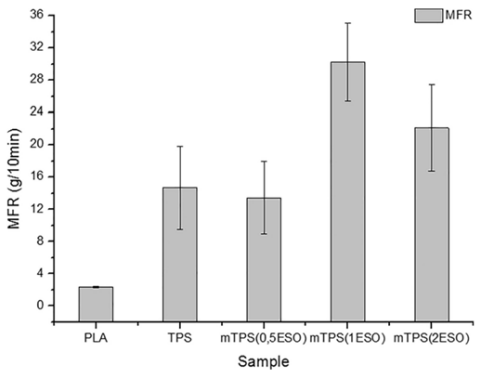

Fig. 2. The effect of the epoxidized soybean oil (ESO) addition on the MFR value of the thermoplastic starch (TPS) samples.

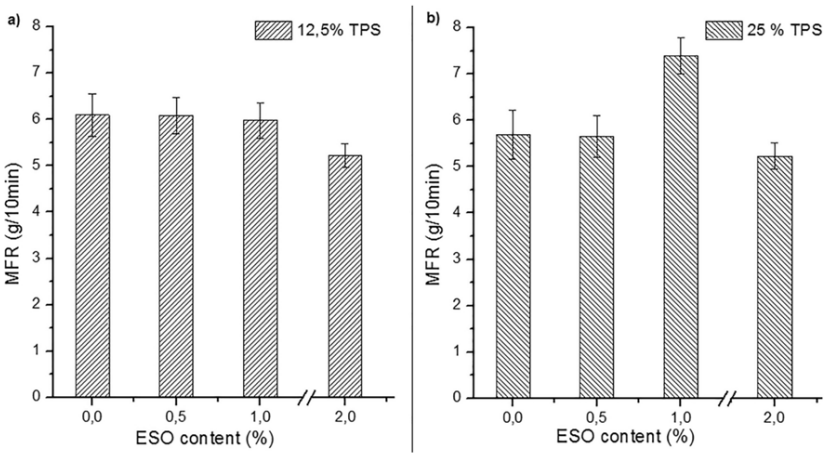

Fig. 3. Effect of the epoxidized soybean oil (ESO) content on the MFR of the a) PLA/TPS blends with 125% of TPS, b) PLA/TPS compositions with 25% of TPS.

plasticizing effect of ESO added to TPS. In this study cross-linking effect was not observed, differently to (Belhassen et al., 2014) study, that observed a decrease of MFR and proved the act of epoxy groups on cross-linking process of TPS. In our work, a catalyst was not used so the cross-linking effect was not observed. Probably, ESO molecules have diffused between TPS chains, acting as a plasticizer and destroyed the occurring hydrogen bonds, what leads to decrease of MFR.

Therefore, the resulting PLA/TPS compositions exhibit also improved degree of flow in comparison to the pure PLA, remaining at a level of 6 g/10 min (Fig. 3). In PLA/TPS compositions containing of 12% TPS, different presence of ESO does not significantly affect the MFR value. Increasing the content of TPS up to 25%, the similar trend in MFR is observed like for TPS modified by ESO (mTPS Fig. 2). For 1% of ESO concentration in PLA/TPS with 25% of TPS, MFR values reached the highest point (7.39 g/10 min). Further increasing the content of the ESO up to 2% results in a reduction of the melt flow rate (5.26 g/10 min). Our findings correlate with Yu-Qiong Xu (Yu-Qiong Xu, 2009) studies. They noted that increasing addition of ESO in the PLA is characterized by a sinusoidal change in value of MFR. In our case, addition of ESO caused plasticization effect by increasing of MFR value. The lack of a catalyst could have contributed to the absence of the branching and cross-linking effect in compositions. However, it should be noted that this effect is not noticeable for the composition containing 12.5% TPS, because of too small ESO content relative to PLA.

3.2. Mechanical characterization

Stress – strain curves of pure PLA and PLA/TPS blends are shown in Fig. 4 (a,b). It can be seen that addition of unmodified (TPS) and modified (mTPS) starch into PLA significantly changed the course of the stress-strain curve. PLA/TPS blends exhibit evident yield point. According to literature reports (Akrami et al., 2016; Ayana et al., 2014; Ferri et al., 2016; Huneault and Li, 2007) the incorporation of thermoplastic starch (TPS) to PLA matrix leads to the increase of flexibility and reduce of tensile strength. In our study, presence of epoxicized soybean oil intensified these effect. The elongation at break increases progressively with the addition of the ESO, reaching up to 5.52% (in samples with 12.5 wt % of TPS and 2% ESO, Fig. 4a) and 8,80% (in samples containing 25 wt % of TPS and 2% ESO, Fig. 4b), respectively. Compared to the pure PLA (2.67%), it is over three-fold increase in the value of elongation at break (Table 3). The tensile strength decrease up to value approximately 50 MPa in PLA/TPS blends generally, relative to the pure PLA (68.14 MPa). It was noticed that, increasing the content of TPS modified by ESO in PLA blends, does not reduce significantly the tensile strength, what is a proof of elastomeric and toughening effect of ESO. Similar observations were reported by Xiong et al. (Xiong et al., 2013). In their study, with the increase of ESO content in PLA and starch matrixes, tensile strength decreased and elongation and break increased. They observed that ESO acted as a plasticizer and also as a compatibilizer which improved interfacial bonding between PLA and starch.

With regard to the hardness, we recorded slightly decreasing tendency with increasing of TPS content (Table 3). The Shore D hardness of pure PLA is 83.53° and it is decreasing up to 82.81° for the PLA/TPS [87.5/12.5] sample. In turn, addition to the PLA/TPS compositions ESO leads to further softening of the material. The evidence is the noticeable decrease in hardness to the value of 77.70° (sample containing 2% ESO, 25%TPS), while hardness of unmodified PLA/TPS with 25% of TPS is equal to 81.55°. This is another confirmation of plasticizing effect of ESO added into PLA/TPS compositions.

Another parameter that describes the functional properties of polymers is impact strength. A slight improvement in impact strength was achieved by blending of unmodified TPS with PLA. It was believed that addition of a ductile and flexible material such as TPS resulted in reduction of brittleness of the PLA. From Table 3 it could be seen the impact-energy absorption of the PLA/TPS blends raising with increasing of ESO content. For the samples with 25% of TPS the highest impact strength value has reached PLA/TPS composition with 2% of ESO (16.96 kJ/m^2). It can be assumed that the PLA/mTPS(2ESO)[75/25] sample show the highest adhesion between PLA and TPS. In turn, for the samples with 25% of TPS and 0.5% or 1% of ESO, the impact strength is unnoticeable (13.92 kJ/m2 and 14.03 kJ/m2, respectively) and probably it is due to too small amount of ESO. Therefore, it should be attributed a significant effect of the addition of ESO to the blends toughness, but only if the ESO content is at least 2%. The impact strength value of all obtained compound does not falls below 10 kJ/m^2, which allows for a statement that as a result of preparing PLA/TPS/ESO blends do not reduce impact strength, compared to pure PLA.

Table 3 summarized the mechanical properties of pure PLA and obtained blends. In terms of mechanical properties our results are passable enough but cannot be strictly comparable to the results found by other researches. Yu-Qiong Xu et al. (Yu-Qiong Xu, 2009) and

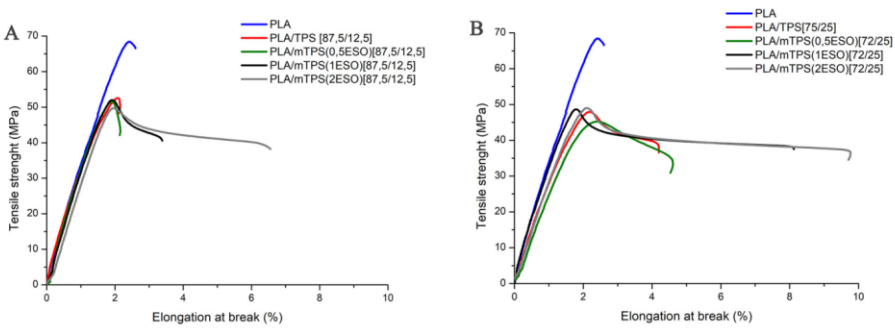

Fig. 4. Evolution of stress-strain curves for PLA and PLA/TPS compositions with different amount of TPS and ESO. A) compositions containing 125% TPS, B) compositions containing 25% TPS.

Vijayarajan et al. (Vijayarajan et al., 2014) added much larger amounts of epoxidized soybean oil to PLA matrix (in the range of 3 up to 20 wt% of ESO). This has led to great improvement of impact strength (up to 47 J/m) and ductility (Vijayarajan et al., 2014) as well as positively influenced on melt strength and rheological properties of PLA (Yu-Qiong Xu, 2009). On the other hand, research on the impact of ESO on the mechanical properties of TPS were led by Belhassen et al. (Belhassen et al., 2014). They proved occurrence of the condensation reaction between the oxirane rings of ESO and the TPS hydroxyl groups. This resulted in enhancement in Young's modulus and tensile strength of TPS/ESO samples, but also caused rigidification effect (lower elongation at break).

Summarizing, the improved mechanical characteristic in a presence of ESO in the PLA/TPS blends mainly might be associated with enhanced interfacial adhesion between PLA and TPS. However, to confirm this thesis in a next step, morphology study was conducted.

3.3. Morphology characterization

The morphology of PLA/TPS[75/25] blends with a various ESO content was examined by SEM and shown in Fig. 5. As the content of the ESO increases, the surface morphology changes. For the unmodified sample (PLA/TPS[75/25]), the morphology is highly inhomogeneous. There are numerous gaps between the TPS and the PLA matrix. Moreover, discontinuities in the structure are visible. TPS occurs in the form of granules (particle size ranges from 0.5 to 2 μm) and tubes (particle length ranges from 3 to 20 μm), suggesting poor dispersion and miscibility of TPS in the PLA matrix due to a large difference in polarity between TPS and PLA polymers. Similar morphology was observed in Ferri et al. study (Ferri et al., 2016). The addition of ESO improved compatibility between TPS and PLA molecules. The addition of only 0.5% ESO (Fig. 5b) resulted in disappearance of the tubes particles and reduction in the number and size of TPS granules. Increasing the ESO content to 2% caused enhancement of interfacial bonding between TPS and TPS phases. Significantly decreased number of black particles were observed, representing TPS granules "ripped out" from PLA matrix. The structure of PLA/mTPS (2ESO) [75/25] is more homogeneous. The TPS granules appear to be strongly embedded in the PLA matrix (Fig. 5d). Hence, the assumption that the addition of ESO improves the miscibility and interphase adhesion of TPS to PLA molecules. Similar effect of ESO presence in PLA/TPS composition was observed by Xiong et al. (Xiong et al., 2013).

3.4. Thermal properties

Table 4 and Fig. 6 (a,b,c) present the results of differential scanning calorimetry (DSC) of PLA/TPS compositions with different content of TPS and ESO. The glass transition temperature (T_g), cold crystallization temperature (T_{cc}), melting temperature (T_m) and the heats of melting and cold crystallization (ΔH_m, ΔH_{cc}) are given.

The neat PLA shows a glass transitions (T_g) at 60.6 °C, a cold crystallization peak (T_{cc}) at 105.6 °C and a sharp melting peak (T_m) about 168 °C. In turn, T_g of TPS is about 52.6 °C, T_m reaches 166.1 °C and the T_{cc} does not appear (Fig. 6a). In case of all prepared compositions T_g is between T_g of pure PLA and TPS, what suggests the good miscibility between the components. However according to the literature the immiscibility of PLA and TPS was proved by Muller et al. (Müller et al., 2012), which is also in accordance with our SEM results as we very clearly observe two-phase morphology for all compositions studied. The examined compositions have small amounts of TPS and due to this some thermal parameters for it are not traced in DSC thermograms. Moreover the thermal transitions for TPS are very weak in comparison of PLA. Occurrence of two endothermic peaks is attributed to the phenomenon of lamellar rearrangement and polymorphism of PLA

Table 3
Summary of results from the mechanical tests of PLA/TPS compositions.

Composition	Tensile strength MPa	Elongation at break %	Impact strength kJ/m^2	Hardness °Sh D
PLA	68.14 ± 0.24	2.67 ± 0.07	13.71 ± 0.27	83.57 ± 1.26
PLA/TPS [87,5/125]	52.65 ± 0.34	2.20 ± 0.16	16.64 ± 1.91	82.81 ± 0.78
PLA/TPS [75/25]	47.87 ± 0.32	4.83 ± 0.52	14.07 ± 0.98	81.55 ± 0.57
PLA/mTPS (0,5ESO) [87,5/125]	51.60 ± 0.57	2.57 ± 0.66	13.56 ± 0.95	79.88 ± 1.47
PLA/mTPS (0,5ESO) [75/25]	45.82 ± 0.78	3.78 ± 0.61	13.92 ± 1.14	78.73 ± 2.03
PLA/mTPS (1ESO) [87,5/125]	52.00 ± 0.16	3.81 ± 1.01	11.84 ± 1.59	80.12 ± 1.87
PLA/mTPS (1ESO) [75/25]	48.76 ± 0.56	7.19 ± 0.91	14.03 ± 2.66	79.14 ± 1.74
PLA/mTPS (2ESO) [87,5/125]	48.26 ± 1.88	5.52 ± 1.62	10.29 ± 3.86	80.49 ± 1.25
PLA/mTPS (2ESO) [75/25]	49.04 ± 0.16	8.80 ± 1.04	16.96 ± 3.54	77.70 ± 1.89

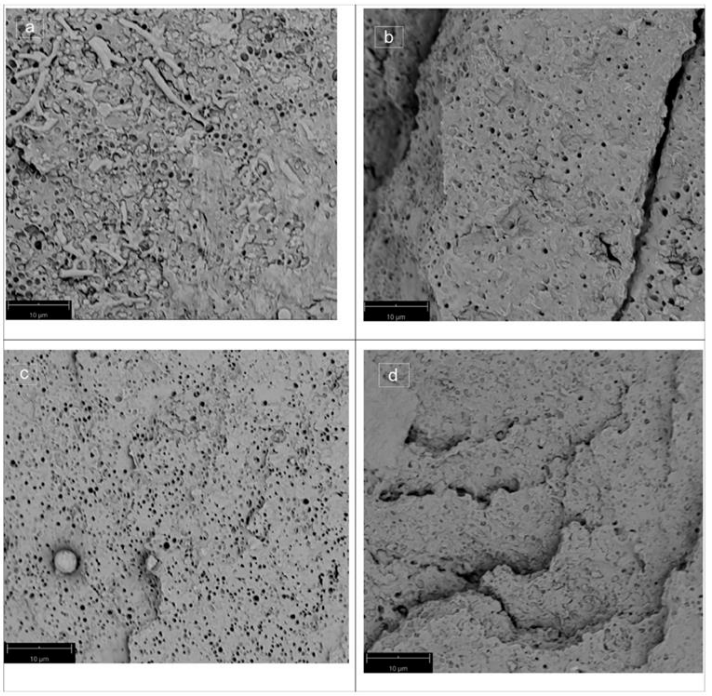

Fig. 5. The fractured surfaces of PLA/TPS[75/25] blends with increasing content of ESO; a) 0%, b) 0,5%, c) 1%, d) 2%, ESO wt%. Magnification x5000.

Table 4
Thermal analysis data for pure PLA and the respective compositions with different content of TPS and ESO.

Composition	T_g [°C]	T_{cc} [°C]	ΔH_{cc} [J/g]	Main T_m [°C]	ΔH_m [J/g]
PLA	60.6	105.6	35.6	168.1	46.3
TPS	52.6	–	–	166.1	0.6
PLA/TPS [87,5/125]	58.4	103.3	33.9	166.8	34.4
PLA/TPS [75/25]	58.1	106.8	27.1	165.2	29.6
PLA/mTPS (0,5ESO) [87,5/125]	58.2	100.5	26.2	166.8	34.5
PLA/mTPS (0,5ESO) [75/25]	59.0	106.0	24.7	166.2	28.4
PLA/mTPS (1ESO) [87,5/125]	57.6	100.7	29.0	165.8	33.6
PLA/mTPS (1ESO) [75/25]	55.7	102.2	30.5	165.8	34.5
PLA/mTPS (2ESO) [87,5/125]	57.2	101.1	30.3	166.2	33.0
PLA/mTPS (2ESO) [75/25]	57.7	107.39	23.45	165.50	27.48

crystalline structure (Cartier et al., 2000; Martin and Årous, 2001; Tábi et al., 2010). Moreover TPS is known as a good crystallization nucleate for PLA (Madhavan Nampoothiri et al., 2010). Some slight increase in T_{cc} of PLA in PLA/TPS/ESO composition are observed after the addition 2% of ESO (Fig. 6b), suggesting small disturbing effect in PLA crystallization (decrease in delta H_{cc}), thus stimulating effect in partial miscibility at the phase border. This might be very valuable information for the processing of the blends. Additionally, adding of 2% of ESO to the composition PLA/mTPS (2ESO)[75/25]) decreases T_g and Tm of blends, what confirms it as a good plasticizer for the composition of PLA and TPS. Summarizing the data of DSC, it should be noted that T_g of potato TPS and PLA are very close, what can complicate the interpretation of the results of DSC and speculations on the morphology of compositions.

3.5. Water resistance

Water resistance of PLA/TPS blends was analyzed by the swelling ratio and mass loss behavior during storage in water under ambient condition. The results shown in Fig. 7 and Fig. 8 revealed that in all cases pure PLA shows minimal swelling ratio and mass loss rate with less than 0.55% and 0.35% after 48 h, respectively. As was presumed, the increase of the starch content in the compound manifested by the higher values in both cases. Contemplating the effect of the ESO adjunct on the resistance to water of prepared compounds found that ESO delays the two processes. In presence of 2%ESO the swelling ratio reaches about 1.5% and 2.75% after 48 h, at a content of 12.5% and 25% TPS, respectively. The mass loss test exhibit similar behavior. Unmodified PLA/TPS[87,5/125], PLA/TPS[75/25] showed the greatest mass loss (about 1.5% and 2.3% after 48 h). While, the increase of ESO content brought the reduction in value which reflect the amount of the 0.55% for PLA/TPS(2ESO)[87.5/12.5] and 0.95% for PLA/TPS(2ESO)[75/25], respectively. It is assumed that presence of plasticized starch (TPS) promoted hydrolytic degradation, thereby causing reduction of dimensional stability. However, presence of ESO resulting in improved the swelling ratio and mass loss behavior, relative to unmodified PLA/TPS compositions.

3.6. Stimulated composting

According to ASTM D5338-98, 2003 (ASTM D5338-98, 2003) standard, composting is a controlled process of biological degradation

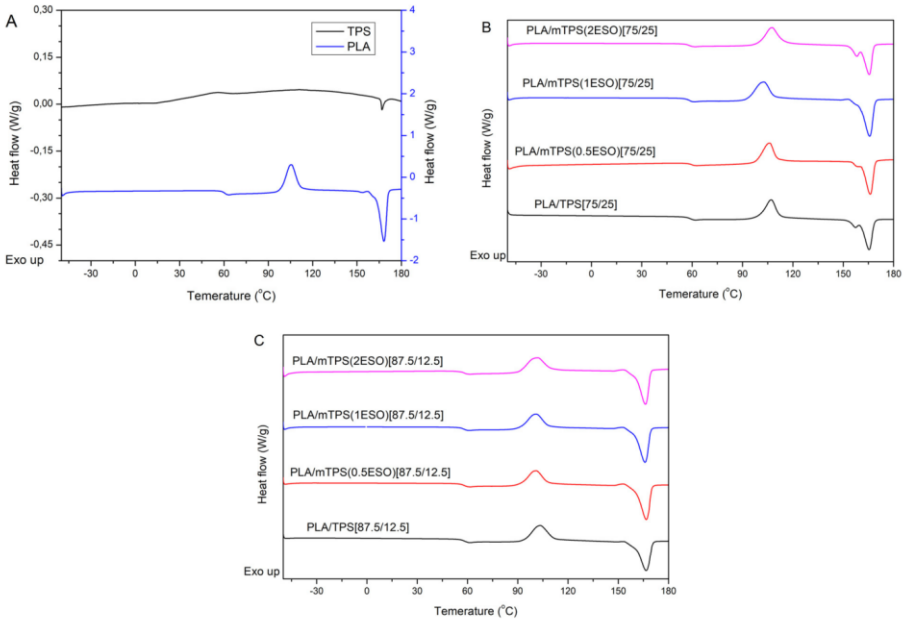

Fig. 6. DSC thermograms of pure PLA and the respective compositions with different content of TPS and ESO. A) PLA and TPS, B) compositions containing 25% TPS, C) compositions containing 12.5% TPS.

with the use of microorganisms under strictly controlled conditions. A biodegradable material is converted to CO2, water, inorganic compounds and biomass. The microorganisms in the process of polymer degradation release enzymes which cause a chain scission of the polymer into monomers (Lau et al., 2009). To confirm the suitability of the obtained innovative materials for use in the short-life application packaging industry as an alternative for commonly used petroleum-based polymers, compostable tests was commissioned. The composting processes is illustrated in Fig. 9. The data from testing by COBRO lab clearly confirm that the materials decomposed completely. During 57 days of incubation, all samples were disintegrated to dimension smaller than 2 mm in diameter. According to PN-EN 14,806:2010 standard, all were completely degraded in the composting conditions.

4. Conclusions

This work is motivated by current demands of the market which seeks for less expensive alternatives for PLA. In this study, a new compositions based on PLA, modified by TPS and ESO was prepared to improve PLAs ductility and reduce the products cost without compromising biodegradation. To confirm the efficiency of drafted compositions, their rheological, mechanical and thermal properties, water resistance and ability to composting were studied. Growth in MFR value leads to an increased susceptibility to injection and blow molding processes. From the technological point of view these increases the variety of products for short life application. Further, to confirm the suitability of obtained PLA/TPS blends in various branches of the

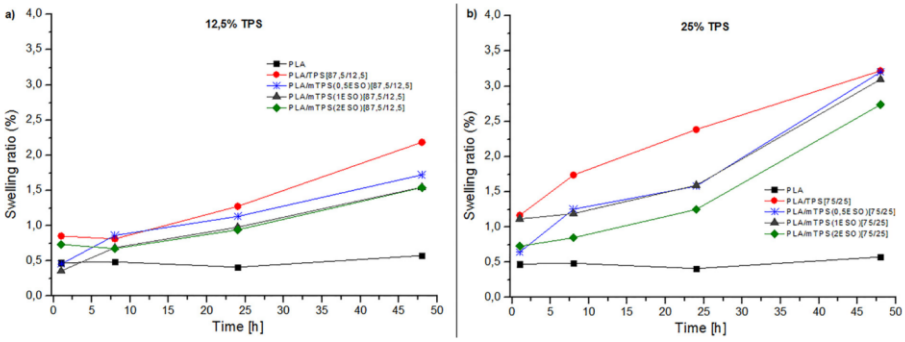

Fig. 7. Swelling ratio behavior of PLA and PLA/TPS compositions with different content of TPS and ESO.

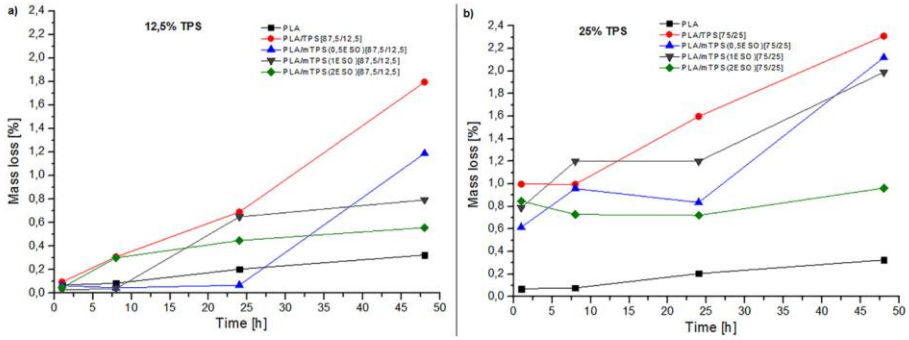

Fig. 8. Mass loss behavior of PLA and PLA/TPS compositions with different content of TPS and ESO.

Fig. 9. The processes of composting test of PLA and PLA/TPS compositions (black arrow represents the compost material, red arrows correspond to the pieces of the samples). A) preparation for test, B) within 15 days of initiation of a study, C) sample on day 30 from the beginning of test– the samples degrades almost completely, D) end of test, the process of sieving – no residue (For interpretation of the references to colour in this figure legend, the reader is referred to the web version of this article).

packaging industry, the mechanical properties were characterized. The addition of ESO leads to softer materials, improved impact strength (up to 16,69 kJ/m$^{2)}$, tensile and ductile properties (elongation at break ~ 8.8%), compared to the native PLA, what has been confirmed by SEM examination of fractured surfaces. The presence of ESO in the compositions delayed the water diffusion into blends matrix. This might improve products dimensional stability, exposed to short-term water acting. The prepared thermoplastic starch (TPS) modified by epoxidized soybean oil (ESO) requires the same machines as well to the processing of pure PLA. Possibility of replacing up to 25% of PLA through modified mTPS allows to reduces the costs of the product as well as maintain quite similar properties and ability to composting relative to pure PLA. Moreover in our previous studies on TPS/ESO it is clear that ESO added to TPS speeds up composting processing time (Janik et al., 2017).

References

Akrami, M., Ghasemi, I., Azizi, H., Karrabi, M., Seyedabadi, M., 2016. A new approach in compatibilization of the poly(lactic acid)/thermoplastic starch (PLA/TPS) blends. Carbohydr. Polym. 144, 254–262. http://dx.doi.org/10.1016/j.carbpol.2016.02.035.

Ali, F., Chang, Y.-W., Kang, S.C., Yoon, J.Y., 2009. Thermal, mechanical and rheological properties of poly (lactic acid)/epoxidized soybean oil blends. Polym. Bull. 62, 91–98. http://dx.doi.org/10.1007/s00289-008-1012-9.

ASTM D5338-98, 2003. Standard Test Method for Determining Aerobic Biodegradation of Plastic Materials Under Controlled Composting Conditions.

Auras, R., Harte, B., Selke, S., 2004. An overview of polylactides as packaging materials. Macromol. Biosci. 4, 835–864. http://dx.doi.org/10.1002/mabi.200400043.

Ayana, B., Suin, S., Khatua, B.B., 2014. Highly exfoliated eco-friendly thermoplastic starch (TPS)/poly (lactic acid)(PLA)/clay nanocomposites using unmodified nanoclay. Carbohydr. Polym. 110, 430–439. http://dx.doi.org/10.1016/j.carbpol.2014.04.024.

Belhassen, R., Vilaseca, F., Mutjé, P., Boufi, S., 2014. Thermoplasticized starch modified by reactive blending with epoxidized soybean oil. Ind. Crops Prod. 53, 261–267. http://dx.doi.org/10.1016/j.indcrop.2013.12.039.

Carmona, V.B., Corrêa, A.C., Marconcini, J.M., Mattoso, L.H.C., 2015. Properties of a biodegradable ternary blend of thermoplastic starch (TPS), poly(ε-caprolactone) (PCL) and poly(lactic acid) (PLA). J. Polym. Environ. 23, 83–89. http://dx.doi.org/10.1007/s10924-014-0666-7.

Cartier, L., Okihara, T., Ikada, Y., Tsuji, H., Puiggali, J., Lotz, B., 2000. Epitaxial crystallization and crystalline polymorphism of polylactides. Polym. (Guildf). 41, 8909–8919. http://dx.doi.org/10.1016/0032-3861(94)90933-4.

Clasen, S.H., Müller, C.M.O., Pires, A.T.N., 2015. Maleic anhydride as a compatibilizer and plasticizer in TPS/PLA blends. J. Braz. Chem. Soc. http://dx.doi.org/10.5935/0103-5053.20150126.

Ferri, J.M., Garcia-Garcia, D., Sánchez-Nacher, L., Fenollar, O., Balart, R., 2016. The effect of maleinized linseed oil (MLO) on mechanical performance of poly(lactic acid)-thermoplastic starch (PLA-TPS) blends. Carbohydr. Polym. 147, 60–68. http://dx.doi.org/10.1016/j.carbpol.2016.03.082.

Gregory, M.R., 2009. Environmental implications of plastic debris in marine settings–entanglement, ingestion, smothering, hangers-on, hitch-hiking and alien invasions. Philos. Trans. R. Soc. Lond. B. Biol. Sci. 364, 2013–2025. http://dx.doi.org/10.1098/rstb.2008.0265.

Guarás, M.P., Alvarez, V.A., Ludueña, L.N., 2016. Biodegradable nanocomposites based on starch/polycaprolactone/compatibilizer ternary blends reinforced with natural and organo-modified montmorillonite. J. Appl. Polym. Sci. 133. http://dx.doi.org/10.1002/app.44163.

Huneault, M.A., Li, H., 2007. Morphology and properties of compatibilized polylactide/thermoplastic starch blends. Polym. (Guildf). 48, 270–280. http://dx.doi.org/10.1016/j.polymer.2006.11.023.

Imre, B., Pukánszky, B., 2013. Compatibilization in bio-based and biodegradable polymer blends. Eur. Polym. J. 49, 1215–1233. http://dx.doi.org/10.1016/j.eurpolymj.2013.01.019.

Jalalvandi, E., Majid, R., Ghanbari, T., Ilbeygi, H., 2015. Effects of montmorillonite (MMT) on morphological, tensile, physical barrier properties and biodegradability of polylactic acid/starch/MMT nanocomposites. J. Thermoplast. Compos. Mater. 28, 496–509. http://dx.doi.org/10.1177/0892705713486129.

Janik, H., Sienkiewicz, M., Wawrowska, M., Wiecierzycka, K., Przybytek, A., 2017. Degradation of modified TPS in natuaral and industrial compost. In: Mukbaniani, O., Abadie, M., Tatrishvili, T. (Eds.), Chemical Engineering of Polymers. Production of Functional and Flexible Materials. Apple Academic Press, CRC Press, pp. 397–406.

Kale, G., Kijchavengkul, T., Auras, R., Rubino, M., Selke, S.E., Singh, S.P., 2007. Compostability of bioplastic packaging materials: an overview. Macromol. Biosci. 7, 255–277. http://dx.doi.org/10.1002/mabi.200600168.

Karagoz, S., Ozkoc, G., 2013. Effects of a diisocyanate compatibilizer on the properties of citric acid modified thermoplastic starch/poly(lactic acid) blends. Polym. Eng. Sci. 53. http://dx.doi.org/10.1002/pen.23478. n/a-n/a.

Kaseem, M., Hamad, K., Deri, F., 2012. Thermoplastic starch blends: a review of recent works. Polym. Sci. Ser. A 54, 165–176. http://dx.doi.org/10.1134/S0965545X1202006X.

Khan, B., Bilal Khan Niazi, M., Samin, G., Jahan, Z., 2016. Thermoplastic starch: a possible biodegradable food packaging material-a review. J. Food Process Eng. 0. http://dx.doi.org/10.1111/jfpe.12447.

Khoo, R., Chow, W., 2015. Mechanical and thermal properties of poly(lactic acid)/sugarcane bagasse fiber green composites. J. Thermoplast. Compos. Mater. http://dx.doi.org/10.1177/0892705715616857.

Lau, A.K., Cheuk, W.W., Lo, K.V., 2009. Degradation of greenhouse twines derived from natural fibers and biodegradable polymer during composting. J. Environ. Manage. http://dx.doi.org/10.1016/j.jenvman.2008.03.001.

Leadprathom, J., Suttiruengwong, S., Threepopnatkul, P., Seadan, M., 2010. Compatibilized polylactic Acid/Thermoplastic starch by reactive blend. J. Met. Mater. Miner. 20, 87–90.

Lim, L.-T., Auras, R., Rubino, M., 2008. Processing technologies for poly(lactic acid). Prog. Polym. Sci. 33, 820–852. http://dx.doi.org/10.1016/j.progpolymsci.2008.05.004.

Luckachan, G.E., Pillai, C.K.S., 2011. Biodegradable polymers- a review on recent trends and emerging perspectives. J. Polym. Environ. 19, 637–676. http://dx.doi.org/10.1007/s10924-011-0317-1.

Madhavan Nampoothiri, K., Nair, N.R., John, R.P., 2010. An overview of the recent developments in polylactide (PLA) research. Bioresour. Technol. 101, 8493–8501. http://dx.doi.org/10.1016/j.biortech.2010.05.092.

Martin, O., Årous, L.A., 2001. Poly(lactic acid): plasticization and properties of biodegradable multiphase systems. Polymer (Guildf). 42, 6209–6219.

Martin, O., Avérous, L., 2001. Poly(lactic acid): plasticization and properties of biodegradable multiphase systems. Polymer (Guildf). 42, 6209–6219. http://dx.doi.org/10.1016/S0032-3861(01)00086-6.

Mohanty, A.K., Misra, M., Hinrichsen, G., 2000. Biofibres, biodegradable polymers and biocomposites: an overview. Macromol. Mater. Eng. (276–277), 1–24. http://dx.doi.org/10.1002/(SICI)1439-2054(20000301)276:1<1::AID-MAME1>3.0.CO;2-W.

Müller, C.M.O., Pires, A.T.N., Yamashita, F., 2012. Characterization of thermoplastic starch/poly(lactic acid) blends obtained by extrusion and thermopressing. J. Braz. Chem. Soc. 23, 426–434. http://dx.doi.org/10.1590/S0103-50532012000300008.

Nafchi, A.M., Moradpour, M., Saeidi, M., Alias, A.K., 2013. Thermoplastic starches: properties, challenges, and prospects. Starch/Staerke 65, 61–72. http://dx.doi.org/10.1002/star.201200201.

Parulekar, Y., Mohanty, A.K., 2007. Extruded biodegradable cast films from polyhydroxyalkanoate and thermoplastic starch blends: fabrication and characterization. Macromol. Mater. Eng. 292, 1218–1228. http://dx.doi.org/10.1002/mame.200700125.

PlasticsEurope, 2016. Plastics – the Facts 2016. An Analysis of European Plastics Production, Demand and Waste Data.Plastics – the Facts 2016. An Analysis of European Plastics Production, Demand and Waste Data.

Shen, L., Haufe, J., Patel, M.K., 2009. Product Overview and Market Projection of Emerging Bio-Based Plastics.

Siracusa, V., Rocculi, P., Romani, S., Rosa, M.D., 2008. Biodegradable polymers for food packaging: a review. Trends Food Sci. Technol. 19, 634–643. http://dx.doi.org/10.1016/j.tifs.2008.07.003.

Tábi, T., Sajó, I.E., Szabó, F., Luyt, A.S., Kovács, J.G., 2010. Crystalline structure of annealed polylactic acid and its relation to processing. Express Polym. Lett. 4, 659–668. http://dx.doi.org/10.3144/expresspolymlett.2010.80.

Teixeira, E., de, M., Curvelo, A.A.S., Corrêa, A.C., Marconcini, J.M., Glenn, G.M., Mattoso, L.H.C., 2012. Properties of thermoplastic starch from cassava bagasse and cassava starch and their blends with poly (lactic acid). Ind. Crops Prod. 37, 61–68. http://dx.doi.org/10.1016/j.indcrop.2011.11.036.

Vijayarajan, S., Selke, S.E.M., Matuana, L.M., 2014. Continuous blending approach in the manufacture of epoxidized soybean-plasticized poly(lactic acid) sheets and films. Macromol. Mater. Eng. 299, 622–630. http://dx.doi.org/10.1002/mame.201300226.

Wang, H., Sun, X., Seib, P., 2001. Strengthening blends of poly(lactic acid) and starch with methylenediphenyl diisocyanate. J. Appl. Polym. Sci. 82, 1761–1767. http://dx.doi.org/10.1002/app.2018.

Wang, N., Yu, J., Chang, P.R., Ma, X., 2008. Influence of formamide and water on the properties of thermoplastic starch/poly(lactic acid) blends. Carbohydr. Polym. 71, 109–118. http://dx.doi.org/10.1016/j.carbpol.2007.05.025.

Woothikanokkhan, J., Kasemwananimit, P., Sombatsompop, N., Kositchaiyong, A., Isarankura na Ayutthaya, S., Kaabbuathong, N., 2012. Preparation of modified starch-grafted poly(lactic acid) and a study on compatibilizing efficacy of the copolymers in poly(lactic acid)/thermoplastic starch blends. J. Appl. Polym. Sci. 126, E389–E396. http://dx.doi.org/10.1002/app.36896.

Wu, C.-S., 2005. Improving polylactide/Starch biocomposites by grafting polylactide with acrylic acid - characterization and biodegradability assessment. Macromol. Biosci. 5, 352–361. http://dx.doi.org/10.1002/mabi.200400159.

Xing, C., Matuana, L.M., 2016. Epoxidized soybean oil-plasticized poly(lactic acid) films performance as impacted by storage. J. Appl. Polym. Sci. 133, 1–8. http://dx.doi.org/10.1002/app.43201.

Xiong, Z., Yang, Y., Feng, J., Zhang, X., Zhang, C., Tang, Z., Zhu, J., 2013. Preparation and characterization of poly(lactic acid)/starch composites toughened with epoxidized soybean oil. Carbohydr. Polym. 92, 810–816. http://dx.doi.org/10.1016/j.carbpol.2012.09.007.

Yang, Y., Tang, Z., Xiong, Z., Zhu, J., 2015. Preparation and characterization of thermoplastic starches and their blends with poly(lactic acid). Int. J. Biol. Macromol. 77, 273–279. http://dx.doi.org/10.1016/j.ijbiomac.2015.03.053.

Yu-Qiong Xu, J.-P.Q., 2009. Mechanical and rheological properties of epoxidized soybean oil plasticized poly(lactic acid). J. Appl. Polym. Sci. 112, 3185–3191. http://dx.doi.org/10.1002/app.

Zhang, J.-F., Sun, X., 2004. Mechanical properties of poly(lactic acid)/Starch composites compatibilized by maleic anhydride. Biomacromolecules 5, 1446–1451. http://dx.doi.org/10.1021/bm0400022.

Zhang, Y., Rempel, C., Liu, Q., 2014. Thermoplastic starch processing and characteristics—a review. Crit. Rev. Food Sci. Nutr. 54, 1353–1370. http://dx.doi.org/10.1080/10408398.2011.636156.

4.6 PAPER 6: PLA–Potato Thermoplastic Starch Filament as a Sustainable Alternative to Conventional PLA Filament: Processing, Characterization and FFF 3D Printing

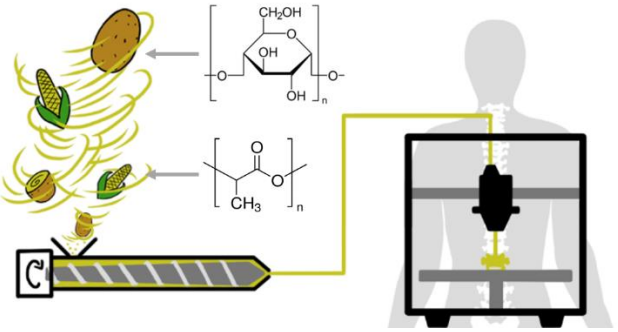

Graphical abstract, source: DOI:(10.1021/acssuschemeng.0c09413)

Authors (percentage share): Agnieszka Haryńska(corresponding author) (60%), Helena Janik (10%), Maciej Sienkiewicz (10%), Barbara Mikolaszek (10%), Justyna Kucińska-Lipka (10%)

Journal: ACS Sustainable Chemistry & Engineering

DOI: doi.org/10.1021/acssuschemeng.0c09413

Index: Q1, IF_{2019}=7.632, MNSiW = 140 pts

CRediT: Conceptualization (lead), Data Curation (lead), Formal Analysis (lead), Investigation (lead: FTIR and Raman spectroscopies, XRD, MFR, tensile and compression strength tests, impact strength, hardness, water contact angle, DSC, TGA, DMA, degradation studies, laboratory simulated composting)**,** Methodology (lead), Project Administration (in part), Visualization (lead), Writing – Original Draft Preparation (lead), Writing – Review & Editing (lead).

Realized doctoral research tasks:

II (filament formation) – formation of 3D-printable filament using developed PLA/TPS composition on a technical scale in a continuous manner *via* filament-forming system presented in PAPER 3.

III (filament characterization) – a comprehensive characterization of the developed PLA/TPS filament and the commercial counterpart – PLA filament (FlashForge PLA™).

IV (evaluation of the filament stability) – analysis of structural, thermal and rheological properties of the filaments before and after the 3D printing process;

V (3D printing) – preparation of personalized anatomical 3D models by the segmentation of the CT scan *via* 3D Slicer software; design of digital 3D models of test samples and porous structures (gyroid and cancellous bone) *via* Autodesk Inventor software; optimization of the 3D printing parameters.

VI (examination of the printouts in terms of their application in medicine) – study of the degradability and compostability; evaluation of the quality and accuracy of obtained personalized anatomical models, and porous structures by

comparing them with virtual models and models obtained using commercial PLA filament.

Material code: PLA/TPS, PLA(FF)

BRIEF DESCRIPTION OF THE PUBLICATION

Discussed topics: latest literature reports on bio-filaments for extrusion-based 3D printing.

Scope of the publication: formation of the bio-filament in a continuous manner; comparison of the filament properties before and after FFF 3D printing; evaluation of filament biodegradability and compostability; preparation of digital 3D models of bone vertebrae directly from CT scan of the spine; design and 3D printing of porous structures and personalized anatomical models; optimization of 3D printing parameters.

Novelty of the publication: fabrication of the fully plant-based and compostable filament for FFF 3D printing, containing PLA enriched with potato thermoplastic starch (TPS) and epoxidized soybean oil (ESO).

Main scientific achievement: increased susceptibility to hydrolytic degradation and disintegration in composting conditions of the developed PLA/TPS/ESO filament comparing to the commercial PLA filament, while maintaining comparable printability.

Outline: The article presents a comprehensive characterization of a novel bio-based filament that was formed using the PLA/TPS composition developed at the earlier stage of the research (PAPER 5). The work particularly focuses on assessing the stability, compostability and printability of the developed filament and its counterpart – commercial PLA filament (FlashForge PLA™). The results present: (i) parameters necessary to form a stable PLA/TPS bio-filament, in a continuous manner, (ii) structural, thermal and mechanical characterization, (iii) results of incubation in PBS and canola oil, (iv) water contact angle measurements (v) simulated composting study, and (vi) 3D printing of personalized bone vertebrae as well as gyroid and cancellous bone-like porous structures. The results indicated that the developed bio-filament shows higher hydrophilicity, improved susceptibility to hydrolytic degradation, and thus, enhanced compostability comparing to the commercial PLA. The spectroscopic and thermal analysis confirmed the stability of the PLA/TPS during the 3D printing process. Applicable printability of the developed filament was demonstrated by high-quality printouts of personalized anatomical models and porous structures. The developed composition is a modern solution in the bio-filaments sector and promising in 3D printing of medical devices such as porous tissue scaffolds or more sustainable disposable patient-matched preoperative models.

ACS Sustainable Chemistry & Engineering

pubs.acs.org/journal/ascecg

Research Article

PLA–Potato Thermoplastic Starch Filament as a Sustainable Alternative to the Conventional PLA Filament: Processing, Characterization, and FFF 3D Printing

Agnieszka Haryńska,* Helena Janik, Maciej Sienkiewicz, Barbara Mikolaszek, and Justyna Kucińska-Lipka

Cite This: *ACS Sustainable Chem. Eng.* 2021, 9, 6923–6938

Read Online

ACCESS | Metrics & More | Article Recommendations | Supporting Information

ABSTRACT: The growing popularity of the fused filament fabrication (FFF) 3D printing technology in science, industry, and in-home use is associated with an increased demand for high-quality polymer filaments. This study presents an in-depth characterization and analysis of a self-made bio-based polylactide (PLA)/thermoplastic potato starch (TPS) filament dedicated for the FFF 3D printing technology. The obtained results were compared with the commercial PLA filament (FF). The series of conducted studies (i.e., Fourier-transform infrared spectroscopy, Raman spectroscopy, differential scanning calorimetry, thermogravimetric analysis, and dynamic mechanical analysis) revealed that both of the investigated filaments are stable under FFF 3D printing conditions. The mechanical test showed a correlation between the print orientation and raster angle on the strength features. The most favorable strengths values were recorded for the ZX_0° configuration, which were ∼18/22 MPa of tensile strength and ∼9/18 kJ m^{-2} of Charpy impact strength for the PLA/TPS filament and FF, respectively. Also, it was observed that the developed bio-filament has a more hydrophilic surface and is more susceptible to hydrolytic degradation in the phosphate-buffered saline solution than the FF. The composting study (according to the EN ISO 20200 standard) revealed that the commercial PLA printouts remain intact, while the PLA/TPS samples showed a mass loss of 19%. Finally, the remarkable printability of PLA/TPS was successfully demonstrated by FFF 3D printing of personalized anatomical models and complex porous structures.

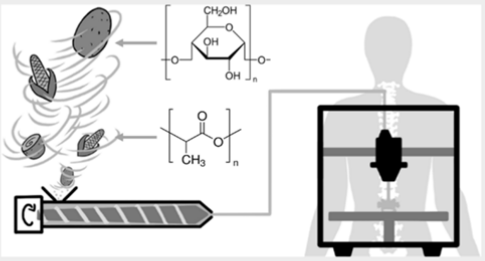

KEYWORDS: *fused filament fabrication, 3D printing, potato thermoplastic starch, polylactide, material characterization, bio-based filaments*

INTRODUCTION

The use of additive manufacturing (AM) technologies in industry and science has become widespread nowadays. These methods are irreplaceable in rapid prototyping as well as more and more often used in the production of finished products. The example of the AM technologies that is particularly popular in the industry, medicine, and home use is the fused filament fabrication (FFF). This highly available technology primarily uses thermoplastic-based polymers as the raw material. The most popular materials (filaments) for FFF 3D printing (3DP) are acrylonitrile butadiene styrene (ABS), polylactide (PLA), polyamide (PA), and thermoplastic elastomer (TPE).[1] Nevertheless, along with the growing interest in this molding method, the amount of petrochemical polymers used is constantly increasing. As prototyping involves the formation of disposable products, the amount of FFF 3D-printed waste reaches a very alarming level. While the recycling of unmodified thermoplastics is not regarded as a problem, the effective recovery of raw materials from modified 3D printout waste (blends and composites) is much more difficult. Therefore, new solutions on fossil fuels-based filament substitutes with less negative environmental impact are being sought.[2]

More and more attention is being paid to the development of bio-filaments for FFF 3DP, which are based on materials that are biodegradable and/or obtained from renewable resources. The most recent literature reports regarding this topic are presented in Table 1. The developed materials are, in most cases, PLA-based composites modified with natural powders (walnut shell powder[4]) or managed eco-wastes (spend coffee grounds[5] and spruce pulp fibers[3]). Other studies focus on the use of recyclates as efficient feedstocks for FFF 3D printers. Idrees et al.[6] proposed a filament based on waste polyethylene terephthalate

Received: January 2, 2021
Revised: March 29, 2021
Published: May 10, 2021

https://doi.org/10.1021/acssuschemeng.0c09413
ACS Sustainable Chem. Eng. 2021, 9, 6923–6938

Table 1. Latest Literature Reports on Bio-Filaments for 3D Printing in the FFF Technology

bio-filaments					
type of filament	composition	short description	material properties[b]	suggested application	refs
fiber-based composites	PLA/TMP[a]	development of biocomposite filaments of PLA with modified spruce thermomechanical pulp fibres (TMP) (10 and 20 wt %)	tensile strength = 10−23 MPa, water contact angle of selected samples up to 100° (highly hydrophobic properties)	antibacterial 3D-printed devices	3
particle-based composites	PLA/WSP[a]	studies of bio-based composite filaments based on the PLA matrix with a walnut shell powder (WSP) modifier (5 wt %)	melt flow index (MFI, 160 °C, 3.8 kg) = 8−18 g 10 min^{-1}, compressive strength = 212−276 MPa, Young modulus = 2.5−3.0 GPa, tensile strength = 48−52 MPa	trabecular bone tissue scaffolds	4
	PLA/Ox-SSG[a]	fabrication and characterization of bio-based PLA filaments loaded with oil-extracted spent coffee grounds (Ox-SCG) (5−20 wt %)	toughness = 5−25 MJ m^{-3}	personalized prosthesis	5
	PET/Biochar	development of sustainable filaments from recycled PET bottles enhanced with biochar derived from packaging waste (0.5−5 wt %)	Young modulus = 0.7−09. GPa, tensile strength = ∼50 MPa	a sustainable, recycle-based alternative for automotive and engineering applica-tion	6
nanocomposite	PA-11/sepiolite nanoclay[a]	development of fully biorenewable filaments based on a PA-11 monomer (11-amino-undecanoic, castor beans origin) modified with natural clay (1, 3, and 7 wt %)	Young modulus = 0.7−1.15 GPa, tensile strength = 27−47 MPa, strain at break = 5−38%	biorenewable alternative to PLA filaments with higher printing temperature for engineering application	7
	PHBH/CNC[a]	studies of bio-based PHBH filaments modified with functionalized cellulose nanocrystals (CNC) (5−20 wt %)	disintegration ratio in a laboratory-scale composting test (60th day of the test) = 55−80%	external medical devices, surgical implants, tissue scaffolds	8
polymer blends	TPS/ABS	development of partly bio-based filaments composed of 30 wt % debranched-with-α-isoamylase thermoplastic starch (TPS) and acrylonitrile butadiene styrene (ABS)	impact strength (Izod, notched) = 8−18 J m^{-1}, flexuralmodulus = 2.1−2.5 GPa, tensiles-trength = 34−48 MPa	household gadgets, inductrial design, architecture	9
	PBS/PLA	fabrication and characterization of biodegrad-able filaments consisting of the mixture of PBS with PLA (20−60 wt %)	tensile strength = 16−21 MPa	architectural design	10
	PLA/PBAT	formulation of biofilaments with increased impact strength from PLA-based blends containing 10, 20, and 30% of poly(butylene adipate-co-terephthalate (PBAT)	Impact strength (Izod, notched) = 30−719 J m^{-1}, Young modulus = 2.2−3.0 GPa, tensile strength = 40−63 MPa, elongation at break = 7.6−84%	not specified	11

[a]Fully bio-based. [b]The given mechanical properties refer to FFF 3D printouts made using developed filaments.

(PET) bottles with the addition of biochar (derived from packaging waste) as a sustainable alternative to conventional filaments. Another interesting solution seems to be a modification of poly(3-hydroxybutyrate-*co*-3-hydroxyhexa-noate) (PHBH) with cellulose nanocrystals (CNC), proposed by Giubilini et al.[8] As a result, a printable FFF filament with enhanced thermal and mechanical properties as well as improved compostability was obtained. This product combines both compostability and fully renewable origin; therefore, it can be considered as "double green". However, the relatively high production costs of PHBH and CNC may hamper the introduction of this product at an industrial scale. Thus, nowadays, it seems reasonable to follow the "double-ECO" approach proposed by Tanabe[12] which takes into consideration not only the environmental and ecological issues but also an economical aspect of the production.

In our previous research, we developed a biodegradable and compostable polymer composition based on renewable and natural-origin ingredients.[13] The composition consists of PLA and thermoplastic potato starch (TPS) modified with epoxidized soybean oil (ESO). As a result, we improved PLA's ductility as well as reduced the costs of the granulate without compromising biodegradability and compostability. In the next step, we started research on the use of the developed composition as a sustainable material for FFF 3DP. Therefore, in this study, we present the full characteristics of self-made PLA/TPS filament which can be a sustainable alternative to the commonly used petrochemical filaments. Moreover, to facilitate direct comparison of the formed PLA/TPS filament with commercially available products, all of the presented studies were also carried out for the FlashForge PLA filament. The schematic flowchart showing the steps of the work is presented in Figure 1. Structural, thermal, and mechanical properties, as well as wettability, susceptibility to hydrolysis, and disintegration in composting conditions, were evaluated. Furthermore, spectroscopic and thermal studies were carried out for both

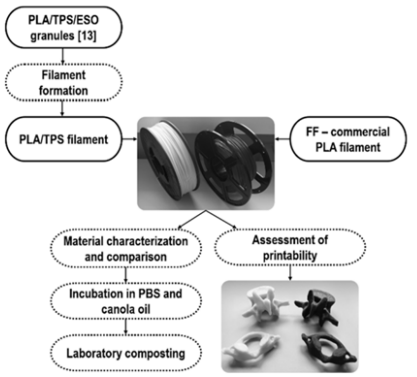

Figure 1. Schematic flowchart representing the steps of the work.

https://doi.org/10.1021/acssuschemeng.0c09413
ACS Sustainable Chem. Eng. 2021, 9, 6923−6938

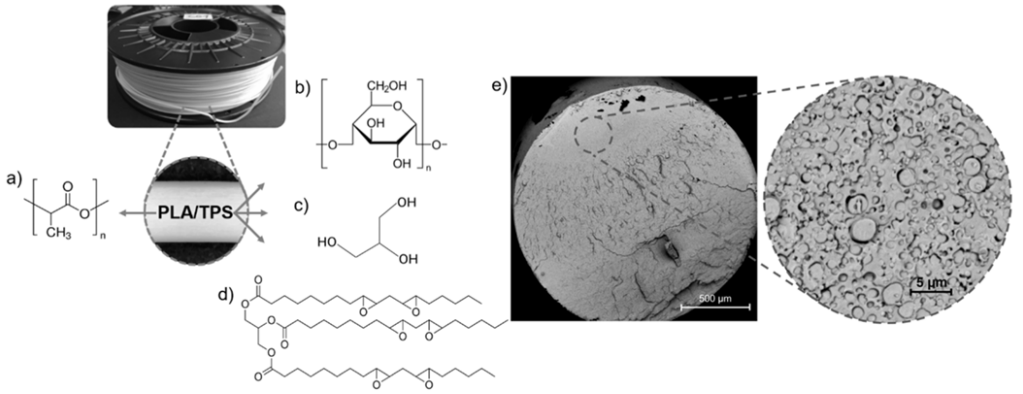

Figure 2. Scheme of the PLA/TPS filament composition: (a) PLA, (b) potato starch, (c) glycerin, and (d) ESO and (e) SEM image of the PLA/TPS filament (in cross-section view).

filaments and the formed printouts to assess the stability of the material under FFF 3DP conditions. Finally, the FFF printability of the proposed novel bio-filament was evaluated and compared with that of commercial PLA printouts. For this purpose, we printed (FFF 3DP) personalized anatomical models (cervical and lumbar vertebrae) and complex-shaped porous structures (gyroid and cancellous bone-like structure). To our best knowledge, we have not found so far any literature reports on PLA-based filaments modified with TPS for FFF 3DP. Thus, the presented research may be an interesting offer for other scientists or industries looking for bio-based filaments with increased compostability and adequate printability.

EXPERIMENTAL SECTION

Materials. The PLA/TPS granulate used to obtain the PLA/TPS_F filament was previously developed and described in detail in our earlier article.[13] The composition selected for this work contained fully plant-based-origin biodegradable raw materials, that is, 60 wt % PLA (7032D transparent injection grade, NatureWorks, USA, MFR = 7 g 10 min^{-1} at 210 °C and 2.16 kg) and 40 wt % TPS (Figure 2). TPS was obtained by melt extrusion of the following mixture: native potato starch (ZetPezet, Poland, humidity 16%), plant pharmaceutical-grade glycerin, used as a plasticizer (TechlandLab, Poland, ρ = 1.26 g cm^3), and ESO (Brenntag, Germany), which served as a reactive modifier. The wt % ratio of the TPS components was as follows: potato starch 65.7%; glycerin 33.3%; and ESO 1%.

A wildly available commercial PLA filament produced by FlashForge (Zhejiang, China) was selected as the reference material. The FlashForge PLA filament (FF) (blue colour, Ø = 1.75 mm) is characterized by the producer in terms of printing conditions (printing temperature: 190−220 °C and bed temperature: 50−60 °C) and basic material properties (density: 1.24 g cm^{-1}, yield strength: 62 MPa, tensile break: 15%, and impact strength: 4.2 kJ m^{-2}). It is also described as environmentally friendly and biodegradable. According to the material safety data sheet, the FF contains 95% of PLA, 4% of TPE, and 1% of additives in the form of mineral oils. Symbols and description of studied materials are presented in Table 2.

Filament (PLA/TPS_F) Formation. The filament-forming system used to obtain the PLA/TPS filament (Ø = 1.75 mm) consisted of a granulator dryer (50 °C/5 h), a single-screw extruder (L/D = 32, with three heating barrel zones and two head zones), two cooling tubes filled with water (40 °C/22 °C) and equipped with calibrators (Ø = 2 and 1.8 mm), a laser diameter measurement system (laser sensor accuracy 0.01 mm), the puller (pulling velocity ∼70 rpm), and a spool winding system. The extrusion temperature profile of barrels zones was I—140 °C, II—160 °C, and III—168 °C and for head zones IV—170 °C and V—172 °C. The temperature of the melt was 176 °C, the head pressure was 21 ± 2 bar, and the extrusion velocity was set at 35 rpm. The scheme and detailed description of the applied filament-forming system are presented in our previous article.[14]

Table 2. Symbols and Description of Materials Used in the Study

		composition (wt %)			
			TPS		
symbol	description	PLA	potato starch	plant glycerin	ESO
PLA/TPS_F	filament	60	26.3	13.3	0.4
PLA/TPS_P	printout				
symbol	description	PLA	thermoplastic elastomer		mineral oils
FF_F	filament	95	4		1
FF_P	printout				

3D Printer, Test Samples, Anatomical Model Design, and 3D Printing Settings. Prusa i3 MK3S (Prusa Research, Prague, Czech), an FFF-based 3D printer, with PrusaSlicer software (2.20 version) was used to print the studied details. Autodesk Inventor software (Autodesk, Warszawa, Poland) was used to prepare SLT files of test specimens (for tensile, compression, and impact tests). The 3D printing settings of all test samples used for characterization are listed in Table S1, and dimensions of samples for strength tests are presented in Figure S1 (the Supporting Information). The L3 and C1 vertebrae were selected as exemplary anatomical models, while the gyroid and cancellous bone were selected as porous structures. Vertebrae models L3 and C1 were prepared by the segmentation of the CT scan of the spine of a healthy woman. The segmentation process was conducted via 3D Slicer software (https://www.slicer.org/, 4.10.2 version). 3D Slicer is an open-source software platform for visualization and medical image computing.[15] The scheme of the segmentation procedure of personalized anatomical models is presented in Figure S2. In turn, the description of porous models (the gyroid and cancellous bone) and detailed 3D printing settings are shown in Tables S2 and S3 (the Supporting Information).

Characterization of the Filaments and Printouts. A series of studies including spectroscopy [Fourier-transform infrared (FTIR) and Raman], X-ray diffraction (XRD), thermal studies [differential scanning calorimetry (DSC) and thermogravimetric analysis (TGA)], dynamical mechanical analysis (DMA), melt flow rate (MFR) measurements, mechanical properties tests (tensile, Charpy impact, and compression tests), and water contact angle (wCA) measurements

https://doi.org/10.1021/acssuschemeng.0c09413
ACS Sustainable Chem. Eng. 2021, 9, 6923−6938

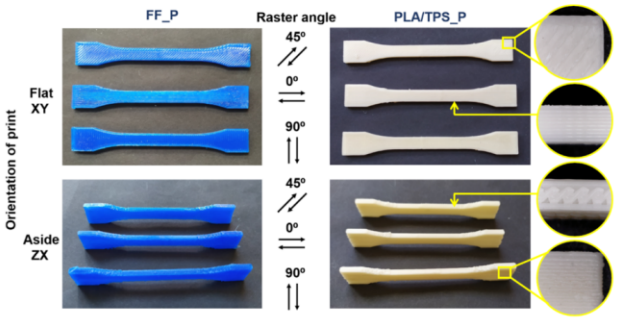

Figure 3. View of the build orientation and raster angle of test specimens.

were conducted on both materials to characterize and compare the FF with the self-made PLA/TPS one.

Spectroscopic Studies. The infrared spectra of the samples were collected via an attenuated total reflectance FTIR Nicolet 8700 spectrometer (Thermo Fisher Scientific, Waltham, USA). The spectral range was 4000−500 cm^{-1}, resolution 4 cm^{-1}, and 64 scans per measurement. The study was carried out at room temperature. The Raman spectra were obtained using a confocal micro-Raman system (inVia, Renishaw, UK) equipped with a red laser (785 nm) operating at 50% of the total power (50 mW).

XRD Analysis. XRD analysis was conducted via the Rigaku Intelligent X-ray diffraction system SmartLab (Rigaku Corporation, Tokyo, Japan) equipped with a sealed tube X-ray generator (a copper target; operated at 40 kV and 30 mA). Data were collected in the 2θ range of 5−50° with a scan speed of 2° min^{-1} and a scan step of 0.01°.

Thermal Properties. Thermal characteristic was studied by DSC and TGA. DSC measurements were collected using a Netzsch 204F1 Phoenix apparatus (Netzsch, Germany) under a nitrogen atmosphere (20 ml min^{-1}) at the temperature range of 25−220 °C and a heating/cooling rate of 5 °C min^{-1}. The sample weight was ∼6 mg. In turn, a Netzsch TG 209 instrument (Netzsch, Germany) was used to collect TGA data. The temperature range was 35−600 °C with a heating rate of 10 °C min^{-1} under a nitrogen atmosphere (sample weight ∼7 mg). The degree of PLA crystallinity ($X_{c\ PLA}$) was calculated based on the following formula 1

$$X_{c\ PLA}\ (\%) = \left(\frac{\Delta H_m - \Delta H_{cc}}{\Delta H_m^0}\right) \times \frac{1}{w_{PLA}} \times 100\% \quad (1)$$

where ΔH_{cc}, ΔH_m, and ΔH_m^0 represent the heat of cold crystallization, heat of melting, and melting of 100% crystalline PLA (93 J g^{-1}[16]), respectively. The $1/w_{PLA}$ factor takes into account the actual content of PLA in the tested samples.

Dynamic Mechanical Analysis. The dynamical mechanical test was performed via a DMA Q800 analyzer (TA Instruments, USA) under the single cantilever bending mode with 1.0 Hz frequency of an oscillatory deformation (sample dimension 40 × 10 × 2 mm^3). The temperature range was −100 to 130 °C (heating rate 4 °C min^{-1}).

Rheological Properties. The MFR and melt volume rate (MVR) of the samples were measured by a Zwick/Roell load plastometer (M-Flow, BFN-001, Zwick, Poland) in accordance with the ISO 1133:2005 standard. The measurement was conducted at four different temperatures (180, 190, 200, and 210 °C) under a load of 2.16 kg. Five repetitions were made for each sample, and the result was presented as an average (n = 5).

Water Contact Angle. The wCAs of the samples were determined with a ramé-hart 90-U3 goniometer and DROPimage Pro software (ramé-hart, USA). Before measurements, the sample surface was degreased and a 2 μL droplet of deionized (DI) water was deposited. Then, the images were collected. Six repetitions were made for each sample, and the result was calculated as an average (n = 6). The test was carried out on flat surfaces of the printouts (infill density = 100% and raster angles of 0 and 90°).

Mechanical Properties. The hardness of the printed samples was measured using the Shore D-type durometer (Zwick/Roell, Germany) according to the ISO 868 standard. Fifteen repetitions per sample were made, and the results were averaged. The tensile tests were performed on printed dumbbell-shaped specimens using a Zwick/Roell Z020 universal tensile machine equipped with an adapter for determining the Young modulus. The measurements were carried out according to the ISO 527 standard at room temperature. The cross-head speed was 5 mm min^{-1}, and the initial force was 1 N. At least six samples were tested, and results were averaged. The Charpy impact strength was determined using a pendulum impact tester (Zwick/Roell HIT5.5P) with a 5 J hammer according to the ISO 179 standard (unnotched). The uniaxial compression test was carried out on cubic specimens via a Zwick/Roell Z020 machine. Samples were compressed until 25% strain was reached at a rate of 5 mm min^{-1} (five samples per series). The brittleness (B) of samples was calculated based on eq 2 formulated by Brostow et al.[17]

$$B = \frac{1}{\varepsilon_b \times E'} \quad (2)$$

where ε_b (%) is the tensile elongation at break and E' (Pa) represents the value of the storage modulus (at a temperature of 25 °C) which was determined by DMA. To facilitate the presentation of the obtained values, the brittleness is expressed as (% Pa 10^{-10}).

Detailed information on test specimen design and dimensions are shown in Figure S1. The tensile and impact tests, as well as brittleness, were rated depending on the infill raster angle (0, 45, and 90°) and the orientation of the printout in relation to the plane of the printer's build table (flat XY and aside ZX) (Figure 3).

Degradation Studies. Filaments (FF_F and PLA/TPS_F) were incubated in 0.1 M phosphate-buffered saline (PBS, Sigma-Aldrich) and food-grade canola oil for 30 days at 37 °C. The filaments were cut into pieces (∼3 mm length) and then dried and weighed (m_0) in a thermobalance (Radwag MAX50/SX, Radom, Poland) at 60 °C. Thus, the prepared samples were placed in 50 mL polypropylene Falcon tubes and immersed with 35 mL of the appropriate medium. Three samples per series were tested, and results were averaged. At each respective time point (1 h, 5 h, 1, 3, 7, 14, and 30 days), samples were carefully removed. In the case of PBS incubation, samples were further rinsed with DI water and dried in a laboratory oven at 50 °C for 48 h. Subsequently, the pH of PBS residues was also monitored (pH-100 ATC, Voltcraft, Germany). Mass loss (Ms) was calculated as follows 3

$$M_s\ (\%) = \frac{m_0 - m_x}{m_0} \times 100\% \quad (3)$$

where (m_0) is the initial mass of the sample and (m_x) is the residual mass.

Furthermore, incubation in 0.1 M PBS was monitored by FTIR measurements and a scanning electron microscope (Phenom Pro Generation 5, Thermo Fisher, Eindhoven, Netherlands, AV = 5 kV).

https://doi.org/10.1021/acssuschemeng.0c09413
ACS Sustainable Chem. Eng. 2021, 9, 6923−6938

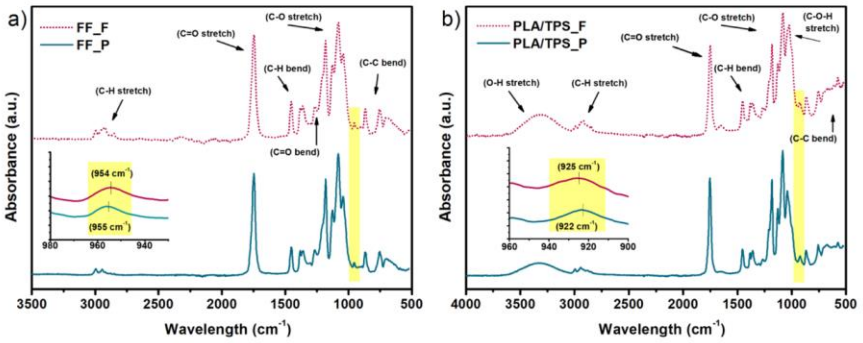

Figure 4. FTIR spectra of (a) FF and (b) PLA/TPS filaments and printouts.

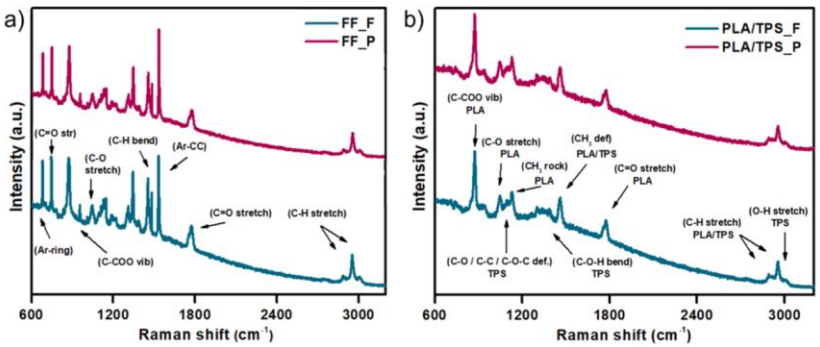

Figure 5. Raman spectra of (a) FF and (b) PLA/TPS filaments and printouts.

In the case of incubation in canola oil, in addition to the mass loss, the degree of swelling (Sw %) was also determined. For this purpose, after removing the sample from the medium, excess oil was gently removed from the surface with a paper towel, and then, the sample was weighed. The Sw % was calculated based on the following formula 4

$$\text{Sw}\ (\%) = \frac{m_x - m_0}{m_x} \times 100\% \tag{4}$$

Laboratory-Simulated Composting. Evaluation of the degree of disintegration of the printouts (FF_P and PLA/TPS_P) under a laboratory-scale composting environment was carried out according to the EN ISO 20200 standard. The composition of the composting mixture is given in Table S4. The initial pH of the compost was 5.95 and relative humidity over 90% (water was added periodically to the containers during the test according to the procedure given in the ISO standard to ensure constant humidity). Printed samples with the dimensions of 1.5 cm length, 1 cm width, and 2 mm thickness were tested (three samples for each material). The samples were dried (60 °C, 48 h) and weighed before testing. Then, the samples were put in polypropylene reactors filled with compost and placed in a bioreactor (48 °C for up to 60 days). To ensure aerobic conditions, the containers were opened and flipped each week. At each time interval (7, 14, 30, 50, and 60 days), samples were carefully removed, rinsed with DI water, dried, and weighed. The degree of disintegration (D %) was calculated based on mass loss measurements (eq 5), where (m_0) is the initial mass of the sample and (m_y) is the dry mass of the tested sample at different composting periods. The composting process was monitored via mass measurements, optical photos of the sample's surface (magnification ×20, Delta Optical Generic, Pro, Mińsk Mazowiecki, Poland), scanning electron microscopy (SEM), and FTIR spectroscopy.

$$D\ (\%) = \frac{m_0 - m_y}{m_0} \times 100\% \tag{5}$$

RESULTS AND DISCUSSION

Structural Characterization (FTIR Spectroscopy, Raman Spectroscopy, and XRD). The results of the FTIR studies are shown in Figure 4. Spectroscopic studies were conducted on both filaments (FF_F and PLA/TPS_F) and printouts (FF_P and PLA/TPS_P) to evaluate the structural stability during the FFF 3D printing (3DP) process.

Analyzing the spectrum of the commercial filament (FF_F), the presence of functional group characteristics for PLA was noted (Figure 4a). The absorption band visible in the range of 2380−3010 cm^{-1} corresponds to the symmetric and asymmetric stretching of the CH_3 group. The C═O stretching vibration occurred at 1748 cm^{-1}. The band at 1452 cm^{-1} is attributed to the CH_3 asymmetric bending vibration. The band at 1264 cm^{-1} is associated with the C═O bending vibration, whereas the bands at 1179, 1083, and 1043 cm^{-1} correspond to the C−O−C stretching vibration of PLA-ester groups. In turn, the spectrum of the PLA/TPS filament shows additional bands derived from TPS, that is, a broad signal at 3310 cm^{-1} (O−H stretching vibration), a band at 1020 cm^{-1} (deformation of C−O, glucose ring), and signals in the region of 1080−1100 cm^{-1} (C−O stretching of the C−O−H group).[18]

https://doi.org/10.1021/acssuschemeng.0c09413
ACS Sustainable Chem. Eng. 2021, 9, 6923−6938

Since the FFF 3DP is a high-temperature process, some changes in the polymer structure could be expected. However, no visible changes between FF_F and FF_P spectra were noted. According to Jia,[19] the bands in the region of 921 and 955 cm^{-1} can be responsible for crystalline and amorphous phases of the PLA, respectively. In the case of FF_F, the intensity of the band at 955 cm^{-1} (amorphous) matches well with the literature data.[19] This suggests the larger share of the amorphous state of PLA and indicates that the crystallization process as a result of the 3DP did not occur. The PLA/TPS filament showed a small "crystalline" band at 925 cm^{-1}, which slightly decreased after the printing process (Figure 4b). This might suggest that due to the fast cooling rate during FFF 3DP, the degree of the crystalline phase decreased slightly. There was also a slight decrease in the intensity of the −OH-derived signal in the PLA/TPS printout, which may be related to the reduction of hydrogen bonds as a result of the 3DP process. It is also worth noting that in the PLA/TPS_P spectrum, the band at ∼1652 cm^{-1} appeared. This range corresponds to the presence of water molecules or C═C bond vibrations resulting from the decomposition of the material.[20] However, no changes in the intensity or positions of the main bands were noted; thus, it can be observed that the materials during the 3DP process were stable. Therefore, the signal at ∼1652 cm^{-1} probably comes from the dampness of the material.

To expand chemical structure analysis of the filaments, the complementary technique, that is, Raman spectroscopy, was performed (Figure 5).

The obtained spectrum for the FF_F sample was generally in line with the FTIR results. Characteristic signals derived from PLA were noted: symmetric and asymmetric vibrations of −CH (2951 and 2887 cm^{-1}, respectively); the C═O carbonyl group (1774 cm^{-1}); CH_3 asymmetric modes (1453 cm^{-1}); C−O stretching (1045 cm^{-1}); C−COO vibration (874 cm^{-1}), and C═O stretching at 749 cm^{-1}.[19,21] Moreover, the presence of additional strong signals in regions characteristic for aromatic structures was also noted at 1532 and 690 cm^{-1}. Those additional signals come from the −CH stretching vibration of the aromatic ring (1532 cm^{-1}) and the bending vibration of the Ar ring (690 cm^{-1}), as Raman spectroscopy is relatively sensitive to these structures.[22,23] According to the information from the manufacturer, the FF, apart from PLA, contains additional substances, that is, TPE (4%) and mineral oils (up to 1%). Both additives contain aromatic carbons in their structure, which correspond to the additional signals located on the Raman spectrum. In turn, the Raman spectrum of PLA/TPS_F (Figure 5b) significantly complemented the characteristics of the composition. In addition to the PLA-derived bands, that is, C−H stretching (2954 and 2889 cm^{-1}); C═O stretching (1775 cm^{-1}); C−H bending (1458 cm^{-1}); C−O stretching (1042 cm^{-1}), and C−COO vibrations (878 cm^{-1}), the TPS-derived bands were noted. They corresponded to the peaks at 3010 cm^{-1} (−OH stretching) and 1309 cm^{-1} (C−O−H bending) as well as to the range of deformation modes in the glycoside bond present in the TPS structure (C−O, C−C, and C−O−C deformative vibrations in the range of 1088−1129 cm^{-1}).[18,24] However, when analyzing the spectroscopic results of both of the studied materials, no significant changes in the spectra of filaments and printouts were observed. There was no carbonyl peak splitting, which would indicate re-crystallization as a result of the printing process. Further, there were no visible bands shifts or changes in their intensity; hence, the structural stability of both studied materials under given printing conditions can be pre-confirmed.

For further structural analysis, both materials were studied by means of XRD (Figure 6).

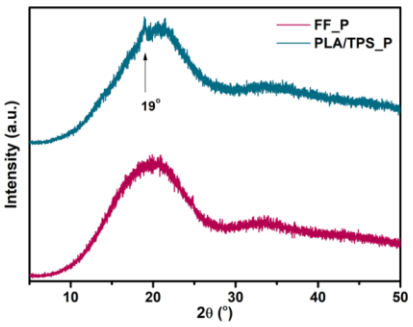

Figure 6. XRD spectra of FF_P and PLA/TPS_P.

The XRD analysis of FF_P showed a broad hump in the range of 2θ equal to 10−25°, which is characteristic for amorphous-based PLA.[21,25] This confirms the previous spectroscopic considerations that confirmed the amorphous nature of the studied FF. PLA/TPS_P showed a similar course with a slight peak at 2θ = 19°. According to Bulatović et al.,[26] TPS is formed by the process of plastification and destruction of the native starch crystalline structure; hence, the TPS shows a semi-crystalline-to-amorphous behavior. Thus, a slight peak at 2θ = 19° can correspond to residues of the A-type crystals present in the native starch.[27] Nevertheless, the mild course of the XRD plot and the lack of clear peaks corresponding to the crystal structure indicate a high proportion of the amorphous phase in both tested materials.

Thermal and Thermomechanical Properties of the FF and PLA/TPS Filament and Printout. Thermal characteristics of both materials before and after the printing process are presented in Figure 7. First, DSC measurements were performed. The results are shown in Figure 7a,b, and the corresponding numerical values are listed in Table 3. Based on the thermograms, the glass transition temperature region (T_g), cold crystallization (T_{cc}), crystalline phase transition (T_{ct}), melting temperature (T_m), heat of cold crystallization (ΔH_{cc}), heat of melting (ΔH_m), and degree of crystallinity (X_c) were determined.

The glass transition of polymers is a gradual phenomenon that takes place in a certain temperature range.[28,29] Although the so-called glass transition temperature (within the meaning of a single temperature value) is an incorrect concept, to facilitate comparison and analysis, Table 3 summarizes the single T_g values corresponding to the midpoint of the heat capacity change recorded in DSC scans. The commercial FF_F PLA filament showed a T_g at 67.4 °C, a T_{cc} at 96.6 °C, a T_{ct} at 156.3 °C, and a melting point at 171.9 °C. The calculated degree of crystallinity was 12.2%. The characteristic exothermic peak (T_{ct}) is associated with PLA polymorphism. These values are typical for PLA filaments and do not significantly differ from the literature data.[30] As a result of the FFF 3DP process (FF_P sample), a shift of the T_g value (∼3 °C) toward lower temperatures was noted. This suggests a very slight increase in the mobility of the polymer chains in the amorphous state.

The glass transition, melting point, and degree of crystallinity for the PLA/TPS filament were found to be 70.8 °C, 165.2 °C,

https://doi.org/10.1021/acssuschemeng.0c09413
ACS Sustainable Chem. Eng. 2021, 9, 6923−6938

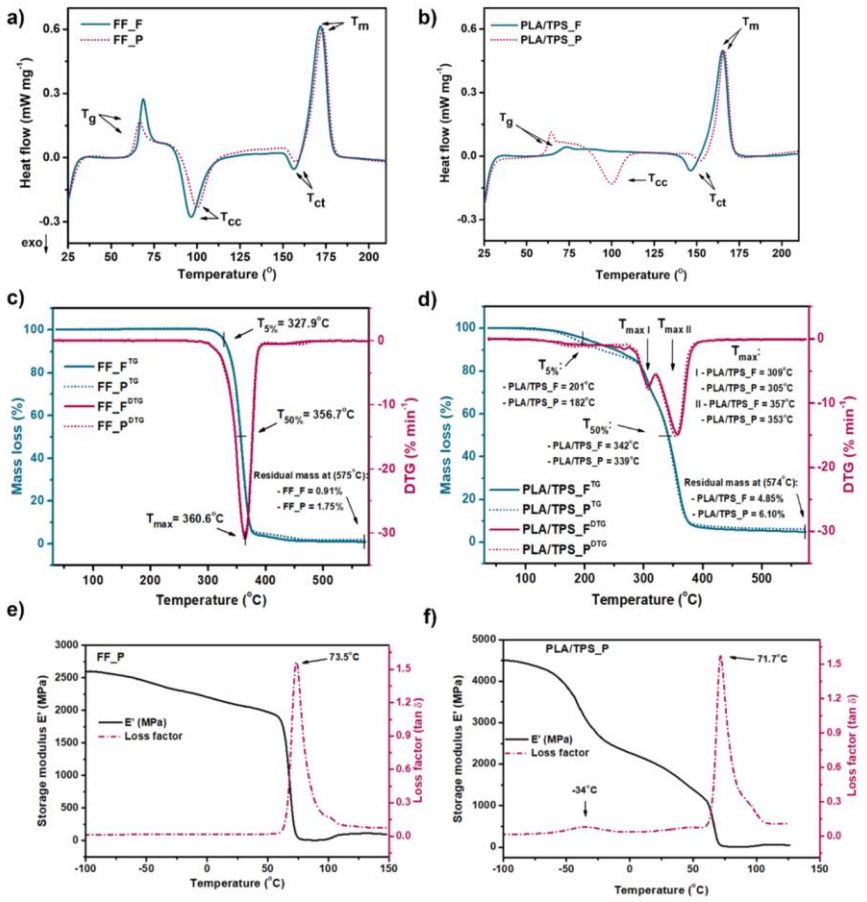

Figure 7. Thermal and thermomechanical characteristics of the FF and PLA/TPS filament and printout; (a,b) DSC curves (first heating run), (c,d) thermogravimetric curves TG and DTG, and (e,f) DMA results.

Table 3. Values of DSC Measurements for the FF and PLA/TPS Filament and Printout (First Heating Run)

sample	T_g[a] (°C)	T_{cc} (°C)	ΔH_{cc} (J g^{-1})	T_{ct} (°C)	T_m (°C)	ΔH_m (J g^{-1})	$X_{c\ PLA}$ (%)
FF_F	67.4	96.6	22.3	156.3	171.9	33.1	12.2
FF_P	64.7	100	19.8	157.3	172.9	30.9	12.6
PLA/TPS_F	70.8			146.5	165.2	25.9	46.3
PLA/TPS_P	63.1	100	12.6	151.9	166.1	22.3	17.4

[a]The value provided in the table corresponds to the midpoint of the heat capacity change recorded in DSC scans.

and 46.3%, respectively. No cold crystallization process was found in the thermogram of the formed PLA/TPS filament (Figure 7b). This indicates sufficient cooling time during the filament-formation process to achieve a very high degree of crystallinity of the sample ($X_{c\ PLA}$ = 46.3%). The printed sample (PLA/TPS_P) showed a cold crystallization transformation at 100 °C during DSC analysis, which indicates that the cooling rate for the printout process was higher than the one for filament making. What is more, a significant reduction in the degree of crystallinity to 17.4% was observed. It follows that the 3DP process significantly affects the degree of crystallization of the PLA/TPS filament. Therefore, when planning a 3DP process with this filament as a feedstock, the above considerations should be taken into account. Moreover, the manufacturer can manipulate with a cooling rate or annealing after printing to achieve various values of crystallinity and thus different properties of the material. In this manner, by post-treatment (annealing), it is possible to obtain details with a relatively higher thermal resistance, hardness, or increased resistance to solvents.[31] Furthermore, a decrease of the T_g by 7 °C relative to

https://doi.org/10.1021/acssuschemeng.0c09413
ACS Sustainable Chem. Eng. 2021, 9, 6923−6938

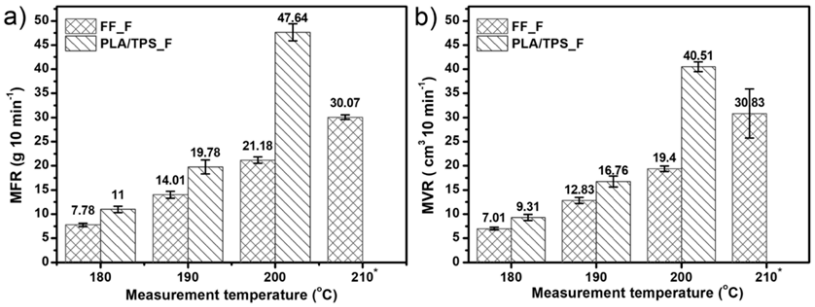

Figure 8. MFR (a) and MVR (b) results for the FF and PLA/TPS filament. The load was 2.16 kg. * At 210 °C, the melt fluidity of PLA/TPS_F was too high, and it was not possible to receive the data.

that of the PLA/TPS filament was also noted. Such a decrease in the glass transition temperature of the printed sample may be related to the destruction of hydrogen bonds occurring in the PLA/TPS structure and thus the increase in the mobility of the polymer chains. It is consistent with the FTIR results, which showed a clear decrease in the intensity of the −OH band of the PLA/TPS_P sample compared to that of PLA/TPS_F.

Subsequently, the thermal stability of both filaments and printouts was determined based on the TGA measurements. The curves show the amount and rate of change in the mass of a sample as a function of temperature. Obtained curves and their derivatives (DTG) are shown in Figure 7c,d. The thermograms of the commercial filament and printout indicated a single-stage degradation course, and their curves overlap to a large extent. The thermal stability (T_{offset}) of FF_F and FF_P was around 320 °C, while the complete decomposition takes place above 500 °C. There was no effect of the 3DP process on the course of the FF thermograms.

In turn, the thermal stability of PLA/TPS_F was ∼200 °C. The PLA/TPS material as a two-component composition showed a two-stage degradation course with distinctly separated DTG peaks (Figure 7d), thus confirming the polymer phase separation.[32] The first DGT peak ($T_{max\ I}$) for the PLA/TPS_F sample corresponds to the decomposition of TPS at 309 °C, while destruction of the PLA takes place at 357 °C ($T_{max\ II}$). The T_{offset} for the PLA/TPS_P sample dropped by 19 °C, while the $T_{max\ I}$ and $T_{max\ II}$ dropped by 4 °C. The decrease in thermal stability was probably related to the dropped crystallinity degree of PLA/TPS_P observed after the 3DP process. Thus, unlike the FF_F, the thermal stability of the PLA/TPS filament is slightly changed due to the 3DP process. Moreover, the 3D printing temperature of PLA/TPS_F should not exceed ∼190 °C to avoid possible degradation and release of glycerin vapors originally contained in TPS ($T_{5\%}$ = 201 °C).

DMA results are presented in Figure 7e,f. The curves show the temperature dependence of storage modulus (E') and loss factor (damping factor). As a standardized sample size is required for DMA measurements, the test was performed only for printed samples (FF_P and PLA/TPS_P). The maximum of the loss factor curves indicates the relaxation processes occurring near the glass transition temperature region of polymers[33] and was observed at 73.5 °C for FF_P and 71.7 °C for PLA/TPS_P. The value of E' in the glassy state region of FF_P was above 2550 MPa and decreased rapidly after exceeding 65 °C (700 MPa). The maximum amplitude of the damping factor for FF_P reached 1.55 which corresponds to an impeccable damping property. The loss factor curve of PLA/TPS_P (Figure 7f) revealed the presence of an additional transition peak at −34 °C. It is most likely related to the α-relaxation of the TPS molecules.[34,35] It can also be seen that FF_P is characterized by significantly higher values of the E' over the entire temperature range than those for PLA/TPS_P and thereby exhibits greater stiffness.

Conducted thermal and thermo-mechanical studies showed a similar trend in thermal characteristics of both filaments. Moreover, the tests revealed that the 3DP process does not significantly affect the properties of the commercial filament. On the other hand, the printing process slightly changes the degree of crystallinity of the PLA/TPS_P sample, which results in a slight deterioration of the thermal stability of the PLA/TPS printouts. The two-phase nature of the prepared PLA/TPS composition was also confirmed. It has also been observed that due to the addition of TPS into PLA, the T_m of the composition is lowered; thus, effectively, the temperature of 3D printing is reduced.

MFR and MVR Results. The MFR and MVR characterize the flow velocity of thermoplastics under thermal processing. These values express the number of grams or volumes of material pressed during 10 min through a die of a specific diameter under specific load and temperature. The MFR/MVR values are also inversely proportional to the dynamic viscosity of the melt as well as allow for a quick and easy way to estimate the appropriate printing temperature for the tested filament. Furthermore, according to Wang et al.,[36] the MFR/MVR is related to the inter-layer adhesion of details formed by FFF 3DP. Thus, it is worth paying attention to this study. The MFR/MVR results of commercial PLA (FF_F) and self-made PLA/TPS_F are presented in Figure 8.

The FF_F showed an MFR ranging from ∼8−30 g 10 min^{-1} at 180 and 210 °C, respectively. The proportional increase in the index (by about 7 g 10 min^{-1} per 10 °C) with the increasing measurement temperature was noted. This proves the high stability of the material and a wide range of effective plasticizing temperature and thus a comparatively wide range of possible 3DP temperatures. When compared to other commercial PLA filaments, the MFR value of the FF_F sample was relatively high. The PLA filament from Prusa (Prusament PLA) indicates that MFR = 10.4 g 10 min^{-1} and that of Ultimaker PLA and Fiberlogy R-PLA around 6 g 10 min^{-1} (at 210 °C, 2.16 kg). These values were over 3 times lower than those recorded for FF_F (MFR = 30 g 10 min^{-1}). This may be due to the lower molecular weight of FF PLA or the presence of additives (TPE and mineral oils)

https://doi.org/10.1021/acssuschemeng.0c09413
ACS Sustainable Chem. Eng. 2021, 9, 6923−6938

Table 4. Summarized Result of Mechanical Studies of FF_P and PLA/TPS_P

sample	print orientation	raster angle (deg)	Young modulus (GPa)	ultimate tensile strength (MPa)	elongation at break (%)	Charpy impact strength eU[a] (kJ m^{-2})	hardness (Sh D)	brittleness (% Pa 10^{-10})
FF_P	*XY*	0	1.62 ± 0.25	15.81 ± 5.19	2.97 ± 1.26	13.31 ± 1.47	79 ± 2	1.611
		45	1.69 ± 0.31	15.21 ± 4.58	2.67 ± 0.46	9.00 ± 1.01	78 ± 3	1.792
		90	1.597 ± 0.08	15.36 ± 3.05	1.83 ± 0.29	7.59 ± 1.33	78 ± 1	2.615
	ZX	0	2.03 ± 0.13	21.81 ± 3.36	4.28 ± 0.75	18.48 ± 1.63		1.118
		45	1.53 ± 0.22	5.83 ± 2.29	5.28 ± 0.55	15.84 ± 1.87		0.906
		90	2.19 ± 0.64	11.83 ± 3.06	3.68 ± 0.73	12.98 ± 0.88		1.300
PLA/TPS_P	*XY*	0	1.47 ± 0.36	24.72 ± 1.21	3.83 ± 0.31	7.65 ± 0.94	60 ± 2	1.355
		45	1.45 ± 0.37	9.35 ± 1.78	1.25 ± 0.12	4.97 ± 1.11	62 ± 2	4.152
		90	1.93 ± 0.47	14.86 ± 1.42	3.11 ± 1.19	3.88 ± 1.31	61 ± 3	1.669
	ZX	0	1.51 ± 0.38	17.85 ± 1.31	4.61 ± 0.11	9.73 ± 1.04		1.126
		45	1.53 ± 0.35	17.28 ± 1.41	3.78 ± 0.52	5.91 ± 0.64		1.373
		90	1.74 ± 0.41	16.87 ± 2.15	2.57 ± 0.78	4.44 ± 0.91		2.019

[a]eU—unnotched Charpy specimen.

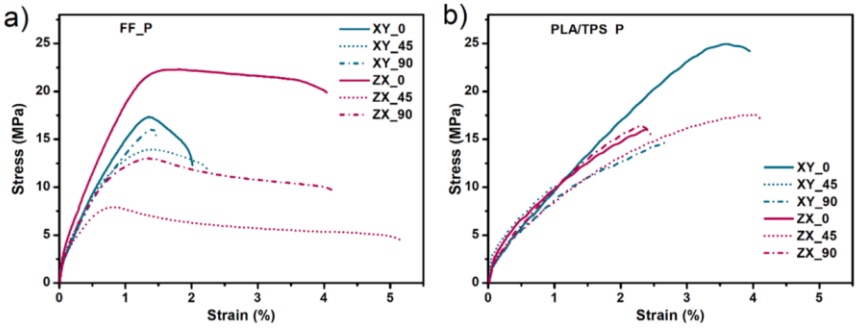

Figure 9. Average tensile stress−strain curves of FF_P (a) and PLA/TPS_P (b) depending on the build orientation and raster angle.

that act as PLA plasticizers, thus increasing MFRs under test conditions.

The MFR value of self-made PLA/TPS_F was in the range of 11 g 10 min^{-1} at 180 °C to 47 g 10 min^{-1} (200 °C). The rising trend of the index with the test temperature was much larger and more irregular compared to that of commercial FF_F. At 210 °C, the melt viscosity of PLA/TPS_F was too low to collect measurement data. In the temperature range of 200−210 °C, the initial material decomposition was recorded (color change and gas formation). Therefore, the 3DP temperature of the PLA/TPS filament should not exceed 200 °C. Due to the lack of research on the PLA filament modified with TPS in the literature, the discussion on PLA/TPS_F MFR values is difficult. However, considering the MFR threshold value for PLA filaments reported by Wang et al.[36] (∼10 g min^{-1}, at 2.16 kg), it can be concluded that the printing temperature for PLA/TPS_F at ∼180 °C is proper.

As the MFR increases, the melt fluidity becomes higher. Thus, it can be assumed that it is easier for the 3DP extruder to push the molten plastic through the die, and therefore, the printing speed can be higher. Nevertheless, it should be remembered that the high MFR may be also related to the low molecular weight of the polymer or its partial degradation under the measurement conditions, which can significantly deteriorate the print quality. Therefore, when analyzing the MFR of filaments for 3DP, one should also simultaneously consider the data derived from DSC and TGA.

Effect of the Print Orientation and Raster Angle on Mechanical Properties (Tensile and Impact Strength and Brittleness). Since there are no specific standards for testing the mechanical properties of FFF 3DP filaments so far, the tensile and impact strength tests were performed taking into account two types of print orientation (*XY* and *ZX*) and three values of raster angle (0, 45, and 90°). The results are summarized in Table 4.

The results of the tensile test of the FF_P samples in the *XY* configuration showed no visible dependence on the raster angle. The Young modulus was in the range of 1.6−1.7 GPa, the tensile strength was around 15−16 MPa, and the elongation at break was at 1.8−3.0%. It was noticed that in the *ZX* orientation, the FF_P samples showed higher strength parameters than that in *XY*, in particular, the Young modulus and elongation at break (∼22 GPa and 4.5%, respectively). Furthermore, the Charpy impact strength of FF_P_*ZX* samples was significantly higher than that of FF_P_*XY*. In turn, considering the raster angle, it was observed that the FF_P_0° system showed the highest overall strength parameters, while the FF_P_90° system exhibited the lowest impact strength (∼7.6 kJ m^{-2}) and the FF_P_45° system had the lower tensile strength.

For the PLA/TPS system, again the samples printed at a raster angle of 90° showed the lowest impact strength; in turn, *ZX*_0° had the highest values of elongation at break (4.6%) as well as tensile (17.8 MPa) and impact strengths (9.7 kJ m^{-2}). However, the Young modulus in both print orientations (*XY* and *ZX*) was

https://doi.org/10.1021/acssuschemeng.0c09413
ACS Sustainable Chem. Eng. 2021, 9, 6923−6938

the highest for the 90° raster angle. In the case of PLA/TPS material, it is difficult to clearly determine which orientation of the printout (*XY* and *ZX*) shows the most favorable values.

As FFF printouts cannot be treated as a continuous material (isotropic material),[37] the assessment of the mechanical properties of such products is difficult. The stress−strain curves of FF_P and PLA/TPS_P are presented in Figure 9. It should be noted that the course of the FF_P curves more closely resembles those of ductile materials than that of PLA/TPS_P. Here,[13] we noticed that the addition of the TPS composition to pure PLA increases the elongation at break while lowering the tensile strength. However, these studies were carried out on injected-molded (continuous) test samples. Thus, it can be assumed that due to insufficient interlayer adhesion of FFF 3D-printed specimens, the effect of increased ductility of PLA/TPS_P samples was not observed.[37]

Summarizing, for both studied filaments, the *ZX*_0° configuration showed the most favorable strength parameters. Similar observations were reported by Chacón et al.[38] In the article, the influence of a number of FFF 3DP parameters on the mechanical properties of PLA was investigated. It was found that the on-edge (*ZX*) print orientation exhibits the most optimal mechanical properties in terms of strength, stiffness, and ductility. However, studies conducted by Dave et al.[39] have shown that the flat orientation (*XY*) of PLA printouts possesses the highest tensile strength. The presented discrepancies indicate the need to take into account additional printing conditions (layer height, flow rate, print speed, temperature conditions, etc.) when comparing the mechanical properties of resulting printouts.[40] Thus, it is highly desirable to standardize methods of assessing the mechanical properties of details obtained with FFF 3DP in order to be able to effectively test and compare new filaments.[37]

Generally, the concept of material brittleness is recognized indirectly—not quantitatively, for example, by evaluation of the results of the tensile test. It is related to the analysis of the fracture surface type or the character of the stress−strain curve. However, these methods constitute a qualitative analysis—they only provide information on whether the material is brittle- or ductile-type. Recently, Brostow et al.[17] proposed an equation that allows for quantitative validation of the material's brittleness. According to this definition, the brittleness (B) is inversely proportional to the product of tensile elongation at break (ε_b) and storage modulus (E'). Thus, when these values increase, the value of B decreases. In our considerations, the storage modulus value is constant for each of the tested materials and equal to 2090 MPa for FF and 1927 MPa for PLA/TPS (data were taken from Figure 7e,f at 25 °C), while the ε_b parameter is variable and depends on the printout configuration (as shown in Table 4). Thus, the samples with the highest ε_b trend are predicted to be the least brittle (B = 0.906 for FF_*ZX*_45° and B = 1.126 for PLA/TPS_*ZX*_0°). However, comparing these materials to others tested by[41] the obtained value of B, which is in the range of around 1.0−4.0 (see Table 4), suggests rather high brittle properties. For comparison, Hytrel (TPE which represents ductile-type materials with a very high elongation at break) exhibits a brittleness (B) of less than 0.1, whereas unmodified polystyrene (known as a brittle-type polymer) has a value of around 9.0.[41]

Effect of Infill Density on Compression Strength. The uniaxial compression test was another study aimed at characterizing the mechanical properties of FF_P and PLA/TPS_P. Samples with three different infill densities were studied (25, 50, and 100%), and the results are displayed in Table 5.

Table 5. Results of the Compression Test for FF_P and PLA/TPS_P Samples

infill density	25%	50%	100%
	yield strength (MPa)		
FF_P	20.44 ± 0.63	34.64 ± 4.77	82.49 ± 8.32
	compression strength (MPa)		
PLA/TPS_P	9.44 ± 2.53	19.65 ± 3.83	30.13 ± 0.91

The compressive strength of the printouts increases with the increase in the degree of infill.[42] This effect is more visible for the FF_P samples where a more than 4-fold increase in the yield strength was noted. For PLA/TPS_P, the increase in compressive strength was proportional to the increase in the infill density, reaching a value of ∼30 MPa (100% infill).

The course of the compression curves is presented in Figure 10. The stress−strain curves of the FF_P samples showed a clear yield point (*), while for PLA/TPS_P, the course is mild and characteristic for elastic polymers (Figure 10b). Therefore, for PLA/TPS_P samples, the inflection point of the curves (marked as #) was adopted as the compressive strength.

Water Contact Angle. During the measurement of the contact angle, significant changes in the wettability values were noticed depending on the direction of the sample arrangement on the measuring table and thus the sample's raster angle. Changing the raster angle to 90° significantly increased the hydrophobicity of both samples. The wCA of FF_P was ∼75 for 0° raster angle and around 111 for 90° raster angle, which correspond to the moderately hydrophilic to hydrophobic surface nature (Table 6). PLA/TPS_P showed a more hydrophilic surface with the wCA ranging from 63 to 81°. The difference in wettability between FF_P and PLA/TPS_P is related to the presence of TPS, which, being a highly hydrophilic material, lowers the contact angle of PLA.[43] However, such large differences in the wCA depending on the raster angle should be considered in terms of surface morphology and not of the material properties.

According to the literature, PLA shows poor hydrophilicity in the range 70−95° of the static wCA.[44] However, these values refer to a solid PLA surface (continuous material, most commonly obtained by plastic molding) and not to FFF 3DP printouts, which are characterized by many defects (voids) and discontinuities in the structure.[45]

The surface of the FFF 3DP samples consists of connected layers of polymer fibers of a given thickness and height. As a result, the printed surface (on a micro-scale) is wavy. Thus, due to the unevenness of the surface, the applied drop of water wets the material depending on the direction of the fibers on which it is placed, which radically changes the contact angle. The above considerations are confirmed by the Modi and Prakash[46] study, in which they proved that the orientation and raster angle of the FFF 3D-printed parts significantly affect the wettability of PLA. They found huge differences in the values of the PLA wCA, ranging from 40 to 75° for 0 and 90° raster angles, respectively.

Therefore, we believe that the standard method of contact angle measurement does not provide reliable data. The influence of the surface shape on the wCA should be minimized by significantly reducing the measuring droplet. Otherwise, the sample's data regarding the printing parameters and printout

https://doi.org/10.1021/acssuschemeng.0c09413
ACS Sustainable Chem. Eng. 2021, 9, 6923−6938

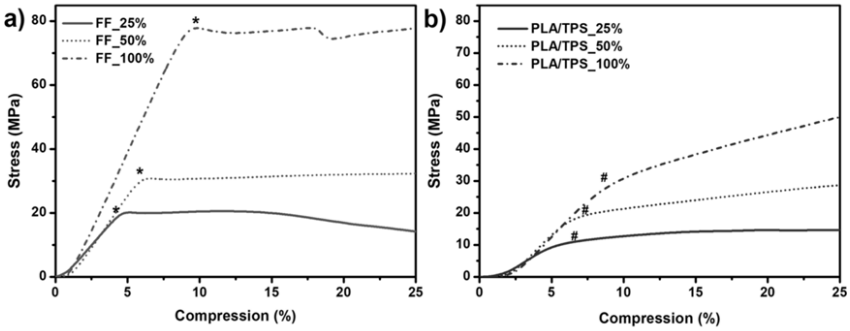

Figure 10. Averaged compressive stress−strain curves of FF_P (a) and PLA/TPS_P (b) depending on the infill density. * Yield strength; # compression strength.

Table 6. CAs of FF_P and PLA/TPS_P with Different Raster Angles (0 and 90°)

Sample	FF_P		PLA/TPS_P	
Raster angle	0°	90°	0°	90°
wCA (°)	75.77 ± 4.35	111.46 ± 4.29	63.03 ± 1.79	81.54 ± 2.43

design should be precisely specified to allow the reliable comparison of the printout surface properties.

Incubation of the Filaments in 0.1 PBS Solution and Canola Oil (Mass Loss, Swelling, and pH Measurements). PLA, as a representative of biodegradable polymers, undergoes hydrolytic degradation in the PBS environment, which might proceed through the surface or bulk erosion mechanism.[47] However, in the case of solid PLA with a relatively high molecular weight (so-called injection or extrusion grades), the PBS degradation might proceed up to 5 years.[48] Therefore, PLA belongs to the long-term degrading biopolymers. Besides temperature, pH, and molecular weight, the ability of water to diffuse into the PLA matrix is the main factor that controls the degradation process.[47] Consequently, to estimate the degradability of both filaments, the incubation in 0.1 M PBS solution at 37 °C for 30 days was performed. During the PBS incubation, the weight change, the pH of the solution, and SEM images were recorded. Figure 11a,b represents the mass loss of the samples and the pH change of the PBS buffer with respect to the immersion time for FF_F and PLA/TPS_F, respectively.

The recorded change in the weight of the FF filament during 30 days of PBS incubation not exceeding 0.1%, as well as the relatively constant pH (7.50−7.48), indicates the stability of the material under given conditions. This is confirmed by SEM photos, which show no changes in the morphology of the surface or the cross-section of FF_F (Figure S3). This is in line with other studies of PLA degradation in the PBS medium, in which no mass changes or drops in pH were recorded during the 56 days of study.[49]

In turn, during the incubation of the PLA/TPS filament in PBS, significant changes in both mass and pH were noted. Thermoplastic starch, as a material sensitive to water, enhances significantly the degradation process of the PLA/TPS filament. The mean mass loss after the first hour was 1.3%, and after 3 days, it increased sharply to 13%. At the end of the study, a mass loss of 14.5% was noted. At the same time, a drop in pH was observed, down to 7.38 after 3 days and 7.27 after 30 days of incubation. The acidification of the electrolyte could be related to material hydrolysis which results in oligomer and monomer formation.[50] The resulting PLA-carboxyl end groups,[51] as well as TPS-origin glucose, glycerin, or ESO, could lower the pH due to the dissociation in the PBS solution. The SEM images (Figure S3) of the PLA-TPS_F surface after 30 days of incubation show numerous cracks and discontinuities in the structure (red arrows), while the cross-view shows the formation of a fibrous-like structure that may have arisen as a result of washing out of the TPS particles from the PLA matrix. The resulting surface defects of the PLA/TPS structure may additionally facilitate the diffusion of water in the inner part of the filament, and thus increase the susceptibility to degradation of PLA itself.[52] Such an effect is highly desirable as we consider the developed filament to be biodegradable.

To confirm the above considerations, the FTIR spectra of the filament samples before (0 d) and after 30 days (PBS_30d) of PBS incubation were compared (Figure 11e,f). In the case of FF_PBS_30d, the spectrum did not change significantly. There was a slight decrease in the intensity of the band derived from the C═O group (1748 cm^{-1}), while the rest of the spectrum remained intact. The degradation of PLA/TPS_F proceeded mostly through the destruction of bonds originating from TPS (−OH 3310 cm^{-1}, −C−O 1020 cm^{-1}, and −COH 1080 cm^{-1}). The PLA-origin aliphatic CH_2 and ester groups (C═O 1747 cm^{-1}) were also broken. Thus, it can be assumed that the erosion of TPS and the resulting surface roughness, cracks, and voids promote hydration and thus facilitate degradation of PLA.

https://doi.org/10.1021/acssuschemeng.0c09413
ACS Sustainable Chem. Eng. 2021, 9, 6923−6938

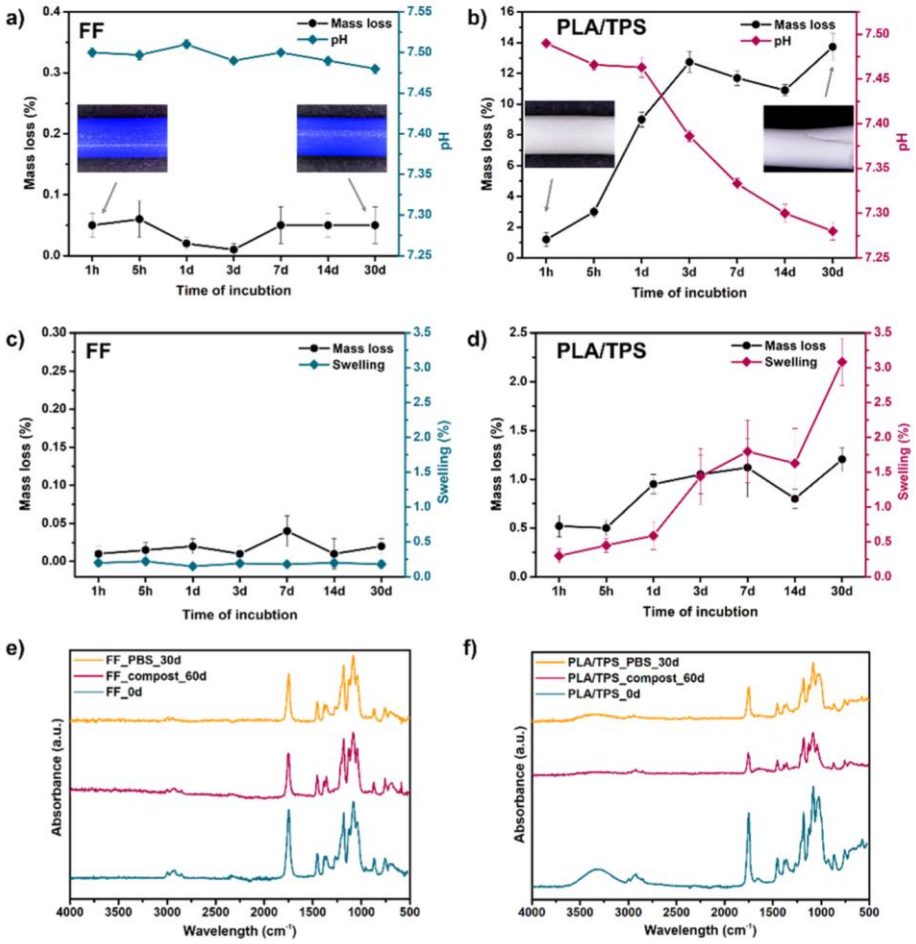

Figure 11. Results of degradation studies in 0.1 M PBS solution of (a) FF_F and (b) PLA/TPS_F. SEM images showing the process of PBS incubation are presented in the Supporting Information (Figure S3). The results of incubation in canola oil of (c) FF_F and (d) PLA/TPS_F. FTIR spectra of (e) FF_F and (f) PLA/TPS_F after 30 days of incubation in PBS and 60 days of composting.

For further characterization of studied filaments, the mass loss and swelling in contact with food-grade canola oil was investigated (Figure 11c,d). As expected, the FF filament showed high resistance to oil. Both the weight loss and the swelling ratio of the samples were unnoticeable, whereas the PLA/TPS_F swelling was ∼3% and the weight loss was 1.2% after 30 days of testing. Thus, PLA/TPS_F shows moderate resistance to oil contact.

Results of Laboratory-Scale Composting. The laboratory composting study was conducted to assess the filament's susceptibility to disintegration in composting conditions. It should be noted that this study cannot be regarded as an assessment of the biodegradability of the bioplastic.[53] According to the EN 13432 standard, bioplastics marked as compostable should show a disintegration of 90% (into pieces smaller than a sieve with 2 mm of the mesh) over 90 days at 58 °C in the simulated compost.

Figure 12 shows the results of the composting test of FF and PLA/TPS 3D printouts. FF_P samples exhibited high composting resistance. There was no change in the weight during the test (Figure 12a), and the morphology of the samples was not intact. The discoloration of the samples was observed from about the 30th day of composting (Figure 12b). The surface of the sample remained homogeneous and smooth (Figure 12c) up to the 50th day of the study. Single surface cracks were recorded only after 60 days (Figure S4). However, the recorded FTIR spectrum of the sample after 60 days of the test (Figure 11e, FF_compost_60d) showed a noticeable decrease in the intensity of the bands, resulting from the vibration of the C═O (stretching at 1748 cm^{-1} and bending at 1264 cm^{-1}) and C−O (stretching at 1043 cm^{-1}) bonds was

https://doi.org/10.1021/acssuschemeng.0c09413
ACS Sustainable Chem. Eng. 2021, 9, 6923−6938

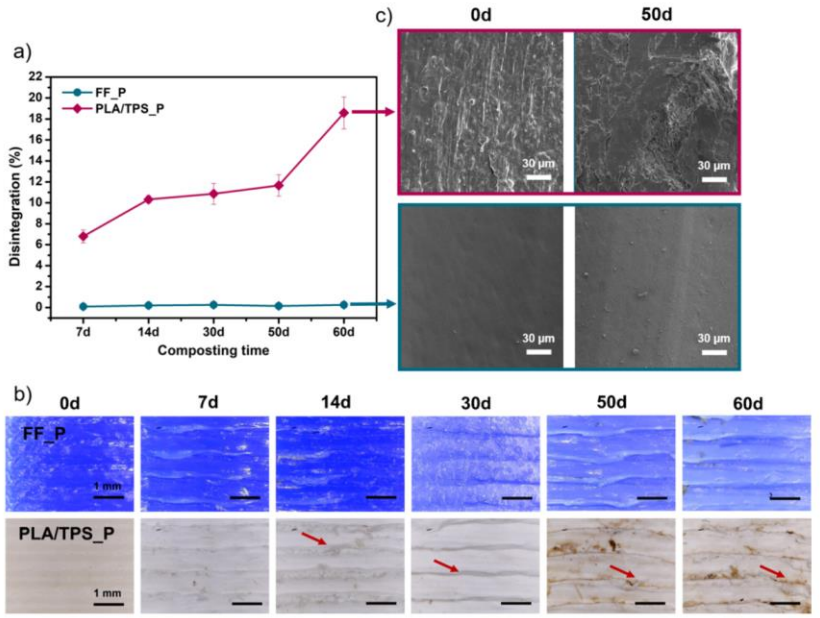

Figure 12. Results of a laboratory-scale composting test of FF_P and PLA/TPS_P: (a) disintegration degree over composting time, (b) optical microscopy images of samples before (0 d) and after 7, 14, 30, 50, and 60 days of composting (red arrows indicate progressive cracks and discontinuities of the PLA/TPS sample surface), and (c) representative SEM micrographs of the sample surface before (0 d) and after 50 days of composting (more SEM images are presented in the Supporting Information; Figures S4 and S5).

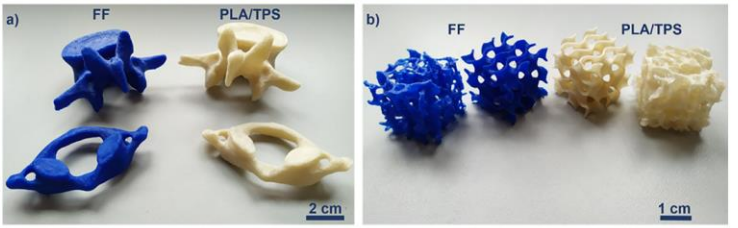

Figure 13. FFF 3D-printed FF and PLA/TPS complex structures: (a) personalized anatomical models of vertebrae C1 (atlas) and L3, (b) porous gyroid, and cancellous bone-like structure printouts. Detailed information on models and the 3DP process is presented in the Supporting Information (Figure S2 and Tables S2 and S3). More optical photos of the printouts can be found in Figure S6.

observed, which may indicate the initial destruction of the surface layer of the FF_P printouts. Nevertheless, overall, the FF_P was left practically intact under the 60 days of simulated composting. In turn, PLA/TPS_P showed an evident trend of an increased degree of disintegration during the composting time. Already after 7 days of incubation, a disintegration degree of 7% was noted, and at the end of the study, it reached over 18% (Figure 12a). Optical microscopy images showed the formation of cracks and defects on the sample's surface from the 14th day of testing. SEM micrographs revealed a high roughness and heterogeneity of the PLA/TPS_P surface compared to that of FF_P. At the beginning of composting, the TPS cavities were observed (14th day), where pinholes in the PLA/TPS_P structures were formed (Figure S5). The initially changed surface started to erode, and the destruction proceeded deeper into the structure, thereby destroying the sample in its entire volume. The FTIR spectrum confirms the above considerations (Figure 11f). There was a clear degradation of bonds originating mainly from TPS. Signals from vibrations of −OH (3310 cm^{-1}) and C−O groups (a glucose ring at 1020 cm^{-1}) were flattened, and the intensity of the whole spectrum significantly decreased. Therefore, the addition of TPS contributed to an increase in the susceptibility to the disintegration of PLA under composting conditions. This is most likely related to the facilitated penetration of moisture into the material and the presence of glucose (as a result of TPS degradation), which acts as a nutrient medium for the microorganisms present in the compost.[52]

The results of laboratory composting presented by Arrieta et al.[54,55] shows a disintegration rate of PLA of over 90% within 35 days. In turn, the study by Quiles-Carrillo et al.[56] conducted at

https://doi.org/10.1021/acssuschemeng.0c09413
ACS Sustainable Chem. Eng. 2021, 9, 6923−6938

the same conditions (ISO 20200) reveals a disintegration of the PLA/TPS (40 wt % TPS) blend of over 90% after 57 days of composting. However, it should be noted that the above data refer to samples in the form of thin films with thicknesses of 0.1 and 1 mm, respectively. Therefore, it is difficult to compare these results with the values obtained for solid FF and PLA/TPS printouts. However, the findings of our earlier studies on the PLA/TPS/ESO composition (which was used to form the PLA/TPS filament) revealed that this material was completely disintegrated after 57 days of simulated composting[13] (the study was carried out on thin sheets with 2 mm thickness).

Printability Assessment—FFF 3D Printing of Anatomical Models and Porous Structures. Finally, to illustrate the usefulness of the developed PLA/TPS filament, complex-shaped details were printed and compared with those obtained from the commercial filament. The resulting printouts are presented in Figure 13. To allow a fair comparison of the printability of both filaments, they were printed with the same 3D printing settings. The only difference was the printing temperature, which was 215 °C for the FF_F and 185 °C for the PLA/TPS filament.

First, the personalized STL files of two types of vertebrae were converted from an abdominal CT scan. The scheme illustrating the process of segmentation and conversion is illustrated in Figure S2 (the Supporting Information). Thus, obtained projects required the use of support structures to ensure a good quality of printouts; hence, detachable-type supports were introduced. The printing process in both cases ran smoothly, and the printing times were ∼5.5 and 2 h for L3 and C1 vertebrae, respectively. As a result, personalized anatomical models with high surface mapping and quality and good dimensional stability were obtained. No shrinkage effect was noticed. Printouts with the PLA/TPS filament did not differ in quality in any way from those obtained from FF_F. Similar observations were made in the case of 3D printing porous structures (which were printed without the use of support structures). The gyroid project was very well mapped. No defects or discontinuities in the structure were observed for both the FF and PLA/TPS gyroid printouts (Figure 13b). Nevertheless, some issues were encountered in cancellous bone-like printouts. As this sponge-like structure possesses many overhangs and very thin walls, it is highly demanding for FFF 3D printing. The printout from the FF filament turned out to be defectless. In turn, in the case of PLA/TPS, some defects of the printout surface were noted. Pores of the cancellous bone-like structure were partially blocked by the so-called stringing, that is, thin threads made of the material leaking out of the printing nozzle (hotend) in an uncontrolled manner. However, this phenomenon can be minimized by changing the printing parameters such as speed, temperature, or the retraction distance. More challenges faced during 3DP with the PLA/TPS filament are described in Table S5 (the Supporting Information).

Summarizing, we can state that our developed bio-filament is suitable for effective FFF 3DP, and the printouts thus formed do not differ in quality from those obtained using available commercial filaments.

■ CONCLUSIONS

In this work, we presented an extensive characteristic of a self-made bio-filament for FFF 3DP, consisting of PLA modified with TPS. For comparative purposes, the properties and printability of the PLA/TPS filament were confronted with those of the FlashForge PLA filament—the commercially available FFF filament. Our approach, namely, replacing up to 40% of PLA with TPS, resulted in considerable improvement of hydrophilicity, susceptibility to hydrolytic degradation, and thus enhancement of compostability in contrast to that of commercial PLA printouts. Furthermore, we demonstrated that the PLA/TPS filament shows a comparable printability to its commercial counterpart and is suitable for FFF 3DP of both personalized anatomical models as well as complex porous structures. We also believe that the developed filament might challenge traditional petroleum-based filaments as a more environmentally friendly alternative.

Furthermore, our results challenge/question commercial terms of marking filaments (e.g., PLA) as "biodegradable/eco-friendly". The use of a biopolymer as a base material cannot determine its final "bio-properties". The addition of printability-improving agents (oils and plasticizers) or fillers and pigments, at the stage of filament formation, may cause numerous changes in the pristine properties of the biopolymer (including a decrease in biodegradability). Due to that, the final product cannot be recognized as "eco-friendly", although it is based on biodegradable polymers. Therefore, to verify the filament's "eco-friendly" character, additional research should be carried out to establish whether a final product is truly biodegradable or it is only partly bio-based.

■ ASSOCIATED CONTENT

Supporting Information

The Supporting Information is available free of charge at https://pubs.acs.org/doi/10.1021/acssuschemeng.0c09413.

Test sample preparation; preparation and description of the virtual models; SEM images of the degradation study in 0.1 M PBS; laboratory composting—compost composition and SEM images; images of printed anatomical models and porous structures; and description of challenges faced during 3D printing with the PLA/TPS filament (PDF)

■ AUTHOR INFORMATION

Corresponding Author

Agnieszka Haryńska − *Department of Polymers Technology, Faculty of Chemistry, Gdansk University of Technology (GUT), 80-233 Gdansk, Poland;* orcid.org/0000-0001-8017-6070; Email: agnieszka.harynska@pg.edu.pl

Authors

Helena Janik − *Department of Polymers Technology, Faculty of Chemistry, Gdansk University of Technology (GUT), 80-233 Gdansk, Poland*

Maciej Sienkiewicz − *Department of Polymers Technology, Faculty of Chemistry, Gdansk University of Technology (GUT), 80-233 Gdansk, Poland*

Barbara Mikolaszek − *Department of Pharmaceutical Technology, Faculty of Pharmacy, Medical University of Gdansk, 80-416 Gdansk, Poland;* orcid.org/0000-0001-5894-7705

Justyna Kucińska-Lipka − *Department of Polymers Technology, Faculty of Chemistry, Gdansk University of Technology (GUT), 80-233 Gdansk, Poland*

Complete contact information is available at: https://pubs.acs.org/10.1021/acssuschemeng.0c09413

Author Contributions

A.H. conceptualization, methodology, software, validation, investigation, writing—original draft, writing—review and editing, visualization, project administration. H.J. conceptualization, resources, writing—review and editing. M.S. material conceptualization, writing—review and editing. B.M. investigation (SEM), writing—review and editing. J.K.-L. resources, writing—review and editing.

Funding

Part of the research realized at the Gdansk University of Technology (GUT) was financed by the Ministry of National Education via the Knowledge & Technology Transfer Center at the GUT under the program Innovation Incubator Plus.

Notes

The authors declare no competing financial interest.

The raw data required to reproduce these findings cannot be shared at this time due to technical or time limitations. Nevertheless, they can be made available on request.

■ ACKNOWLEDGMENTS

We acknowledge Paulina Kosmela for technical help in conducting DSC, TGA, and DMA studies.

■ REFERENCES

(1) Wickramasinghe, S.; Do, T.; Tran, P. FDM-Based 3D Printing of Polymer and Associated Composite: A Review on Mechanical Properties, Defects and Treatments. *Polymers* **2020**, *12*, 1529.

(2) Sanchez-Rexach, E.; Johnston, T. G.; Jehanno, C.; Sardon, H.; Nelson, A. Sustainable Materials and Chemical Processes for Additive Manufacturing. *Chem. Mater.* **2020**, *32*, 7105−7119.

(3) Filgueira, D.; Holmen, S.; Melbø, J. K.; Moldes, D.; Echtermeyer, A. T.; Chinga-Carrasco, G. Enzymatic-Assisted Modification of Thermomechanical Pulp Fibers to Improve the Interfacial Adhesion with Poly(Lactic Acid) for 3D Printing. *ACS Sustainable Chem. Eng.* **2017**, *5*, 9338−9346.

(4) Song, X.; He, W.; Yang, S.; Huang, G.; Yang, T. Fused Deposition Modeling of Poly (Lactic Acid)/Walnut Shell Biocomposite Filaments-Surface Treatment and Properties. *Appl. Sci.* **2019**, *9*, 4892.

(5) Chang, Y.-C.; Chen, Y.; Ning, J.; Hao, C.; Rock, M.; Amer, M.; Feng, S.; Falahati, M.; Wang, L.-J.; Chen, R. K.; Zhang, J.; Ding, J.-L.; Li, L. No Such Thing as Trash: A 3D-Printable Polymer Composite Composed of Oil-Extracted Spent Coffee Grounds and Polylactic Acid with Enhanced Impact Toughness. *ACS Sustainable Chem. Eng.* **2019**, *7*, 15304−15310.

(6) Idrees, M.; Jeelani, S.; Rangari, V. Three-Dimensional-Printed Sustainable Biochar-Recycled PET Composites. *ACS Sustainable Chem. Eng.* **2018**, *6*, 13940−13948.

(7) Herrero, M.; Peng, F.; Núñez Carrero, K. C.; Merino, J. C.; Vogt, B. D. Renewable Nanocomposites for Additive Manufacturing Using Fused Filament Fabrication. *ACS Sustainable Chem. Eng.* **2018**, *6*, 12393−12402.

(8) Giubilini, A.; Siqueira, G.; Clemens, F. J.; Sciancalepore, C.; Messori, M.; Nystrom, G.; Bondioli, F. 3D Printing Nanocellulose-Poly(3-Hydroxybutyrate-Co-3-Hydroxyhexanoate) Biodegradable Composites by Fused Deposition Modeling. *ACS Sustainable Chem. Eng.* **2020**, *8*, 27.

(9) Kuo, C.-C.; Liu, L.-C.; Teng, W.-F.; Chang, H.-Y.; Chien, F.-M.; Liao, S.-J.; Kuo, W.-F.; Chen, C.-M. Preparation of Starch/Acrylonitrile-Butadiene-Styrene Copolymers (ABS) Biomass Alloys and Their Feasible Evaluation for 3D Printing Applications. *Composites, Part B* **2016**, *86*, 36−39.

(10) Ou-Yang, Q.; Guo, B.; Xu, J. Preparation and Characterization of Poly(Butylene Succinate)/Polylactide Blends for Fused Deposition Modeling 3D Printing. *ACS Omega* **2018**, *3*, 14309−14317.

(11) Andrzejewski, J.; Cheng, J.; Anstey, A.; Mohanty, A. K.; Misra, M. Development of Toughened Blends of Poly(Lactic Acid) and Poly(Butylene Adipate- Co-Terephthalate) for 3D Printing Applications: Compatibilization Methods and Material Performance Evaluation. *ACS Sustainable Chem. Eng.* **2020**, *8*, 6576−6589.

(12) Tanabe, I. Double-ECO Model Technologies for an Environmentally-Friendly Manufacturing. *Procedia CIRP* **2016**, *48*, 495−501.

(13) Przybytek, A.; Sienkiewicz, M.; Kucińska-Lipka, J.; Janik, H. Preparation and Characterization of Biodegradable and Compostable PLA/TPS/ESO Compositions. *Ind. Crops Prod.* **2018**, *122*, 375.

(14) Haryńska, A.; Carayon, I.; Kosmela, P.; Brillowska-Dąbrowska, A.; Łapiński, M.; Kucińska-Lipka, J.; Janik, H. Processing of Polyester-Urethane Filament and Characterization of FFF 3D Printed Elastic Porous Structures with Potential in Cancellous Bone Tissue Engineering. *Materials* **2020**, *13*, 4457.

(15) Kikinis, R.; Pieper, S. D.; Vosburgh, K. G. 3D Slicer: A Platform for Subject-Specific Image Analysis, Visualization, and Clinical Support. In *Intraoperative Imaging and Image-Guided Therapy*; Jolesz, F. A., Ed.; Springer New York: New York, NY, 2014; pp 277−289.

(16) Pyda, M.; Bopp, R. C.; Wunderlich, B. Heat Capacity of Poly(Lactic Acid). *J. Chem. Thermodyn.* **2004**, *36*, 731−742.

(17) Brostow, W.; Hagg Lobland, H. E.; Narkis, M. Sliding Wear, Viscoelasticity, and Brittleness of Polymers. *J. Mater. Res.* **2006**, *21*, 2422−2428.

(18) Nobrega, M. M.; Olivato, J. B.; Müller, C. M. O.; Yamashita, F. Biodegradable Starch-Based Films Containing Saturated Fatty Acids: Thermal, Infrared and Raman Spectroscopic Characterization. *Polimeros* **2012**, *22*, 475−480.

(19) Jia, W.; Luo, Y.; Yu, J.; Liu, B.; Hu, M.; Chai, L.; Wang, C. Effects of High-Repetition-Rate Femtosecond Laser Micromachining on the Physical and Chemical Properties of Polylactide (PLA). *Opt. Express* **2015**, *23*, 26932.

(20) Antończak, A. J.; Stępak, B. D.; Szustakiewicz, K.; Wójcik, M. R.; Abramski, K. M. Degradation of Poly(l-Lactide) under CO2 Laser Treatment above the Ablation Threshold. *Polym. Degrad. Stab.* **2014**, *109*, 97−105.

(21) Mallick, S.; Ahmad, Z.; Touati, F.; Bhadra, J.; Shakoor, R. A.; Al-Thani, N. J. PLA-TiO2 Nanocomposites: Thermal, Morphological, Structural, and Humidity Sensing Properties. *Ceram. Int.* **2018**, *44*, 16507−16513.

(22) Haryńska, A.; Carayon, I.; Kosmela, P.; Szeliski, K.; Łapiński, M.; Pokrywczyńska, M.; Kucińska-Lipka, J.; Janik, H. A Comprehensive Evaluation of Flexible FDM/FFF 3D Printing Filament as a Potential Material in Medical Application. *Eur. Polym. J.* **2020**, *138*, 109958.

(23) Schrader, B. Raman Spectroscopy of Mineral Oil Products. Part I: NIR/FT-Raman Spectra of Polycyclic Aromatic Hydrocarbons. *Appl. Spectrosc.* **1991**, *45*, 1230−1232.

(24) Peidayesh, H.; Ahmadi, Z.; Khonakdar, H. A.; Abdouss, M.; Chodák, I. Fabrication and Properties of Thermoplastic Starch/Montmorillonite Composite Using Dialdehyde Starch as a Crosslinker. *Polym. Int.* **2020**, *69*, 317−327.

(25) Tao, Y.; Shao, J.; Li, P.; Shi, S. Q. Application of a Thermoplastic Polyurethane/Polylactic Acid Composite Filament for 3D-Printed Personalized Orthosis. *Mater. Technol.* **2019**, *53*, 71−76.

(26) Bulatović, V. O.; Mandić, V.; Kučić Grgić, D.; Ivančić, A. Biodegradable Polymer Blends Based on Thermoplastic Starch. *J. Polym. Environ.* **2020**, *29*, 492.

(27) Teixeira, E. D. M.; De Campos, A.; Marconcini, J. M.; Bondancia, T. J.; Wood, D.; Klamczynski, A.; Mattoso, L. H. C.; Glenn, G. M. Starch/Fiber/Poly(Lactic Acid) Foam and Compressed Foam Composites. *RSC Adv.* **2014**, *4*, 6616−6623.

(28) Kalogeras, I. M.; Hagg Lobland, H. E. The Nature of the Glassy State: Structure and Glass Transitions. *J. Mater. Educ.* **2012**, *34*, 69−94.

(29) Kalogeras, I. M.; Brostow, W. Glass Transition Temperatures in Binary Polymer Blends. *J. Polym. Sci., Part B: Polym. Phys.* **2009**, *47*, 80−95.

(30) Matos, B. D. M.; Rocha, V.; da Silva, E. J.; Moro, F. H.; Bottene, A. C.; Ribeiro, C. A.; dos Santos Dias, D.; Antonio, S. G.; do Amaral, A. C.; Cruz, S. A.; de Oliveira Barud, H. G.; Silva Barud, H. d. Evaluation of Commercially Available Polylactic Acid (PLA) Filaments for 3D Printing Applications. *J. Therm. Anal. Calorim.* **2019**, *137*, 555−562.

(31) Benwood, C.; Anstey, A.; Andrzejewski, J.; Misra, M.; Mohanty, A. K. Improving the Impact Strength and Heat Resistance of 3D Printed Models: Structure, Property, and Processing Correlationships during Fused Deposition Modeling (FDM) of Poly(Lactic Acid). *ACS Omega* **2018**, *3*, 4400−4411.
(32) Turco, R.; Ortega-Toro, R.; Tesser, R.; Mallardo, S.; Collazo-Bigliardi, S.; Boix, A. C.; Malinconico, M.; Rippa, M.; Di Serio, M.; Santagata, G. Poly (Lactic Acid)/Thermoplastic Starch Films: Effect of Cardoon Seed Epoxidized Oil on Their Chemicophysical, Mechanical, and Barrier Properties. *Coatings* **2019**, *9*, 574.
(33) Menard, K. P. *Dynamic Mechanical Analysis: A Practical Introduction*, 2nd ed.; CRC Press, 2008.
(34) B, A.; Suin, S.; Khatua, B. B. Highly Exfoliated Eco-Friendly Thermoplastic Starch (TPS)/Poly (Lactic Acid)(PLA)/Clay Nanocomposites Using Unmodified Nanoclay. *Carbohydr. Polym.* **2014**, *110*, 430.
(35) Park, H.-M.; Li, X.; Jin, C.-Z.; Park, C.-Y.; Cho, W.-J.; Ha, C.-S. Preparation and Properties of Biodegradable Thermoplastic Starch/Clay Hybrids. *Macromol. Mater. Eng.* **2002**, *287*, 553−558.
(36) Wang, S.; Capoen, L.; D'hooge, D. R.; Cardon, L. Can the Melt Flow Index Be Used to Predict the Success of Fused Deposition Modelling of Commercial Poly(Lactic Acid) Filaments into 3D Printed Materials? *Plast., Rubber Compos.* **2018**, *47*, 9−16.
(37) García-Domínguez, A.; Claver, J.; Camacho, A. M.; Sebastián, M. A. Considerations on the Applicability of Test Methods for Mechanical Characterization of Materials Manufactured by FDM. *Materials* **2020**, *13*, 28.
(38) Chacón, J. M.; Caminero, M. A.; García-Plaza, E.; Núñez, P. J. Additive Manufacturing of PLA Structures Using Fused Deposition Modelling: Effect of Process Parameters on Mechanical Properties and Their Optimal Selection. *Mater. Des.* **2017**, *124*, 143−157.
(39) Dave, H. K.; Patadiya, N. H.; Prajapati, A. R.; Rajpurohit, S. R. Effect of Infill Pattern and Infill Density at Varying Part Orientation on Tensile Properties of Fused Deposition Modeling-Printed Poly-Lactic Acid Part. *Proc. Inst. Mech. Eng., Part C* **2019**, 1−17.
(40) Popescu, D.; Zapciu, A.; Amza, C.; Baciu, F.; Marinescu, R. FDM Process Parameters Influence over the Mechanical Properties of Polymer Specimens: A Review. *Polym. Test.* **2018**, *69*, 157−166.
(41) Brostow, W.; Hagg Lobland, H. E. Brittleness of Materials: Implications for Composites and a Relation to Impact Strength. *J. Mater. Sci.* **2010**, *45*, 242−250.
(42) Fadhil Alani, T.; Ali, H.; Abbas, D.; Mohammad Othman, D.; Basil Ali, H.; Author, C. Effect of Infill Parameter on Compression Property in FDM Process. *Int. J. Eng. Res. Appl.* **2017**, *7*, 16−19.
(43) Esmaeili, M.; Pircheraghi, G.; Bagheri, R.; Altstädt, V. Poly(Lactic Acid)/Coplasticized Thermoplastic Starch Blend: Effect of Plasticizer Migration on Rheological and Mechanical Properties. *Polym. Adv. Technol.* **2019**, *30*, 839−851.
(44) Biresaw, G.; Carriere, C. J. Correlation between Mechanical Adhesion and Interfacial Properties of Starch/Biodegradable Polyester Blends. *J. Polym. Sci., Part B: Polym. Phys.* **2001**, *39*, 920−930.
(45) Tronvoll, S. A.; Welo, T.; Elverum, C. W. The Effects of Voids on Structural Properties of Fused Deposition Modelled Parts: A Probabilistic Approach. *Int. J. Adv. Manuf. Technol.* **2018**, *97*, 3607−3618.
(46) Modi, U.; Prakash, S. Wettability of 3D Printed Polylactic Acid (PLA) Parts. *AIP Conf. Proc.* **2019**, *2148*, 030052.
(47) Elsawy, M. A.; Kim, K.-H.; Park, J.-W.; Deep, A. Hydrolytic Degradation of Polylactic Acid (PLA) and Its Composites. *Renew. Sustain. Energy Rev.* **2017**, *79*, 1346−1352.
(48) Saha, S. K.; Tsuji, H. Effects of Molecular Weight and Small Amounts of D-Lactide Units on Hydrolytic Degradation of Poly(l-Lactic Acid)S. *Polym. Degrad. Stab.* **2006**, *91*, 1665−1673.
(49) Chouzouri, G.; Xanthos, M. Degradation of Aliphatic Polyesters in the Presence of Inorganic Fillers. *J. Plast. Film Sheeting* **2007**, *23*, 19−36.
(50) Gorrasi, G.; Pantani, R. Hydrolysis and Biodegradation of Poly(Lactic Acid). *Advances in Polymer Science*; Springer New York LLC, 2018; Vol. 279, pp 119−151.
(51) Chamas, A.; Moon, H.; Zheng, J.; Qiu, Y.; Tabassum, T.; Jang, J. H.; Abu-Omar, M.; Scott, S. L.; Suh, S. Degradation Rates of Plastics in the Environment. *ACS Sustainable Chem. Eng.* **2020**, *8*, 3494−3511.
(52) Rodrigues, C. A.; Tofanello, A.; Nantes, I. L.; Rosa, D. S. Biological Oxidative Mechanisms for Degradation of Poly(Lactic Acid) Blended with Thermoplastic Starch. *ACS Sustainable Chem. Eng.* **2015**, *3*, 2756−2766.
(53) Ruggero, F.; Gori, R.; Lubello, C. Methodologies to Assess Biodegradation of Bioplastics during Aerobic Composting and Anaerobic Digestion: A Review. *Waste Manage. Res.* **2019**, *37*, 959−975.
(54) Arrieta, M. P.; López, J.; Rayón, E.; Jiménez, A. Disintegrability under Composting Conditions of Plasticized PLA−PHB Blends. *Polym. Degrad. Stab.* **2014**, *108*, 307−318.
(55) Arrieta, M. P.; López, J.; Hernández, A.; Rayón, E. Ternary PLA-PHB-Limonene Blends Intended for Biodegradable Food Packaging Applications. *Eur. Polym. J.* **2014**, *50*, 255−270.
(56) Quiles-Carrillo, L.; Montanes, N.; Pineiro, F.; Jorda-Vilaplana, A.; Torres-Giner, S. Ductility and Toughness Improvement of Injection-Molded Compostable Pieces of Polylactide by Melt Blending with Poly(ε-Caprolactone) and Thermoplastic Starch. *Materials* **2018**, *11*, 2138.

https://doi.org/10.1021/acssuschemeng.0c09413
ACS Sustainable Chem. Eng. 2021, 9, 6923−6938

SUPPORTING INFORMATION

PLA–potato thermoplastic starch filament as a sustainable alternative to conventional PLA filament: processing, characterization and FFF 3D printing

Agnieszka Haryńska[1*], Helena Janik[1], Maciej Sienkiewicz[1], Barbara Mikolaszek[2], Justyna Kucińska-Lipka[1]

[1] Department of Polymers Technology, Faculty of Chemistry, Gdansk University of Technology (GUT), Narutowicza Street 11/12, 80-233, Gdansk, Poland

[2] Department of Pharmaceutical Technology, Faculty of Pharmacy, Medical University of Gdansk, Al. Gen. J. Hallera 107, 80-416, Gdansk, Poland

* Correspondence: agnieszka.harynska@pg.edu.pl

Total number of pages: 7 (Page S1-S7)

Total number of tables: 5 (Table S1-S5)

Total number of figures: 6 (Figure S1-S6)

Contents

1. Preparation of the samples for testing – 3D printing settings, dimentions of samples

Table S1 3D printing settings of the test samples used for the characterization of both tested materials.

3D printing parameter	FF	PLA/TPS
Extrusion temperature (°C)	215	180
Bed temperature (°C)	60	
Cooling	Fan on	
Printing speed (mm s^{-1})	20	
Layer height (mm)	0.2	
Nozzle diameter (mm)	0.4	
Shell number	2	

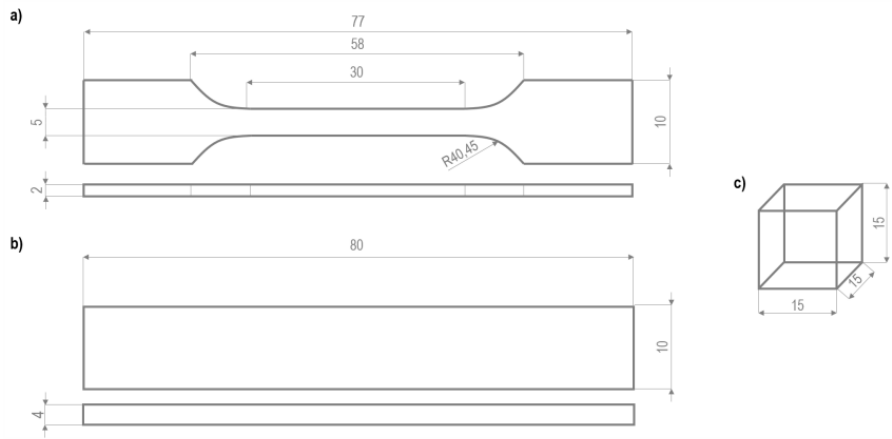

Figure S1 Dimentions of tested samples. a) dumbbell-shaped tensile specimen (ISO 527-2, 1BA), b) Charpy impact test specimen (ISO 179-1, unnotched), c) cubic compression test specimen

2. Preparation and description of the virtual models (vertebra C1, L3, cancellous bone, gyroid)

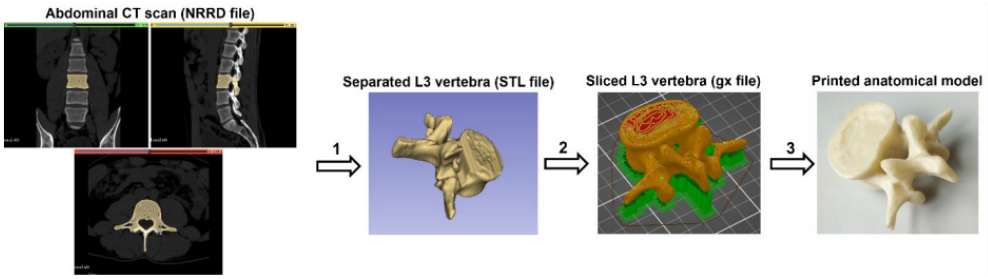

Figure S2 Scheme of the procedure used during the preparation of personalized anatomical models (vertebra C1, and L3). The scale of printouts 1:1

1 → Conversion of CT scan into STL file (segmentation, slicing, modeling)

2 → Conversion of STL file into gx code (optimization, assigning printing settinngs, supports architecture, slicing)

3 → 3D printing and post-processing/finishing (supports removal, polishing)

Table S2 View of models of porous structures. The gyroid structure was designed in Autodesk Inventor software. The cancellous bone STL file was downloaded from NIH 3D Print Exchange – an opensource community (https://3dprint.nih.gov/).

Gyroid	Cancellous bone
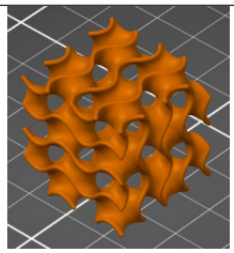	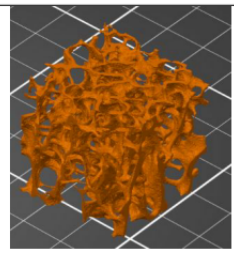
25 × 25 × 25 mm	25 × 25 × 25 mm

Table S3 3D printing settings of anatomical models and porous structures.

3D printing parameter	Vertebra L3	Vertebra C1 (atlas)	Cancellous bone	Gyroid
Print time	5 h 30 min	2 h	1 h 12 min	1 h 6 min
Used filament (m)	12.62	4.35	0.95	1.42
Extrusion temperature (°C)	215(FF) / 185 (PLA/TPS)			
Bed temperature (°C)	60			
Cooling	Fan on			
Printing speed (mm s^{-1})	Contour 20, Infill 80, Supports 40			
Layer height (mm)	0.18			
Nozzle diameter (mm)	0.4			

3. SEM images of the samples during degradation studies in 0.1 M PBS

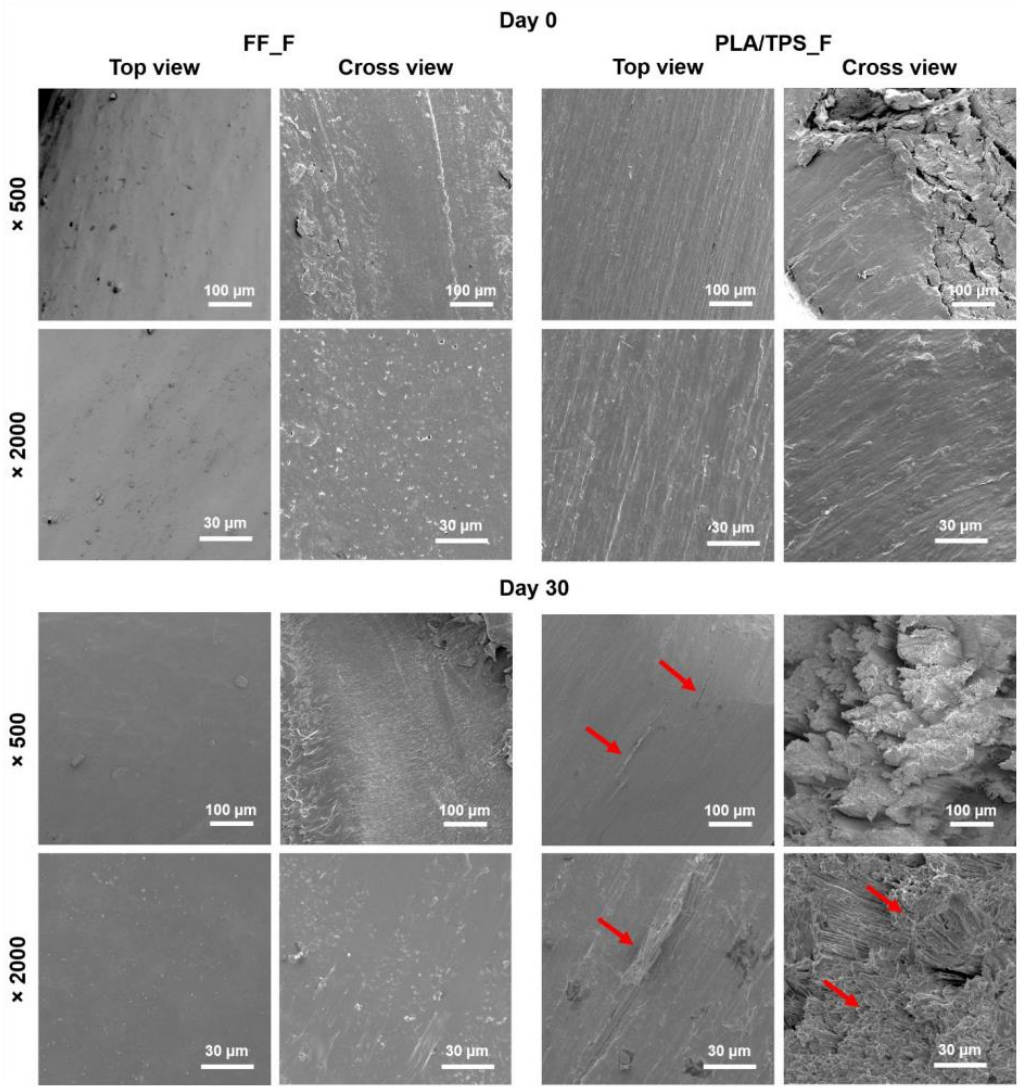

Figure S3 SEM images taken before (day 0) and at the end (day 30) of the degradation studies in 0.1 M PBS solution of FF and PLA/TPS filaments. Top view – the surface of the filament, cross-view – side view of the filament. Red arrows point out the changes in filament morphology during the incubation time (cracks, fibre-like structure).

4. Laboratory compost - composition

Table S4 Composition of laboratory compost (EN ISO 20200:2015)

Component	Content (%)
Sawdust	40
Rabbit food	30
Compost	10
Potato starch	10
Sugar	5
Canola oil	4
Urea	1
All	100
+ Water	55

5. SEM images of the samples during laboratory-scale composting test

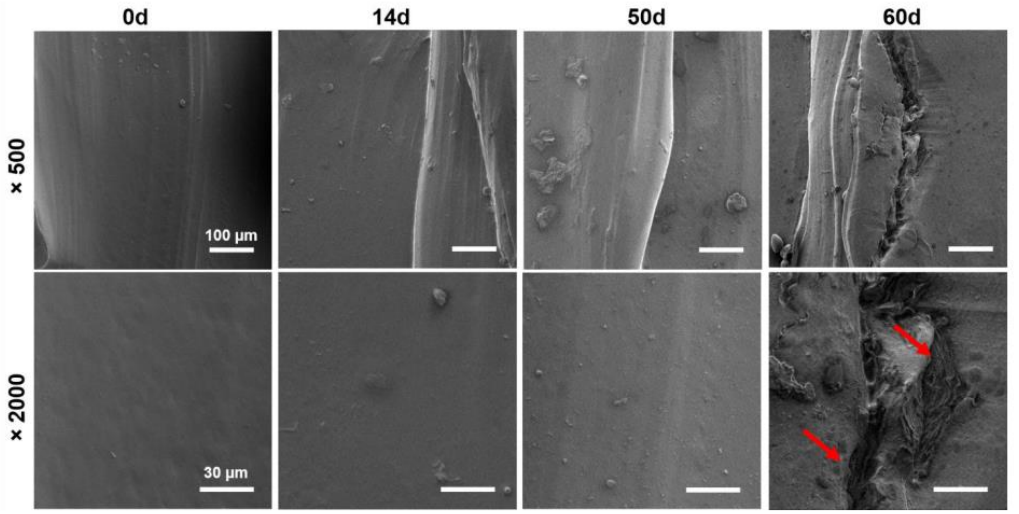

Figure S4 SEM images of the FF_P during a laboratory-scale composting test. The red arrows indicate cracks in the surface of the sample formed during the composting process.

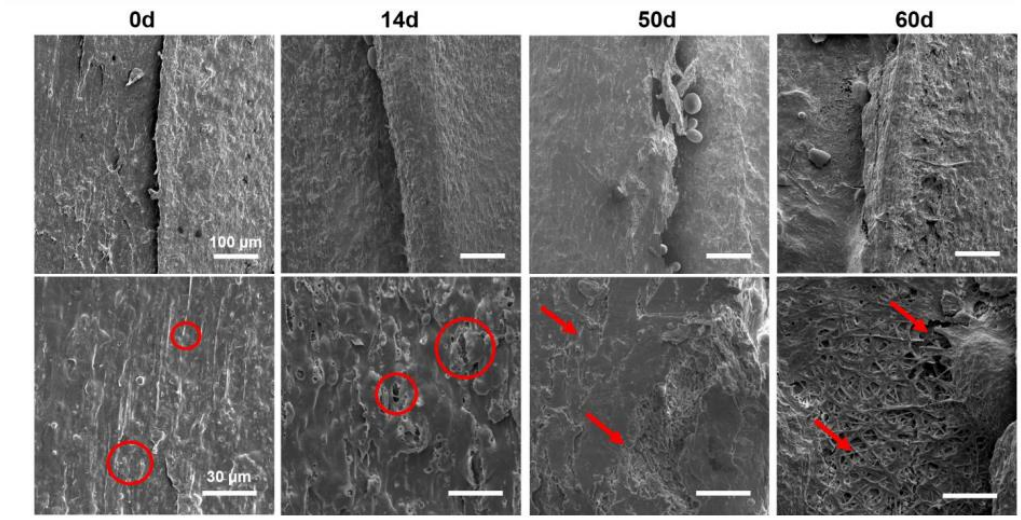

Figure S5 SEM images of the PLA/TPS_P during a laboratory-scale composting test. The red circles show the TPS granules distributed in the PLA matrix (0d) and the places of TPS cavities (14d). The red arrows represent changes in the morphology of the sample, which remained during the composting process (pinholes, cracks, cavities).

6. Images of printed anatomical models and porous structures

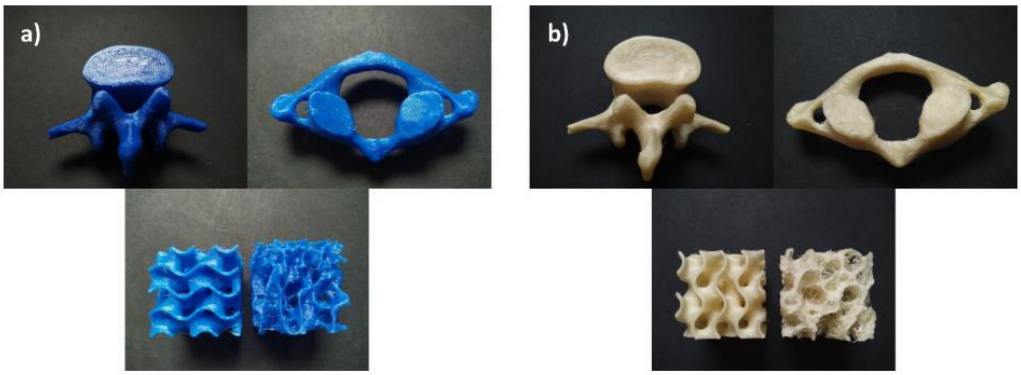

Figure S6 The view of printed with (a) FF_F and (b) PLA/TPS_F anatomical models and porous structures.

7. Description of challenges faced during 3D printing with the PLA/TPS filament

Table S5 Observations recorded during the optimization of 3D printing parameters of the PLA/TPS filament.

Issue	Comment
Printing temperature	The temperature range was set to 180-185°C which corresponds to a relatively narrow printing temperature range. This is due to the two-component nature of the PLA/TPS filament. Below the temperature of 180°C, the nozzle becomes clogged with insufficiently molten PLA, while above 185°C, the degradation of the TPS occurs (the glycerin contained in it begins to evaporate, the filament is destabilized, and thus deforming the printout).
Printing speed	The optimal printing speed was set to 5-40 mm s^{-1}. The underextrussion phenomenon (gaps between the layers of the printed object) take places at a higher print speed. The filament slips on the drive gear, resulting in the irregular feeding of the material.
Adhesion to the build plate	Printouts adhere well to the build plate – the use of glue is not necessary. However, when printing complex structures, it is recommended to heat the build plate to temperature of 60°C.
Shrinkage effect	High dimensional tolerance of the printed objects. Shrinkage effect negligible.
Cooling the printout	It is highly recommended to cool the printout during printing (fan on).

CHAPTER V

SUMMARY AND CONCLUSIONS

5.1 Summary

In the presented doctoral dissertation, research on the preparation of new polymer materials, formation, and detailed characterization of new medical-grade filaments for extrusion-based 3D printers (FDM™/FFF) was undertaken. A method of synthesizing biocompatible poly(ester urethanes) with different susceptibility to hydrolytic degradation without the use of a catalyst was developed. For this purpose, aliphatic isocyanate (HDI) and crystallizable (PCL), as well as non-crystallising (PEBA) (not used in such applications so far) polyols, were used. Moreover, a fully plant-based and compostable polylactide-starch composition with improved impact strength was obtained and well described. Epoxidized soybean oil (ESO) was used as a novel reactive compatibilizer that improved the miscibility of the composition while retaining compostability. Subsequently, two types of filaments were obtained and well characterized, i.e. medical-grade, degradable poly(ester urethane) filaments [TPU(PEBA), TPU(PCL)] and bio-based polylactide-starch filament [PLA/TPS]. This required adaptation of the apparatus and optimization of the filament-forming process which was carried out both in continuous and discontinuous manner. The filament formation process was presented and discussed. The critical steps and parameters leading to the stable 3D printable filament has been captured complementing the current state of knowledge. A method for the stability assessment of the filaments *via* analyzing selected properties before and after the 3D printing process was proposed. Subsequently, several types of porous 3D structures were designed and personalized anatomical models were prepared directly from the CT scans. Obtained digital models were then 3D printed using the developed filaments. Finally, selected printouts were subjected to a series of preliminary biological tests (*in vitro*) to assess their potential for medical use.

In the first stage of research **[PAPER 1,2]**, work was undertaken on the uncatalytic synthesis of poly(ester urethanes) using a standard two-step procedure (prepolymer method). Besides the selection of apparatus, the amounts of reagents and the synthesis parameters had to be adjusted. The first step of the synthesis involved the reaction of excess diisocyanate (HDI) with a selected polyol (PCL/PEBA) resulting in a prepolymer mixture of isocyanate-terminated oligomers with unreacted HDI residues (8% excess of NCO groups). The synthesis was carried out for at least 3 hours at 80-90°C. The course of the pre-polymerization was monitored by measuring

the number of free isocyanate groups during the process (acidimetric titration). The second step covered the so-called chain extension reaction by adding BDO to the prepolymer mixture. Intensive mixing lasted up to 3 minutes and the mixtures were poured into heated molds in which the gelling process took place (80°C, at least 3 h). The chain extender was added in four different molar ratios, thus changing the content of the rigid segments (HS) of poly(ester urethanes). In this way, a series of samples were obtained that differ in the type of soft segment (crystalline or amorphous) and the content of rigid segments (HS% 27-29%). The chemical structure of the obtained TPU was analysed using spectroscopic techniques (FTIR, Raman). Synthesis without the use of a catalyst caused an increase in the time and intensity of mixing in the extension step as well as doubling the gelling time of the samples compared to catalyzed systems ($SnOct_2$, DBTDL). However, as the mechanical properties of uncatalyzed TPUs did not differ significantly from synthesized systems, further research was continued only on non-catalized TPU samples. The mechanical properties of both developed systems TPU(PEBA) and TPU(PCL) were within the range of commercial counterparts (Texin®, Despoman®, and MillaMed®), namely the tensile strength at break of 20-30 MPa, elongation at break of 500-730%, and hardness of 25-37 Shore D. The MFR study was used to assess the suitability of the obtained TPUs for processing into a filament. The results showed sufficient flow and viscosity of the melt with the value in the range of 30-50 g per 10 min (at 200°C, load of 5 kg) for selected TPUs. The water contact angle (wCA) measurements revealed that TPU(PCL) system is hydrophobic with the contact angle over 100°, and TPU(PEBA) system is rather hydrophilic (wCA below 75°). The studies of accelerated degradation showed that polyurethanes with amorphous soft segments were more prone to degradation as the mass loss progressed much faster and the final value was around 90%, whereas for TPU(PCL) was below 50% after one month of incubation. The absorption of selected polyurethanes in water and phosphate buffer PBS (37°C, 3 days) did not exceed 2%wt. which proves the stability of the materials under given conditions. Indirect cytotoxicity tests using MTT assay revealed that the cell viability regarding a control group was above 70% for all the synthesized samples. According to the ISO 10993:5 standard, material with cell viability over 70% (compared to control group) can be considered as cytocompatible and non-toxic. The short-term hemocompatibility test of the selected TPUs showed that the materials did not affect the tested blood parameters in basic blood count. Undertaken efforts resulted in the

successful synthesis of uncatalyzed poly(ester urethane) systems that exhibit a wide range of properties and meet the pre-requirements of medical-grade materials. Moreover, the use of various types of polyols in TPU synthesis allowed customizing degradability and wettability, thus extending the range of potential applications of formed polyurethanes, from hydrophilic fast-degradable to hydrophobic slow-degradable systems.

In the next stage of the research **[PAPER 1,2]**, the obtained materials (described above) were formed into filaments using melt-extrusion process. The filament formation of the synthesized TPU(PCL) and TPU(PEBA) was carried out with the use of laboratory extruders. The apparatus was not adapted to the formation of dimensionally stable filaments, therefore the process was carried out in a discontinuous manner, obtaining only small amounts of filament (short sections with a stable diameter). The optimization of the process consisted in the selection of temperatures, the speed of extrusion, feeding ratio, the method of collecting the extrudate, and the design of an appropriate forming nozzle. The observation of the process allowed to conclude that the main factor determining the successful formation of an elastic filament with a constant diameter in a discontinuous manner is maintaining a stable value of head pressure. It is possible while maintaining the appropriate dosing ratio combined with the optimal temperature profile ensuring sufficient melt viscosity. Thermoplastic elastomers are characterized by high melt strength and viscosity, therefore their extrusion is more demanding. Using a molding nozzle with a too-small diameter (below 1.5 mm) may lead to too high flow resistance in the area of extruder head (adapter and die zones). In this case, an attempt to reduce the melt viscosity by increasing the temperature of the head zones (adapter and die zone) most often leads to overheating and material degradation. It should be noted that the diameter of the molding nozzle does not determine the filament diameter due to the common phenomenon of extrudate swelling (Baruss effect). Although the degree of swelling can be reduced to some extent by modelling the geometry of the flow channel, the shear rate, and the pressure-temperature conditions, obtaining a strictly defined and constant dimension is extremely difficult. Thus, the simplest way to obtain dimensionally stable extrudate with a strictly defined diameter in a discontinuous manner is to let the force of gravity shape the filament. Collecting the extrudate from the appropriate height (relative to the extrudate nozzle) combined with proper cooling allows obtaining filament with a given diameter in

a relatively undemanding way. The filament diameter was controlled manually using an electric caliper and the extrudate was cooled with air with appropriately positioned fans. However, such system was insufficient to form the filament continuously and only fragments were collected. In summarizing, the optimized parameters leading to the formation of TPU(PEBA) filament samples with a diameter of 1.75 mm were as follows, extrusion temperature in the range of 160-210°C, extrusion speed of 20 rpm, head pressure around 16-18 bar, dosage ratio of 100 g per 30 sec. The values given are relative and correspond to double-screw extruder with nine heating zones and screw with L/D ratio of 22. The custom-made molding nozzle diameter was 1.5 mm. In turn parameters ensuring stable filament of TPU(PCL) were as follows, extrusion temperature in the range of 175-200°C, the rotation speed of 40-50 rpm, head pressure of 17 bar, dosage ratio of 30-50 g per 1 min. These values correspond to single screw extruder with two heating zones. The diameter of molding nozzle was 1.9 mm. The samples of TPU(PEBA) and TPU(PCL) filaments thus obtained were further tested on the FFF 3D printer. Unfortunately, due to the insufficient length of the obtained TPUs filaments reliable data on printability was not obtained. In addition, it was not possible to print the designed structures. Nonetheless, the obtained TPU filaments were also carefully characterized and by comparing the results with those of cast TPUs, it was proved that the filament-formation process does not deteriorate the properties of the material, which remains biocompatible and hemocompatible.

The unsatisfactory results from the discontinuous filament formation work as well as the lack of literature data on the formation of filaments for 3D printing prompted me to research using a more advanced system that would allow obtaining sufficient amounts of filament in a continuous manner. Therefore, in the third stage of the research, a complex filament-forming system was used, with which attempts were made to form filaments using synthesized TPUs. The work on such a system required, however, large amounts of feedstocks (over 10 kg of each TPU pellet), which at that time were beyond my reach to synthesize. As a consequence, the optimization of the filament-forming process was carried out with the use of commercial poly(ester urethane) (Epaline® 390 A) **[PAPER 3]**. Unlike the laboratory setups, the molding system used had calibration zones, a laser diameter sensor, and the spool winding system. Thus, in addition to selecting the appropriate extrusion parameters, the optimization included setting parameters of the calibration zones (type and temperature of cooling medium, diameter of calibrators) and winding system (pulling

velocity). Maintaining constant head pressure along with adequate cooling of the extrudate and pulling velocity has proven to be key factors in continuously forming flexible filaments. The proposed method of cooling on a water surface with gradually decreasing temperature, together with the proper extrudate drying system limited the filament over-stretching and ensured diameter stability. Among the many tested process parameters, the **PAPER 3** presents and describes those leading to obtaining TPU(E) filament with a constant diameter (1.75 mm ± 0.01 mm) and suitable for FFF/FDM 3D printing. Melt extrusion parameter were as follows, extrusion temperature in the range of 155-193°C, extrusion speed of 50 rpm, head pressure around 62 bar, continuous dosage. The values given are relative and correspond to single-screw extruder with five heating zones, screw with L/D ratio of 32, and molding nozzle diameter of 2 mm. In conclusion, the description of the filament-formation line, including all the necessary processing parameters and apparatus needed to obtain elastic filament complements the current state of knowledge in the field of processing 3D printable filaments in a continuous manner.

Subsequent research stage covered characterization of TPU(E) filament *via* structural (FTIR, Raman, H-NMR), thermal (DSC, TGA), mechanical (tensile test, hardness), and rheological (MFR) tests. The stability of the filament under 3D printing conditions was evaluated by comparing the structural and thermal data of the filament with the data obtained for the printouts. The results showed that TPU(E) filament remains stable under FFF 3DP, however, slight changes were observed. FTIR spectra revealed that in the region of -NH groups (wavelength of 3400-3200 cm^{-1}) the band shifted towards higher values and the peak representing the H-bonded -NH groups decreased significantly as a result of the 3D printing process. Thus, the proportion of hydrogen bonded -NH groups in the polyurethane structure is reduced. However, there was no change in the areas corresponding to the ester and urethane bonds. DSC thermograms of the TPU(E) filament and the printout showed the T_g in a very close range of 40°C, and therefore the transition of the soft phase of TPU(E) was not affected. Two melting peaks were observed, the total heat enthalpy of which was relatively low (and did not change significantly due to the 3D printing process), which suggests a small proportion of crystalline phases in the tested samples. Change in the value of the T_c of the hard segments was negligible and ranged from 164-168°C. Thermal stability of the TPU(E) filament and the printout, determined on the basis of TGA thermograms, was very similar (T_{onset} of 300°C) and the complete decomposition

in both cases occurred near 475°C (T_{offset}). Determined DTG curves showed a two-stage material decomposition, which confirmed the segmental structure of TPU(E). Measurement of the melt flow rate (MFR) showed a slight increase after the 3DP process which is in line with the results of FTIR (reduction of H-bonding in the TPU structure). Taking into account the above test results, no deterioration of the material properties of the developed TPU(E) filament was found as a result of the 3D printing process. Subsequently, series of *in vitro* studies (long-term, and short-term degradation, cytotoxicity, wettability) were performed. Once the results confirmed the potential of the TPU(E) filament as medical-grade material, work began on the design of digital models with the use of 3D modelling platforms (Autodesk Inventor, 3D Slicer).

The project assumed the preparation of highly porous and flexible structures that can be used in tissue engineering as the so-called scaffolds. Therefore, structures of high porosity and complexity were prepared, differing in the architecture and size of the pores as well as the degree of their order. As a consequence, a number of different scaffolds and specimens for tensile testing were designed and printed on a FFF printer using developed TPU(E) filament. It required prior selection of optimal 3D printing parameters. The optimized basic settings for printing were as follows: extrusion temperature of 210-225°C, bed temperature of 60-65°C, printing speed of 20 mm s^{-1}. The crucial factor covered proper cooling with air of the printout during the process. The overall printability of TPU(E) was remarkable. Used nozzle with a diameter of 0.2 mm allowed the formation of pores with dimensions even below 0.3 mm. Scaffolds porosity ranged from 50-80% depending on the type of porous structure. The printouts were characterized by high print accuracy (over 97%), which is highly desirable when forming complex structures for tissue engineering. The Young modulus and tensile strength of printed dumbbell-shaped specimens ranged 0.19-0.21 GPa and 29-31 MPa, respectively, depending on the given printing parameters (infill orientation). The compression strength of the scaffolds was in the range of 0.12-1.05 MPa. Along with *in vitro* cytotoxicity, long-term incubation in PBS, and short-term degradation studies, incubation in simulated body fluid (SBF) was performed as it is an effective method to assess the bioactivity of a material in terms of its ability to form apatite. The effect of incubation in SBF on the scaffolds was monitored *via* SEM, EDS, weight measurements, and compression test. The results of *in vitro* studies showed that the scaffolds are stable up to 6 months of incubation in

PBS (with a degree of swelling below 2%), meet the requirements of biocompatibility (ISO 10993:5), are rather hydrophilic with the wCA of 76°, exhibit degradability of long-term tissue-engineered constructs, and are prone to mineralization following SBF incubation. SEM complemented by EDS measurements revealed the formation of carbonated-hydroxyapatite (C-HAp) crystals within 14 days, which significantly strengthened the scaffolds. The compressive strength increased by up to 50% from the initial value after 28 days of SBF incubation. Moreover, a strong correlation was found between the compressive strength, and the type of scaffold architecture. The scaffolds with the highest degree of pore ordering and lowest porosity had the highest compressive strength (~1 MPa), at the same time the strongest effect of HAp enhancement was noted for scaffolds with the lowest degree of pores order and the highest porosity (from 0.12 MPa to 0.20 MPa). The obtained TPU(E) filament is suitable for FFF 3D printing of complex porous structures that have potential as scaffolds in cancellous bone tissue engineering.

In order to confront the obtained filaments with commercial products, I was looking for the medical polyurethane filaments for FFF/FDM 3D printing. However, no such solutions had been found. Moreover, a lack of specified standards for filaments testing, and also unsystematic and often insufficient data provided by filament manufacturers encouraged me to carry out detailed research on a selected commercial filament labelled as medical-grade. Bioflex® used to be one of the few commercially available filaments marked as flexible and medical-grade. Therefore in the next stage of research **[PAPER 4]**, a comprehensive evaluation of Bioflex® filament was performed to compare the performance of the commercial product with the developed filaments. Besides, its potential in medical applications was assessed using the same methods as for TPU (E) filament. A detailed analysis of the structural, thermal, thermomechanical, and tensile results revealed that the Bioflex® belongs to the group of thermoplastic copolyester-ether elastomers (TPC) with poly(tetramethylene oxide) (PTMO) as a soft segment. DCS thermograms showed T_g of -68.7°C and a relatively low crystallinity degree of HS (according to low heat enthalpy). One-step decomposition was observed with a thermal stability of 368°C (T_{onset}), suggesting a small share of HS segments or a close decomposition temperature of both types of segments. In turn, both spectroscopic, thermal, and rheological tests have shown that the printing temperature of 220°C does not degrade the material and the properties do not deteriorate. The FTIR and Raman spectra as

well as DSC and TG thermograms of Bioflex® filament and printout almost overlapped. Therefore, it was found that there were no changes at the microstructural level in the tested material. There were also differences in the material data contained in the technical data sheet (TDS) and those obtained from the conducted tests. The measured hardness, tensile strength, elongation at break, and Young modulus of Bioflex® printouts were lower than those given in TDS, 22 Sh D (27 Sh D TDS), ~12-14 MPa (16 MPa TDS), 650-750% (800% TDS), and 0.16-0.19 MPa (35 MPa TDS), respectively. Besides, a significant impact of 3D printing parameters (raster angle and printout orientation) on the strength properties of the printouts has been observed. The overall strength profile of the sample printed with a raster angle of ±45° was higher than those with a raster angle of 0/90°. The wettability of the filament was average with a water contact angle was of 69°. The *in vitro* tests of the printed porous structures confirmed the biocompatibility (ISO 10993:5) and the moderate ability to the formation of apatite during SBF incubation. The first pellet-like crystals were observed within 1 month of incubation. EDS analysis of the crystals revealed the presence of elements corresponding to HAp fortified with carbon and oxygen elements. Ramman spectrum showed the presence of carbonate groups thus indicating the formation of carbonated-hydroxyapatite (C-HAp). Accelerated degradation showed high resistance to hydrolysis in a concentrated media of 2M HCl and 5M NaOH with a mass loss of 1.5% and 10%, respectively, over 28 days of incubation. The test results allowed to classify Bioflex® as suitable for 3D printing of medical devices and biostable items with high elasticity and resistance to aggressive environments. Attention also was drawn to inaccuracies in the presented material data regarding filaments that should be regulated. Moreover, the conducted research allowed for the comparison of the formed TPU(E) filament with its commercial counterpart. Due to the different materials chemistry of both filaments (TPU and TPC), only the stability under printing conditions, printability, and the quality of the obtained prints were considered, which can be regarded as comparable.

Further stage of the research was devoted to the development of bio-filament using plant based feedstocks, as an alternative biomaterial for PLA filament commonly used in medicine. The literature on the subject indicated that, apart from excessive stiffness, PLA is characterized by an insufficient biodegradation rate, therefore attempts were made to prepare fast-biodegradable and compostable composition of PLA modified with thermoplastic starch (TPS) **[PAPER 5]**. To ensure proper

plasticization of TPS and compatibility between PLA and TPS, epoxidized soybean oil (ESO) was used as a modifier and enhancer of glycerine plasticizer. Using melt extrusion, a series of PLA/TPS/ESO compositions, differed in content of ESO and TPS compared to PLA, were obtained. The results of mechanical, thermal, and rheological properties as well as incubation in water and SEM of fractured surfaces allowed to select compositions with the most favourable properties. The addition of unmodified TPS to PLA resulted in improved ductility and impact toughness while deteriorating tensile strength and water resistance compared to pure PLA. Modification of TPS with ESO resulted in better plasticization and thus compatibilization between PLA and TPS. SEM observation of the fractured surfaces showed an increase in the homogeneity and hence the compatibility between the PLA and TPS phases with the increase in ESO content. The addition of ESO to TPS resulted in a significant increase in the MFR (over 30 g 10 min^{-1}) value as well as there was a shift in the values of T_g and T_m towards lower temperatures along with an increasing share of ESO in PLA/TPS compositions which confirmed the plasticizing effect. Moreover, the addition of ESO improved the water resistance of the blends, as swelling ratio and mass loss decreased with the increase in ESO content. Both developed compositions and pure PLA (NatureWorks) completely disintegrated within 57 days in laboratory composting (ISO 20200:2015). Replacement of 25% PLA with ESO-modified thermoplastic starch led to improvement in ductility and impact strength while maintaining similar processability and increased biodegradability compared to pure PLA.

The developed bio-compositions (PLA/TPS/ESO), derived only from rapidly renewable plant sources, showed promising properties as an alternative to the widely used PLA. Moreover thy are more economic than PLA itself. Besides the packaging industry, extrusion-based 3D printing mainly utilize PLA filaments. As PLA filaments are marked as eco-friendly and easy to print, they are commonly used, among others in medicine, in the design of operational planning systems, artificial organs for educational aids, or prototypes of personalized implants. Such activities produce a lot of disposable waste which is expected to be no less harmful than the petrochemical ones. Therefore, in the last stage of research, efforts were made to develop bio-filament with increased biodegradability for medical application as an effective raw material to 3D printing personalized anatomical models or educational systems **[PAPER 6]**. Using the previously described continuous filament forming system, PLA/TPS/ESO filament was obtained which consisted of 40% TPS (modified with 1% of ESO). The temperature

profile was in the range of 140-172°C with the melt temperature of 176°C. The head pressure was kept constant at 21 bar and the extrusion velocity did not exceed 35 rpm. The cooling system was filled with water while calibrators were of 2 and 1.8 mm diameter. These process parameters resulted in a stable filament with a 1.75 mm diameter, which was further optimized on FFF 3D printer. Contrary to the flexible TPU(E) filament, the PLA/TPS filament was characterized by relatively narrow range of printing temperature (180-185°C). It requires strict control of the process, as above the temperature of 185°C, the TPS is destabilized (T_{onset} around 185°C), which is manifested by the evaporation of the plasticizer (glycerine). In turn, below the temperature of 180°C, insufficient plasticization of PLA occurs, which lead to clogging of the printer nozzle. The optimal printing speed was up to 40 mm s^{-1}. It was observed that heating (60°C) the build plate during printing promotes adhesion and reduces the shearing effect. The optimized 3D printing setup was used to prepare various test specimens. To confront the resulted PLA/TPS filament with commercial product, a comprehensive characterization was also conducted for the FlashForge PLA® filament PLA(FF). The FTIR and Raman spectra showed structural stability of both filaments under 3D printing conditions. The additional signals characteristic for aromatic structures were found in the Raman spectrum of PLA(FF), which correspond to the filament modifiers such as plasticizers (mineral oils), print enhancers (TPE) etc. A slight decrease in the intensity of -OH derived signal (~3310 cm^{-1}) in the PLA/TPS printout was noted, which is related to the reduction of H-bonding resulting from the 3DP process. There was also a slight decrease in the so-called crystalline band (~925 cm^{-1}) suggesting a decrease in the crystalline phase of the PLA/TPS composition due to the fast cooling of the printout. The XRD spectra indicated rather an amorphous character of both filaments with slight residues of the crystalline phase (A-type crystals) derived from native starch. Thermal stability of the PLA(FF) was relatively high, reaching over 300°C while for the PLA/TPS was much lower and oscillated around 200°C. Such outstanding thermal stability of the commercial filament probably comes from the modifiers and fillers used in the production process. Two-stage decomposition confirmed phase separation of PLA/TPS. Degree of crystallinity (X_c), (calculated from DSC measurements), of the PLA(FF) was around 12% and did not change after 3DP. In turn, X_c of the PLA/TPS filament reached over 46% and decreased to 17% indicating that by selecting the degree of cooling of the printout or by additional post-treatment (annealing), the degree of crystallinity can be adjusted

and thus customizing the properties. The shift of T_g towards lower temperatures resulting from the 3DP process can be associated with the increased mobility of the PLA/TPS chains (destruction of H-bonding), which is in line with FTIR considerations. The storage modulus values over entire temperature range of PLA(FF) were significantly higher than those for PLA/TPS suggesting grater material stiffens. The MFR value of PLA(FF) was around 8 g 10 min^{-1} and 11 g 10 min^{-1} for PLA/TPS filament (at 180°C, 2.16 kg load) which corresponds to the range of commercial PLA filaments. A sharp increase in MFR value resulting from increasing the measurement temperature to 200°C (MFR above 47 g 10 min-1) confirms the previous considerations on the thermal stability of PLA/TPS filament and points out that the printing temperature should be lower than 200°C. Examination of mechanical properties included tensile test, Charpy impact test, compression test, and hardness, at the same time effect of the print orientation, raster angle and infill density was investigated. The strength parameters correlated with the given printing parameters indicating anisotropic properties of the FFF printouts, however the overall strength values of the commercial PLA were slightly higher than for PLA/TPS. The biggest difference was noted for the impact toughness, which for PLA(FF) samples was about 2 times higher. Elongation at break was in a rather similar range of 2-5%. Relatively low ductility and impact toughness parameters of PLA/TPS printouts indicate insufficient adhesion between successive print layers, as the values determined for continuous (injected) samples, were significantly higher. Besides, the stress-strain curves of the injected PLA/TPS samples reflected ductile materials while those of the printed specimens showed a rather fragile nature. The conducted research allowed to select the print configuration with the most favorable strength parameters, which corresponded to the *ZX* print orientation (so-called on-edge) and the raster angle of 0°. As the surface of details 3D printed with FFF is not flat and is characterized by an evenly pleated structure, determination of wettability *via* goniometer using the sessile drop technique is challenging and can lead to unreliable data. The reported values of the water contact angle for the printouts from PLA(FF) were extremely different, and were ~111° and 75°, for raster angles 90° and 0°, respectively, which corresponds to the hydrophobic to moderate hydrophilic surface nature. Similar trend was observed for PLA/TPS printouts, however the measured values were lower and ranging from 81° to 63°. The difference in wettability between both filaments is related to the presence of highly hydrophilic TPS that lowers the wCA of PLA.

Therefore, special attention should be paid to the degree of corrugation of the surface and the wCA data should first be analyzed in relation to the raster angle of a given sample, and then to the chemistry of the material. Incubation in PBS (30 days, 37°C) supplemented with pH measurements, SEM images, and FTIR analysis allowed to estimate the susceptibility to hydrolytic degradation of both tested filaments. The results indicated the stability of commercial PLA filament under given conditions. The mean sample weight remained intact, the pH of the solution was stable, the morphology of the surface did not change, and the FTIR spectrum showed no structural changes. Different data were registered for the PLA/TPS filament as the degradation was intense. Already after 5h of incubation, the mass loss was noticeable and reached over 13% after 3 days. At the same time drop in pH was noted, down to 7.27 within 30 days. This is most likely due to the dissociation of the released residues acidifying the solution, such as glucose or glycerine as well as carbonyl-ends groups of fragmented PLA since the degradation proceeded mostly through the destruction of TPS-origin bonds (-OH, -C-O and -COH) and PLA-origin -CH_2, and C=O groups. The SEM images showed numerous changes in PLA/TPS surface morphology (voids, cracks, roughness) resulting from PBS incubation. Thus, the formed PLA/TPS is more prone to the degradation than PLA(FF) which remain untouched. Moreover, it was found that degradation proceeded by both erosions of TPS and PLA, which is a desirable effect as solid PLA is rather resistant to hydrolysis. The initial erosion of the TPS disrupts the surface which is presumed to favor the penetration of water molecules into the sample and thus initiates PLA degradation. The laboratory-scale composting showed that the PLA(FF) printouts were practically intact over 60 days of study while the disintegration degree of PLA/TPS printouts reached over 18%. The optical and SEM microscopy showed that the surface of PLA(FF) samples remained homogenous and smooth, and discoloration occurred after 30 days of composting. In turn, numerous cracks, defects and an increase in roughness were noticed on the PLA/TPS surface from the 14th day of incubation. The FTIR spectrum after 60 days of composting showed slight structural variations in the PLA(FF) sample (mainly changes in the intensity of the bands derived from the ester groups) while the TPS-origin bonds were disturbed and the entire spectrum showed structural degradation of the PLA/TPS samples. This suggests that the commercial PLA filaments, are significantly modified at the production stage (improved processability, addition of fillers and pigments), thus affecting biodegradability and compostability.

Finally to access the potential of developed bio-filament in medical applications, various 3D models of anatomical units and porous structures were designed. 3D models of vertebra C1 and L3 were prepared directly from the CT scan of the human spine. For this purpose, tools for 3D modelling, segmentation, and slicing were used (3D Slicer, PrusaSlicer software). The resulted digital models were optimized for 3D printing (support architecture and printing setup were customized). The resulted printouts of personalized anatomical models and porous structures obtained with developed PLA/TPS filament showed high dimensional stability and surface mapping. The quality of the printouts was comparable to that of commercial PLA filament, even for very complex porous structures. Thus, the usefulness of the obtained filament for 3D printing for medical applications was confirmed.

The novelty of the PhD thesis covers the formation of new elastic filaments using experimental poly(ester urethanes) that are degradable and biocompatible as well as the development of a new polylactide-starch bio-filament with printability comparable to commercial products. In the case of elastic filaments, the developed method of synthesis allowed to obtain TPUs without the use of an organometallic catalyst. While a properly selected forming nozzle and optimized extrusion parameters allowed for the formation of dimensionally stable samples of TPU filament in a discontinuous manner. The test results showed that the experimental filaments are biocompatible and prone to degradation, and the molding process does not affect their stability and bio-properties. According to developed bio-filament, the addition of TPS into pure PLA increased biodegradability without significant deterioration of mechanical properties, whereas the incorporation of epoxidized soybean oil (ESO) improved compatibility and hence the ductility and impact strength of the bio-composition. A professional production line was used, allowing for the continuous formation of a high-quality PLA/TPS bio-filament. The proposed method of assessing the stability of the experimental filaments allows for the ongoing monitoring of the suitability of the material for 3D printing. A summarized list of the dissertation's novelties is presented in **Table 6**.

Table 6 A collective list of scientific and technological novelties in the presented dissertation.

	Polyurethane-based filaments [TPU(PCL)/TPU(PEBA)]	**Bio-based filament (PLA/TPS)**
Scientific novelty of the research	- synthesis of thermoplastic polyurethanes without the use of a catalyst, limiting the possible negative impact of organometallic catalysts on the human body; - synthesis of biocompatible poly(ester urethane) based on amorphous polyol (PEBA) with enhanced susceptibility to accelerated degradation	- the use of epoxidized soybean oil (ESO) as reactive modifier, thus improving interfacial adhesion and ductile properties of PLA/TPS blends; - development of a fully plant-based filament (PLA/TPS) with enhanced compostability and printability comparable to commercial PLA filament.
Technological novelty of the research	- developing a processing window for filament formation by extrusion process of medical-grade elastic poly(ester urethanes) in a discontinuous manner	- developing a processing window and description of the filament formation by extrusion process of a new bio-filament in a continuous manner; - design and 3D printing of porous structures and personalized anatomical models with remarkable surface mapping and dimensional stability, which are characterized by improved decomposition ratio in composting conditions compared to commercial PLA printouts.

5.2 Final conclusions

Based on the presented research results, the following general conclusions were drawn.

Regarding thermoplastic elastomer filaments for FFF/FDM 3D printing:

- The elimination of the catalyst in the synthesis of poly(ester urethanes) extended the synthesis and gelation time.
- As a result of adjusting the process parameters, apparatus, and the ratio of reagents, cast materials with satisfactory properties were obtained. Analysis of the FTIR and Raman spectra showed complete conversion of the end groups of the reactants and formation of urethane groups partially associated with hydrogen bonds. The analysis of the TGA and DCS measurements indicated the presence of micro-phase separation and segmented structure of the synthesized aliphatic poly(ester urethanes) TPU(PEBA)/TPU(PCL) which show thermal stability in the range of 250-260°C.

- The mechanical properties of the obtained new uncatalyzed aliphatic poly(ester urethanes) TPU(PEBA)/TPU(PCL) are within the range of commercial medical-grade polyurethane systems such as Desmopan®, Texin®, or MillaMed®.
- The use of amorphous PEBA polyol (as opposed to the commonly used semicrystalline PCL) for the synthesis of medical polyurethanes allows for obtaining a system with increased susceptibility to hydrolytic degradation and greater hydrophilicity.
- The process of forming medical-grade TPU(PEBA)/TPU(PCL) filaments does not cause significant structural and thermal changes and the material remains biocompatible and/or hemocompatible.
- The key factors of the filament-forming process, both in a continuous and discontinuous manner, are maintaining a constant head pressure and gradual cooling of the extrudate.
- The use of an extensive filament forming system enriched with calibration systems, cooling tubs, and a pulling and winding system allows for continuously obtaining flexible filaments with a constant diameter suitable for 3D printing in FFF technology.
- The FFF 3D printing process did not deteriorate the material properties of the developed TPU(E) and commercial Bioflex® filaments and the printouts remained biocompatible.
- Accelerated degradation study in concentrated media (5M NaOH and 2M HCl) showed that the TPU(PEBA) filament can be classified as a prone to degradation, TPU(PCL) filament as moderate-degradable, TPU(E) filament as a long-degradable, and Bioflex® as a non-degradable systems.
- It has been proven that the 3D printing parameters affects mechanical properties of the printouts. Attention was also paid to inaccuracies in the material data provided by filament manufacturers and the need to introduce standards for testing filaments and regulation on how to present material data of commercial products especially those of medical application.
- The TPU(E) and Bioflex's ability to mineralize as a result of incubation in SBF was confirmed by SEM, EDS, and Raman studies. More prone to mineralization was TPU(E). The resulting crystals correspond to the minerals of carbonated-

hydroxyapatite (C-HAp), which is considered to be more like the natural apatite of hard tissues than synthetic HAp.

- Developed TPU(E) filament is suitable to FFF 3D printing of elastic porous scaffolds differing in architecture, shape and dimensions of the pores (0.1-1 mm diameter) with a print accuracy above 97% in three dimensions.
- It has been observed that the susceptibility to mineralization differs depending on the type of porous structure. The G3D type scaffold with the lowest pore ordering and the highest porosity showed the highest degree of HAp deposition and a 55% increase in compressive strength due to SBF incubation. It can be assumed that the increase in the specific surface area promotes the release of hydroxyapatite.
- Strength parameters (Young modulus ~0.2 GPa , tensile strength ~30 MPa, compressive strength ~1 MPa), biocompatibility, as well as susceptibility to mineralization under SBF exposure allow to pre-qualify the developed TPU(E) filament for FFF 3D printing of cancellous bone tissue scaffolds.
- The printability and overall performance of the developed flexible TPU(E) filament are comparable to commercial counterpart - Bioflex®.

Regarding bio-based thermoplastic filaments for FFF/FDM 3D printing:

- The addition of epoxidized soybean oil (ESO) to potato starch enhanced the plasticizing effect and improved compatibility between PLA and TPS phases, resulting in improved elongation at break, impact strength, and water resistance compared to the unmodified PLA/TPS composition.
- The PLA/TPS filament has been developed exclusively from natural, and quickly renewable raw materials. Replacing up to 40% of PLA with ESO-modified TPS resulted in considerable improvement of wettability, hydrolytic degradability, and thus disintegration ratio in composting, in contrast to that of commercial PLA filament.
- Commercial PLA printouts PLA(FF) were shown to be non-biodegradable (specimens remained intact) under laboratory simulated composting conditions (60 days, 58°C, 90% humidity).
- A strong correlation was observed between the 3D printing parameters (raster angle, print orientation) and the strength properties of the printouts of thermoplastics (PLA(FF), PLA/TPS) unlike those obtained from thermoplastic

elastomers. This suggests differences in interlayer adhesion which is higher in the case of flexible filaments.

- Despite the fact that as a result of the FFF 3D printing process there were slight structural and thermal changes, no degradation or deterioration in the material properties of the developed PLA/TPS bio-filament were found.
- It has been shown that the water contact angle (wCA) of samples printed in FFF 3D printing technology is strictly dependent on the printing parameters and surface orientation (raster angle, path width, layer height, nozzle diameter, etc.). Therefore, the wCA measurements must contain information on the above 3DP settings to allow the reliable comparison of printouts' wettability.
- The PLA/TPS filament is suitable to FFF 3D printing of personalized anatomical models and porous structures with high surface mapping and satisfactory dimensional stability.
- The printability and overall performance of the developed bio-based PLA/TPS filament are comparable to commercial counterpart - PLA FlashForge® filament.

The main achievements of the doctoral dissertation include:

1) Optimization of the synthesis parameters and characterization of new uncatalyzed, aliphatic poly(ester urethanes), differing in the type of soft segment and thus susceptibility to degradation for biomedical application [PAPER 1,2].
2) Description of the continuous filament-formation line, including all the necessary processing parameters, apparatus, and critical points leading to high-quality flexible filament [PAPER 3].
3) Design and 3D printing of porous structures that meet the prerequisites of cancellous bone porous tissue scaffolds, using formed poly(ester urethane) filament TPU(E) [PAPER 3].
4) Understanding the influence of 3D printing on the physicochemical, thermal, mechanical, and biological properties of medical filaments. The stability of the tested filaments was found and it was confirmed that the 3D printing process did not affect the biocompatibility of the material [PAPER 1-4].

5) Preparation of fully plant-based filament with enhanced biodegradability and comparable printability to commercial PLA filament [PAPER 6].

Summarizing the above conclusions and achievements, it can be stated that the developed filaments for 3D printing in the FFF/FDM® technology are valuable and attractive alternative for medical purposes, and the conducted research supplements the current knowledge in the field of synthesis, forming, and characterization of materials for extrusion-based 3D printers. The developed filaments can be used for 3D printing of the following details (**Figure 9**):

- long- and short-term porous structures for tissue engineering applications;
- personalized anatomical models for surgical training systems and pre-operative planning procedures;
- artificial organs as teaching aids for medical students;
- customized laboratory equipment.

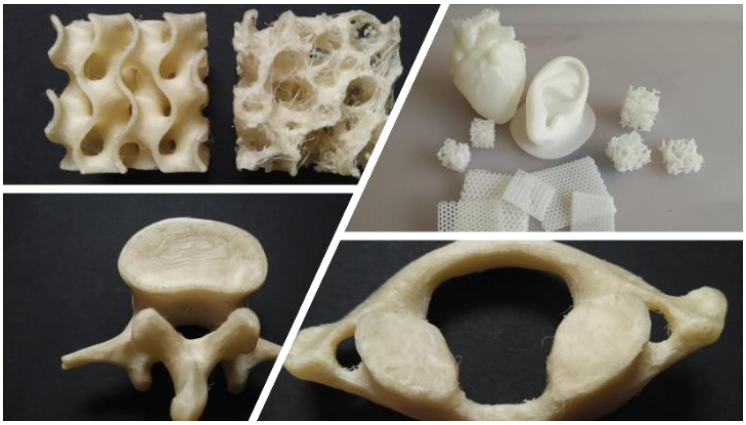

Figure 9 An example of products printed with the use of filaments developed in the dissertation.

Nevertheless, there are still many properties to investigate and improve, and many possible applications to evaluate for the studied filaments.

Postscriptum

The nature of graduation thesis is to follow the well-trodden paths but in your own shoes. Despite this sometimes rocky and arduous journey, this dissertation has been put forward to reflect what I believe to be valuable and noteworthy, and knowledge on a range of subjects from the understanding of bio-polymers to potential novel solutions regarding medical filaments for FFF 3D printing. I hope the issues I have raised will benefit future researchers who by adding their own efforts contribute to the improvement of the human condition and the state of nature.

5.3 Personal data and list of scientific achievements

Personal data

Agnieszka Haryńska, MSc Eng. (maiden name Przybytek)

Affiliation	Gdańsk University of Technology, Faculty of Chemistry, Department of Polymer Technology
Scopus ID	57202500947
Orcid ID	0000-0001-8017-6070

List of scientific achievements

H-index:	**7** (Scopus), **9** (Google Scholar)
Total Impact Factor ($\sum_{IF}$)	**29,45**
Total MEiN pts ($\sum_{MEiN}$)	**970**
Total citations	**188** (Scopus), **257** (Google Scholar)
Number of articles (JCR list)	**9**
Number of articles (outside the JCR list)	**1**
Number of books chapters	**2**
Participation in international conferences	**4** (oral presentation), **1** (poster presentation)
Participation in nationwide (polish) conferences	**3** (oral presentation), **1** (poster presentation)
Exhibitor at international trade fairs	**3**
Participation in research projects	**2**

Detailed list of scientific achievements

Articles in the JCR list with a Journal Index Factor:

1) **Haryńska A.**, Janik H., Sienkiewicz M,. Mikolaszek B,. Kucińska-Lipka J. PLA–potato thermoplastic starch filament as a sustainable alternative to conventional PLA filament: processing, characterization and FFF 3D printing. *ACS Sustain. Chem. Eng.* 2021, 9(20), 6923-6938, doi.org/10.1021/acssuschemeng.0c09413.
(Q1, IF_{2020}=8.198, MEiN=140 pts) **[PhD Paper 6]**

2) **Haryńska A.**, Carayon I., Kosmela P., Szeliski K., Łapiński M., Pokrywczyńska M., Kucińska-Lipka J., Janik, H. A comprehensive evaluation of flexible FDM/FFF 3D printing filament as a potential material in medical application. *Eur. Polym. J.* 2020, *138*, doi:10.1016/j.eurpolymj.2020.109958. (Q1, IF_{2019}=3.862, MEiN=100 pts) **[PhD Paper 4]**

3) **Haryńska A.**, Carayon I., Kosmela P., Brillowska-Dąbrowska A., Łapiński M., Kucińska Lipka J., Janik H. Processing of Polyester-Urethane Filament and Characterization of FFF 3D Printed Elastic Porous Structures with Potential in Cancellous Bone Tissue Engineering. *Materials (Basel).* 2020, *13*, 4457,

doi:10.3390/ma13194457.
(Q2, IF_{2019}=3.057, MEiN=140 pts) **[PhD Paper 3]**

4) **Haryńska A.**, Kucinska-Lipka J., Sulowska A., Gubanska I., Kostrzewa M., Janik H. Medical-Grade PCL Based Polyurethane System for FDM 3D Printing—Characterization and Fabrication. *Materials (Basel).* 2019, *12*, 887, doi:10.3390/ma12060887.
(Q2, IF_{2019}=3.057, MEiN=140 pts) **[PhD Paper 2]**

5) **Haryńska A.**, Gubanska I., Kucinska-Lipka J., Janik H. Fabrication and Characterization of Flexible Medical-Grade TPU Filament for Fused Deposition Modeling 3DP Technology. *Polymers (Basel).* 2018, *10*, 1304, doi:10.3390/polym10121304.
(Q1, IF_{2018}=3.164, MEiN=100 pts) **[PhD Paper 1]**

6) **Haryńska A. (Przybytek A.)**, Sienkiewicz M., Kucińska-Lipka J., Janik H. Preparation and characterization of biodegradable and compostable PLA/TPS/ESO compositions. *Ind. Crops Prod.* 2018, *122*, doi:10.1016/j.indcrop.2018.06.016.
(Q1, IF_{2018}=4.244, MEiN=200 pts) **[PhD Paper 5]**

7) Kucińska-Lipka J., Gubańska I., Lewandowska A., Terebieniec A., **Haryńska A. (Przybytek A.)**, Cieśliński H. Antibacterial polyurethanes, modified with cinnamaldehyde, as potential materials for fabrication of wound dressings, *Polym. Bull.* 2018, doi:10.1007/s00289-018-2512-x.
(Q2, IF_{2018}=1.597, MEiN=40 pts)

8) Janik H., Sienkiewicz M., **Haryńska A. (Przybytek A.)**, Guzman A., Kucinska-Lipka J., Kosakowska A. Novel Biodegradable Potato Starch-Based Compositions as Candidates in Packaging Industry, Safe for Marine Environment. *Fibers Polym.* 2018, *19* (6), 1166–1174. doi:10.1007/s12221-018-7872-1.
(Q2, IF_{2018}=1.595, MEiN=70 pts)

9) **Haryńska A. (Przybytek A.)**, Gubańska I., Kucińska-Lipka J., Janik H. Polyurethanes as a potential medical-grade filaments for the use in Fused Deposition Modeling 3D printers – a brief review. *Fibers Text. East. Eur.,* 2018, 6,doi:10.5604/01.3001.0012.5168.
(Q4, IF_{2018}=0.677, MNiSW=40 pts)

Articles without a Journal Index Factor:

1) **Haryńska A. (Przybytek A.)**, Janik H., Kucińska-Lipka J. Thermoplastic Elastomer Filaments and Their Application in 3D Printing. *Elastomery,* 2016, *20* (4), 32–39.

Books chapters:

1) Kucińska-Lipka J., Janik H., Sulowska A., **Haryńska A. (Przybytek A.)**. The Influence of PEG on Morphology of Polyurethane Tissue Scaffold. In *Science*

and Technology of Polymers and Advanced Materials Applied Research Methods; Mukbaniani, O., Tatrishvili, T., Abadie, M., Eds.; Taylor & Francis: New York, 2019 ISBN 9780429425301.

2) Janik H., Sienkiewicz M., Wawrowska M., Wiecierzycka K., **Haryńska A. (Przybytek A.).** Degradation of Modified TPS in Natuaral and Industrial Compost. In *Chemical Engineering of Polymers. Production of Functional and Flexible Materials*; Mukbaniani, O., Abadie, M., Tatrishvili, T., Eds.; Apple Academic Press, CRC Press, 2017; pp 397–406.

International conferences:

1) **Haryńska A.**, Lesner D., Janik H.: "*3D printing of bone structure prototype",* X International Scientific-Technical Conference "Advance in Petroleum and Gas Industry and Petrochemistry, 18-23.05.2020, Lviv, Ukraine. – **on-line oral presentation**

2) **Haryńska A.**: *"Circular economy – sustainable cutlery",* BalticSea Youth Camp, 8-11.06.2019, Gdańsk, Wyspa Sobieszewska, Poland. – **plenary lecture**

3) **Haryńska A.,** Kucińska-Lipka J., Gubańska I., Janik H.: "*Evaluation of medical-grade TPU systems based on different polyols, dedicated to FDM 3D printing technology",* European Congress and Exhibition on Advanced Materials and Processes EUROMAT 2019, 1-5.09.2019, Stockholm, Sweden. – **oral presentation**

4) **Haryńska A. (Przybytek A).,** Kucińska-Lipka J., Gubańska I., Janik H.: *"Physico-mechanical properties of novel uncatalyzed polyurethanes suitable for fabrication of tissue scaffolds by various techniques",* 5th International Conference on Polymer Processing and Characterization, 27-29.09.2017, Gdańsk University of Technology, Gdańsk, Poland. – **oral presentation**

5) **Haryńska A. (Przybytek A.),** Kucińska-Lipka J., Gubańska I., Janik H.: "*The effect of calcium glycerophosphate (GPCa) on physico-chemical, mechanical and biological properties of polyurethanes applicable in bone tissue engineering",* 5th International Conference on Polymer Processing and Characterization, 27-29.09.2017, Gdańsk University of Technology, Gdańsk, Poland. – **poster presentation**

Nationwide (polish) conferences:

1) **Haryńska A. (Przybytek A.),** Lewandowska A., Gubańska I., Kucińska-Lipka J., Janik H.: "*Optymalizacja procesu formowania alifatycznych PUR do druku 3D w technologii FDM" (ang. Optimization of the process of forming aliphatic PUR for 3D printing in FDM technology),* IX Kongres Technologii Chemicznej, 3-7.09.2018, Gdańsk University of Technology, Gdańsk, Poland. – **oral presentation**

2) **Haryńska A. (Przybytek A.)**, Lewandowska A., Gubańska I., Kucińska-Lipka J., Sienkiewicz M., Janik H.: *„Otrzymywanie nowych poliuretanów dla celów medycznych o właściwościach elastycznych do zastosowania w drukarkach FDM" (ang. Preparation of new polyurethanes for medical purposes with flexible properties for use in FDM printers),* I Ogólnopolska Konferencja Naukowa Polimery w Medycynie, 18.05.2018, Instytut Biopolimerów i Włókien Chemicznych, Łódź, Poland – **oral presentation**

3) **Haryńska A. (Przybytek A.),**: *„Przegląd specjalistycznych materiałów do druku w technologii FDM" (ang. Review of specialized materials for 3D printing in FDM technology),* Pomorskie Dni Druku 3D Industry, 25-26.09.2018, Gdynia, Poland – **plenary lecture**

4) **Haryńska A. (Przybytek A.)**, Ziółkowska M., Sienkiewicz M., Kucińska-Lipka J., Janik H. *„Badanie podatności na kompostowanie kompozycji poliestrowo-skrobiowych modyfikowanych gumą arabską" (ang. Study of the compostability of polyester-starch compositions modified with arabic gum)*, IX Kongres Technologii Chemicznej, 3-7.09.2018, Politechnika Gdańska– **poster presentation**

International trade fairs:

1) Exhibitor – *"Biodegradable and compostable disposable cutlery"* at Perspektywy Women In Tech Summit 2019, 13-14.11.2019, Warsaw, Poland

2) Exhibitor – *"BioGranAqua - biodegradable and compostable polymer granules for the production of support filaments for FFF 3D printing, PurGranMed - biocompatible polymer granules for the production of medical-grade flexible filaments for FFF 3D printing"* at 10th International 3D Printing Days, 10-12.04.2018, Kielce, Poland

3) Exhibitor – *"Biodegradable thermoplastic polymer compositions, method of their preparation and application"* at Technicon Innovations, The International Industrial Technology Fair, 22-23.10.2015, Gdańsk, Poland

Research projects:

1) Project contractor *"Biodegradable thermoplastic polymer composition, method of its production and application"* The project was financed under the Innovation Incubator+ program, implemented by the Center for Knowledge and Technology Transfer of the Gdansk University of Technology.

2) Project contractor – *"Novel elastic and support filaments for 3D printing".* The project was financed under the Innovation Incubator+ program, implemented by the Center for Knowledge and Technology Transfer of the Gdansk University of Technology.

Popularization of science:

1) Coordinator of science and technology workshops: *„Pokaz procesów przetwórstwa, przetwarzania i kompostowania polimerów biodegradowalnych" (ang. Demonstration of the processing and composting of biodegradable polymers)* during Baltic Science Festival 2017 and 2018, Gdańsk, Poland

2) Co-cordinator of science and technology workshops: *„Świecący polimer z ziemniaka – zrób to sam! Biodegradowalne i kompostowalne polimery" (ang. Glowing polymer from potato - do it yourself! Biodegradable and compostable polymers)* during Baltic Science Festival 2017 and 2018, Gdańsk, Poland

University scholarships:

1) Gdańsk University of Technology Rector's scholarship for the best PhD students in the academic years 2016/17, 2018/19 and 2019/20.

2) Pro-quality scholarship in the academic years 2016/17, 2018/19 and 2019/20.

3) Task scholarship within the project Integrated Development Program of the Gdansk University of *Technology* POWR.03.02.00-IP.08-00-DOK/16, 1.09.2017 – 30.03.2022.

University awards:

1) The main award of the best product in the competition of 10th International 3D Printing Days and the Association of Technology Initiatives Poland for the product "BioGranAqua". International trade fairs, 10-12.04.2018, Kielce, Poland. Authors: Janik H, Kucińska-Lipka J, Sienkiewicz M, Gubańska I, **Przybytek A**, Lewandowska A.

2) Gold Medal in the Innovations competition for "*Biodegradable thermoplastic polymer compositions, method of their production and application*", at Technicon Innovations, The International Industrial Technology Fair, 22-23.10.2015, Gdańsk, Poland

3) Professor Jerzy Młynarczyk Award of Pomeranian District Basketball Association for people combining outstanding results in science with sports achievements (pol. *Nagroda imienia Profesora Jerzego Młynarczyka Pomorskiego Okręgowego Związku Koszykówki dla osób łączących wybitne wyniki w nauce z osiągnięciami w sporcie*), 2019 edition, Gdańsk, Poland.

4) The Most Valuable Player (MVP) of the Polish Academic Basketball Championship 2019, 23-26.05.2019, Warszawa, Poland.

5) Honorable mention in the plebiscite for The Best Athlete of the Gdańsk University of Technology (pol. *Wyróżnienie w plebiscycie na najlepszego sportowca Politechniki Gdańskiej*), season 2017/2018, Gdańsk, Poland

6) Two-time Academic Polish Champion in women's basketball with the Gdansk University of Technology team, Kraków 2018, Warszawa 2019.

7) Academic Polish Champion in women's 3x3 basketball with the Gdansk University of Technology team, Wilkasy 2022.

8) Academic Polish Vice-champion in women's basketball with the Gdansk University of Technology team, Opole 2022.

9) Five-time gold medalist of the Polish Academic Basketball Championships in the category of Technical Universities with the Gdansk University of Technology team, Warszawa 2015, Lublin 2016, Kraków 2018, Warszawa 2019, Opole 2022.

10) Gold medalist of the Polish Academic 3x3 Basketball Championships in the category of Technical Universities with the Gdansk University of Technology team, Wilkasy 2022.

11) Fourth place in the European Universities Basketball Championship EUSA, Poznań 2019.

Acknowledgments

This work could not have been created without the participation and help of people to whom I would like to express my gratitude at this point.

- I would like to acknowledge my scientific leader, **professor dr hab. inż. Helena Janik**, for the invitation and introduction to the world of science, and for the trust, great kindness, support in my sports carrier, and given knowledge, both scientific and life. Her great scientific and life wisdom is an inspiration.

- I would also like to acknowledge my supervisor, **dr hab. inż. Justyna Kucińska-Lipka,** for the opportunity to follow my own, sometimes very winding and time-consuming scientific paths, and also for a kindness and good mood, support in my sports carrier and always a positive attitude.

- I would also like to thank **dr inż. Maciej Sienkiewicz** for the practical knowledge passed on to me in the field of operating machinery and measuring devices.

- I would also like to thank all the **employees of the Department of Polymer Technology** for all their comments and scientific tips.

- Many thanks to **PhD students and young researchers** of the Department of Polymer Technology (**especially dr inż. Iga Carayon**), for maybe short but always positive and hilarious moments.

- Special thanks to my family, especially my **mother Wiesia**, who took great care of my baby daughter so that I could finish this doctoral dissertation.

Last but not least. The greatest thanks and appreciation to the person who carried the burden and hardships of my doctorate. For your constant faith in me and support in my scientific and sports career. For your everyday care, tonnes of sacrifices, and unimaginable effort. **Thank you my husband.**

Appendix 1 - Material data on commercial medical-grade polyurethanes

Table A1 Summary of commercially available medical-grade polyurethane. Data taken from company safety data sheets. *HS – hardness, Tsb – ultimate tensile strength, Eb – elongation at break. * ISO 10993 Part 1 "Biological Evaluation of Medical Devices" tests for **30-day** indirect blood contact applications. ** The United States Pharmacopeia (USP). USP Class VI Plastic Tests are designed to evaluate the biological reactivity of various types of plastics materials in vivo.*

Trade name	Grade	Chemical description	Mechanical properties	Recommended application	Biological test	Company
TEXIN®	RxS285	Aromatic polyester-based TPU	TSb= 37,9 MPa, Eb =500%, Flexural modulus = 27,6 MPa, HS = 85º ShA	dental ligature, tubing, luers, wound dressings, fabric coatings, packaging, soft touch grips	Biocompatibility(ISO 10993-1*), USP Class VI**	Bayer Material Science LLC
	RxT50D – 90A	Aromatic polyether-based TPU	HS 70º ShA to 65º ShD, TSb 25,5 – 51,7 MPa, Eb 370 – 770 %, Flexular modulus 14,5 – 420 MPa	anesthetic connectors, catheters, flexible tubing, seals, gaskets		
DESMOPAN®	5377A 6064A 6072A 6088A	Aromatic polyether/ester-based TPU	HS 60º ShA to 75º ShD, TSb 25 – 50 MPa, Eb 470 – 880 %,	wound dressings, fabric coatings, packaging and films, surgical drapes, catheters, tubing, soft grip	Biocompatibility (ISO 10993-1*), Cytotoxicity (ISO 10993-5), Skin irritation, Skin sensitization (ISO 10993-10)	
	9370AU 9380AU 9392AU	Aromatic polyether-based TPU				
ChronoFlex®	AL	Aliphatic polycarbonate-based TPU	HS 75º ShA to 75º ShD,TSb 27 – 60 MPa, Eb 350 – 750 %	long and short term implants, disposable medical products,	USP Class VI**, Cytotoxicity (ISO 10993-5), Skin irritation (ISO 10993-10), Skin sensitization (ISO 10993-10), Pyrogenicity (ISO 10993-11)	AdvanSource biomaterials
	C	Aromatic polycarbonate-based TPU	HS 75º ShA to 75º ShD, Tsb 37 – 55 MPa, Eb 300 – 500 %			
ChronoSil®	-	polycarbonate based silicone TPU	HS 75º ShA to 75º ShD, Tsb 22 – 70 MPa, Eb 350 – 650 %		USP Class VI**, Cytotoxicity (ISO 10993-5)	

Trade name	Grade	Chemical description	Mechanical properties	Recommended application	Biological test	Company
Bionate®	I, II	Polycarbonate-based TPU	HS 80º ShA to 75º ShD, TSb 46 – 63 MPa, Eb 240 – 530 %, Flexular modulus range from 41 – 1790 MPa	long-term implants, cardiovascular electrostimulation, neurostimulation, vascular, artificial heart, cardiac assist and diagnostic devices, hip and knee joints	USP Class VI**, Ames Mutagenicity test, Humoral Immunological Study, Systemic Toxicity (ISO 10993-11), Sensitization: Magnusson and Kligma – no dermal sensitization, Carcinogenicity:2 years/rats – non carcinogenic.	DMS
BioSpan®	SPU S SPU F SPU	Segmented polyether TPU	HS 70º ShA. TSb 38,6 – 42 MPa, Eb 847 – 960 %, Flexular modulus range from 10 – 20 MPa	artificial hearts, interventional cardiology balloons, drug eluting stents and spinal implants.	USP (cytotoxicity, pyrogen, muscle implementation 14, 120 days/rats, intracutaneous injection), Hemolysis, Sensitization:Magnusson and Kligman – weak allergic potential, Ames Mutagenicity Assay Chromosome Aberration Balb/c-3T3 Cell Transformation,	
CarboSil®	20,5	Silicone-polycarbonate-based TPU	HS 80º ShA to 55º ShD,TSb 35 – 43 MPa, Eb 340 – 470 %	cardiovascular and nervous system electrostimulation, continuous glucose monitoring, drug eluting and orthopedic implants.	Intracutaneous, Maximization Sensitization Study (ISO 10993-10), Genotoxicity - *in viro* chromosal abrration, Bacterial reverse mutation (saline extract, 95% ehtanol extract), Mouse Bone Marrow Micronucleus (ISO 10993-3), USP Pyrogen Study, Cytotoxicity, Hemolysis, Muscle implementation 2,12 weeks (ISO 10993-6), 26 week Carcinogenicity Study in the Transgenic ras H2 Mouse Model	
Elasthane®	-	Aromatic, polyether-based TPU	HS 80º ShA to 75º ShD, TSb 43 – 60 MPa,Eb 300 – 600 %, Flexular modulus range from 36 –2000 MPa	cardiovascular, neurostimulation and orthopedic implants	Cytytoxicity – non cytotoxic, Hemocompatybility – non-hemolytic	

Trade name	Grade	Chemical description	Mechanical properties	Recommended application	Biological test	Company
PurSil®	20,35	Silicone-polyether-based TPU	HS 80º ShA to 83º ShA,TSb 25 – 32 MPa, Eb 500 – 565 %, Flexular modulus range from 38 –43 MPa	medical devices, including ophthalmic, anastomotic, and continuous glucose monitoring.	Cytotoxicity (ISO 10993-5), Sensitization Tests, Irritation Test (ISO 10993-10), Genotoxicity (bacterial reverse mutation, in vitro chromosomal aberration) (ISO 10993-3), In Vitro Hemolysis Study (ISO 10993-4), Subchronic Intravenous Toxicity ISO 10993-11),	
DegraPol®	-	Polyester-urethane (Hard Segment – PHB-diol, trimetilexametilene diisocyanate TMDI), (Soft Segment – polycaprolactole-dyglicol-diol)	no data found	Tissue scaffolds (cardiac and cartilage tissue engineer, nerve guidance channel)	Cytocompatibility, subcutaneous implantation (rats), cell (HCS) seeding and response to material	ab Medica
Parker	ALC 95A, 95A-B20	aliphatic polycarbonate-based TPU	HS 95,96º ShA, TSb 0,02, 0,034 MPa,Eb 400, 460 %, Flexular modulus range from 0,075, 0,13 MPa (ASTM D 790)	vascular access devices, tracheotomy, urological, dialysis devices, disposable tretment devices	USP Class VI**, Cytotoxicity, Hemolysis (ISO 10993-4)	PARKER
MillaMed®	PU2055 PU2075	Aliphatic polyether-based TPU	HS 55,75º ShA,Tsb 15, 32 MPa, Eb 540, 565 %, Flexular modulus range from 0,075, 0,13 MPa (ASTM D 790)	short term implants (up to 29 days)	USP Class VI**, Cytotoxicity (ISO 10993-5)	TSE
Carbothane ®	PC	Aliphatic Polycarbonate-based TPU	HS 70º ShA to 69º ShD TSb 50 – 67 MPa, Eb 325 – 600 %	medical bags, wound dressings and tapes, catheters, tubing, bone and tissue scaffolds, artificial knees and hips, long/short term implants, ndovascular medical devices	USP Class VI**, Cytotoxicity (ISO 10993-5), Hemolysis (ISO 10993-4)	Lubrizol
	AC	Aromatic Polycarbonate-based TPU	HS 77º ShA to 56º ShD, TSb 50 – 67 MPa, Eb 300 – 400 %			

Trade name	Grade	Chemical description	Mechanical properties	Recommended application	Biological test	Company
	PC B20	Aliphatic Polycarbonate-based TPU+ 20% of barium sulfate	HS 75º ShA to 71º ShD, TSb 50 – 65 MPa, Eb 300 – 570 %			Lubrizol
	AC B20	Aromatic Polycarbonate-based TPU+ 20% of barium sulfate	HS 78º ShA to 56º ShD, TSb 57 – 69 MPa, Eb 300 – 400 %			
Tecoflex®	EG	Aliphatic polyether-based TPU	HS 72º ShA to 67º ShD, TSb 40 – 57 MPa, Eb 310 – 660 %		no data found	
Pellethane®	2363-5863	Aromatic polyether-based TPU	HS 81º ShA to 76º ShD,TSb 30 – 48 MPa, Eb 450 – 700 %		USP Class VI**	
	5855	Aromatic polyester-based TPU	HS 92º ShA, 70º ShD, TSbt 29, 62 MPa, Eb 160%, 450 %			
Pathway®	-	Aliphatic polyether-based TPU	HS 62 ºShA to 83 ºshD	Controlled drug release, implantable drug delivery, drug eluting devices	Amnes Mutagenicity Assay (ISO 10993-3), Hemolysis (ISO 10993-4), Cytotoxicity (ISO 10993-5), Irritancy, Muscule implementation (ISO 10993-6), Skin sensitization (ISO 10993-10) – 0% Grade 1, System Toxicity (ISO 10993-11)	

Appendix 2 - Co-authors' statements and contributions

PAPER 1 → Haryńska A., Gubanska I., Kucinska-Lipka J., Janik H. *Fabrication and Characterization of Flexible Medical-Grade TPU Filament for Fused Deposition Modeling 3DP Technology*. Polymers (Basel). 2018, *10*, 1304, doi:10.3390/polym10121304.

L.P.	NAME AND SURNAME	SHARE %	SIGNATURE
1	**Agnieszka Haryńska**	**40**	Agnieszka Haryńska
2	Iga Carayon (Gubańska)	20	Carayon
3	Justyna Kucińska-Lipka	20	Kucińska-Lipka
4	Helena Janik	20	H Janik

PAPER 2 → Haryńska A., Kucinska-Lipka J., Sulowska A., Gubanska I., Kostrzewa M., Janik H. *Medical-Grade PCL Based Polyurethane System for FDM 3D Printing—Characterization and Fabrication*. Materials (Basel). 2019, *12*, 887, doi:10.3390/ma12060887.

L.P.	NAME AND SURNAME	SHARE %	SIGNATURE
1	**Agnieszka Haryńska**	**50**	Agnieszka Haryńska
2	Justyna Kucińska-Lipka	15	Kucińska-Lipka
3	Agnieszka Sulowska	10	Agnieszka Sulowska
4	Iga Carayon (Gubańska)	10	Carayon
5	Marcin Kostrzewa	5	Marcin Kostrzewa
6	Helena Janik	10	H Janik

PAPER 3 → Haryńska A., Carayon I., Kosmela P., Brillowska-Dąbrowska A., Łapiński M., Kucińska-Lipka J., Janik H. *Processing of Polyester-Urethane Filament and Characterization of FFF 3D Printed Elastic Porous Structures with Potential in Cancellous Bone Tissue Engineering*. Materials (Basel). 2020, *13*, 4457, doi:10.3390/ma13194457.

L.P.	NAME AND SURNAME	SHARE %	SIGNATURE
1	**Agnieszka Haryńska**	**50**	Agnieszka Haryńska
2	Iga Carayon	10	Carayon
3	Paulina Kosmela	5	Kosmela
4	Anna Brillowska-Dąbrowska	10	
5	Marcin Łapiński	5	
6	Justyna Kucińska-Lipka	10	Kucińska-Lipka
7	Helena Janik	10	H Janik

PAPER 4 → Haryńska A., Carayon I., Kosmela P., Szeliski K., Łapiński M., Pokrywczyńska M., Kucińska-Lipka J., Janik, H. *A comprehensive evaluation of flexible FDM/FFF 3D printing filament as a potential material in medical application.* Eur. Polym. J. 2020, *138*, doi:10.1016/j.eurpolymj.2020.109958.

L.P.	NAME AND SURNAME	SHARE %	SIGNATURE
1	**Agnieszka Haryńska**	**50**	
2	Iga Carayon	10	
3	Paulina Kosmela	5	
4	Kamil Szeliski	5	
5	Marcin Łapiński	5	
6	Marta Pokrywczyńska	5	
7	Justyna Kucińska-Lipka	10	
8	Helena Janik	10	

PAPER 5 → Haryńska A. (Przybytek A.), Sienkiewicz M., Kucińska-Lipka J., Janik H. *Preparation and characterization of biodegradable and compostable PLA/TPS/ESO compositions.* Ind. Crops Prod. 2018, *122*, doi:10.1016/j.indcrop.2018.06.016.

L.P.	NAME AND SURNAME	SHARE %	SIGNATURE
1	**Agnieszka Haryńska (Przybytek)**	**30**	
2	Maciej Sienkiewicz	40	
3	Justyna Kucińska-Lipka	10	
4	Helena Janik	20	

PAPER 6 → Haryńska A., Janik H., Sienkiewicz M,. Mikolaszek B,. Kucińska-Lipka J. *PLA-potato thermoplastic starch filament as a sustainable alternative to conventional PLA filament: processing, characterization and FFF 3D printing.* ACS Sustain. Chem. Eng. 2021, 9(20), 6923-6938, doi.org/10.1021/acssuschemeng.0c09413

L.P.	NAME AND SURNAME	SHARE %	SIGNATURE
1	**Agnieszka Haryńska**	**60**	
2	Helena Janik	10	
3	Maciej Sienkiewicz	10	
4	Barbara Mikolaszek	10	
5	Justyna Kucińska-Lipka	10	

Paper 1: Haryńska A., Gubanska I., Kucinska-Lipka J., Janik H. Fabrication and Characterization of Flexible Medical-Grade TPU Filament for Fused Deposition Modeling 3DP Technology. *Polymers (Basel).* **2018**, *10*, 1304, doi:10.3390/polym10121304.

Agnieszka Haryńska: material synthesis and optimization; filament-formation; investigation (acidimetric titration, density, melt-flow rate, tensile test, hardness, FTIR, optical microscopy, accelerated degradation); testing of the 3D printing process; analysis and discussion of the results; data visualization; data curation; literature review; writing an original draft, cover letter, and response on reviewers' comments; preparation of graphical abstract.
My contribution is estimated at 40%.

Agnieszka Haryńska
signature

Iga Carayon (Gubańska): statical analysis; analysis of cells morphology; revision and editing of the manuscript.
My contribution is estimated at 20%.

Carayon
signature

Justyna Kucińska-Lipka: development and design of the methodology; investigation (contact angle, short-term hemocompatibility test, indirect cytotoxicity test).
My contribution is estimated at 20%.

Kucińska-Lipka
signature

Helena Janik: revision and editing of the manuscript; supervision; provision of study materials, reagents, and other analysis tools
My contribution is estimated at 20%.

Janik
signature

Paper 2: Haryńska A., Kucinska-Lipka J., Sulowska A., Gubanska I., Kostrzewa M., Janik H. Medical-Grade PCL Based Polyurethane System for FDM 3D Printing—Characterization and Fabrication. *Materials (Basel).* **2019**, *12*, 887, doi:10.3390/ma12060887.

Agnieszka Haryńska: design of the methodology; material synthesis; filament-formation; investigation (FTIR and Raman spectroscopy, tensile test, hardness, thermal analysis – DSC and TGA, long-term degradation); analysis and discussion of the results; data visualization; data curation; writing an original draft, cover letter, and response on reviewers' comments.
My contribution is estimated at 50%.

Agnieszka Haryńska
signature

Justyna Kucińska-Lipka: conceptualization; investigation (indirect cytotoxicity test); revision of the manuscript; supervision.
My contribution is estimated at 15%.

Kucińska-Lipka
signature

Agnieszka Sulowska: writing literature review; investigation (water absorption, accelerated degradation, optical microscopy).
My contribution is estimated at 10%.

Agnieszka Sulowska
signature

Iga Carayon (Gubańska): statical analysis; revision and editing of the manuscript.
My contribution is estimated at 10%.

Carayon
signature

Marcin Kostrzewa: investigation (contact angle, surface free energy).
My contribution is estimated at 5%.

Marcin Kostrzewa
signature

Helena Janik: revision and editing of the manuscript; provision of study materials, reagents, and other analysis tools.
My contribution is estimated at 10%.

H. Janik
signature

Paper 3: Haryńska A., Carayon I., Kosmela P., Brillowska-Dąbrowska A., Łapiński M., Kucińska-Lipka J., Janik H. Processing of Polyester-Urethane Filament and Characterization of FFF 3D Printed Elastic Porous Structures with Potential in Cancellous Bone Tissue Engineering. *Materials (Basel).* **2020**, *13*, 4457, doi:10.3390/ma13194457.

Agnieszka Haryńska: conceptualization and design of the methodology; literature review; filament-formation; investigation (FTIR and Raman spectroscopy, H-NMR, melt flow rate, tensile and compression tests, hardness, contact angle, surface free energy, long and short-term degradation, SBF incubation, optical microscopy); design of the digital models of the porous structures and test samples; optimization of the 3D printing; analysis and discussion of the results; data visualization; data curation; writing an original draft, cover letter, and response on reviewers' comments; preparation of graphical abstract.
My contribution is estimated at 50%.

Agnieszka Haryńska
signature

Iga Carayon (Gubańska): investigation (cytotoxicity test); revision and editing of the manuscript.
My contribution is estimated at 10%.

Carayon
signature

Paulina Kosmela: carrying out the thermal and thermomechanical tests (DSC, TGA, DMA).
My contribution is estimated at 5%.

Kosmela
signature

Anna Brillowska-Dąbrowska: formal analysis; revision and editing of the manuscript.
My contribution is estimated at 10%.

signature

Marcin Łapiński: carrying out the SEM images and EDS measurements.
My contribution is estimated at 5%.

M Łapiński
signature

Justyna Kucińska-Lipka: conceptualization; revision of the manuscript; provision of study materials, reagents, and 3D printers.
My contribution is estimated at 10%.

Kucińska-Lipka
signature

Helena Janik: formal analysis; revision of the manuscript; supervision.
My contribution is estimated at 10%.

H Janik
signature

Paper 4: Haryńska A., Carayon I., Kosmela P., Szeliski K., Łapiński M., Pokrywczyńska M., Kucińska-Lipka J., Janik, H. A comprehensive evaluation of flexible FDM/FFF 3D printing filament as a potential material in medical application. *Eur. Polym. J.* **2020**, *138*, doi:10.1016/j.eurpolymj.2020.109958.

Agnieszka Haryńska: conceptualization and design of the methodology; literature review; filament-formation; investigation (FTIR and Raman spectroscopy, melt flow rate, tensile and compression tests, hardness, contact angle, surface free energy, accelerated degradation, SBF incubation, optical microscopy); design of the digital models of the porous structures and test samples; optimization of the 3D printing; analysis and discussion of the results; data visualization; data curation; writing an original draft, cover letter, and response on reviewers' comments; preparation of graphical abstract.
My contribution is estimated at 50%.

signature

Iga Carayon (Gubańska): statical analysis; analysis of cells morphology; revision of the manuscript.
My contribution is estimated at 10%.

signature

Paulina Kosmela: carrying out the thermal and thermomechanical tests (DSC, TGA, DMA).
My contribution is estimated at 5%.

signature

Kamil Szeliski: carrying out the cytotoxicity test.
My contribution is estimated at 5%.

signature

Marcin Łapiński: carrying out the SEM images and EDS measurements.
My contribution is estimated at 5%.

signature

Marta Pokrywczyńska: investigation of the cytotoxicity test.
My contribution is estimated at 5%.

signature

Justyna Kucińska-Lipka: revision of the manuscript; provision of study materials, reagents, and 3D printers; supervision.
My contribution is estimated at 10%.

signature

Helena Janik: formal analysis; revision of the manuscript.
My contribution is estimated at 10%.

signature

Paper 5: Haryńska (Przybytek) A., Sienkiewicz M., Kucińska-Lipka J., Janik H. Preparation and characterization of biodegradable and compostable PLA/TPS/ESO compositions. *Ind. Crops Prod.* **2018**, *122*, doi:10.1016/j.indcrop.2018.06.016.

Agnieszka Haryńska: material preparation and extrusion; investigation (melt-flow rate, tensile and impact test, hardness, water resistance, optical microscopy); analysis and discussion of the performed studies; data visualization; data curation; literature review; writing an original draft, cover letter, and response on reviewers' comments.
My contribution is estimated at 30%.

Agnieszka Haryńska
signature

Maciej Sienkiewicz: project administration; conceptualization of the material composition, design of the methodology; investigation (thermal properties – DSC, SEM imagining, supervision of the composting study); revision and editing of the manuscript.
My contribution is estimated at 40%.

Sienkiewicz
signature

Justyna Kucińska-Lipka: revision of the manuscript; supervision.
My contribution is estimated at 10%.

Kucińska-Lipka
signature

Helena Janik: formal analysis; revision and editing of the manuscript; provision of study materials, reagents, and other analysis tools.
My contribution is estimated at 20%.

Janik
signature

Paper 6: Haryńska A., Janik H., Sienkiewicz M,. Mikolaszek B,. Kucińska-Lipka J. PLA–potato thermoplastic starch filament as a sustainable alternative to conventional PLA filament: processing, characterization and FFF 3D printing. *ACS Sustain. Chem. Eng.* **2021**, 9(20), 6923-6938, doi.org/10.1021/acssuschemeng.0c09413

Agnieszka Haryńska: conceptualization, design of the methodology; filament-formation; investigation (FTIR and Raman spectroscopy, XRD measurements, melt-flow rate, tensile, compression and impact tests, hardness, water contact angle, thermal tests – DSC, TGA, DMA, degradation studies and pH measurements, optical microscopy, laboratory simulated composting); design of the digital models of the porous structures, anatomical models and test samples; optimization of the 3D printing; analysis and discussion of the results; data visualization; data curation; literature review; writing an original draft, cover letter, and response on reviewers' comments; preparation of graphical abstract.
My contribution is estimated at 60%.

signature

Helena Janik: formal analysis; revision of the manuscript; provision of study materials, reagents, and other analysis tools.
My contribution is estimated at 10%.

signature

Maciej Sienkiewicz: project administration; design of the material composition.
My contribution is estimated at 10%.

signature

Barbara Mikolaszek: carrying out the SEM images, English proof of the manuscript.
My contribution is estimated at 10%.

signature

Justyna Kucińska-Lipka: manuscript revision; provision of 3D printers and measurement equipment.
My contribution is estimated at 10%.

signature